Fakultät für Maschinenwesen

Modal Quantities and Their Usage for Evaluation of Radiated Sound Power

Lennart Dennis Moheit

Vollständiger Abdruck der von der Fakultät für Maschinenwesen der
Technischen Universität München zur Erlangung des akademischen Grades eines

Doktor-Ingenieurs (Dr.-Ing.)

genehmigten Dissertation.

Vorsitzender:	Prof. Dr. Carlo L. Bottasso
Prüfer der Dissertation:	1. Prof. Dr.-Ing. Steffen Marburg
	2. Prof. Dr. Andrés Prieto

Die Dissertation wurde am 25.05.2020 bei der Technischen Universität München eingereicht und durch die Fakultät für Maschinenwesen am 01.11.2020 angenommen.

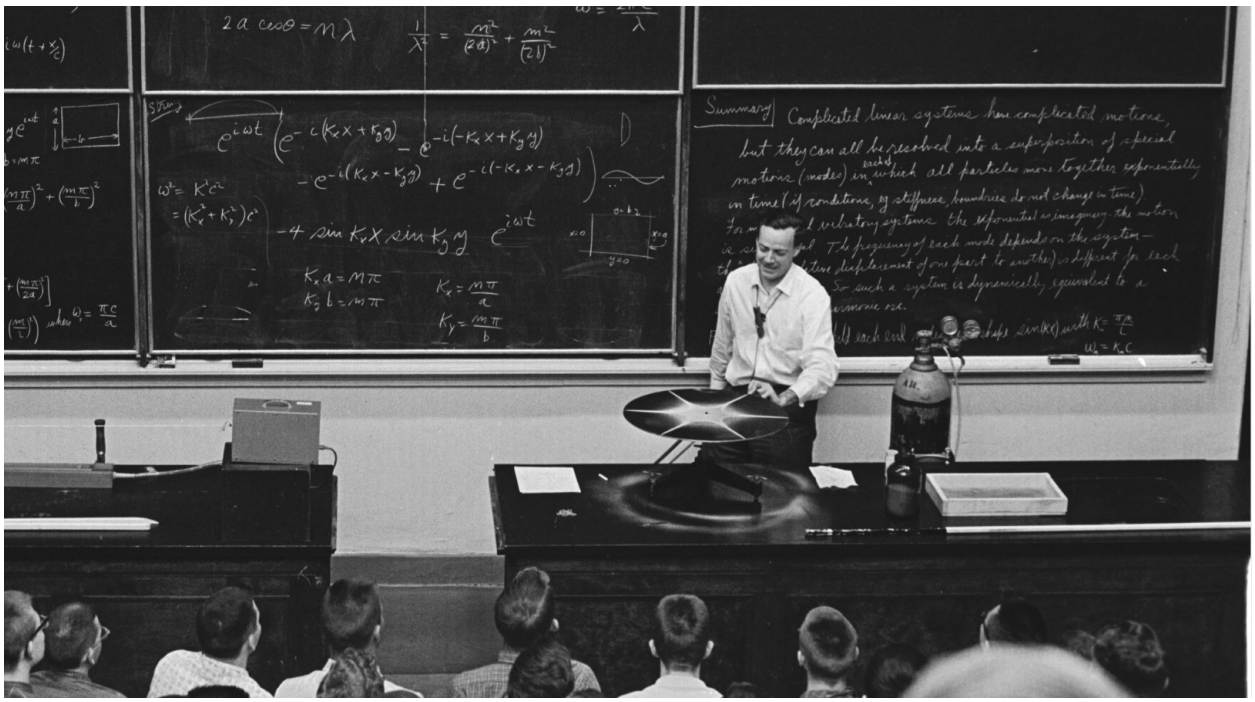

a)

Summary Complicated linear systems have complicated motions, but they can all be resolved into a superposition of special motions (modes) in each of which all particles move together exponentially in time (if conditions, eg stiffness, boundries do not change in time). For mechanical vibratory systems the exponential is imaginary - the motion is sinusoidal. The frequency of each mode depends on the system — the "shape" (relative displacement of one part to another) is different for each allowed frequency. So such a system is dynamically equivalent to a set of independent harmonic osc.

b)

Figure 1: Prof. Richard Feynman lecturing on modes to undergraduates in 1962 (a) and his summary on the topic on the blackboard (b) [1].

Abstract

Exterior problems describe effects in not entirely closed areas. They are an essential field of acoustics in which, for example, unwanted environmental noise from technical equipment needs to be minimized or the exterior noise of vehicles is optimized. In addition, the radiated sound power outdoors is usually used to describe sound sources. Since experimental investigations are often expensive and associated with uncertainties, the use of numerical methods is becoming increasingly important. Despite considerable technical and methodological developments in recent years, the calculation of exterior acoustic problems is still very expensive in terms of time and memory requirements and there is a substantial need to develop efficient methods and algorithms for these problems.

Modal superposition is a well-established and efficient mathematical concept applied in structural dynamics and interior acoustics. However, the transfer to exterior acoustics is complex due to the specific mathematical properties of the systems resulting from the boundary conditions. With the frequency-dependent acoustic radiation modes (ARM) and the frequency-independent normal modes (NM), two modal quantities have been documented in the literature that potentially provide a benefit in efficiency compared to conventionally used harmonic analysis. While ARM based on the boundary element method (BEM) are already widely investigated and used in practice, NM based on the finite and infinite element method (FEM, IFEM) are relatively new and the relationship to ARM is not well understood.

The present dissertation addresses these knowledge gaps and contributes to a deeper understanding of modal quantities in exterior acoustics. Tools and criteria are developed to determine physically relevant modes for the efficient numerical solution of these problems. For the first time, ARM are determined based on the frequency-independent system matrices of FEM and IFEM in order to create the same calculation basis for both modal methods. Their properties and dependencies on the underlying numerical approaches are analyzed in depth and experiences are made for a good balance between efficiency and accuracy. Appropriate models are used to investigate the nature and acoustic significance of the modes, thus developing a deeper understanding of their physical effects. It is described how the modes belong to different groups and criteria and methods for the identification and classification of the different types and their acoustic effects are developed on the basis of mathematical properties of the corresponding eigenvalues and eigenvectors.

Based on the proposed and tested tools, this work presents essential innovations and findings on ARM and NM for the efficient solution of exterior acoustic problems. For the primarily investigated NM and simple radiator geometries with cavities it is shown that, with a considerably reduced modal basis, a very high accuracy (relative error of the sound power compared to harmonic analysis below 1%) can be achieved in wide frequency ranges.

Kurzfassung

Außenraumprobleme beschreiben Effekte in nicht vollständig geschlossenen Gebieten. Sie sind ein wesentliches Aufgabengebiet der Akustik, in dem beispielsweise unerwünschter Umgebungslärm technischer Anlagen minimiert oder die Außengeräusche von Fahrzeugen optimiert werden sollen. Darüber hinaus wird zur Beschreibung von Schallquellen in der Regel die abgestrahlte Schallleistung im Freien herangezogen. Dementsprechend aufwändig und unsicherheitsbehaftet gestalten sich häufig messtechnische Untersuchungen, sodass die Verwendung numerischer Verfahren vermehrt in den Fokus rückt. Die Berechnung akustischer Außenraumprobleme ist trotz erheblicher technischer und methodischer Entwicklungen in den vergangenen Jahren noch immer sehr zeit- und ressourcenintensiv und es besteht ein hoher Bedarf zur Entwicklung effizienter Methoden und Algorithmen für diese Probleme.

Modale Superposition ist ein in strukturdynamischen und Innenraum-akustischen Problemstellungen etabliertes und effizientes numerisches Lösungsverfahren. Allerdings gestaltet sich deren Übertragung auf den akustischen Außenraum aufgrund der spezifischen mathematischen Eigenschaften der Systeme infolge der Randbedingungen aufwändig. Mit den frequenzabhängigen acoustic radiation modes (ARM) und den frequenzunabhängigen normal modes (NM) sind in der Literatur zwei modale Größen dokumentiert, die gegenüber der klassischerweise verwendeten harmonischen Analyse potentiell einen Effizienzvorteil liefern können. Während die ARM auf der Basis der Randelementemethode (BEM) bereits vielfältig untersucht und praktisch eingesetzt werden, sind NM auf der Grundlage von Finite und Infinite Elemente Methode (FEM, IFEM) sowie die Zusammenhänge zu den ARM wenig erforscht.

Die vorliegende Dissertation befasst sich mit diesen Wissenslücken und trägt zu einem tieferen Verständnis modaler Größen in akustischen Außenraumproblemen bei. Zur Ermittlung physikalisch relevanter Moden für die effiziente numerische Lösung der Außenraumakustik werden Werkzeuge und Kriterien entwickelt. Hierfür werden erstmals ARM auf Grundlage der frequenzunabhängigen Systemmatrizen von FEM und IFEM bestimmt, um für die beiden modalen Verfahren die gleiche Berechnungsbasis zu schaffen. Es werden die Eigenschaften und Abhängigkeiten der modalen Verfahren von den zugrundeliegenden numerischen Methoden tiefergehend analysiert und Erfahrungswerte für eine gute Balance zwischen Rechenaufwand und Genauigkeit generiert. Anhand geeigneter Modelle werden die Beschaffenheit und die akustische Bedeutung der Moden untersucht und so ein tiefergehendes Verständnis ihrer physikalischen Effekte entwickelt. Es werden Gruppenzugehörigkeiten beschrieben und Kriterien und Verfahren zur Identifikation und Klassifizierung unterschiedlich gearteter und wirkender Moden anhand mathematischer Eigenschaften der Eigenwerte und -vektoren entwickelt.

Zur effizienten Lösung akustischer Außenraumprobleme stellt diese Arbeit mit den vorgeschlagenen und erprobten Werkzeugen wesentliche Neuerungen und Erkenntnisse zu ARM und NM vor. Für die schwerpunktmäßig untersuchten NM und einfache Strahlergeometrien mit Kavität wird gezeigt, dass mit einer stark reduzierten modalen Basis in weiten Frequenzbereichen eine sehr hohe Genauigkeit (relativer Fehler der Schallleistung gegenüber harmonischer Analyse unter 1%) erzielt werden kann.

Preface / Vorwort

Während dieser scheinbar niemals enden wollenden Arbeit haben mich viele wunderbare Menschen unterstützt, denen ich von Herzen danken möchte. Mein allergrößtes und allerherzlichstes Dankeschön richtet sich an Luzie für ihre unermüdliche und aufopferungsvolle Liebe und Unterstützung, die all dies überhaupt erst möglich gemacht hat, in schönen wie in schweren Zeiten. Ich danke herzlich meiner lieben Familie, die mich von klein auf auf meinem Weg begleitet und unterstützt hat.

Vielmals danken möchte ich Prof. Dr.-Ing. Steffen Marburg für die Betreuung dieser Arbeit und die zahlreichen fruchtbaren Diskussionen und Impulse, die mich immer wieder den roten Faden finden ließen. Danke Dir, lieber Steffen, für die vielen Gelegenheiten, die Welt zu bereisen und viele interessante Menschen kennen zu lernen, für die Freiheiten und das Vertrauen.

Many thanks to Prof. Dr. Andrés Prieto for supervising my thesis and being a very friendly and helpful discussion partner. I enjoyed meeting you in A Coruña and hope to see you again soon in Munich. Furthermore, I would like to thank Prof. Dr. Carlo Bottasso for his guidance through the exam and for his friendly chairmanship.

Many greetings to Sydney, namely to Prof. Dr. Nicole Kessissoglou and Dr. Daipei David Liu at UNSW, as well as to Dr. Herwig Peters. Best thanks for the wonderful time in “Down Under” and for the great introduction to the research topic.

Ganz besonders möchte ich allen Weggefährt:innen an der UniBW und der TU München für die Unterstützung, tolle Zusammenarbeit und schöne Zeit danken, vor allem den “alten Hasen”, die von Anfang an dabei waren: Marcus Mäder, Patrick Langer, Christian Geweth, Theo Kiesel, Johannes Henneberg, Monika Gatt und Kheirollah Sepahvand. Aber natürlich auch jenen, die später an der TUM dazu gestoßen sind, u.a. Ferina Saati, Magdalena Scholz, Caglar Gürbüz, Felix Kronowetter, Martin Eser, Koji Baydoun, Christopher Jelich, Alex Hoppe, Anton Melnikov sowie Jonas und Johannes Schmid (nicht zu vergessen die immer hilfsbereiten Kolleginnen aus dem Sekretariat Elke Reichardt und Martina Sommer). Ich freue mich sehr, viele von euch als Freundinnen und Freunde gewonnen zu haben. Lasst uns in Kontakt bleiben!

Gewidmet dem größten HF aller Zeiten

Attached Publications

[**A**] MOHEIT, L. & MARBURG, S. (2017). Infinite elements and their influence on normal and radiation modes in exterior acoustics. *Journal of Computational Acoustics*, 25(04), 1650020.

[**B**] MOHEIT, L. & MARBURG, S. (2018). Normal modes and modal reduction in exterior acoustics. *Journal of Theoretical and Computational Acoustics*, 26(03), 1850029.

[**C**] MOHEIT, L., ANTHIS, S., HEINZ, J., KRONOWETTER, F. & MARBURG, S. (2020). Analysis of scattering by finite sonic crystals in free field with infinite elements and normal modes. *Journal of Sound and Vibration*, 476, 115291.

List of Prior Publications

[M1] MOHEIT, L. & MARBURG, S. (2015). Vergleich frequenzabhängiger und -unabhägiger Moden der Schallabstrahlung akustischer Außenraumprobleme. In: BECKER, S. (Ed.), *Fortschritte der Akustik 41*.

[M2] MOHEIT, L., PETERS, H. & MARBURG, S. (2015). A comparison of acoustic radiation modes and frequency-independent normal modes in acoustic exterior problems. In: PAVIC, G. (Ed.), *Proceedings of NOVEM 2015*.

[M3] MOHEIT, L. & MARBURG, S. (2016) Konvergenz akustischer Außenraummoden mit infiniten Elementen. In: VORLÄNDER, M. & FELS, J. (Eds.): *Fortschritte der Akustik 42*.

[M4] MOHEIT, L. & MARBURG, S. (2016). Convergence of modes in exterior acoustics problems with infinite elements. In: KROPP, W., VON ESTORFF, O. & SCHULTE-FORTKAMP, B. (Eds.), *Proceedings of the 45th Internoise*, 1640–1648.

[M5] MOHEIT, L. & MARBURG, S. (2017). Eigenwertproblem und modale Superposition im akustischen Außenraum. In: NOLTE, B. & SCHMIDT, G. (Eds.), *Fortschritte der Akustik 43*.

[M6] MOHEIT, L. & MARBURG, S. (2017). Acoustic radiation modes and normal modes in unbounded domains. In: *Proceedings of Meetings on Acoustics* 30(1), 022004.

[M7] MOHEIT, L. & MARBURG, S. (2018). Superposition frequenzunabhängiger Moden im akustischen Außenraum. In: SEEBER, B. (Ed.), *Fortschritte der Akustik 44*.

[M8] MOHEIT, L. & MARBURG, S. (2018). Superposition of frequency-independent normal modes in exterior acoustics. In: GUASCH, O. (Ed.), *Proceedings of NOVEM 2018*, 172082.

[M9] KRONOWETTER, F., MOHEIT, L., ESER, M., SEPAHVAND, K. & MARBURG, S. (2020). Spectral stochastic infinite element method in vibroacoustics. *Journal of Theoretical and Computational Acoustics*, 28(02), 2050009.

[M10] KRONOWETTER, F., BAYDOUN, S. K., ESER, M., MOHEIT, L., & MARBURG, S. (2020). A Benchmark Study on Eigenfrequencies of Fluid-Loaded Structures. *Journal of Theoretical and Computational Acoustics*, 28(02), 2050013.

Contents

CHAPTER 1

Introduction and Outline

In which the physical and mathematical problem is defined and motivated in an engineering context, the related literature is classified and the scientific contribution and objectives of the current work are presented.

1 Problem Formulation and Motivation

In many practical applications in acoustics, free-field conditions apply, i.e. a sound source or the area of interest is not or only partially enclosed by reflective boundaries and sound energy emerges from the system towards infinity. Examples are turbine noise from airplanes, rooms with open windows, and sound radiation from trains or cars on the track. These conditions must also be created if only the characteristics of an acoustic radiator are of interest regardless of its reflecting environment, e.g. for the determination of the sound power of a machine, or if only direct sound paths to a receiver are desired as for recording purposes. Within the scope of this dissertation these problems are referred to as *exterior acoustic problems*. A distinction can be made between full-space and half-space problems. While in the first case the sound source is completely surrounded by a non-reflective outer boundary as one can assume approximately for aircraft in high altitude, the half-space problem denotes a semicircular or semispherical domain in which the even ground is (fully) reflective. This assumption is valid for stationary sound sources or vehicles in outdoor environments. The present work deals with the sound pressure in fluids. Solid structures are considered as obstacles in the fluid-filled domain. Fluid-structure interaction, material inhomogeneities as well as flow phenomena are not considered in this work.

The sound power P is a source-describing energy-related quantity, which refers only to the total radiation of sound by the source, but not to its directionality, the environment or the receiver location. It is often the objective to minimize this quantity for noise control purposes [2]. According to the ISO standard 3745 [3], measurements of the sound power have to be conducted in an anechoic chamber that mimics free-field conditions with the help of porous, highly-absorbing walls. The sound pressure p at a certain point, i.e. the immission, is the consequence of the emission of sound from sources, vibrating surfaces, or reflections by obstacles or in the surrounding room. Mathematically, the spatial sound pressure field can be described by the Helmholtz equation as a function of a harmonic frequency. In order to solve this equation uniquely, boundary conditions need to be specified at the surfaces of the obstacles and at the ground in half-space problems. Another condition at infinity is required in order to satisfy the requirements of the free-field environment. Arnold Sommerfeld calls it *the condition of radiation* [4, p. 189], whereupon

> “the sources must be sources, not sinks, of energy. The energy which is radiated from the sources must scatter to infinity; no energy may be radiated from infinity into [...] the field.”

Since acoustic measurements are often associated with a considerable effort and uncertainties and since laboratories and equipment are expensive and often not available, it is desirable to simulate and predict the acoustic behavior of products emitting sound early in the design phase. Thus, it is the subject of extensive research and development. The utilization of efficient methods and algorithms allows the control and optimization of the radiated sound power during the development of virtual prototypes [5, 6]. There are many suitable numerical methods in the field of computational acoustics with a number of advantages and disadvantages, and their use must be carefully weighed depending on the problem.

Besides accuracy, the related computational costs in storage and time are crucial. In particular, inversions of large-scale matrices in a wide range of frequencies are expensive, so that approaches of model order reduction (MOR) can make a major contribution in terms of efficiency. This includes a reduction of the size of a discrete system or the approximation of the model by an appropriate substitution model [7, 8].

One common MOR technique in structural mechanics and interior acoustics is the concept of modal decomposition. Here, the dynamic behavior of the system is approximated by the superposition of linearly-independent, orthogonal vibration patterns, so-called mode shapes [9–11]. Depending on the frequencies and the location of excitation of the system, the total vibrational behavior is often dominated by only a few modes and can thus be reconstructed with a reduced computational effort when they are known a priori. For numerical models, the modal decomposition can be mathematically conducted by solving an eigenvalue problem to obtain the eigenvalues and eigenvectors with the latter representing the mode shapes. In the literature, modes in (room) acoustics are often restricted or understood as standing waves in finite, bounded domains [12]. However, if the boundary or the domain is partially absorbent, i.e. damping occurs, the complex-valued eigenvectors partially consist of both standing waves and traveling waves [13]. In a similar way, standing and radiating wave forms are found for modal quantities in exterior acoustic problems [14, 15].

Two types of modal methods applied to exterior acoustics are considered within the scope of this dissertation: frequency-dependent acoustic radiation modes (ARM) and frequency-independent normal modes (NM). While on the one hand much research has been published on ARM [14], on the other hand, little is known about NM in exterior acoustic problems [16]. Although several studies have already proven applicability of the normal modes approach [15, 17–19], there is still a lack of physical understanding and knowledge about the individual contribution of single modes to the total superimposed solution [16]. Furthermore, the relationships to ARM and the underlying numerical methods have not yet been sufficiently investigated.

The main objective of this dissertation is the enhancement of computational techniques for the efficient prediction of the radiated sound power of sound sources and the sound pressure field around them under free-field conditions. For this purpose, NM and ARM are further investigated and compared to each other. In particular, the NM approach is refined and gradually brought to practical application.

This dissertation is structured as follows: Following the literature review in the subsequent Sec. 2, three central research questions will be formulated in Sec. 3 of the first chapter. Chapter 1 then concludes with the objectives of the attached publications to address the research gaps. The second part, Ch. 2, deals with the physical principles and methods used and refined in this work. In the subsequent Ch. 3, the main results and developments of the attached publications and the respective individual contributions of the candidate are presented. Chapter 4 is dedicated to the discussion of the novelty of the present work with reference to the literature and occasionally provides a look at possible future research. The appendix finally contains the three publications of the author.

2 Literature Overview

The literature references, which serve as a foundation for this work, are structured thematically. First, an overview of available numerical methods for the calculation of exterior acoustic problems is outlined and a decision is made and justified as to which method is suitable within the scope of this work. Subsequently, modal methods are put into the context of exterior problems in acoustics and the two techniques examined in this thesis are reviewed. Finally, possible practical applications of the considered methods and the requirement for developing efficient algorithms in this context are discussed.

2.1 Numerical Techniques in Exterior Acoustic Problems

With the introduction of computer-aided, numerical methods in the engineering sciences, new possibilities arose in the field of technical acoustics. Numerical or computational acoustics is a field of application of numerical mathematics and describes the approximate calculation of solutions of acoustic wave phenomena with the help of algorithms and computers. At the center of numerical methods is the solution of differential equations, whereby a continuous problem, which may not be solved analytically or only with considerable effort, is discretized and then solved approximatively. Lloyd N. Trefethen defines numerical analysis in his essay published in 1992 [20]. He resolutely contradicts the presumption that "numerical analysis is the study of rounding errors" and instead provides a courageous motivation from a mathematician's point of view [20, p. 5]:

> "[. . .] our central mission is to compute quantities that are typically uncomputable, from an analytical point of view, and to do it with lightning speed."

The scope of this dissertation addresses acoustics in fluids neglecting flow and fluid-structure interaction, underlying the Helmholtz equation for the description of the spatial sound pressure field.

In the following, state-of-the-art numerical methods for the solution of exterior acoustic problems are reviewed and discussed with regard to their suitability for the calculation of the modal quantities being considered. An essential requirement is thus the provision of frequency-independent system matrices.

2.1.1 Boundary Element Method (BEM)

A widely used method in numerical acoustics is the boundary element method (BEM), which is suitable for both interior and exterior acoustic problems. Hereby, Green's function is the fundamental solution of the underlying Kirchhoff-Helmholtz integral equation and implicitly fulfills Sommerfeld's radiation condition [21]. Hence, BEM is attractive for exterior problems because the complexity of the problem can be reduced: Instead of the entire, infinitely large volume domain, only the limiting surfaces of obstacles need to be considered. The resulting system matrices are therefore usually small compared to the

corresponding discretization of the entire or a truncated fluid domain. This is the case with the finite element method (FEM) in combination with suitable free-field boundary conditions. However, BEM matrices are frequency-dependent and dense in contrast to sparse and frequency-independent system matrices in FEM, which significantly increases their memory requirements and reduces their performance during mathematical operations such as matrix inversions. The application in large systems is thus strongly restricted.

Conventional BEM for exterior acoustics suffers from the phenomenon of irregular frequencies. These are derived from the solutions of the interior sound-soft bounded (Dirichlet) problem (cf. Ch. 2, Sec. 1.1) and can be found as non-physical resonances in the exterior domain. The effect is due to non-unique solutions of the underlying boundary integral equation and can be mitigated by application of the Burton and Miller method [22, 23] or CHIEF (combined Helmholtz integral equation formulation) [24, 25].

Moreover, numerical damping is a recently revealed effect for BEM problems that attenuates the sound pressure solution in a non-physical way. It was observed and studied for acoustic interior problems by Marburg [26]. Baydoun et al. [27] and Marburg [28] get to the bottom of the effect, provide a quantification of the phenomenon and relate it to the pollution effect widely known in FEM [29–31].

A quasi-periodic BEM formulation is utilized in the example of Helmholtz-resonators and periodic noise barriers by Fard et al. [32, 33] and by Ziegelwanger et al. [34] by application of the fast multipole method. Fast multipole BEM allows the application of iterative solvers in order to generate system matrices that are as sparsely populated as possible [35, 36]. Fischer and Gaul [37] use the approach for coupled systems with fluid-structure interaction (FSI) and FEM for the simulation of the structural part. Czygan and von Estorff [38] previously described FSI coupled problems by the combination of BEM and nonlinear FEM for effects, such as material nonlinearities or large displacements of obstacles in unbounded fluid-filled domains. Moser et al. [39] present an adapted BEM formulation for an infinite boundary element, which allows the modeling of infinite surfaces by introduction of special mapping functions on the basis of the infinite element method (IFEM).

Reference is made to the textbooks of Ciskowski and Brebbia [40] and Kirkup [41] as well as editions by Wu [42], von Estorff [43], and Marburg and Nolte [44] for more in-depth information on the method.

Due to the frequency dependence of the system matrices generated by the BEM, it is applicable for acoustic radiation modes (cf. Sec. 2.2.1), but not for normal modes (cf. Sec. 2.2.2) that fall within the scope of this work. Therefore, it is not considered except for comparison purposes.

2.1.2 Finite Element Method (FEM)

Probably the most common numerical method in acoustics is the finite element method (FEM), the basics of which are presented in numerous textbooks [21, 43, 45, 46]. The method has its origin in structural mechanical analysis in aircraft construction in the middle of the 20th century when it was derived from

the stiffness method [47, 48]. Clough [49] showed the convergence of the method to analytical solutions by reducing the size of finite elements to which he gave the method's name. The universal applicability of the method ensured rapid dissemination beyond mechanical engineering. This was further reinforced by the development of capable computer technologies. In the 1960s, Craggs [50] and Gladwell [51] published first works in the context of engineering acoustics. The field of application of FEM in acoustics is now very broad. The method is used for structure-borne sound, for airborne sound and even for coupled problems, to name a few examples.

Different formulations of FEM vary primarily in the choice of the discretization method. The most common is probably the (Bubnov–)Galerkin scheme [21, 52]. A thorough derivation of the method will be given in Chapter 2.

One of the weaknesses of FEM is its poor suitability in the high frequency range, which remains a subject of current research [53–55]. The failure of the method at high frequencies with small wavelengths results from a too coarse sampling of physical quantities. This is due to the number of nodes per finite element (i.e. their polynomial order for interpolation) and their relative size in comparison to the wavelength. Although explicitly described in the context of BEM, Marburg's [56, 57] recommendation to use boundary elements of quadratic or even higher order is applicable to finite elements as well. He also proposes rules of element design in computational acoustics.

Harari et al. [58] provide a comprehensive cost comparison between FEM and BEM. Von Estorff [59] presents an overview of procedures that reduce the computational effort and time in numerical acoustics. For instance, this includes the simplification of geometries, improved element formulations, and acoustic transfer functions.

In the case of sound-hard reflecting outer boundaries of the computational domain, the system is regarded as an interior problem as it is often the case in vehicle and room acoustics. This also includes the treatment of partially or completely absorbing surfaces such as seats, carpets or absorber elements on ceilings, which can be represented by the concept of boundary admittances or impedances as demonstrated by Anderssohn and Marburg [60, 61].

The efficient and numerically stable calculation of wave propagation for exterior problems turns out to require special handling: An infinitely large exterior volume cannot be completely discretized and simulated by using a volume-related technique as FEM. To remedy the situation, an artificial boundary is typically introduced to reduce the unbounded free field to a finitely extended computational FE domain around the area of interest. Either absorbing conditions are directly applied to the envelope of the finite element domain or beyond in the form of an additional layer attached to it. They face the challenge of avoiding *spurious reflections* at the artificial outer boundary of the FE domain. The works of Tsynkov [62], Shirron and Babuška [63], and Thompson [54] each give a thorough overview of procedures for the treatment of exterior Helmholtz problems. Three examples of such methods are artificial absorbing boundary conditions (ABC), perfectly matched layers (PML) and the infinte element method (IFEM).

These methods are reviewed in the following.

2.1.3 Artificial Absorbing Boundary Conditions (ABC)

The concept of absorbing boundary conditions (ABC) takes up the lack of a missing free-field boundary condition inherent in FEM. An infinitely large, unbounded medium is artificially truncated. The inner part, which encloses the region of interest, is discretized by finite elements, while the envelope of this computational domain undergoes a special numerical treatment.

ABC are generally classified in local and non-local non-reflecting absorbing boundary conditions. A slightly outdated but still comprehensive overview on these is provided by Givoli et al. [64]. Selected review articles to be referenced here were published by Givoli [65], Tsynkov [62] and Hagstrom [66]. Reference for further information is still made to a book by Givoli [67], to the third chapter in Ihlenburg's book [52] and Givolis contribution to an edition [68].

Low order (local) absorbing boundary conditions, now often regarded as classical ABC, include the two well-known formulations by Engquist and Majda [69] and by Bayliss and Turkel [70]. Local conditions are generally not fully non-reflective at the truncated boundary. Their accuracy can be increased including higher-order derivatives, which substantially raise computational costs and the complexity of implementation [63, 71]. (Local) ABC of higher order, on the other hand, do not only provide improved accuracy, but can also be implemented in practice up to any desired order. These formulations do not contain any higher-order derivatives at all, but the price to pay is the need to introduce *auxiliary* variables [72–74]. The first high-order ABC was devised by Collino [75]. A review on such can be found in Ref. 76. Rabinovich et al. [77] present a comparison of high-order ABC and perfectly matched layers. Levin et al. [78] present a time-reversed algorithm with a second-order Engquist-Majda ABC for the identification of obstacles using wave propagation.

Non-local ABC can be regarded as exact boundary conditions for non-reflecting radiation. The disadvantage of these methods is the fact that all degrees of freedom on the truncated boundary and not only the neighbors (as in the standard FEM) are coupled to each other, leading to dense blocks in the linear system matrices. Moreover, this boundary condition involves an infinite series. It has to be truncated for its numerical use so that the accuracy of the solution can be adjusted by the number of terms of the finite series. The Dirichlet-to-Neumann (DtN) boundary condition is probably the most widely used exact non-local ABC [79, 80]. It relates the unknown field quantity and its derivative, here sound pressure and fluid particle velocity, and can be interpreted as an impedance boundary condition (BC) in the context of acoustics [68, 81]. The inversion, admittance BC, is known as Neumann-to-Dirichlet map (NtD). Unlike the local ABC, the shape of the boundary curve can only take on simple geometries.

For ABC, the frequency independence of the system matrices required for the calculation of normal modes can only be achieved with research and development of specific auxiliary variables [82]. At the

same time, losses of desirable mathematical properties are expected, which is why the approach cannot yet be considered for the numerical analysis in this work, but in principle, the application is conceivable.

2.1.4 Perfectly Matched Layers (PML)

Another approach to satisfy physically meaningful radiation and decay of sound pressure in exterior problems is to surround a truncated domain of finite elements by an artificially damping layer of finitely extended perfectly matched layers (PML). The term perfectly matching refers to their property of non-reflecting transition of acoustic waves into the outer computational domain, where the waves are attenuated rapidly. However, since the PML domain is truncated at a finite distance, reflections occur at its outer boundary, which are usually negligible due to the exponential decay of the sound waves inside the PML [83]. Lassas and Somersalo [84] proved exponential convergence of the numerical solution obtained by PML towards the exact solution as the thickness of the PML layer increases.

PML was first introduced by Berenger [85] in the field of electromagnetics. First applications in exterior acoustics can be ascribed to Turkel and Yefet [86] and to Harari et al. [87]. It is an advantage of PML that they can be used for rectangular, circular and even elliptical domains [88].

Teixeira and Chew [89] present a review on extensions of the PML for general orthogonal curvilinear coordinates and for general media. The two book chapters by Bermúdez et al. [83, 90] provide a thorough survey and review of the method and related publications in the field.

The technique is widespread and implemented in many commercial software packages. It has been used for verification purposes within this work, for which the reported accuracy [83] is sufficient. The system matrices generated by PML are generally frequency-dependent, which leads to more complicated equations and the loss of favorable mathematical properties of the system matrices in case of time-domain implementations [89, 91]. According to the present state of the art, the method is not yet feasible for the calculation of NM without additional developments.

2.1.5 Infinite Element Method (IFEM)

An artificial layer of radially extented *infinite* elements is attached to the envelope of a truncated circular or elliptical FE domain. Unlike absorbing layers, the IFE domain is not artificially dissipative, but rather extents the numerical discretization to an infinite boundary [92]. The basis functions of these elements contain polynomial and exponential functions. They fulfill Sommerfeld's radiation condition to ensure physically meaningful decay of the sound waves while propagating towards infinity. The polynomial interpolation in circumferential direction is inherited from the discretization of the adjoining FE region.

Two essential formulations of the technique differ in the definition of the basis functions, namely the two concepts of Bettess–Burnett and Astley–Leis. Early formulations from the 70s of the twentieth century

were published by Bettess [93] and Bettess and Zienkiewicz [94]. Zienkiewicz et al. [95] adjust the decay rate and integration procedure for 2D problems and obtain high accuracy for several examples. Burnett [96] further develops the approach by introducing 3D, spheroidal infinite elements for the efficient modeling of acoustic fields surrounding obstacles of virtually any practical shape. The Bettess–Burnett IFEM formulation generates symmetric, but frequency-dependent system matrices.

The second essential formulation by Astley is initially known as wave-envelope elements [97–100]. The weighting functions of the variational statement within the method, known as test functions, are divided into either conjugated or unconjugated [92]. This property refers to the relationship of the complex-valued basis and test functions. In the conjugated case, the complex arguments of the exponential functions in both terms are of opposite sign and cancel out each other during multiplication in the integrals. This ensures frequency-independence of the system matrices, but leads to asymmetry due to the different choice of basis and test functions. The conjugated Astley–Leis infinite elements are characterized by an additional geometric factor in the test function [92], which satisfies the variational formulations by Leis [101]. Astley further distinguishes between separable and mapped infinite elements [92].

Demkowicz and Gerdes [102] have proven convergence and reliability of conjugated and unconjugated approaches. Further studies by Shirron and Babuška [63] and Ihlenburg [103] have shown that the stability of the solution of the unconjugated Burnett elements in the exterior domain is low, but they provide a more accurate solution in the inner finite element region compared to Astley–Leis elements, which, however, are more efficient in the exterior.

Comparative works and review articles have been published by Bettess [104], Gerdes [105–107] and Astley et al. [108, 109].

Both formulations were adapted to respective coordinate transformations to apply the infinite elements to 3D, ellipsoidal computational domains, such as by Burnett and Holford [110, 111] or by Astley [112].

Recent developments deal with the improvement of stability and conditioning of the infinite element schemes. Astley and Coyette [113] investigate how the choice of radial basis functions influences the condition number of the system matrices. This effect is illustrated for three formulations: the Bettess–Burnett formulation, the conjugated Burnett formulation and the Astley–Leis formulation. Building on the work by Shirron and Babuška [63], Astley et al. [114] introduce Legendre polynomials for the radial interpolation, thereby increasing the orthogonality of the matrices, which perform much better compared to Lagrange polynomials in terms of conditioning. Dreyer and von Estorff [115, 116] proceed analogously and successfully introduce Jacobi polynomials for radial interpolation. They underpin improved robustness and performance of iterative solvers, employed in practical exterior acoustic problems with an improved formulation compared to the standard Astley–Leis infinite element scheme [117]. Dreyer [118] and Petersen [119] deal in great detail with the numerical properties and efficiency of adaptive finite and infinite element methods in their dissertations. Biermann et al. [120] discuss the pollution effect for high frequencies and suggest higher-order FE shape functions and related

p-FEM concepts with Bernstein polynomials in combination with Krylov subspace methods for iterative solvers.

The property of static system matrices of the Astley–Leis scheme makes the method particularly suitable for problems in the time domain, which is thoroughly presented by Astley et al. [121]. Van Ophem et al. [122] apply model order reduction of a fully-coupled, exterior vibro-acoustic model for time-domain simulations and preserve the stability of the full model while reducing the amount of degrees of freedom significantly. They use this procedure in a time-reversal technique for identifying sound sources and scatterers in exterior problems [123].

The use of the IFEM in media with a fluid flow is discussed in the works of Eversman [124], Hamilton and Astley [125] and Retka et al. [19].

Hohage et al. [126] and Nannen et al. [127] introduce another type of infinite element that is derived from a pole condition as radiation condition. It states that a transformation of the exterior solution belongs to the so-called Hardy space, a mathematical class of functions, which leads to purely outgoing waves. A further formulation by Shirron and Dey [128] for elongated, slender structures reduces or entirely eliminates the need of finite elements in the immediate vicinity of radiators and instead allows the infinite elements to be applied directly to any convex surface. They present both a conjugated and an unconjugated formulation. Yang et al. [129] present a frequency-independent IFE method for the treatment of semi-infinite spaces for soil-structure interaction which, however, does not seem to be further documented in the literature and which requires adaptation for application to exterior acoustic problems.

Due to the fact that both the FEM and the Astley–Leis IFEM provide frequency-independent system matrices, the combination of them is chosen for the numerical implementation in the present work and will be dealt with in more detail in the survey of methods in Chapter 2.

2.2 Modal Methods

Both in the experimental and in the numerical analysis of dynamic and acoustic systems, vibration modes are an essential approach for their description, analysis and solution.

Ewins [9, p. 27] describes the term *vibration modes* in his book on experimental modal testing as

> "[. . .] the various ways in which the structure is capable of vibrating naturally, i.e. without any external forcing or excitation, and so these are called the 'natural' or 'normal' modes of the structure."

In the context of discrete systems and their numerical computation, modal analysis requires the solution of an eigenvalue problem containing the matrices that describe the system. Depending on the formulation and definition of the problem, the eigenvalues obtained generally express the natural frequencies of

the respective modes. In damped systems, the complex eigenvalues also contain informations about their damping behavior. The eigenvectors of the eigenvalue problem represent the orthogonal, linearly independent mode shapes, which Ewins describes in his book.

For the calculation of the dynamic properties of weakly damped solid structures, the tool of modal superposition, i.e. the approximation of the overall dynamic behavior by the weighted sum of a number of modes, is frequently used for linear systems. As a rule of thumb, it can be assumed that all modes with resonance frequencies up to twice the highest frequency of the interested range can be taken into account for vibrating solids in order to obtain a sufficiently accurate approximation [130]. The computational effort of the modal superposition is hardly of any significance compared to the solution of the eigenvalue problem, for which efficient algorithms have been developed in past decades regarding miscellaneous problems [131].

Since structural-dynamic problems can be calculated relatively quickly according to the current state of the art, Marburg [6] argues that more efficient algorithms are required for the calculation of acoustics in fluids for sound radiation and the calculation of the sound power. In a combined FE/BE model, Merz et al. [132] have efficiently minimized the radiation of sound power over a wide frequency range while performing a structural optimization in the example of a submarine. As the solution must be determined separately for each frequency, in harmonic analysis the calculation is particularly expensive in a wide frequency range. The Padé-via-Lanczos approximation offers a possible solution by combining frequency interpolation and model order reduction [133–135].

Although the concept of modes is often associated with standing waves, eigenvectors in unbounded domains can also be interpreted as mode shapes of the fluid. Depending on the excitation and frequency, they are more or less pronounced during modal superposition of the field quantity. For exterior acoustic problems, however, the use of modal methods is less straightforward compared to interior acoustics and for structural dynamics. The calculation of eigenvalue problems becomes more challenging because the boundary conditions may lead to a loss of favorable mathematical properties of the system matrices, such as sparsity and symmetry. In addition, it is discussed in the literature that spectra are continuous for exterior problems and radiation, but may also contain discrete eigenvalues, so-called *trapped modes* [136–140]. One type of vibration mode for unbounded problems in acoustics is based on Hardy space infinite elements as described in the works by Hein et al. [141] and Hohage et al. [126]. By application of the complex scaling method with frequency-independent PML coefficients, Hein et al. [142] and Koch [143] were able to implement a PML formulation for the calculation of exterior modes. This was specifically used for acoustical duct–cavity systems with non-reflecting ends by Hein et al. [144, 145] and Duan et al. [146].

Two types of modes in exterior acoustics are considered in this paper. These are on the one hand the frequency-dependent acoustic radiation modes and on the other hand frequency-independent normal modes. Both concepts are reviewed below. To calculate normal modes, frequency independence of the

system matrices is a fundamental condition. According to the above review of numerical methods for the treatment of exterior acoustic problems, the Astley–Leis IFEM is found to be the most appropriate method.

2.2.1 Frequency-Dependent Modes—Acoustic Radiation Modes (ARM)

With his research on the radiation operator in the quadratic form of the sound power, Borgiotti [147] laid the foundation for acoustic radiation modes in the 1990s. He decomposed an operator equivalent to the acoustic impedance matrix into orthogonal functions of the fluid particle velocities at the surfaces using singular value decomposition. By distinguishing between velocity distributions with high and low radiation efficiencies, Borgiotti presented a first approach of model order reduction. Photiadis [148] studies the frequency-dependence of the radiation modes in exterior acoustics and describes how the weakly radiating modes correspond to subsonic surface wave numbers, whereas efficiently radiating modes correspond approximately to supersonic wave numbers. Since only the real part of the acoustic impedance matrix (containing the sound pressure and the fluid particle velocity) is important for calculating the sound power, Sarkissian [149] subjects this to an eigenvalue analysis and thus obtains ARM according to the present, most common definition. She recognized that the impedance matrix has to be symmetric and further discovered a directly proportional relationship between ARM eigenvalues and radiation efficiency. Cunefare [150] demonstrates that the most powerful radiating modes are already formed with a small number of degrees of freedom (DOF). Additional DOF would primarily reveal modes with a neglectible contribution to the total radiation of sound. Elliott and Johnson [151] show for the sound radiation of a panel, that around 99% of the sound power is determined by only a small number of modes. In order to retain the high accuracy of the approximation at higher frequencies, however, the number grows as the frequency increases.

In their work on convergence and sensitivity of ARM with respect to small fluctuations of the velocity excitation, Cunefare and Currey [152] came to the conclusion that efficiently radiating modes converge quickly and are comparatively insensitive to disturbances. Chen and Ginsberg [153] consider both real and imaginary parts of the acoustic impedance matrix for modal analysis for an estimation of the reactive part of the sound power. Cunefare et al. [14] observed a grouping behavior of the radiation efficiencies or ARM eigenvalues as functions of the frequency. Within these groups, the corresponding eigenvectors represent multipoles of the same order, respectively.

Peters et al. [154] show that although the impedance matrix must be symmetric to determine ARM as widely described in literature [153], it is often generated asymmetrically in practice. They found that this is due to a discretization error of the collocation BEM, which decreases by refining the mesh. Finally, they propose an operation to produce symmetry of the real matrix.

Due to the frequency-dependency of the acoustic impedance matrix, it follows that for each discrete frequency, a single eigenvalue problem has to be solved and the modal superposition has to be conducted.

The orthogonality of the eigenvectors with respect to the matrix is only given for the respective frequency. Since modal analysis is conducted irrespective of excitations, it is sufficient to carry out these calculations only once per geometry assuming the surface shape of the radiator remains unaffected. For changes within the structure and varying velocity boundary conditions on the surfaces, a quick estimation of the expected radiation behavior can be made for a large number of scenarios as shown by Kuijpers et al. [155] and Kessels [156]. By structural optimization a so-called weak radiator could be constructed by Naghshineh et al. [157]. The structural particle velocity distribution on its surface was optimized in certain target frequencies in such a way that the vibration patterns resemble those of mode shapes with low radiation efficiencies.

Studies by Peters et al. [158] are dedicated to the modal decomposition and reduction of ARM in FE/BE coupled systems considering fluid-structure interaction. In a sequel [159], they additionally apply Krylov subspace-based model order reduction (MOR) techniques for the efficient calculation of the fluid-loaded structure. Based on the ARM, Marburg et al. [160] determine surface contributions to the radiated sound power, which they compare to the acoustic intensity. Wu et al. [161] apply fast multipole BEM for an iterative and efficient computation of the radiation modes in the example of a baffled plate. Liu and Maury [162] provide an overview and scope of far-field and near-field ARM and present an improved numerical method, the pressure-velocity method, of the latter modes. Ji and Bolton [163] introduce structure-dependent radiation modes (s-modes) and differentiate these from the conventional acoustic radiation modes (a-modes), providing that s-modes additionally consider frequency-independent normal modes of the structure. The dependence of the modes on frequency and geometry is the subject of the work of Liu et al. [164]. They also investigate an inverse method based on radiation modes, in which these are used to reconstruct and describe the surface motion of a source [165]. Jones et al. [166] address the lack of experimental verifications of ARM and comparisons with other sound power measurement standards over wide frequency ranges.

The eigenvectors of the acoustic radiation modes are limited to degrees of freedom at surfaces of fluid-loaded obstacles and do not permit a view on the sound pressure distribution in the medium beyond the boundaries. This is different for the normal modes considered below.

2.2.2 Frequency-Independent Modes—Normal Modes (NM)

The concept of normal modes underlying this work mainly originates from three works by Marburg [16, 17] and Marburg et al. [15]. The first part [17] introduces the method in the example of a one-dimensional duct with Robin boundary conditions (cf. Sec. 1.1 in Ch. 2) and presents an analytical and a numerical solution as well as an eigenvalue analysis. A first outlook towards reduced modal superposition is given by testing three sorting criteria. For the second part of this series [15], the authors have applied the Astley–Leis IFEM for 2D examples. They use a state-space formulation for the solution of the resulting quadratic eigenvalue problem, which is described by Ruge [167] and by Tisseur and Meerbergen [168],

and provide a workaround for the problem of singular matrices in case of circular domain shapes [100]. Besides well-known multipole mode shapes (e.g. monopoles, dipoles, quadrupoles), cavity modes are found in the case of a open box structure and compared with those of the corresponding closed cavity [15]. In contrast to ARM (cf. Chen and Ginsberg [153]), NM multipoles do not appear in groups with always the same number of modes. The third part of the publication series [16] focuses on the determination of modal sound pressure and sound power contributions. The sorting criteria are refined compared to the first tests and comprehensive investigations for different load cases are presented.

Since normal modes have to be calculated only once for a set of frequency-independent system matrices, the concept seems to be particularly suitable for optimization, if the surface of the radiator remains unchanged and the fluid can be reconstructed by simple matrix-vector operations for varying velocity excitations at the surfaces. Another publication by Marburg et al. [169] can be considered as part four of the above series and takes advantage of this strength. They demonstrate the potential of the application of normal modes in exterior acoustic problems for optimization of a finite beam with the aim to minimize its radiated sound power. The superimposed modes were selected by their individual sound power contribution. Although the results were promising, the performance of the method is not yet competitive in comparison to the classical harmonic analysis since all modes have to be calculated in advance to find identify their specific contribution to sound radiation. From a practical point of view, it can be deduced that the objective must clearly be to identify the most contributing modes a priori.

In the example of a three-dimensional model of a recorder as a long, slender and hollow object, Fuß et al. [18] use an iterative Arnoldi eigenvalue solver to calculate selected weakly-damped normal modes in the proximity of the imaginary axis. Retka and Marburg [19] take flow into consideration by coupling the Galbrun equation to the FEM/IFEM approach and solve the quadratic eigenvalue problem for the orthogonal NM using the example of a duct with openings on both sides under free-field conditions.

In more general terms, the following two works are related to the discussed concept to some extent. By application of the HELS (Helmholtz equation least squares) method, Wu [170] reconstructs the acoustic pressure field radiated from vibrating structures. He superimposed eigenfunctions to obtain the sound pressure in the free field and found HELS to be effective in the low-to-mid frequency range. Astley and Hamilton [171] investigate the stability of IFE schemes for transient wave problems by solving an eigenvalue problem. They discuss the singularity of the mass matrix in the case of circular FE domains, but do not use the eigenfunctions in order to reconstruct the acoustic pressure or sound power solution. Goursaud et al. [172] use FEM in combination with a PML technique where the coefficients do not depend on the frequency to determine normal modes in exterior acoustics. As the numerical results are found to be very sensitive with regard to mesh refinements and in order to distinguish spurious from physical modes, the pseudospectrum [173] is computed to identify poles as the physical eigenvalues.

This dissertation mainly focuses on the further development of this technique and the comparison to the already extensively researched frequency-dependent ARM.

3 Research Questions

This work contributes to the ongoing research in the field of numerical analysis of exterior acoustic problems by means of modal methods. The following research questions arise from the scientific state of the art and form the basis for this work:

1. How can the modes in exterior acoustics be physically interpreted and what dependencies exist towards the underlying concepts and among each other?
2. Which characteristics, relationships and affiliations are inherent in the normal modes and which roles do they play within the continuous spectrum of exterior problems?
3. Which criteria can serve the modal reduction of normal modes for the efficient and accurate solution of applied time-harmonic problems in exterior acoustics?

Three publications are attached to the dissertation to address these central questions.

Publication A
A good compromise between the accuracy of the solution and the requirements for computing resources includes the need to know under which conditions the numerical solution converges and which influence input parameters and discretization methods have on the results. For the two considered types of modes in exterior acoustics ARM and NM, little is known so far about the influence of the properties of finite and infinite elements. In particular, the literature does not document any experience with acoustic radiation modes based on the infinite element method, which was accomplished in this work. The influence of the FE mesh size and of the IFE radial polynomial interpolation on the matrix condition and eigenvalue convergence of ARM and NM is examined in this article. The practical example of a recorder in cross section is used to compare both methods and to discuss the physical significance of the modes in exterior acoustic problems.

Publication B
The properties of the eigenvalues and eigenvectors of the normal modes are currently widely unknown. Also their respective contribution to the reconstruction of the exact sound pressure or sound power solution during modal superposition is not yet sufficiently clarified, which is investigated in this publication for the purpose of an efficient calculation. This includes studies on the position of the eigenvalues in the complex plane, the role of complex conjugated partners and purely real eigenvalues and eigenvectors. Furthermore, the similarities and differences of left and right eigenvectors are discussed. Together they form the orthogonal basis of the normal modes and obviously play different roles in the composition of the solution for sound pressure and sound power. Two similar models are used to distinguish between interior and exterior modes. One of the models has a specially designed cavity whose interior resonance frequencies are roughly known to the authors in advance, so that the eigenvalues can be easily assigned. Furthermore, the authors develop a mathematical criterion for categorizing the NM eigenvectors into

inner, outer and mixed mode shapes. The criterion refers to their sound pressure distribution within the FE domain. For two load cases in the form of surface velocity excitations, different selections of modes from these groups are discussed with respect to the resulting global relative error after modal superposition.

Publication C

The infinite element method is rarely described in the literature for 2D problems and especially for elliptical and half-space computational domains. Hence, there is insufficient experience with the basic requirements and benefits of their calculation, which is studied and discussed in this article using the example of acoustic meta-atoms. The concept of frequency-independent NM is introduced for their analysis and targeted design, whereby the dependencies of the approach on the underlying numerical methods are further investigated. A relationship between the elliptical domain shape and the eigenvalues is found, which may lead to an improved assignment of converging trapped modes within the continuous exterior spectrum and thus to a better understanding and criteria for efficient modal superposition. The NM approach is used to illustrate and interpret the underlying physics of sound insulation by finite sonic crystal noise barriers and meta-atoms, their components. The analysis of absorbing boundary conditions (boundary admittance) using NM contributes to a deepened insight into the physical effects involved. Furthermore, an iterative eigenvalue solver is tested with which it is possible to determine eigenvalues for modal superposition in a specific search space, so that the sound pressure solution can be efficiently and repeatedly determined using reduced modal bases, for example in an optimization procedure.

CHAPTER 2

Methods

In which the modal methods and numerical tools used in this work are presented, the underlying physical principles are introduced and special aspects such as the two-dimensional formulation of the infinite elements, elliptical computational domains and symmetric half-space problems are described.

1 Fundamental Equations

The sound pressure $\tilde{p}(\mathbf{x},t)$ is a location- and time-dependent field quantity in fluids. It describes the fluctuation around the significantly greater ambient (average or equilibrium) atmospheric pressure of the medium p_0 due to sound waves. If these fluctuations are oscillations in the frequency range audible to humans and of appropriate magnitude, one can perceive them as sound. The total pressure is defined here as the sum of atmospheric pressure and sound pressure $p_{total} = p_0 + \tilde{p}$.

The sound pressure and thus all sound events are governed by the acoustic wave equation, a linear partial differential equation of second order. Its derivation can be found in textbooks such as Möser's [12] and Ihlenburg's [52] or in editions by Marburg and Nolte [44], and by Kaltenbacher [174]. In its homogeneous form without source terms it can be written as follows

$$\nabla^2 \tilde{p}(\mathbf{x},t) = \frac{1}{c_f^2} \frac{\partial^2 \tilde{p}(\mathbf{x},t)}{\partial t^2} \qquad \mathbf{x} \in \Omega \subset \mathbb{R}^d \tag{1.1}$$

with d being the space dimension of the domain Ω and c_f being the speed of sound in the fluid. It is derived from three fundamental equations of continuum mechanics [21, 175]:

1. the **balance of mass**, which states that the mass as an integral of density over volume does not change over time,
2. the **balance of momentum** (Newton's 2nd law) saying that the time rate of change of the momentum of a body is equal to the sum of external forces acting on its surfaces, and
3. a **material law (constitutive equation)**, which relates density perturbation and sound pressure to the speed of sound as a material parameter.

In linear acoustics, comparatively small fluctuations of the field quantities around the much greater ambient quantities are assumed. This applies to sound pressure $\tilde{p}$, but also to density pertubation $\tilde{\rho}$ and fluid particle velocity $\tilde{v}$. Excluding the ambient quantities implies that $v_0 = 0$, i.e. the fluid is at rest.

The transition to the frequency domain is achieved with the application of a time-harmonic approach and the separation of variables for the sound pressure. This results in an expression that consists of a function of the spatial sound pressure distribution and an exponential function of frequency and time

$$\tilde{p}(\mathbf{x},t) = \Re\{p(\mathbf{x})e^{-\mathrm{i}\omega t}\}, \tag{1.2}$$

where i is the imaginary unit with $\mathrm{i}^2 = -1$ and $\omega = 2\pi f$ is the angular frequency of the sound pressure oscillation with f being the frequency. Finally, the real part of this product is formed, since the physical quantity sound pressure is a real number. The imaginary part could also be used. This approach is referred to as time-harmonic, which refers to pure tones, i.e. sinusoidal oscillations of a frequency. Any sound pressure field can be understood as a superposition of the partial sound pressure fields of all

harmonic frequencies. The sign in the expression of the exponential function indicates the rotational direction of the complex position vector and therefore the direction of the traveling wave. The choice here is minus resulting in waves propagating outwards, which is consistently applied throughout the entire work.

Inserting the time-harmonic approach of the sound pressure field Eq. (1.2) into the wave equation Eq. (1.1) provides the transition to the frequency domain. The Helmholtz equation is obtained, which describes the spatial sound pressure field at a frequency f

$$\nabla^2 p(\mathbf{x}) + k^2 p(\mathbf{x}) = 0, \qquad \mathbf{x} \in \Omega \subset \mathbb{R}^d \tag{1.3}$$

with the wave number $k = \omega/c_f = 2\pi f/c_f$ being the ratio of the angular frequency and the speed of sound in the fluid.

A distinction is basically made between closed interior and unbounded exterior acoustic problems. Both are schematically illustrated in Fig. 1.

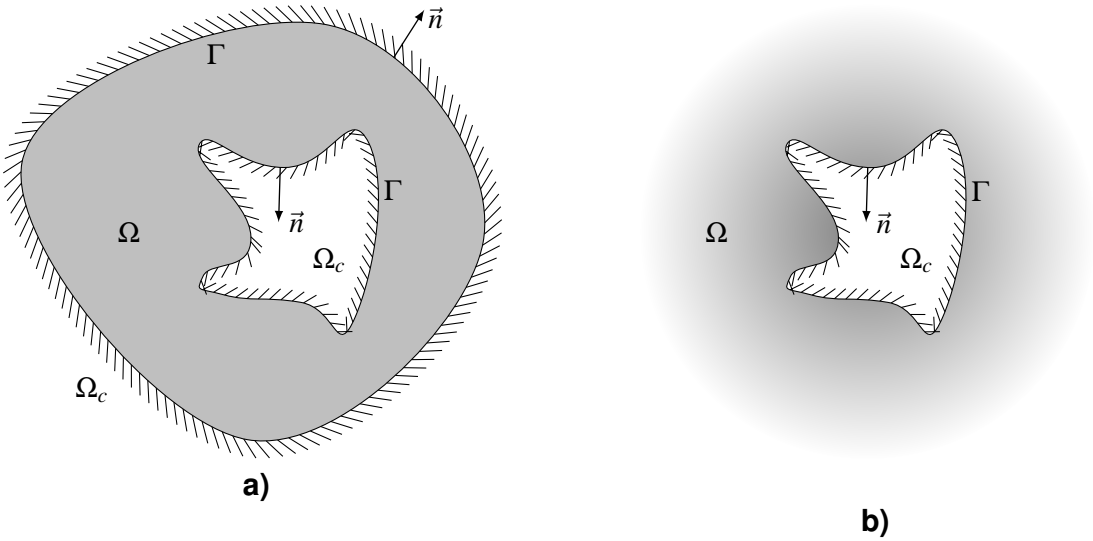

Figure 1: Schematic model domains Ω, complementary domains Ω_c, boundaries Γ and outward normal vectors $\vec{n}$ for: a) interior problems and b) exterior problems.

1.1 Boundary Conditions

The solution of the Helmholtz equation Eq. (1.3) requires the specification of boundary conditions (BC). There are three fundamental types for such boundary value problems, for which further details can be found in textbooks [21, 175, 176]:

- **Dirichlet** BC (first type or essential BC): the sound pressure is explicitly prescribed at the boundary as

$$p(\mathbf{x}) = p_D(\mathbf{x}), \qquad \mathbf{x} \in \Gamma \subset \mathbb{R}^{d-1}, \tag{1.4}$$

  where in the homogeneous case $p_D = 0$, the boundary is considered as sound-soft reflecting.

- **Neumann** BC (second type or natural BC): the normal derivative of the sound pressure towards the boundary is prescribed. It is derived from the linearized Euler equation transferred to the frequency domain, which establishes the relationship between complex sound pressure p and (normal) fluid particle velocity v_f

$$\frac{1}{\mathrm{i}\omega\rho_0}\frac{\partial p}{\partial n}(\mathbf{x}) = v_f(\mathbf{x}), \qquad \mathbf{x} \in \Gamma \subset \mathbb{R}^{d-1}. \tag{1.5}$$

  If the coupling to an adjacent structure is non-dispersive and the fluid particle velocity equals the structural particle velocity $v_s(\mathbf{x}) = v_f(\mathbf{x})$, the boundary is considered to be fully (sound-hard) reflecting.

- **Robin** BC (third type, admittance/impedance BC): the sum of both first and second type BC applies to the boundary. In acoustics, this is often expressed in terms of acoustic admittance $Y(\mathbf{x})$ or impedance $Z(\mathbf{x}) = Y^{-1}(\mathbf{x})$

$$Y(\mathbf{x})p(\mathbf{x}) = v_f(\mathbf{x}) - v_s(\mathbf{x}), \qquad \mathbf{x} \in \Gamma \subset \mathbb{R}^{d-1}. \tag{1.6}$$

  In the specific case that $Z(\mathbf{x}) \to \infty$, which is equivalent to $Y(\mathbf{x}) = 0$, the boundary is sound-hard reflecting so that this in turn amounts to a Neumann BC. If $Z(\mathbf{x}) = 0$, i.e. $Y(\mathbf{x}) \to \infty$, the Robin BC changes to a sound-soft Dirichlet BC.

  Acoustic boundary impedance or admittance are functions of the frequency and depend on the incident angle of the acoustic wave, whereby in the context of the Helmholtz equation only their normal components are considered. They are often normalized with respect to the factor $\rho_0 c$ so that $\tilde{Z} = Z/(\rho_0 c)$ and $\tilde{Y} = \rho_0 c Y$ are dimensionless and then named *specific* impedance or admittance, respectively.

In the context of this work, sound-hard boundaries on the surfaces of inner obstacles are assumed. The boundary condition for the free-field behavior in infinity is provided by Sommerfeld's radiation

condition [4, 52, 177–179], a Robin type BC at infinity, which acts uniformly in all directions

$$\lim_{r\to\infty} r^{\alpha}\left(\frac{\partial}{\partial r} - \mathrm{i}k\right) p(r) = 0, \tag{1.7}$$

where $r = \sqrt{x^2+y^2+z^2}$ is the radial distance to the origin of a source point and $\alpha = (d-1)/2$ with d being the space dimension. The Sommerfeld condition is often stated in the literature in two steps written in the Bachmann–Landau or Big O notation as

$$\begin{aligned} p(r) &= \mathcal{O}\left(r^{-\alpha}\right), \\ \left(\frac{\partial}{\partial r} - \mathrm{i}k\right) p(r) &= o\left(r^{-\alpha}\right) \quad \text{for } r \to \infty. \end{aligned} \tag{1.8}$$

The first expression (*decay condition*) denotes the decay rate of the Helmholtz equation in $p(r)$ in the direction of infinity, i.e. the sound pressure magnitude $|p(r)|$ is asymptotically bounded above by $r^{-\alpha}$ (up to a constant factor). The second expression (*radiation condition*) is equivalent to Eq. (1.7) and describes that the left-hand side is required to decay faster than $r^{-\alpha}$, or, in other words, it is asymptotically dominated by $r^{-\alpha}$ [180]. It can be shown though, that the decay condition is superfluous in the formulation of the exterior boundary value problem, since any function that satisfies both the Helmholtz equation and the radiation condition automatically satisfies the decay condition [52, 179, 181, 182].

It follows from Sommerfeld's radiation condition that the sound pressure $p(r)$ decays in the two-dimensional case ($d = 2$) with $1/\sqrt{r}$ [63], since the acoustic energy of the wavefront is distributed along the growing circumference of the circle with radius r. In the three-dimensional case ($d = 3$), $p(r)$ decays faster with $1/r$. Here the sound energy is distributed on the spherical shell of radius r during the propagation of the wave front. For one-dimensional problems ($d = 1$) such as ducts without lateral expansion, there is no decay at all if the fluid is considered undamped.

Due to their property to provide frequency-independent system matrices, the finite element method (FEM) in combination with the Astley–Leis infinite element method (IFEM) is used in this work to fulfill the radiation condition. They are described in detail in the two following sections.

2 Finite Element Method (FEM)

The aim of the finite element method is to numerically discretize and solve continuous problems, in particular, partial differential equations. The analytic solution is represented by superimposing known functions to determine function values for discrete coordinates on grid points. The model or computational domain Ω is therefore divided into a number of small elements Ω_{el}, e.g. triangles, quadrilaterals, tetrahedra or hexahedrons, which together span a mesh that mimics the continuous shape of the area. The mesh nodes serve as data points for element-wise polynomial interpolation of

the underlying physical quantity. They can be understood as degrees of freedom (DOF) of the system.

Numerical models of Helmholtz problems need to resolve the oscillatory behavior of the exact solution, which is characterized by the wave number k. The accuracy of the discrete FE approximation compared to the continuous (exact) solution is often measured by means of a fixed number of elements per wavelength [52, 57]. From this, a maximum element edge length can be derived to the highest frequency of interest. The literature often mentions a "rule of thumb" of at least six finite elements per wavelength with quadratic (2nd-order) or higher-order polynomial interpolation functions [56, 183]. Figure 1 shows examples of finite element meshes with quadrilateral and triangular elements Ω_{el} for the discretization of a fluid-filled domain Ω. In this work, isoparametric finite elements are considered, i.e. geometry and physics are equally discretized [46].

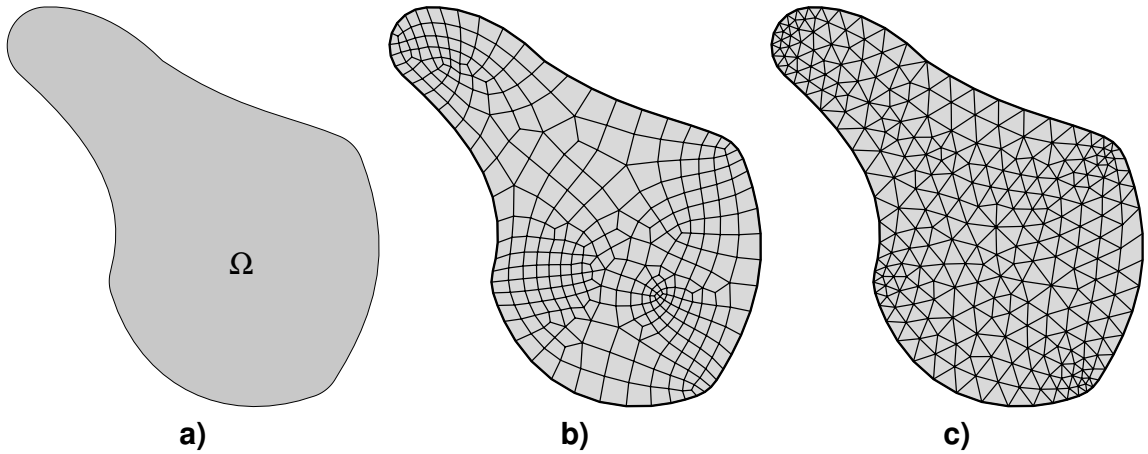

Figure 1: Example geometry Ω for an interior problem (a); meshed geometry with two different element types: (b) quadrilateral and (c) triangular elements Ω_{el}.

Applying the finite element method to the Helmholtz differential equation Eq. (1.3) finally returns a system of linear equations, which is often found in a similar form in the field of mechanical engineering and convenient in further handling:

$$(\mathbf{K} - \mathrm{i}k\mathbf{D} - k^2\mathbf{M})\mathbf{p} = \mathbf{f}, \tag{2.1}$$

with the discrete and frequency-independent system matrices for mass $\mathbf{M}$, damping $\mathbf{D}$ and stiffness $\mathbf{K}$ and the vector $\mathbf{p} = [p_1(\mathbf{x}), \ldots, p_N(\mathbf{x})]^T$ that includes (nodal) sound pressure values p_i at the N data points of a discrete mesh of finite elements. Applying Robin BC, the right-hand side $\mathbf{f}$ contains the boundary mass matrix $\mathbf{\Theta}$ and a vector $\mathbf{v}_s$ with nodal structural particle velocities at boundaries of the computational domain. A sound pressure field other than zero can therefore only be expected if a surface oscillates with a structural particle velocity. The treatment of source terms or incident plane waves in the inhomogeneous Helmholtz equation is not covered here. The procedure is described in the attached publication [C].

A detailed description and derivation of the FEM can be found in numerous textbooks [21, 45, 46, 52, 174]. The basic idea and the essential steps to get from the Helmholtz equation Eq. (1.3) to the system of linear equations Eq. (2.1) are briefly outlined below.

2.1 Derivation and Discretization

In the first step of the finite element method, the Helmholtz equation Eq. (1.3) is transformed into a residual or *weak* formulation. For this purpose, a weighting function, called *test* function $\chi(\mathbf{x})$, is multiplied to Eq. (1.3) and integrated over the whole domain Ω

$$\int_\Omega \chi \left[\nabla^2 p + k^2 p\right] \mathrm{d}\Omega = 0, \tag{2.2}$$

requiring this equality to hold for all test functions in the $H1$ test function space (Hilbert space) instead of Eq. (1.3) for all points in Ω. This relaxes the requirements of the differential equation such that equality is only required in an integral sense by minimizing the weighted residual [52]. The weak form reduces the steadiness requirements for the physical variables by shifting the derivation operators to the test function, resulting in weaker constraints on derivation. For this and all subsequent equations, spatial dependency of all functions is implied (i.e. $p = p(\mathbf{x})$).

The Laplace operator can be resolved by the vectorial equivalent of the product rule. As a result, the divergence operator $\mathrm{div}\, u = \nabla \cdot u$ enters the weak formulation and yields

$$\int_\Omega \nabla \cdot (\nabla p \chi)\, \mathrm{d}\Omega - \int_\Omega \nabla p \cdot \nabla \chi \mathrm{d}\Omega + k^2 \int_\Omega p \chi \mathrm{d}\Omega = 0. \tag{2.3}$$

In the second step, Gauß's theorem (divergence theorem) is used to resolve the divergence operator. It relates the flux of a vector field through a boundary Γ to the behavior of the field inside the boundary [184]

$$\begin{aligned} \int_\Omega \nabla \cdot (\nabla p \chi)\, \mathrm{d}\Omega &= \int_\Gamma \vec{n} \cdot (\nabla p \chi)\, \mathrm{d}\Gamma = \int_\Gamma \frac{\partial p}{\partial n} \chi \mathrm{d}\Gamma \\ &= \mathrm{i}\omega\rho_0 \int_\Gamma (v_f \chi)\, \mathrm{d}\Gamma = \mathrm{i}\omega\rho_0 \int_\Gamma ((Yp + v_s)\chi)\, \mathrm{d}\Gamma. \end{aligned} \tag{2.4}$$

The equation includes the normal derivative of the sound pressure at the surface Γ. A relationship to the fluid particle velocity is given by the linearized Euler equation Eq. (1.5). According to Eq. (1.6), it can be substituted by structural particle velocity and boundary admittance times sound pressure.

Substitution in above equation yields

$$\int_\Omega \nabla p \cdot \nabla \chi \mathrm{d}\Omega - \mathrm{i}\omega\rho_0 \int_\Gamma (Yp\chi)\, \mathrm{d}\Gamma - k^2 \int_\Omega p\chi \mathrm{d}\Omega = \mathrm{i}\omega\rho_0 \int_\Gamma (v_s \chi)\, \mathrm{d}\Gamma, \tag{2.5}$$

where all terms that contain the unknown acoustic pressure p are on the left-hand side and the term on the right-hand side denotes an excitation by a structural particle velocity v_s at a boundary Γ. It should be noted that all quantities still are continuous functions of the position vector $\mathbf{x}$: $p = p(\mathbf{x})$, $\chi = \chi(\mathbf{x})$, $v_f = v_f(\mathbf{x})$, $v_s = v_s(\mathbf{x})$ and $Y = Y(\mathbf{x})$. They are discretized in space in the next step by using N polynomial functions called basis functions $\boldsymbol{\varphi}(\mathbf{x}) = [\varphi_1(\mathbf{x}), \ldots, \varphi_N(\mathbf{x})]^T$ with N being the number of degrees of freedom in the mesh or of a single finite element if the discretization is conducted element-wise. This gives the following expressions with the superscripts of $\boldsymbol{\varphi}$ and φ indicating that for each quantity different basis functions can be chosen, although the basis functions used in this work are the same for all variables

$$p(\mathbf{x}) = \sum_{i=1}^{N} \varphi_i^p(\mathbf{x}) p_i = [\boldsymbol{\varphi}^p(\mathbf{x})]^T \mathbf{p}, \tag{2.6}$$

$$Y(\mathbf{x}) = \sum_{k=1}^{N} \varphi_k^Y(\mathbf{x}) Y_k = \left[\boldsymbol{\varphi}^Y(\mathbf{x})\right]^T \mathbf{Y}, \tag{2.7}$$

$$\chi(\mathbf{x}) = \sum_{j=1}^{N} \varphi_j^\chi(\mathbf{x}) = \boldsymbol{\varphi}^\chi(\mathbf{x}), \tag{2.8}$$

$$v_s(\mathbf{x}) = \sum_{l=1}^{N} \varphi_l^{v_s}(\mathbf{x}) v_{sl} = \left[\boldsymbol{\varphi}^{v_s}(\mathbf{x})\right]^T \mathbf{v}_s. \tag{2.9}$$

The sound pressure p_i, and in the same way the other physical quantities, are no longer functions of $\mathbf{x}$, but represent the discrete value (here: sound pressure) at node i (for Lagrangian basis functions which take the value one at the element nodes). The polynomials of the basis functions as functions of $\mathbf{x}$ interpolate continuous curves between the discrete data points.

Discretization procedures usually differ in the way they relate test and basis functions. In FEM the Bubnov–Galerkin method (classical Galerkin method) is often used, where the test function is equal to the basis function [46].

The approximations Eqs. (2.6) to (2.9) are substituted in the weak formulation Eq. (2.5) and after rearranging it results in

$$\begin{aligned} &\int_\Omega \left[\sum_{i=1}^{N} \nabla\varphi_i^p p_i\right] \cdot \left[\sum_{j=1}^{N} \nabla\varphi_j^\chi\right] \mathrm{d}\Omega - \mathrm{i}\omega\rho_0 \int_\Gamma \left[\sum_{k=1}^{N} \varphi_k^Y Y_k\right] \left[\sum_{i=1}^{N} \varphi_i^p p_i\right] \left[\sum_{j=1}^{N} \varphi_j\right] \mathrm{d}\Gamma \\ &-k^2 \int_\Omega \left[\sum_{i=1}^{N} \varphi_i^p p_i\right] \left[\sum_{j=1}^{N} \varphi_j^\chi\right] \mathrm{d}\Omega = \mathrm{i}\omega\rho_0 \int_\Gamma \left[\sum_{l=1}^{N} \varphi_l^{v_s} v_{sl}\right] \left[\sum_{j=1}^{N} \varphi_j^\chi\right] \mathrm{d}\Gamma, \end{aligned} \tag{2.10}$$

where constant terms as p_i and v_{sl} can be extracted from the integrals. The FEM matrices of the system of linear equations Eq. (2.1) can be formed as follows

$$m_{ij} = \int_\Omega \varphi_i \varphi_j \mathrm{d}\Omega, \tag{2.11}$$

$$\theta_{jl} = \int_\Gamma \varphi_j \varphi_l \mathrm{d}\Gamma, \tag{2.12}$$

$$k_{ij} = \int_\Omega \nabla\varphi_i \cdot \nabla\varphi_j \mathrm{d}\Omega, \tag{2.13}$$

$$\begin{aligned} d_{ij} &= \rho_0 c \int_\Gamma \varphi_i \left(\boldsymbol{\varphi}^T \mathbf{Y}\right) \varphi_j \mathrm{d}\Gamma \\ &= \int_\Gamma \varphi_i \left(\boldsymbol{\varphi}^T \tilde{\mathbf{Y}}\right) \varphi_j \mathrm{d}\Gamma \end{aligned} \tag{2.14}$$

with the mass matrix $\mathbf{M} = [m_{ij}]$, the stiffness matrix $\mathbf{K} = [k_{ij}]$, and the boundary mass matrix $\mathbf{\Theta} = \left[\theta_{jl}\right]$, all of them being sparse, frequency-independent and real, where i, j and l indicate rows and columns of the matrices. $\mathbf{M}$ and $\mathbf{K}$ are symmetrical and have a band structure. In contrast to these two matrices, the boundary mass matrix $\mathbf{\Theta}$ may not be square but rectangular, depending on the type of implementation. The symmetry property and the band structure are thus also no longer given. This circumstance is a result of the fact that when applying a normal structural particle velocity to a boundary, the contribution of each surface finite element that shares a node with others must be provided with its own DOF for this node. For this purpose, additional DOFs were introduced in the code for this work, leading to additional columns in the boundary mass matrix and just as many more rows in the vector for the structural particle velocities.

In the case of a non-zero, complex (normalized) boundary admittance $\tilde{Y} = \rho_0 c Y$, a complex-valued damping matrix $\mathbf{D} = [d_{ij}] \neq \mathbf{0}$ exists. It is symmetric and sparse, but not Hermitian (meaning that it is not equal to its own conjugate transpose). For simplicity's sake, this work does not consider Y as a function of the frequency, so that $\mathbf{D}$ also remains independent of f. A more realistic treatment is described by Marburg and Hardtke [185].

It should be noted that the basis functions $\varphi_i(\mathbf{x})$ shown here are polynomial functions of the global position vector $\mathbf{x} = [x, y, z]^T$. A major strength of finite elements is that they can, even deformed to a certain degree, be transformed from the global coordinate system to a rectilinear reference element in a natural coordinate system with the local element nodes being positioned between 0 and 1 or between -1 and 1, respectively. The use of these natural coordinates makes the derivation of polynomials—they are often called shape functions $N_i(\boldsymbol{\xi})$ of the local coordinates $\boldsymbol{\xi}$ on the reference element—much easier and leads to the definition of a set of standard or parent elements. The shape functions are usually Lagrangian polynomials.

This local, unified consideration of all finite elements can contribute to a substantial acceleration and reduction of computational effort in the element-wise solution of the integrals to the assembly of the system matrices in Eqs. (2.11) to (2.14). The coordinate transformation is not discussed further here, since it is described in detail in the literature [52]. Only this much is to say that it is carried out by means of the Jacobian matrix and its determinant.

The concept of FEM has been developed for the numerical discretization of problems on bounded domains [52]. Problems on unbounded domains involve a domain decomposition and introduction of an artificial boundary, on which the FE discretization can be coupled to a discrete representation of the analytical solution in different ways. Infinite elements can be attached that ensure impedance matching at the transition in a manner typical for Lagrangian shape functions [100]. The method is described in the following section.

3 Infinite Element Method (IFEM)

The treatment of exterior acoustic problems requires the fulfilment of Sommerfeld's radiation condition (cf. Sec. 1.1). In the present work, the mapped (and conjugated) Astley–Leis infinite element method (IFEM) is used for this purpose. Its essential steps are described in this section, mainly on the basis of selected works by Astley et al. [92, 98–100] and by Shirron and Babuška [63]. The interested reader is referred to the literature for further information, see Sec. 2.1.5 in Ch. 1.

The formulation of the infinite elements is much reminiscent of that of the FEM shown in the previous section. The solution of the Helmholtz equation is obtained by approximation of the acoustic pressure using suitable basis functions. These must ensure the smoothness of the physical field quantities on the envelope of the inner domain, represent their wave character and fulfill the Sommerfeld radiation condition. The weighting or test functions contain an exponential term, which is complex-conjugated to the one of the basis functions and eliminated in the product of the two. This property of the Astley–Leis infinite elements eliminates the frequency dependence of the trial solution [92]. The same system of linear equations as in FEM Eq. (2.1) is derived that contains frequency-independent system matrices. During this procedure, the matrices of the FEM are supplemented by new rows and columns for additional degrees of freedom and information is added to existing entries. A further domain of infinite elements is attached to the outer boundary of a spherical (space dimension $d = 2$: circle or ellipse) or spheroidal ($d = 3$: sphere or ellipsoid) FE domain. The general setup for $d = 2$ is depicted in Fig. 1 for full-space and half-space problems. The latter may be used whenever the obstacle is on or near a reflecting surface subjected to normal admittance boundary conditions or to reduce the computational costs if the problem is symmetrical along a mirror axis [186].

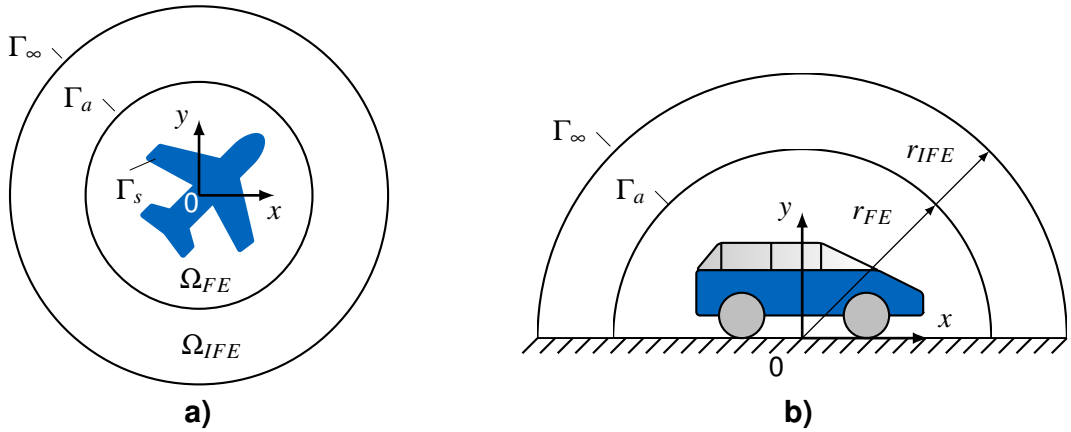

Figure 1: Schematic of two-dimensional ($d = 2$) problems in exterior acoustics: a) full-space and b) half-space FE and IFE domains of radii r_{FE} and r_{IFE}.

3.1 Mapping Concept

The infinite elements are directly connected to the outer boundary of the FE domain and extend the fluid perpendicular to it longitudinally in a radial direction to infinity. Their shape is rectangular for two-dimensional problems ($d = 2$). The outer edge of the FE area is thus a line, regardless of whether triangular or quadrilateral finite elements are used. In the three-dimensional case ($d = 3$), the procedure of the method is completely analogous as the shape of the infinite elements is prismatic. However, the shape of the base faces depends on the type of surface elements of the FE domain. If this is discretized with tetrahedra, the base of the infinite elements is triangular. For hexahedra in the FE region, the prismatic infinite elements have a quadrilateral base.

Fig. 2 illustrates the shape of the elements and the principle of the underlying coordinate transformation in the example $d = 2$. This is, analogous to that of the finite elements, based on the projection of the elements onto a normalized unit element in a system of natural coordinates, which again significantly simplifies the solution of the integrals [52]. Marques and Owen [187] provide the basis for the coordinate

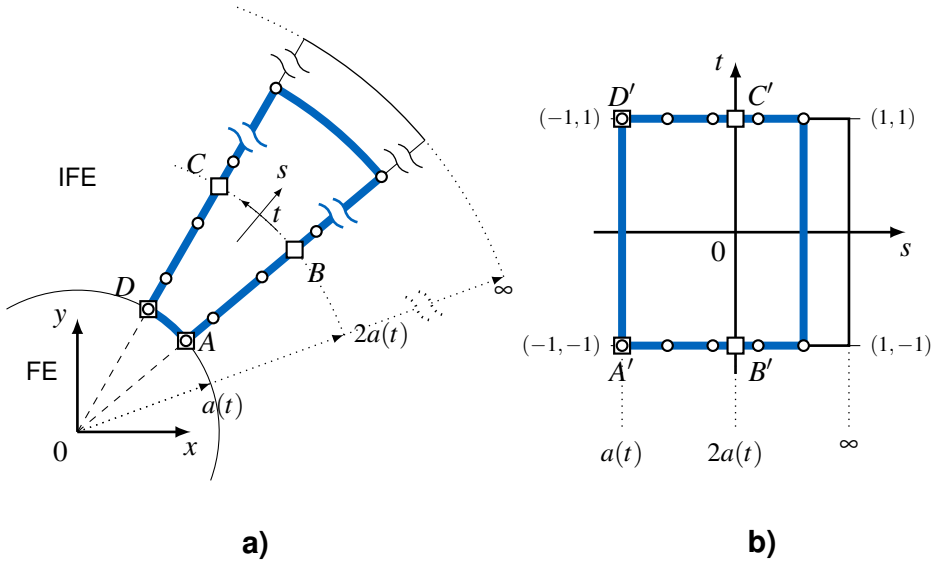

Figure 2: Mapping concept for infinite elements: a) a single element (blue framed) in global cartesian coordinates x, y; b) transformed element in natural coordinates s, t with □ being mapping nodes $A - D$ or $A' - D'$ and ○ representing variable nodes.

transformation. As it can be seen in Fig. 2, the space between the outer envelope of the FE domain and infinity is mapped to a local space between -1 and 1. The local (natural) coordinate for this is s. The extension of the element in circumferential direction is also mapped to the interval -1 to 1. In this work, the coordinate is referred to as t, whereby for the sake of simplicity only two-dimensional problems with a single circumferential interpolation function are considered. Their numerical treatment, e.g. in integration, is analogous to that of one-dimensional FE line elements.

The transformation rule by Marques and Owen [187] for the geometry of an infinite element in physical

coordinates $\mathbf{x}$ is given as follows

$$\mathbf{x} \approx M_a(s) \sum_{i=1}^{n} N_i(s) \mathbf{x}_{a,i} + M_{2a}(s) \sum_{i=1}^{n} N_i(s) \mathbf{x}_{2a,i} \tag{3.1}$$

with $N_i(s)$ being the Lagrangian shape functions and two corresponding mapping functions

$$M_a(s) = -\frac{2s}{1-s} \qquad \text{and} \qquad M_{2a}(s) = -\frac{1+s}{1-s}. \tag{3.2}$$

The mapping nodes with coordinates $\mathbf{x}_{a,i}$ and $\mathbf{x}_{2a,i}$ are positioned at distances $a(t)$ ($s=-1$) from the origin (corresponding to the radius of the outer envelope of the FE domain) and $2a$ ($s=0$), as shown in Fig. 2 in the form of rectangular markers. It follows that $s=1$ for $r \to \infty$ considering the underlying relationship

$$s = 1 - \frac{2a(t)}{r}. \tag{3.3}$$

The radius $a(t)$ is approximated by the sum of Lagrangian shape functions times the nodal radii a_i using the standard FE discretization on the envelope.

The actual infinite element is delimited by discrete interpolation points, called *variable nodes*, on the square in the system of natural coordinates (see Fig. 2 in the form of circular markers). They are (preferably equidistantly) positioned between $s = [-1,1[$, where the nodes on the surface of the FE domain ($r=a$ and $s=-1$) are always part of the infinite elements and there are no variable nodes at infinity ($r=\infty$ and $s=1$) [92]. The contributions of their associated degrees of freedom are added to the corresponding entries of the system matrices.

3.1.1 Two-Dimensional Elliptical IFEM

Elliptical FE domains are desirable if the radiator is of elongated, slim shape and if computer resources can be saved by an adapted form of the computational domain. An ellipse at the origin with foci at $x=\pm f$ satisfies the equation

$$\frac{x^2}{a^2} + \frac{y^2}{b^2} = 1 \tag{3.4}$$

with the semi-major axis a and the semi-minor axis b and $f^2 = a^2 - b^2$ (see Fig. 3).

The coordinate transformation for 3D ellipsoidal infinite elements is well documented in the literature, such as by Burnett and Holford [96, 111] and by Astley et al. [99, 109, 112]. A distinction is usually made between prolate and oblate ellipsoids in which each two of the half-axes of the ellipsoid are of equal length and one, either the longest or the shortest, differs. The two-dimensional system of elliptical coordinates (ρ, ϕ) is derived from the three-dimensional set of equations published by Burnett and

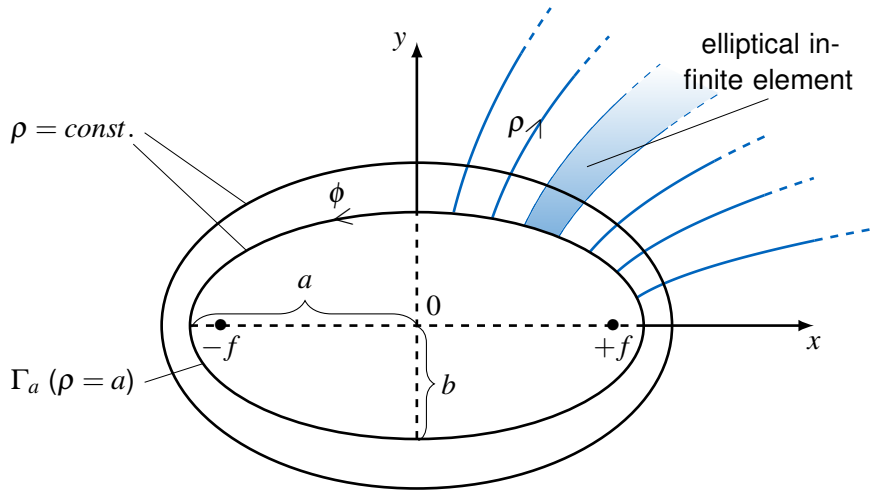

Figure 3: Geometry of elliptical infinite elements and coordinate system with iso-surfaces of ρ and ϕ.

Holford [110], who developed a general transformation for ellipsoids with arbitrary half-axis ratios

$$x = \rho \cos\phi, \tag{3.5}$$

$$y = (\rho^2 - f^2)^{1/2} \sin\phi \tag{3.6}$$

with ρ being the elliptical radial coordinate and ϕ being the elliptical angular coordinate. The reverse transformation can be solved numerically, e.g. by using the Newton-Raphson method. The relationship between natural and physical coordinates as described in the previous section remains valid.

Analogous to the procedure in FEM, the coordinate transformation is incorporated into the integrals of the system matrices in the form of the Jacobian matrix and its determinant. The procedure is described in Refs. [52, 96].

3.2 Derivation and Discretization

The considered boundary value problem in exterior acoustics is formed by the Helmholtz equation in the fluid and by boundary conditions on the surfaces of inner obstacles (cf. Sec. 1.1 and Fig. 1). Analogous to the FEM in interior problems, the Helmholtz equation is reformulated in a weak form (Eq. (2.3)), the boundary conditions are introduced with the Gaussian theorem (Eq. (2.4)) and finally substituted in the weak form (Eq. (2.5)). For exterior problems, however, Sommerfeld's radiation condition from Eq. (1.8) is also taken into account via the Gaussian theorem. This yields

$$\int_\Omega \nabla p \cdot \nabla\chi \,\mathrm{d}\Omega - \mathrm{i}\omega\rho_0 \int_{\Gamma_s} (Yp\chi)\,\mathrm{d}\Gamma - k^2 \int_\Omega p\chi \,\mathrm{d}\Omega - \int_{\Gamma_\infty} \left[\mathrm{i}kp - o\left(r^{-\alpha}\right)\right] \chi \,\mathrm{d}\Gamma = \mathrm{i}\omega\rho_0 \int_{\Gamma_s} (v_s\chi)\,\mathrm{d}\Gamma \tag{3.7}$$

with $p = p(\mathbf{x})$ and $\chi = \chi(\mathbf{x})$ being the sound pressure and the test function, and $v_s = v_s(\mathbf{x})$ and $Y = Y(\mathbf{x})$ being the structural particle velocity and the boundary admittance, which are not part of the exterior domain and thus not considered for the IFEM. $\alpha = (d-1)/2$ contains the space dimension d. The domain Ω approximates infinite extension for $r \to \infty$ and the integral term in the equation above vanishes for an appropriate choice of p and χ that satisfy the radiation condition. The trial solution for the approximation of the sound pressure is given by

$$p(\mathbf{x},\omega) \approx \sum_{i=1}^{n} p_i(\omega)\varphi_i(s,t,\omega) = \mathbf{p}(\omega)\boldsymbol{\varphi}(s,t,\omega), \tag{3.8}$$

where p_i are the nodal sound pressure values obtained from the solution of the system of linear equations Eq. (2.1) and $\boldsymbol{\varphi}(s,t,\omega) = [\varphi_i(s,t,\omega)]$ are basis functions of s and t defined as

$$\varphi_i(s,t,\omega) = I_i(s,t)e^{-\mathrm{i}k\mu(s,t)}. \tag{3.9}$$

The frequency-dependent basis functions are constructed utilizing an interpolation function $I_i(s,t)$ and an exponential function containing the imaginary number i, the wave number k and a phase term μ with

$$\mu(s,t) = a(t)\frac{1+s}{1-s}. \tag{3.10}$$

The interpolation function consists of the product of two polynomials for radial $P^s(s)$ and transverse $P^t(t)$ interpolation and a geometric factor to satisfy Sommerfeld's radiation condition. It vanishes at infinity for $s = 1$ and, in contrast to the case $d = 3$, it is framed by a root for $d = 2$ [63]

$$I_i(s,t) = \sqrt{\frac{(1-s)}{2}}P_j^t(t)P_k^s(s). \tag{3.11}$$

All combinations j,k of the two polynomial functions $P_j^t(t)$ (FE interpolation at the infinite element base) and $P_k^s(s)$ (radial interpolation) are numbered via the index i for the corresponding interpolation function $I_i(s,t)$. In accordance to the *hat shape* of Lagrangian shape functions—in the corresponding node they always take the value 1 and at all other data points the value 0—exactly the value 1 is required at the transition to the standard FE discretization.

Lagrangian Astley–Leis elements lead to a high matrix condition for high polynomial degrees. Astley et al. proposed Legendre polynomials as an alternative [113, 114]. Von Estorff et al. [116] and Dreyer et al. [115] prove the poor suitability of Lagrange polynomials of high orders and achieve better matrix conditions with Legendre and Jacobi polynomials. A detailed description of those is given by Dreyer [118] and in the attached publication [A]. For polynomials other than Lagrange, an additional shift may be required to meet the transition condition [115]. The circumferential interpolation in t-direction is inherited by the FE discretization at the envelope.

The given form of the basis functions resembles the Atkinson–Wilcox expansion [52, 178, 188], a

fundamental solution to the exterior Helmholtz problem and a series of terms of the form r^{-n} with $n \in \mathbb{N}^+$ or $r^{-n/2}$ for space dimension $d = 2$ (cf. [63, 95]). The expression is apparent in the form of the coordinate transformation in Eq. (3.3). In connection with the preceding geometric factor in Eq. (3.11), this means that infinite elements of the radial order m are able to represent the radiation behavior of acoustic multipoles of the order $m-1$ [100].

The test functions $\chi(s,t,\omega)$ of the Astley–Leis IFEM use the complex conjugates of the basis functions with an additional geometric weighting factor $D(s) = (a/r)^2 = (1-s)^2/4$, which is the major difference to the Bettess–Burnett formulation, where a Bubnov–Galerkin scheme is used, i.e. basis and test function are identical. The test functions according to Astley and Leis are given by

$$\chi(\mathbf{x},\omega) \approx \left(\frac{1-s}{2}\right)^2 \sum_{i=1}^{n} p_i(\omega)\varphi_i^*(s,t,\omega) = D(s)\mathbf{p}(\omega)\boldsymbol{\varphi}^*(s,t,\omega), \tag{3.12}$$

where the $*$-operator indicates complex conjugation. The product of the complex conjugated exponential terms in the basis functions and in the test functions leads to the elimination of the frequency-dependence in the weak formulation. The obtained stiffness, damping and mass matrices of the system are thus independent of frequency (under the assumption of a fluid without damping or thermal losses).

By inserting the expressions of the trial and test functions Eqs. (3.8) and (3.12) into the weak formulation Eq. (3.7), a system of linear equations is derived in the same form as for the FEM in Eq. (2.1) with the following integral expressions for the element matrices $\mathbf{K} = [k_{ij}]$, $\mathbf{D} = [d_{ij}]$ and $\mathbf{M} = [m_{ij}]$:

$$k_{ij} = \int_\Omega [(I_i \nabla D + D\nabla I_i)\cdot\nabla I_j]\,\mathrm{d}\Omega, \tag{3.13}$$

$$d_{ij} = \frac{1}{c_f}\int_\Omega [DI_i\nabla\mu\cdot\nabla I_j - I_iI_j\nabla D\cdot\nabla\mu - DI_j\nabla I_i\cdot\nabla\mu]\,\mathrm{d}\Omega, \tag{3.14}$$

$$m_{ij} = \frac{1}{c_f^2}\int_\Omega [DI_iI_j\,(1-\nabla\mu\cdot\nabla\mu)\cdot\nabla I_j]\,\mathrm{d}\Omega, \tag{3.15}$$

where c_f is the speed of sound in the fluid. It is important to note that $\mathbf{M}$ is singular for circular or spherical domain shapes [100].

4 Normal Modes (NM)

The homogeneous form of the discrete system of linear equations in Eq. (2.1) can be understood as a quadratic eigenvalue problem (QEVP) [168]. Based on a state-space linearization proposed by Ruge [167], Marburg et al. [15] introduce the concept of normal modes to exterior acoustic problems on the basis of frequency independent FE and IFE system matrices (cf. literature overview Sec. 2 in

Chapter 1). The linearized eigenvalue problem (EVP) to be solved is:

$$\left(\overbrace{\begin{bmatrix} \mathbf{M} & \mathbf{0} \\ \mathbf{0} & -\mathbf{K} \end{bmatrix}}^{\mathbf{A}} - \kappa \overbrace{\begin{bmatrix} \mathbf{0} & \mathbf{M} \\ \mathbf{M} & \mathbf{D} \end{bmatrix}}^{\mathbf{B}} \right) \overbrace{\begin{bmatrix} -\mathrm{i}k\mathbf{p} \\ \mathbf{p} \end{bmatrix}}^{\mathbf{z}} = \begin{bmatrix} \mathbf{0} \\ \mathbf{0} \end{bmatrix} \tag{4.1}$$

with the eigenvalues $\kappa = -\mathrm{i}k$, the eigenvectors $\mathbf{z}$ and the hypermatrices $\mathbf{A}$ and $\mathbf{B}$ of the size $2N \times 2N$. A left-sided and a right-sided EVP results from the asymmetry of $\mathbf{K}$ and $\mathbf{D}$ [15, 100]

$$(\mathbf{A} - \kappa\mathbf{B})\mathbf{x}_z = \mathbf{0} \quad \text{and} \quad \mathbf{y}_z^T(\mathbf{A} - \kappa\mathbf{B}) = \mathbf{0}, \tag{4.2}$$

where the index z denotes that the eigenvectors $\mathbf{x}$ and $\mathbf{y}$ are of the size $2N \times 1$ and must be truncated for the entries in the lower half that are associated to the sound pressure, cf. vector $\mathbf{z}$. Eq. (4.2) can be rewritten in terms of the modal matrices $\mathbf{Y}$ and $\mathbf{X}$, which diagonalize $\mathbf{A}$ and $\mathbf{B}$ such that α_j and β_j can be found on the resulting diagonals with $\kappa_j = \alpha_j/\beta_j$ being the j^{th} NM eigenvalue

$$\mathbf{Y}_z^T\mathbf{A}\mathbf{X}_z = \mathrm{diag}(\alpha_1,\ \ldots,\ \alpha_{2N-\delta}) \quad \text{and} \quad \mathbf{Y}_z^T\mathbf{B}\mathbf{X}_z = \mathrm{diag}(\beta_1,\ \ldots,\ \beta_{2N-\delta}) \tag{4.3}$$

The rank deficiency δ results from the circumstance that in the case of circular FE domains, $\mathbf{M}$ is singular for IFE DOF [100]. Fur that purpose, Marburg et al. [15] propose a subdivision of the mass matrix into FE and IFE DOF. Empty rows and columns are removed from the hypermatrices and the EVP can be solved.

Marburg [17] proposes a scaling of the eigenvalues with the factor $c_f/2\pi$ that leads to a form in which $\Im\{\kappa_j\}$ corresponds to the resonance frequency of the j^{th} mode and $\Re\{\kappa_j\}$ represents a damping term.

4.1 Modal Sound Pressure and Sound Power

The modal sound pressure solution of the NM approach is provided by Marburg [16, 17] for right-hand side excitations $\mathbf{f} = \mathrm{i}\omega\rho_0\boldsymbol{\Theta}\mathbf{v}_s$ in the form of a fluid particle velocity $\mathbf{v}_s$ on the surfaces of obstacles

$$\mathbf{p} = -\sum_{m=1}^{2N-\delta} \frac{\mathbf{y}_{\Gamma m}^T\mathbf{f}_\Gamma}{\alpha_m + \mathrm{i}k\beta_m}\mathbf{x}_m. \tag{4.4}$$

The index Γ indicates that only boundary DOF are considered in the scalar product with the excitation $\mathbf{f}$ and since this is only defined on the surfaces of scatterers.

Modal sound power contributions P_m can be derived from substitution of the sound pressure according

to Eq. (4.4) in the discrete form $P = 0.5\Re\left\{\mathbf{p}_\Gamma^T \boldsymbol{\Theta}_{\Gamma\Gamma} \mathbf{v}_\Gamma^*\right\}$ [16]

$$P = -\frac{1}{2}\Re\left\{\frac{1}{\mathrm{i}\omega\rho_f}\sum_{m=1}^{2N-\delta}\frac{\mathbf{y}_{\Gamma,m}^T\mathbf{f}_\Gamma}{\alpha_m + \mathrm{i}k\beta_m}\mathbf{x}_{\Gamma,m}^T\mathbf{f}_\Gamma^*\right\}. \tag{4.5}$$

5 Acoustic Radiation Modes (ARM)

The determination of the acoustic radiation modes is based on the eigenvalue problem of the real and symmetric acoustic impedance matrix $\mathbf{Z}_R$ [154]. This can be derived from the discretized quadratic form of the sound power in terms of vectorial fluid particle velocities at the surfaces Γ of the radiator [189]:

$$P = \frac{1}{2}\Re\left\{\int_\Gamma p(\mathbf{x})v_f^*(\mathbf{x})\mathrm{d}\Gamma(\mathbf{x})\right\} \approx \frac{1}{2}\Re\{\mathbf{p}_\Gamma^T\boldsymbol{\Theta}_{\Gamma\Gamma}\mathbf{v}_\Gamma^*\} = \frac{1}{2}\mathbf{v}_\Gamma^T\Re\{\mathbf{Z}\}\mathbf{v}_\Gamma^* = \frac{1}{2}\mathbf{v}_\Gamma^T\mathbf{Z}_R\mathbf{v}_\Gamma^*, \tag{5.1}$$

where discretizations according to Eqs. (2.6) and (2.9) are applied. The index Γ indicates that only degrees of freedom on the surface of the obstacle(s) are considered. Chen and Ginsberg [153] prove that the vectorial velocities are excluded from the real part operator in the quadratic form. They also present a modified ARM concept based on the quadratic form of sound pressure instead of velocities and introduce reciprocity relations to correlate the two sets of surface responses. They show that the (appropriately scaled) eigenvalue magnitudes indicate the radiated modal sound power.

$\mathbf{Z}$ is often calculated from the frequency-dependent BEM matrices $\mathbf{G}$ and $\mathbf{H}$ by rearranging the well-known relation $\mathbf{H}\mathbf{p}_\Gamma = \mathbf{G}\mathbf{v}_\Gamma$ to $\mathbf{p}_\Gamma^T$ and substituting it in the above discrete expression of the sound power [154]. According to Peters et al. [154], the symmetry of the real impedance matrix is not necessarily given and therefore may have to be produced, for which they present a suitable approach.

In this work it could be demonstrated by the author [A, M6] that the acoustic impedance matrix can also be obtained on the basis of the discretization by FEM and IFEM. This can be done by splitting up the discrete system of linear equations Eq. (2.1) into degrees of freedom (DOF) in the fluid (subscript $\circ$), those at the surface of the inner obstacles (Γ) and mixed DOF

$$\begin{bmatrix}\mathbf{A}_{\Gamma\Gamma} & \mathbf{A}_{\Gamma\circ}\\ \mathbf{A}_{\circ\Gamma} & \mathbf{A}_{\circ\circ}\end{bmatrix}\begin{bmatrix}\mathbf{p}_\Gamma\\ \mathbf{p}_\circ\end{bmatrix} = \mathrm{i}\omega\rho_f\begin{bmatrix}\boldsymbol{\Theta}_{\Gamma\Gamma} & \boldsymbol{\Theta}_{\Gamma\circ}\\ \boldsymbol{\Theta}_{\circ\Gamma} & \boldsymbol{\Theta}_{\circ\circ}\end{bmatrix}\begin{bmatrix}\mathbf{v}_\Gamma\\ \mathbf{v}_\circ\end{bmatrix} = \begin{bmatrix}\mathbf{f}_\Gamma\\ \mathbf{f}_\circ\end{bmatrix}. \tag{5.2}$$

The transposed sound pressure vector at Γ follows as

$$\mathbf{p}_\Gamma^T = \mathrm{i}\omega\rho_f\mathbf{v}_\Gamma^T\left[\boldsymbol{\Theta}_{\Gamma\Gamma} - \mathbf{A}_{\Gamma\circ}\mathbf{A}_{\circ\circ}^{-1}\boldsymbol{\Theta}_{\circ\Gamma}\right]^T\left[\mathbf{A}_{\Gamma\Gamma} - \mathbf{A}_{\Gamma\circ}\mathbf{A}_{\circ\circ}^{-1}\mathbf{A}_{\circ\Gamma}\right]^{-T}. \tag{5.3}$$

This leads to the acoustic impedance matrix $\mathbf{Z}_A$, whose real part has to be symmetrized.

Furthermore, the author [M6] shows that the real part of the symmetrized normal modes impedance

matrix can be used for the calculation of the ARM

$$\mathbf{Z}_{NM} = \mathrm{i}\omega\rho_f \boldsymbol{\Theta}^T \left(\mathbf{Y}_\Gamma \mathrm{diag}\left(F_m\right) \mathbf{X}_\Gamma^T\right) \boldsymbol{\Theta}, \tag{5.4}$$

where $\mathbf{X}_\Gamma$ and $\mathbf{Y}_\Gamma$ are the NM modal matrices for boundary DOF and $F_m = 1/(\alpha_m + \mathrm{i}k\beta_m)$ is a frequency-dependent factor that can be found in the NM sound pressure solution Eq. (4.4).

Regardless of the underlying method (BEM, FEM/IFEM or similar), the acoustic impedance matrix is frequency dependent and therefore its eigenvalue problem must be solved for each frequency. The resulting ARM eigenvalues $\lambda_j(\omega)$ are thus functions of the frequency. Their corresponding right eigenvectors illustrate the vibration modes on the surfaces of the radiators.

CHAPTER 3

Major Results of Attached Publications

In which the main results and novelty character of the attached publications are summarized. Furthermore, the candidate's individual contribution to the three articles is indicated.

- *Analyses of convergence and basic requirements of modal quantities in exterior acoustics. It is presented how ARM and NM can be determined on the same basis of finite and infinite elements. The impact of the choice of mesh size, interpolation polynomials and their degree is investigated. The results are compared for both methods. Moreover, their physical meaning is illustrated by a practical example.* ***(Publication A)****.*

- *Development of a criterion to identify cavity modes and exterior multipole modes. The properties and relevance of NM are evaluated by means of the sound pressure distribution of the eigenvectors and their individual frequency-dependent contribution to the radiated sound power, where the position of the eigenvalues in the complex plane is of particular interest. The differences between left and right eigenvectors are elaborated. The quality of reduced modal bases is measured by the relative error of the superposed sound power.* ***(Publication B)****.*

- *Application of the normal modes approach in the practical context of finite sonic crystal noise barriers and acoustic meta-atoms in free field. The potential for the reduction of computational effort through half-space and elliptic domain shapes is discussed for 2D IFEM and NM, while the resulting errors serve to estimate prerequisites for the analyses. It is shown how the NM approach can contribute to the dimensioning and design of meta-atoms and sonic crystals without the aim to optimize an array.* ***(Publication C)****.*

Publication A

Infinite Elements and Their Influence on Normal and Radiation Modes in Exterior Acoustics

This article addresses the influence of the finite element mesh, the choice of polynomials for the radial interpolation of the infinite elements as well as their degree on normal modes and acoustic radiation modes in exterior acoustics. It contributes to the application of modal methods under free-field conditions by providing empirical knowledge for the balancing of computational costs and accuracy for the sound pressure and sound power solution. Three types of polynomials for the radial interpolation of the infinite elements are considered, which are discussed in the literature: Lagrange, Legendre and Jacobi polynomials. It is confirmed that the condition of the dynamic stiffness matrix becomes very poor for Lagrangian polynomials for degrees greater than or equal to eight, whereas the other polynomials show a much better condition even for higher polynomial degrees.

A novel approach is presented to determine the acoustic impedance matrix Z (and thus also ARM) based on FEM and IFEM instead of on the basis of the commonly used boundary element method. Consequently, both ARM and NM can be calculated on the same basis and comparability of the results is achieved. The convergence of three significant cavity modes (trapped modes) is examined in detail in the example of a recorder cross-section and it is found that the eigenvalues for both modal methods each converge to different values for IFEM polynomials of even and of odd degree. The assignment of the eigenvalues is achieved by means of the modal assurance criterion (MAC) to match the corresponding eigenvectors. The eigenvalues of the acoustic radiation modes converged only close to their resonance peaks, whereas in the frequency ranges besides them the eigenvalue curves are virtually identical for all polynomials and all polynomial degrees from two to twenty despite the large differences in matrix condition numbers. No clear tendency, however, is found for convergence of eigenvalues from above or below. The comparison of normal modes and acoustic radiation modes is in very good agreement with the eigenfrequencies for the investigated mode shapes.

With regard to a balanced relationship between computational effort and accuracy, this paper provides insights into which degree of discretization and which orders of interpolation polynomials are essentially required for computations of ARM and NM in exterior acoustic problems using FEM and Astley–Leis IFEM. On the basis of the chosen example, the reader is given an impression of the physical characteristics and significance of the eigenvectors.

Publication B

Normal Modes and Modal Reduction in Exterior Acoustics

The work offers the reader an in-depth study of the characteristics of normal modes in exterior acoustics. It aims to analyze the role of cavity and multipole modes as well as of purely real and complex eigenvalues and -vectors for the radiation of sound. The assignment of NM eigenvalues in the complex plane to groups is presented, for which purpose a model with a duct-like cavity is considered, whose resonances are roughly known in advance. The investigations illustrate how the continuous spectrum of the exterior space appears in the form of discrete eigenvalues in lines as a result of the discretization by IFEM and modal decomposition by NM.

A novel approach is presented to the reader to distinguish between NM by their sound pressure distribution in the eigenvectors, which is concentrated either at the outer boundary of the FE domain or in the inner region at the surfaces of inner obstacles. The criterion developed for this purpose (eigenvector distribution ratio) forms the basis for a reliable distinction and thorough analysis of the spectrum. Left and right eigenvectors are studied, which result from the asymmetry of the IFE matrices and which together form the orthogonal basis of NM. The modal assurance criterion (MAC) is used to determine that both are virtually identical for the degrees of freedom in the FE domain, but differ for the degrees of freedom of the infinite elements. For cavity modes, however, both eigenvectors are also virtually identical in the IFE domain. It could also be observed that left eigenvectors radiate much further into the surrounding free field than their respective counterparts. In addition, the two oscillate in opposite phase to each other.

Within this work, criteria for the identification of physically relevant modes are developed and the accuracy of reduced modal bases are measured by the superimposed radiated sound power level (SWL). It is described how modal SWL contributions behave as functions of the frequency and it is shown that those modes of complex conjugated partners with negative imaginary parts are mainly responsible for the emission of sound in the region of the cavity resonance frequencies. The publication presents an error estimation for reduced modal bases during superposition for two load cases to induce different modes. Therefore, a velocity excitation is applied inside the cavity and on the outer surface of the radiator, respectively. It becomes apparent that relative SWL errors of less than $1\,\%$ can be achieved in wide frequency ranges, where purely real modes suffice approximately for external excitations but fail around the resonance frequencies of the cavity. This becomes particularly clear with the internal excitation for which cavity resonances dominate the SWL spectrum. These are found to be very well represented by the complex cavity modes with negative imaginary parts.

Publication C

Analysis of Scattering by Finite Sonic Crystals in Free Field With Infinite Elements and Normal Modes

This publication introduces Astley–Leis infinite elements and NM for both harmonic and modal analysis of the sound insulation by finite sonic crystal noise barriers—arrays of (locally) periodically arranged scatterers—and their components in free field. To verify the method and to determine the minimum requirements and maximum efficiency for discretization and accuracy, convergence and error studies are presented for the first time on elliptical IFE domains in 2D. It is found that the coordinate transformation leads to a local error maximum for aspect ratios close to 1.4 for all frequencies and meshes and that the requirements for counterbalancing errors due to elliptical domains by a higher-order radial polynomial interpolation of the infinite elements are growing with increasing frequency. The article shows that individual NM eigenvalue magnitudes of exterior multipole modes behave indirectly proportional to the half-axis ratios of the underlying elliptical FE domains. Their convergence suggests the presence of trapped modes—discrete eigenvalues in the continuous spectrum of the exterior space.

In the example of a circular and a c-shaped obstacle, the insertion loss of single meta-atoms is measured and the sound insulating effect of the cavity can be assigned to the first and the two higher-order Helmholtz resonator modes. The article describes that the mitigation of sound pressure also involves an amplification at another frequency with the result that both effects have to be weighted. The largest sound insulation is actually not achieved at the resonance frequencies of the cavity, respectively, but the eigenfrequencies rather seem to approximate the inflection points of the curve. It is shown that the application of a boundary admittance inside the cavity, e.g. to model absorption or as a result of contamination by dust or soil, results in a reduced sound insulation by the resonator. By considering narrow, elliptical as well as half-space FE domains, the potential for increasing efficiency of the approach is studied.

The idea of this article is to present the NM concept as an appropriate and novel tool for the investigation, design and optimization of the acoustic properties of locally periodic, finite sonic crystals and arbitrarily shaped meta-atoms without being embedded in a periodic arrangement but isolated in free field. The underlying, sound-insulating effects, e.g. Bragg scattering and absorption by Helmholtz resonators, are studied and the individual contribution of single modes is illustrated to derive specific acoustical and numerical optimization measures.

1 Individual Contributions of the Candidate

Publication A

The author conceived and conducted the analyses including the coding. He evaluated and discussed the results and wrote the article.

Publication B

The research question of this article was derived by the author from preliminary work by the co-author. Designing the model, developing the eigenvector distribution ratio, carrying out criteria for grouping modes and modal reduction is the author's contribution. This also includes planning and performing the studies, developing the code and writing the article.

Publication C

The investigations on half-space problems, the c-shaped meta-atom, the boundary admittance and sonic crystals were planned and carried out by the author and recorded in the article. The preceding manuscript of a co-author with fundamental studies on meta-atom level has been substantially revised by the author and in the peer-review process.

CHAPTER 4

Discussion

In which the novelty that has been generated by this work in the field of numerical and modal methods in exterior acoustics is outlined. It is discussed with reference to the literature by addressing the research questions posed in the introduction.

Discussion

This dissertation provides novel scientific contributions to the Astley–Leis infinite element method (IFEM) and to both acoustic radiation modes (ARM) and normal modes (NM) in exterior acoustics.

In order to answer the research questions derived from the problem definition and literature review in the introductory Ch. 1, tools for numerical calculations and subsequent scientific studies were developed. This includes a 2D IFEM code and interfaces to software for geometry and FE mesh generation as well as for providing the FEM system matrices. For reasons of efficiency, the functionality for handling half-space and elliptical computational domains was also developed.

The scope of this work covers 2D problems in order to keep the computation time and memory requirements low. For fundamental studies on the modes in exterior acoustics, the complete modal basis must first be determined before individual eigenpairs could a priori be filtered. However, this limitation is not a disadvantage, since most statements that are valid in 2D are usually also valid for later application in 3D problems and are at the same time easier to visualize and interpret.

During the studies on the influence of infinite elements on modes in exterior acoustics, several interesting observations were made. It could be confirmed for two-dimensional problems that the condition of the system matrices also becomes very large and leads to errors in the sound pressure solution with Lagrangian polynomials greater than or equal to the eighth order for radial interpolation of the IFEM [**A**]. So far, this has only been discussed for one- and three-dimensional problems [113–115]. For the first time, it could also be shown for 2D problems [**A**] that, as described by Astley et al. [109], Legendre polynomials resolve this problem and can be used for higher polynomial degrees with a significantly lower condition number of the matrix. The results of Dreyer [118] and Dreyer et al. [117] on the advantages of using Jacobi polynomials could also be confirmed in 2D [**A**]. They are a generalized form of Legendre polynomials which resemble the form of the IFE interpolation function by the specific choice of exponents [**A**]. On the other hand, it was observed that the effort for the calculation of the element integrals considerably increased with Legendre and Jacobi polynomials compared to standard Lagrange polynomials, which requires efficient algorithms for a practical implementation. This applies in particular for highly repetitive analyses, e.g. parameter studies, optimization and uncertainty analyses [M9].

In this dissertation, experiences with elliptical IFE domains in 2D have been documented for the first time and detailed error analyses have been published [**C**]. For ellipsoidal domains in 3D, the IFEM has been described in the works of Burnett and Holford [110, 111] and Astley [99]. It could be observed [**C**] that the error for elliptical computational domains strongly increases compared to circular domains with a slightly elliptical shape. At a ratio of about 1.4, it showed a flat maximum, which is apparently due to numerical inaccuracies of the coordinate transformation [**C**]. As expected from experiences in 3D [190], it could be shown that the accuracy of the sound pressure solution in exterior space coincides with the radial interpolation order of the infinite elements [**A**]. With increasing frequency, the global relative error

could be lowered, however, it resulted in higher demands on the polynomial degree [**C**].

Since half-space problems and the propagation of sound waves over impedance planes in exterior acoustic problems are suitable for many practical applications and in order to increase the efficiency of symmetric problems [117, 186, 191, 192], experiences were generated by this work using 2D IFEM [**C**].

The presented results and experiences could be used for an applied study on finite sonic crystal noise barriers and their components, acoustic meta-atoms [193]. Both were analyzed using FEM/IFEM for the first time [**C**]. It could be shown that this approach is very well suited for their calculation and design. The advantages of considering finite arrays in the free field compared to infinite, periodic arrays have been worked out. Especially at the edges of real noise barriers, diffraction effects lead to a deterioration of the mitigation of sound, which has to be considered in practical application [194, 195]. In the literature, Floquet-Bloch periodicity boundary conditions are often applied to the boundaries of a unit cell in which the analysis is conducted and the behavior is generalized to the infinite, periodic arrangement [196, 197]. A characteristic of these arrays are so-called stop bands, which are frequency ranges with complete sound insulation of incident acoustic waves. They can be visualized in dispersion curves [198, 199]. In contrast to them, finite sonic crystal noise barriers do not exhibit stop bands with complete sound isolation. Frequency ranges with high insertion losses were found to be in good agreement [**C**] compared to arrays of the same design in a waveguide in Ref. [198].

The procedure described in this thesis [**C**] allows the investigation and acoustic design of the meta-atoms independently of their environment and its influences, such as the lattice width of the sonic crystal array or its pattern (triangular, square, honeycomb lattice [200, 201]). With the separate consideration of the components and the arrays in free field, this thesis presents IFEM as a suitable tool for the analysis of both sonic crystals and acoustic meta-atoms and for the calculation of a realistic insertion loss. In addition, individual defects in the array that are not subject to any periodicity condition could be examined. In publication [**C**], the method was used to calculate the insertion loss of an individual meta-atom with absorbing admittance boundary conditions to break down the underlying effects to the minimum level. This is a novelty since in other studies [202, 203], boundary admittances are investigated in infinite sonic crystal lattices, but not individually at meta-atom level. By means of all these investigations, this work deepened the knowledge about two-dimensional Astley–Leis IFEM in exterior acoustic problems.

A central concern of this dissertation is the investigation and further development of modal quantities in exterior acoustics. The focus is on the frequency-independent NM, which—in contrast to ARM being state-of-the art in exterior acoustics [152]—have been little investigated so far. The work of Marburg [16, 17] and Marburg et al. [15] forms the basis of the research by introducing the NM concept to exterior acoustics, however, several knowledge gaps remain. One of these is the dependence of NM on the formulation and parameters of the Astley–Leis IFEM. It could be shown in Ref. [**A**] that the choice of Legendre or Jacobi polynomials for radial interpolation has no noticeable influence on the NM eigenvalues and -vectors compared to commonly used Lagrange polynomials (at least for orders smaller

than or equal to eight). Their failure for higher orders is a criterion for exclusion, especially when using elliptical or ellipsoidal FE computational domains with an increased need for radial interpolation [112],[**C**]. For further studies on the influence of the IFEM on NM, this dissertation provides convergence studies of their eigenvalues with increasing order of radial interpolation to provide empirical values for the numerical requirements of the method [**A**]. For the first time, it could be shown that two different NM eigenvalue convergences were obtained for even and odd polynomial degrees. By describing the distribution of the eigenvalues in the complex plane in more detail and discussing the differences between even and odd polynomial degrees [**A**],[**B**], the work of Marburg et al. [15] could be supplemented.

With the specific selection of models, a contribution to the physical interpretation of the NM could be made in Refs. [**A**],[**C**], which up to now have been mostly investigated on the basis of simple, theoretical models [15, 16, 19]. Fuß et al. [18] and Retka [204], however, used NM to study the physics of a 3D recorder in free field, which was taken up and further investigated in this work in 2D [**A**]. Three representative mode shapes, which are effective in different regions within the hollow body, were used to illustrate the tone (=eigenfrequency) generation in the recorder in a simplified form by neglecting flow effects [204]. The applicability of the method was thus practically motivated by analyzing mode shapes regarding their physical relevance. In a second example, finite sonic crystal noise barriers and the associated acoustic meta-atoms were investigated using the technique [**C**]. The advantages over harmonic analysis of the problems were highlighted, which, as described above, have not been calculated by IFEM in the free field so far. Diffraction effects at the ends of the finite lattice could be described and visualized by NM. They subsequently cause the sound insulating effect of the crystal to vary and weaken spatially. The normal modes of a single c-shaped meta-atom in free field have been investigated and it was possible to prove the Helmholtz resonator mode to be responsible for its sound insulation besides two additional higher-order cavity modes [**C**]. For all three, this was demonstrated by the insertion loss (IL) as a function of the frequency and it was also shown that the highest effectiveness might not be observed in the cavity's natural frequencies (cf. Fard et al. [33]) but rather approximately at the inflection points of the IL curve, which has an ascending and a descending peak around these frequency points [**C**]. The described approach determines the acoustic effectiveness of arbitrarily shaped meta-atoms in the free field, e.g. *Matryoska*-type [198, 205], *Mie*-type [206, 207] meta-atoms or shapes optimized with regard to their acoustic properties [208, 209]. They could thus be investigated and designed completely independent of the embedding in a periodic array.

In the example of a single c-shaped meta-atom under free-field conditions, it was demonstrated that an absorbing admittance boundary condition inside the cavity weakens the effect of amplification and attenuation of IL around the resonance frequencies [**C**]. The NM eigenfrequencies slightly increase with the introduction of the boundary admittance. However, an additional sound mitigation other than that around the cavity resonance frequencies could not be observed in the considered frequency range. Since other studies on absorbing surfaces of sonic crystal arrays describe an additional benefit [202, 203], further research on this aspect is desirable. Further research and development is still crucial for an

advanced understanding and efficiently superimposed solution of completely fluid-structure coupled modal problems under free-field conditions [6].

Since NM eigenvectors can be visualized in the entire exterior domain, physical effects in the fluid could be illustrated and the complex-valued eigenvalues and -vectors could be related to their acoustic effect, e.g. in the form of a frequency-dependent insertion loss [**C**]. In the example of sonic crystals with c-shaped meta-atoms, eigenvectors could subjectively be assigned to groups of modes of the same operating principle. Modes within such a group resonated at slightly different frequencies, in which, for instance, individual resonators or groups of resonators oscillated, but never all of them at the same time. They together provided sound insulation across a certain frequency range. This behavior is observed in a similar way for modes of rotor blades in other studies [210, 211].

So far, no studies have been published on normal modes in exterior acoustics for half-space problems. Their suitability and potential for memory reduction in computational analysis in case of symmetric problems could be demonstrated [**C**]. Another novelty is the calculation of NM for elliptical domain shapes [**C**]. At a first glance, these have the advantage compared to circular shapes that they save DOF within the FE domain due to their slim shape, which could closely approach the obstacle. However, this advantage might be canceled out by the greatly increased requirements for the radial interpolation order of the infinite elements. It became apparent that advantages and disadvantages of elliptical domains have to be weighed up depending on the problem, since no general statement could be made so far. Elliptical domains do not have a singular mass matrix [100] compared to circular domains used so far (cf. Marburg [16]), which affects the properties of the state-space matrices in the NM eigenvalue problem. This could be useful for the selection of suitable eigenvalue solvers in future studies.

For a number of NM eigenvalues in elliptical domains a direct relationship to their semi-axis ratio could be found [**C**]. This finding is very useful for the identification and assignment of NM, e.g. for convergence studies and assigning modes to groups, because the modal assurance criterion (MAC) [212] is only suitable for the matching of eigenvectors within unchanged domain shapes, as it was applied in [**A**].

The second research gap outlined in the introduction poses the question of the roles of modes within the continuous spectrum of the exterior acoustic field. The mathematically continuous exterior spectrum [181] was modeled and discretized using FEM and IFEM and decomposed into discrete eigenvalues. The existence of discrete eigenvalues in the continuous spectrum for exterior problems (*trapped modes*) could be shown e.g. by Jones [136] and Hein et al. [142]. The structure of the complex plane of NM eigenvalues observed by Marburg et al. [15] and further investigated in [**A**][**B**] shows traces of lines, curves and point clouds in which the eigenvalues seem to be grouped. Using the *eigenvector distribution ratio* introduced in publication [**B**], mode shapes could be sorted according to their sound pressure distribution within the computational domain: eigenvectors with a concentration of sound pressure along the surfaces of inner obstacles, with a concentration at the envelope of the FE domain and mixed forms [**B**]. The first group of eigenvectors reliably reveals the internal resonances of obstacles with

cavities, while modes with a strong sound pressure distribution at the transition of FE and IFE domains are multipoles. This criterion might be the basis for a more detailed, refined grouping according to multipole groups. Within each multipole group, eigenvalues could be assigned to each other for variable domain shapes via the above described ratio of eigenvalues and semi-axes [**C**]. It was assumed that these particular modes could be identified as converging trapped modes using this criterion, which, however, has to be confirmed in future research. With an increasing radial interpolation order, the number of multipoles that are not subject to this property grows [**C**]. This could indicate that they are non-physical and do not contribute to the actual sound radiation, which would need further investigation.

The analysis of the position and distribution of groups of normal modes in the complex plane is required for the a priori determination of physically relevant modes and their targeted calculation. Following the example of Marburg [16], the sound power solution of a radiator with one cavity was analyzed for a purely external and a internal surface velocity excitation [**B**]. Low-order cavity modes could thus be identified as essential for the modally superposed sound pressure or sound power solution. The presented findings could be supplement to the considerations on sorting criteria presented by Marburg in Ref. [16] and Marburg et al. [17]. Besides the ascending sorting by eigenvalue or modal sound power contribution to the overall sound power, these were two approaches according to a term F_m, which is related to the NM eigenvalues (cf. Eqs. (4.4) and (5.4)). Furthermore, Marburg [16] considered the difference between modal and actual frequency as a sorting criterion. Taking into account the clustering presented in [**B**], these criteria could be used much more efficiently, since a preselection and reduction of the modal basis by means of iterative eigenvalue solvers is possible. With regard to the modal sound power contributions shown in [**B**], this becomes apparent in a meaningful representation in the complex plane. Here, it was revealed for the first time that the sound radiation of the NM cavity modes is mainly caused by the complex conjugated partners with negative imaginary parts. It could be shown that the global relative error of a modal basis reduced to these modes leads to promising results in a wide frequency range. However, the addition of exterior multipole modes is essential [**B**]. Unpublished studies by the author showed with promising results for simple geometries that considering modes from the groups of low multipole orders and the first up to ten cavity modes could be sufficiently accurate. Further empirical evidence is to be collected and documented in future research work.

This work compared NM left and right eigenvectors and visualized them in the IFE domain for the first time [**B**]. It could be shown that both were virtually identical in the FE domain. For cavity modes with a very high concentration of the sound pressure around inner obstacles of the FE domain (cf. eigenvector distribution ratio), this also applied in the IFE domain. For multipoles it could be observed that the left eigenvectors radiate significantly further into the free field than their respective counterparts. Furthermore, they oscillated in phase opposition to each other [**B**].

In addition to cavity and multipole modes, a number of non-physical mathematical artifacts, namely spurious modes [213] were computed, due to the overdetermination by the state-space linearization and high-order interpolation polynomials. They were characterized by the fact that their eigenvectors

showed subjectively random and irregularly distributed sound pressure values. Apparently, these did not substantially contribute to the physical effect of sound radiation [**B**]. The identification of these non-relevant modes was, to a certain extent, quite reliably done by the eigenvector distribution ratio. For the solution of the quadratic eigenvalue problem of a displacement-based Helmholtz equation, Bermúdez et al. [214] presented lowest-order Raviart–Thomas finite elements, which did not produce spurious modes compared to ordinary finite elements. Whether this or similar approaches could help to suppress spurious modes in the sound-pressure-based exterior acoustic problem could be the subject of future research.

With the improved knowledge of the distribution of eigenvalues in the complex plane and with the help of iterative solvers, eigenvalues could be determined specifically in certain regions of the complex plane. Fuß et al. [18] used an iterative Arnoldi eigenvalue solver for a 3D problem to determine weakly damped NM eigenvalues along the imaginary axis. With the knowledge gained from [**B**], the search region in the complex plane could be narrowed down and their approach could possibly achieve even better results. In this dissertation, the Matlab solver `eig` (based on the QZ algorithm) was used for full ARM and NM eigenvalue problems, while alternative techniques are often not available due to the properties of the hypermatrices (e.g. asymmetry). Furthermore, the software libraries SLEPc and PETSc [215, 216] were used for the iterative solution of the linearized NM eigenvalue problem. Depending on the problem (e.g. circular or elliptic domain shape), different libraries and methods are suitable or not, while in this work [**C**], good experience could be made with the direct solver preconditioner `PCLU` based on LU factorization in combination with `KSPPREONLY` [217].

As with most related studies, this work focused on NM in 2D exterior acoustic problems with the exception of the work of Fuß et al. [18] in 3D. It is assumed that the majority of the results and methods used could be transferred to realistic 3D problems. An exception are unpublished criteria developed by the author for the identification and grouping of multipoles, which are based on the eigenvector distribution ratio [**B**]. These are based on the analysis of zero crossings and the distribution and amplitudes of the sound pressure minima and maxima of the eigenvectors along the outer, circular FE boundary. A similar analysis is not conceivable for three-dimensional problems, but the analyses of the complex plane provided information about the position and grouping of the NM cavity and multipole modes, which is most probably still valid for 3D problems and needs to be verified in further research.

The scientific novelty that this work contributes to the ARM was presented in the first attached publication [**A**]. For the first time, it could be shown that ARM can be calculated on the basis of FEM and IFEM [M6][**A**], whereas they are usually calculated using BEM in most other studies [14, 154]. Therefore, the investigations on the influence of the infinite elements on ARM in terms of radial polynomial order and type of interpolation polynomial also represent a novelty. Analogous to NM, two different convergences of ARM eigenvalues for even and odd polynomial degrees could be observed. In the prior publication [M6], it was shown that ARM could also be determined using the real part of the NM impedance matrix (requiring a symmetrization according to Peters et al. [154]). These ARM showed very good agreement

with those of calculations using BEM or using FEM/IFEM. Moreover, for the ARM eigenvalues based on BEM, non-physical resonance frequencies (*irregular frequencies*) could be observed in [M6], whose peaks could be minimized to a negligible level by using the Burton–Miller formulation [23, 218].

The main motivation for research on modal methods in exterior acoustics is the need to develop efficient algorithms and procedures for accelerated solutions in the unbounded fluid [6]. Compared to harmonic analysis, modal methods have the advantage that they can simplify and reduce the numerical model (ideally to a minimum of complexity) while providing a sufficiently accurate solution. This procedure is state of the art in structural dynamics and interior acoustics [9, 219, 220]. Depending on the application, harmonic analysis is sometimes more, sometimes less suitable when using FEM and Astley–Leis IFEM with their frequency-independent system matrices compared to the frequency-dependent BEM [59] or other methods [54]. Even though the efficiency of harmonic analysis with FEM and IFEM was not measured against them, it appeared that the advantage of frequency independence could possibly often be compensated by the higher number of DOF compared to BEM. This effect becomes particularly clear in elliptical domains with a higher demand on the radial interpolation of the IFEM [**C**]. Future research could address the lack of experiences on the performance of harmonic analyses and of the two modal methods in exterior acoustics and complement them with comparisons to other MOR techniques [8].

A central research question posed at the beginning highlights the lack of experience in comparing ARM and NM and their physical interpretation. By calculating ARM on the basis of the NM impedance matrix, they could be connected and the knowledge of their relationship deepened [**A**][M6]. The essential similarities and differences between the two modal quantities were demonstrated [**A**]. In accordance to other studies [14, 15], it could be shown that both methods result in cavity modes and groups of multipole modes [**B**]. The limitation of ARM eigenvectors to the surfaces of inner obstacles results in a different view of the multipoles compared to the normal mode shapes whose oscillation can be illustrated in the entire fluid. However, even these differ in detail in their appearance from those which Prieto [221] determines on the basis of FEM and a frequency-independent PML [172], which opens up several new research opportunities. For the cavity modes, a direct comparison is possible, e.g. using MAC [212]. The physical interpretation of sound radiation using NM could be enhanced by the experience gained from the examples of tone generation in the recorder [**A**] and finite sonic crystals [**C**], where various physical effects could be visualized, e.g. Bragg scattering and Helmholtz resonator effects. Numerous other practical applications of the two modal methods are conceivable in the field of vehicle acoustics for the simulation of pass-by sound or the calculation of equipment or engine noise under free field conditions with the aim to reduce computational effort in comparison to commonly used harmonic analysis [117]. For a large-scale industrial application of the methods, however, their efficiency has to be increased. The present work provides a further important contribution to this.

Bibliography

[1] Harvery, T., “The Feynman lectures on physics first year photos (1961-62),” 1962, California Institute of Technology. [Online]. Available: https://www.feynmanlectures.caltech.edu/Photos1_toc.html

[2] Koopmann, G. H. and Fahnline, J. B., *Designing quiet structures: A sound power minimization approach*. Elsevier, 1997.

[3] ISO 3745:2012„ “Acoustics–determination of sound power levels and sound energy levels of noise sources using sound pressure–precision methods for anechoic rooms and hemi-anechoic rooms,” *International Organization for Standardization*, 2012.

[4] Sommerfeld, A., *Partial differential equations in physics*. Academic press, 1949, Vol. 1.

[5] Belegundu, A., Salagame, R., and Koopmann, G., “A general optimization strategy for sound power minimization,” *Structural Optimization*, Vol. 8, No. 2-3, pp. 113–119, 1994.

[6] Marburg, S., “Developments in structural-acoustic optimization for passive noise control,” *Arch. Comput. Methods Eng.*, Vol. 9, No. 4, pp. 291–370, 2002.

[7] Benner, P., Mehrmann, V., and Sorensen, D. C., *Dimension reduction of large-scale systems*. Springer, 2005, Vol. 45.

[8] Besselink, B., Tabak, U., Lutowska, A., Van de Wouw, N., Nijmeijer, H., Rixen, D. J., Hochstenbach, M., and Schilders, W., “A comparison of model reduction techniques from structural dynamics, numerical mathematics and systems and control,” *J. Sound Vib.*, Vol. 332, No. 19, pp. 4403–4422, 2013.

[9] Ewins, D. J., *Modal testing: Theory, practice and application*. Research Studies Press LTD., 2000, Vol. 2.

[10] Fahy, F. J. and Gardonio, P., *Sound and structural vibration: Radiation, transmission and response*. Elsevier, 2007.

[11] Blevins, R. D., *Formulas for dynamics, acoustics and vibration*. John Wiley & Sons, 2015.

[12] Möser, M., *Engineering acoustics*. Springer, 2014.

[13] Unruh, O., “Schallabstrahlcharakteristik von Platten mit inhomogener Dämpfung und komplexen Schwingungseigenformen,” Ph.D. dissertation, Institut für Adaptronik und Funktionsintegration, TU Braunschweig, Braunschweig, 2015.

[14] Cunefare, K. A., Currey, M. N., Johnson, M. E., and Elliott, S. J., “The radiation efficiency grouping of free-space acoustic radiation modes,” *J. Acoust. Soc. Am.*, Vol. 109, No. 1, pp. 203–215, 2001.

[15] Marburg, S., Dienerowitz, F., Horst, T., and Schneider, S., “Normal modes in external acoustics. Part II: Eigenvalues and eigenvectors in 2D,” *Acta Acustica united with Acustica*, Vol. 92, No. 1, pp. 97–111, 2006.

[16] Marburg, S., “Normal modes in external acoustics. Part III: Sound power evaluation based on superposition of frequency-independent modes,” *Acta Acustica united with Acustica*, Vol. 92, No. 2, pp. 296–311, 2006.

[17] Marburg, S., “Normal modes in external acoustics. Part I: Investigation of the one-dimensional duct problem,” *Acta Acustica united with Acustica*, Vol. 91, No. 6, pp. 1063–1078, 2005.

[18] Fuß, S., Hawkins, S. C., and Marburg, S., “An eigenvalue search algorithm for the modal analysis of a resonator in free space,” *J. Comput. Acoust.*, Vol. 19, No. 01, pp. 95–109, 2011.

[19] Retka, S. and Marburg, S., “An infinite element for the solution of Galbrun equation,” *ZAMM-Journal of Applied Mathematics and Mechanics/Zeitschrift für Angewandte Mathematik und Mechanik*, Vol. 93, No. 2-3, pp. 154–162, 2013.

[20] Trefethen, L. N., “The definition of numerical analysis,” Cornell University, Tech. Rep., 1992.

[21] Marburg, S. and Nolte, B., “A unified approach to finite and boundary element discretization in linear time–harmonic acoustics,” in *Computational Acoustics of Noise Propagation in Fluids - Finite and Boundary Element Methods*, Marburg, S. and Nolte, B., Eds. Berlin, Heidelberg: Springer Berlin Heidelberg, 2008, pp. 1–34.

[22] Burton, A. and Miller, G., “The application of integral equation methods to the numerical solution of some exterior boundary-value problems,” *Proceedings of the Royal Society of London. Series A, Mathematical and Physical Sciences*, pp. 201–210, 1971.

[23] Marburg, S., “The Burton and Miller method: Unlocking another mystery of its coupling parameter,” *J. Comput. Acoust.*, Vol. 24, No. 01, p. 1550016, 2016.

[24] Schenck, H. A., “Improved integral formulation for acoustic radiation problems,” *J. Acoust. Soc. Am.*, Vol. 44, No. 1, pp. 41–58, 1968.

[25] Benthien, W. and Schenck, A., “Nonexistence and nonuniqueness problems associated with integral equation methods in acoustics,” *Computers & Structures*, Vol. 65, No. 3, pp. 295–305, 1997.

[26] Marburg, S., “Numerical damping in the acoustic boundary element method,” *Acta Acustica united with Acustica*, Vol. 102, No. 3, pp. 415–418, 2016.

[27] Baydoun, S. K. and Marburg, S., “Quantification of numerical damping in the acoustic boundary element method for two-dimensional duct problems,” *J. Theoret. Comput. Acoust.*, Vol. 26, No. 03, p. 1850022, 2018.

[28] Marburg, S., “A pollution effect in the boundary element method for acoustic problems,” *J. Theoret. Comput. Acoust.*, Vol. 26, No. 02, p. 1850018, 2018.

[29] Bayliss, A., Goldstein, C. I., and Turkel, E., “On accuracy conditions for the numerical computation of waves,” *J. Comput. Phys.*, Vol. 59, No. 3, pp. 396–404, 1985.

[30] Deraemaeker, A., Babuška, I., and Bouillard, P., “Dispersion and pollution of the FEM solution for the Helmholtz equation in one, two and three dimensions,” *Int. J. Numer. Methods Eng.*, Vol. 46, No. 4, pp. 471–499, 1999.

[31] Ihlenburg, F., “The medium-frequency range in computational acoustics: Practical and numerical aspects,” *J. Comput. Acoust.*, Vol. 11, No. 02, pp. 175–193, 2003.

[32] Fard, S. M., Peters, H., Kessissoglou, N., and Marburg, S., "Three-dimensional analysis of a noise barrier using a quasi-periodic boundary element method," *J. Acoust. Soc. Am.*, Vol. 137, No. 6, pp. 3107–3114, 2015.

[33] Fard, S., Peters, H., Marburg, S., and Kessissoglou, N., "Acoustic performance of a barrier embedded with Helmholtz resonators using a quasi-periodic boundary element technique," *Acta Acustica united with Acustica*, Vol. 103, No. 3, pp. 444–450, 2017.

[34] Ziegelwanger, H., Reiter, P., and Conter, M., "The three-dimensional quasi-periodic boundary element method: Implementation, evaluation, and use cases," *Int. J. Comp. Methods and Experimental Measurements*, Vol. 5, No. 3, pp. 404–414, 2017.

[35] Fischer, M., Gauger, U., and Gaul, L., "A multipole Galerkin boundary element method for acoustics," *Eng. Anal. Boundary Elem.*, Vol. 28, No. 2, pp. 155–162, 2004.

[36] Gumerov, N. A. and Duraiswami, R., *Fast multipole methods for the Helmholtz equation in three dimensions*. Elsevier, 2005.

[37] Fischer, M. and Gaul, L., "Fast BEM–FEM mortar coupling for acoustic–structure interaction," *Int. J. Numer. Methods Eng.*, Vol. 62, No. 12, pp. 1677–1690, 2005.

[38] Czygan, O. and von Estorff, O., "Fluid-structure interaction by coupling BEM and nonlinear FEM," *Engineering Analysis With Boundary Elements - ENG ANAL BOUND ELEM*, Vol. 26, pp. 773–779, 10 2002.

[39] Moser, W., Duenser, C., and Beer, G., "Mapped infinite elements for three-dimensional multi-region boundary element analysis," *Int. J. Numer. Methods Eng.*, Vol. 61, No. 3, pp. 317–328, 2004.

[40] Ciskowski, R. D. and Brebbia, C. A., *Boundary element methods in acoustics*. Springer, 1991.

[41] Kirkup, S. M., *The boundary element method in acoustics*. Integrated sound software, 2007.

[42] Wu, T. W., *Boundary element acoustics fundamentals and computer codes*. WIT Press, Southampton, 2000.

[43] von Estorff, O., *Boundary elements in acoustics: Advances and applications*. Wit Pr/Computational Mechanics, 2000, Vol. 9.

[44] Marburg, S. and Nolte, B., *Computational Acoustics of Noise Propagation in Fluids - Finite and Boundary Element Methods*. Berlin, Heidelberg: Springer Berlin Heidelberg, 2008.

[45] Zienkiewicz, O. C. and Taylor, R. L., *The finite element method for solid and structural mechanics*. Butterworth-Heinemann, 2005.

[46] Bathe, K.-J., *Finite element procedures*. Klaus-Jürgen Bathe, 2006.

[47] Turner, M., Clough, R., Martin, H., and Topp, L., "Stiffness and deflection analysis of complex structures," *J. Aeronaut. Sci.*, Vol. 23, No. 9, pp. 805–823, 1956.

[48] Samuelsson, A. and Zienkiewicz, O. C., "History of the stiffness method," *Int. J. Numer. Methods Eng.*, Vol. 67, No. 2, pp. 149–157, 2006.

[49] Clough, R. W., "The finite element method in plane stress analysis," in *Proceedings of 2nd ASCE Conference on Electronic Computation, Pittsburgh Pa., Sept. 8 and 9, 1960*, 1960.

[50] Craggs, A., "The use of simple three-dimensional acoustic finite elements for determining the natural modes and frequencies of complex shaped enclosures," *J. Sound Vib.*, Vol. 23, No. 3, pp. 331–339, 1972.

[51] Gladwell, G., "A variational formulation of damped acousto structural vibration problems," *J. Sound Vib.*, Vol. 4, No. 2, pp. 172–186, 1966.

[52] Ihlenburg, F., *Finite element analysis of acoustic scattering*. Springer Science & Business Media, 2006, Vol. 132.

[53] Zienkiewicz, O. C., "Achievements and some unsolved problems of the finite element method," *Int. J. Numer. Methods Eng.*, Vol. 47, No. 1-3, pp. 9–28, 2000.

[54] Thompson, L. L., "A review of finite-element methods for time-harmonic acoustics," *J. Acoust. Soc. Am.*, Vol. 119, No. 3, pp. 1315–1330, 2006.

[55] Harari, I., "A survey of finite element methods for time-harmonic acoustics," *Comput. Methods Appl. Mech. Eng.*, Vol. 195, No. 13-16, pp. 1594–1607, 2006.

[56] Marburg, S., "Six boundary elements per wavelength: Is that enough?" *J. Comput. Acoust.*, Vol. 10, No. 01, pp. 25–51, 2002.

[57] Marburg, S. and Schneider, S., "Influence of element types on numeric error for acoustic boundary elements," *J. Comput. Acoust.*, Vol. 11, No. 03, pp. 363–386, 2003.

[58] Harari, I. and Hughes, T. J., "A cost comparison of boundary element and finite element methods for problems of time-harmonic acoustics," *Comput. Methods Appl. Mech. Eng.*, Vol. 97, No. 1, pp. 77–102, 1992.

[59] Von Estorff, O., "Efforts to reduce computation time in numerical acoustics–an overview," *Acta Acustica united with Acustica*, Vol. 89, No. 1, pp. 1–13, 2003.

[60] Anderssohn, R. and Marburg, S., "Nonlinear approach to approximate acoustic boundary admittance in cavities," *J. Comput. Acoust.*, Vol. 15, No. 01, pp. 63–79, 2007.

[61] Marburg, S. and Anderssohn, R., "Fluid structure interaction and admittance boundary conditions: Setup of an analytical example," *J. Comput. Acoust.*, Vol. 19, No. 01, pp. 63–74, 2011.

[62] Tsynkov, S. V., "Numerical solution of problems on unbounded domains. a review," *Appl. Numer. Math.*, Vol. 27, No. 4, pp. 465–532, 1998.

[63] Shirron, J. J. and Babuška, I., "A comparison of approximate boundary conditions and infinite element methods for exterior Helmholtz problems," *Comput. Methods Appl. Mech. Eng.*, Vol. 164, No. 1, pp. 121–139, 1998.

[64] Givoli, D., Patlashenko, I., and Keller, J. B., "High-order boundary conditions and finite elements for infinite domains," *Comput. Methods Appl. Mech. Eng.*, Vol. 143, No. 1-2, pp. 13–39, 1997.

[65] Givoli, D., "Non-reflecting boundary conditions," *J. Comput. Phys.*, Vol. 94, No. 1, pp. 1–29, 1991.

[66] Hagstrom, T., "Radiation boundary conditions for the numerical simulation of waves," *Acta Numerica*, Vol. 8, pp. 47–106, 1999.

[67] Givoli, D., *Numerical methods for problems in infinite domains*. Elsevier, 2013, Vol. 33.

[68] Givoli, D., "Computational absorbing boundaries," in *Computational acoustics of noise propagation in fluids–finite and boundary element methods*. Springer, 2008, pp. 145–166.

[69] Engquist, B. and Majda, A., "Absorbing boundary conditions for numerical simulation of waves," *Proceedings of the National Academy of Sciences*, Vol. 74, No. 5, pp. 1765–1766, 1977.

[70] Bayliss, A. and Turkel, E., "Radiation boundary conditions for wave-like equations," *Commun. Pure Appl. Math.*, Vol. 33, No. 6, pp. 707–725, 1980.

[71] Bayliss, A., Gunzburger, M., and Turkel, E., "Boundary conditions for the numerical solution of elliptic equations in exterior regions," *SIAM J. Appl. Math.*, Vol. 42, No. 2, pp. 430–451, 1982.

[72] Guddati, M. N. and Tassoulas, J. L., "Continued-fraction absorbing boundary conditions for the wave equation," *J. Comput. Acoust.*, Vol. 8, No. 01, pp. 139–156, 2000.

[73] Givoli, D. and Neta, B., "High-order non-reflecting boundary scheme for time-dependent waves," *J. Comput. Phys.*, Vol. 186, No. 1, pp. 24–46, 2003.

[74] Hagstrom, T. and Warburton, T., "A new auxiliary variable formulation of high-order local radiation boundary conditions: Corner compatibility conditions and extensions to first-order systems," *Wave Motion*, Vol. 39, No. 4, pp. 327–338, 2004.

[75] Collino, F. *et al.*, "High order absorbing boundary conditions for wave propagation models. Straight line boundary and corner cases," in *Second International Conference on Mathematical and Numerical Aspects of Wave Propagation (Newark, DE, 1993)*. SIAM Philadelphia, PA, 1993, pp. 161–171.

[76] Givoli, D., "High-order local non-reflecting boundary conditions: A review," *Wave Motion*, Vol. 39, No. 4, pp. 319–326, 2004.

[77] Rabinovich, D., Givoli, D., and Bécache, E., "Comparison of high-order absorbing boundary conditions and perfectly matched layers in the frequency domain," *Int. J. Num. Methods Biomedical Eng.*, Vol. 26, No. 10, pp. 1351–1369, 2010.

[78] Levin, T., Turkel, E., and Givoli, D., "Obstacle identification using the TRAC algorithm with a second-order ABC," *Int. J. Numer. Methods Eng.*, Vol. 118, No. 2, pp. 61–92, 2019.

[79] Keller, J. B. and Givoli, D., "Exact non-reflecting boundary conditions," *J. Comput. Phys.*, Vol. 82, No. 1, pp. 172–192, 1989.

[80] Givoli, D. and Keller, J. B., "A finite element method for large domains," *Comput. Methods Appl. Mech. Eng.*, Vol. 76, No. 1, pp. 41–66, 1989.

[81] Grote, M. J. and Keller, J. B., "Nonreflecting boundary conditions for time-dependent scattering," *J. Comput. Phys.*, Vol. 127, No. 1, pp. 52–65, 1996.

[82] Givoli, D., Personal communication, Vienna, Austria, 2017.

[83] Bermúdez, A., Hervella-Nieto, L., Prieto, A., and Rodríguez, R., "Perfectly matched layers," in *Computational Acoustics of Noise Propagation in Fluids - Finite and Boundary Element Methods*, Marburg, S. and Nolte, B., Eds. Springer Berlin Heidelberg, 2008, pp. 167–196.

[84] Lassas, M. and Somersalo, E., "On the existence and convergence of the solution of PML equations," *Computing*, Vol. 60, No. 3, pp. 229–241, Sep 1998.

[85] Berenger, J.-P., "A perfectly matched layer for the absorption of electromagnetic waves," *J. Comput. Phys.*, Vol. 114, No. 2, pp. 185–200, 1994.

[86] Turkel, E. and Yefet, A., "Absorbing PML boundary layers for wave-like equations," *Appl. Numer. Math.*, Vol. 27, No. 4, pp. 533–557, 1998.

[87] Harari, I., Slavutin, M., and Turkel, E., "Analytical and numerical studies of a finite element PML for the Helmholtz equation," *J. Comput. Acoust.*, Vol. 8, No. 01, pp. 121–137, 2000.

[88] Bunting, G., Prakash, A., Walsh, T., and Dohrmann, C., "Parallel ellipsoidal perfectly matched layers for acoustic Helmholtz problems on exterior domains," *J. Theoret. Comput. Acoust.*, Vol. 26, No. 02, p. 1850015, 2018.

[89] Teixeira, F. and Chew, W., "Complex space approach to perfectly matched layers: A review and some new developments," *Int. J. Numer. Modell. Electron. Networks Devices Fields*, Vol. 13, No. 5, pp. 441–455, 2000.

[90] Bermúdez, A., Hervella-Nieto, L., Prieto, A., and Rodríguez, R., "Perfectly matched layers for time-harmonic second order elliptic problems," *Arch. Comput. Methods Eng.*, Vol. 17, No. 1, pp. 77–107, 2010.

[91] Diaz, J. and Joly, P., "A time domain analysis of PML models in acoustics," *Comput. Methods Appl. Mech. Eng.*, Vol. 195, No. 29-32, pp. 3820–3853, 2006.

[92] Astley, R. J., "Infinite elements," in *Computational Acoustics of Noise Propagation in Fluids - Finite and Boundary Element Methods*, Marburg, S. and Nolte, B., Eds. Berlin, Heidelberg: Springer Berlin Heidelberg, 2008, pp. 197–230.

[93] Bettess, P., "Infinite elements," *Int. J. Numer. Methods Eng.*, Vol. 11, No. 1, pp. 53–64, 1977.

[94] Bettess, P. and Zienkiewicz, O., "Diffraction and refraction of surface waves using finite and infinite elements," *Int. J. Numer. Methods Eng.*, Vol. 11, No. 8, pp. 1271–1290, 1977.

[95] Zienkiewicz, O. C., Bando, K., Bettess, P., Emson, C., and Chiam, T. C., "Mapped infinite elements for exterior wave problems," *Int. J. Numer. Methods Eng.*, Vol. 21, No. 7, pp. 1229–1251, 1985.

[96] Burnett, D. S., "A three-dimensional acoustic infinite element based on a prolate spheroidal multipole expansion," *J. Acoust. Soc. Am.*, Vol. 96, No. 5, pp. 2798–2816, 1994.

[97] Astley, R. J. and Eversman, W., "Finite element formulations for acoustical radiation," *J. Sound Vib.*, Vol. 88, No. 1, pp. 47–64, 1983.

[98] Astley, R., Macaulay, G., and Coyette, J., "Mapped wave envelope elements for acoustical radiation and scattering," *J. Sound Vib.*, Vol. 170, No. 1, pp. 97–118, 1994.

[99] Astley, R., "Mapped spheroidal wave-envelope elements for unbounded wave problems," *Int. J. Numer. Methods Eng.*, Vol. 41, No. 7, pp. 1235–1254, 1998.

[100] Astley, R. J., Macaulay, G. J., Coyette, J.-P., and Cremers, L., "Three-dimensional wave-envelope elements of variable order for acoustic radiation and scattering. Part I. Formulation in the frequency domain," *J. Acoust. Soc. Am.*, Vol. 103, No. 1, pp. 49–63, 1998.

[101] Leis, R., *Initial boundary value problems in mathematical physics*. Courier Corporation, 2013.

[102] Demkowicz, L. and Gerdes, K., "Convergence of the infinite element methods for the Helmholtz equation in separable domains," *Numerische Mathematik*, Vol. 79, No. 1, pp. 11–42, 1998.

[103] Ihlenburg, F., "On fundamental aspects of exterior approximations with infinite elements," *J. Comput. Acoust.*, Vol. 8, No. 01, pp. 63–80, 2000.

[104] Bettess, P., *Infinite elements. 1992*. Penshaw Press, 1992.

[105] Gerdes, K., "A summary of infinite element formulations for exterior Helmholtz problems," *Comput. Methods Appl. Mech. Eng.*, Vol. 164, No. 1, pp. 95–105, 1998.

[106] Gerdes, K., "The conjugated vs. the unconjugated infinite element method for the Helmholtz equation in exterior domains," *Comput. Methods Appl. Mech. Eng.*, Vol. 152, No. 1-2, pp. 125–145, 1998.

[107] Gerdes, K., "A review of infinite element methods for exterior Helmholtz problems," *J. Comput. Acoust.*, Vol. 8, No. 01, pp. 43–62, 2000.

[108] Astley, R. J., "Infinite elements for wave problems: A review of current formulations and an assessment of accuracy," *Int. J. Numer. Methods Eng.*, Vol. 49, No. 7, pp. 951–976, 2000.

[109] Astley, R. and Hamilton, J., "Numerical studies of conjugated infinite elements for acoustical radiation," *J. Comput. Acoust.*, Vol. 8, No. 01, pp. 1–24, 2000.

[110] Burnett, D. S. and Holford, R. L., "An ellipsoidal acoustic infinite element," *Comput. Methods Appl. Mech. Eng.*, Vol. 164, No. 1-2, pp. 49–76, 1998.

[111] Burnett, D. S. and Holford, R. L., "Prolate and oblate spheroidal acoustic infinite elements," *Comput. Methods Appl. Mech. Eng.*, Vol. 158, No. 1-2, pp. 117–141, 1998.

[112] Astley, R. and Coyette, J.-P., "The performance of spheroidal infinite elements," *Int. J. Numer. Methods Eng.*, Vol. 52, No. 12, pp. 1379–1396, 2001.

[113] Astley, R. J. and Coyette, J.-P., "Conditioning of infinite element schemes for wave problems," *Commun. Numer. Methods Eng.*, Vol. 17, No. 1, pp. 31–41, 2001.

[114] Astley, R., Hamilton, J., and Wilkinson, B., "Accuracy and conditioning of infinite element schemes for exterior acoustics," in *Proc. of the Seventh Int. Conf. on Sound and Vibration, Garmisch-Partenkirchen*, 2000, pp. 2171–2178.

[115] Dreyer, D. and von Estorff, O., "Improved conditioning of infinite elements for exterior acoustics," *Int. J. Numer. Methods Eng.*, Vol. 58, No. 6, pp. 933–953, 2003.

[116] von Estorff, O., Petersen, S., and Dreyer, D., "Efficient infinite elements based on Jacobi polynomials," in *Computational Acoustics of Noise Propagation in Fluids - Finite and Boundary Element Methods*, Marburg, S. and Nolte, B., Eds. Springer Berlin Heidelberg, 2008, pp. 231–250.

[117] Dreyer, D., Petersen, S., and von Estorff, O., "Effectiveness and robustness of improved infinite elements for exterior acoustics," *Comput. Methods Appl. Mech. Eng.*, Vol. 195, No. 29-32, pp. 3591–3607, 2006.

[118] Dreyer, D., *Efficient infinite elements for exterior acoustics*. Shaker, 2004.

[119] Petersen, S., *Adaptive finite und infinite Elementemethoden in der Akustik*. Shaker, 2007.

[120] Biermann, J., von Estorff, O., Petersen, S., and Wenterodt, C., "Higher order finite and infinite elements for the solution of Helmholtz problems," *Comput. Methods Appl. Mech. Eng.*, Vol. 198, No. 13-14, pp. 1171–1188, 2009.

[121] Astley, R., Coyette, J.-P., and Cremers, L., "Three-dimensional wave-envelope elements of variable order for acoustic radiation and scattering. Part II. Formulation in the time domain," *J. Acoust. Soc. Am.*, Vol. 103, No. 1, pp. 64–72, 1998.

[122] van Ophem, S., Atak, O., Deckers, E., and Desmet, W., "Stable model order reduction for time-domain exterior vibro-acoustic finite element simulations," *Comput. Methods Appl. Mech. Eng.*, Vol. 325, pp. 240–264, 2017.

[123] Van Ophem, S. and Desmet, W., "Time-reversed infinite elements and their application to scatterer and source identification," in *INTER-NOISE and NOISE-CON Congress and Conference Proceedings*, Vol. 257, No. 1. Institute of Noise Control Engineering, 2018, pp. 751–762.

[124] Eversman, W., "Mapped infinite wave envelope elements for acoustic radiation in a uniformly moving medium," *J. Sound Vib.*, Vol. 224, No. 4, pp. 665–687, 1999.

[125] Hamilton, J. A. and Astley, R. J., "Acoustic propagation on irrotational mean flows using transient finite and infinite elements," *AIAA Journal*, Vol. 43, No. 1, pp. 124–134, 2005.

[126] Hohage, T. and Nannen, L., "Hardy space infinite elements for scattering and resonance problems," *SIAM J. Numer. Anal.*, Vol. 47, No. 2, pp. 972–996, 2009.

[127] Nannen, L. and Schädle, A., "Hardy space infinite elements for Helmholtz-type problems with unbounded inhomogeneities," *Wave Motion*, Vol. 48, No. 2, pp. 116–129, 2011.

[128] Shirron, J. J. and Dey, S., "Acoustic infinite elements for non-separable geometries," *Comput. Methods Appl. Mech. Eng.*, Vol. 191, No. 37-38, pp. 4123–4139, 2002.

[129] Yang, Y.-B., Kuo, S.-R., and Hung, H.-H., "Frequency-independent infinite elements for analysing semi-infinite problems," *Int. J. Numer. Methods Eng.*, Vol. 39, No. 20, pp. 3553–3569, 1996.

[130] Freymann, R., *Strukturdynamik: Ein anwendungsorientiertes Lehrbuch*. Springer-Verlag, 2011.

[131] Balay, S., Gropp, W. D., McInnes, L. C., and Smith, B. F., "Efficient management of parallelism in object oriented numerical software libraries," in *Modern Software Tools in Scientific Computing*, Arge, E., Bruaset, A. M., and Langtangen, H. P., Eds. Birkhäuser Press, 1997, pp. 163–202.

[132] Merz, S., Kessissoglou, N., Kinns, R., and Marburg, S., "Minimisation of the sound power radiated by a submarine through optimisation of its resonance changer," *J. Sound Vib.*, Vol. 329, No. 8, pp. 980–993, 2010.

[133] Malhotra, M. and PINSKY, P. M., "Efficient computation of multi-frequency far-field solutions of the Helmholtz equation using Padé approximation," *J. Comput. Acoust.*, Vol. 8, No. 01, pp. 223–240, 2000.

[134] Wagner, M. M., Pinsky, P. M., and Malhotra, M., "Application of Padé via Lanczos approximations for efficient multifrequency solution of Helmholtz problems," *J. Acoust. Soc. Am.*, Vol. 113, No. 1, pp. 313–319, 2003.

[135] Baumgart, J., Marburg, S., and Schneider, S., "Efficient sound power computation of open structures with infinite/finite elements and by means of the Padé-via-Lanczos algorithm," *J. Comput. Acoust.*, Vol. 15, No. 04, pp. 557–577, 2007.

[136] Jones, D., "The eigenvalues of $\nabla 2u + \lambda u = 0$ when the boundary conditions are given on semi-infinite domains," in *Mathematical Proceedings of the Cambridge Philosophical Society*, Vol. 49, No. 4. Cambridge University Press, 1953, pp. 668–684.

[137] Werner, P., "Ein Resonanzphänomen in der Theorie akustischer und elektromagnetischer Wellen," *Mathematical methods in the applied sciences*, Vol. 6, No. 1, pp. 104–128, 1984.

[138] Werner, P., "Zur Asymptotik der Wellengleichung und der Wärmeleitungsgleichung in zweidimensionalen Außenräumen," *Mathematical methods in the applied sciences*, Vol. 7, No. 1, pp. 170–201, 1985.

[139] Hein, S., Hohage, T., Koch, W., and Schöberl, J., "Acoustic resonances in a high-lift configuration," *J. Fluid Mech.*, Vol. 582, pp. 179–202, 2007.

[140] Koch, W., "Acoustic resonances and trapped modes in annular plate cascades," *J. Fluid Mech.*, Vol. 628, pp. 155–180, 2009.

[141] Hein, S., Koch, W., and Nannen, L., "Fano resonances in acoustics," *J. Fluid Mech.*, Vol. 664, pp. 238–264, 2010.

[142] Hein, S., Hohage, T., and Koch, W., "On resonances in open systems," *J. Fluid Mech.*, Vol. 506, pp. 255–284, 2004.

[143] Koch, W., "Acoustic resonances in rectangular open cavities," *AIAA Journal*, Vol. 43, No. 11, pp. 2342–2349, 2005.

[144] Hein, S. and Koch, W., "Acoustic resonances and trapped modes in pipes and tunnels," *J. Fluid Mech.*, Vol. 605, pp. 401–428, 2008.

[145] Hein, S., Koch, W., and Nannen, L., "Trapped modes and Fano resonances in two-dimensional acoustical duct-cavity systems," *J. Fluid Mech.*, Vol. 692, pp. 257–287, 2012.

[146] Duan, Y., Koch, W., Linton, C. M., and McIVER, M., "Complex resonances and trapped modes in ducted domains," *J. Fluid Mech.*, Vol. 571, pp. 119–147, 2007.

[147] Borgiotti, G. V., "The power radiated by a vibrating body in an acoustic fluid and its determination from boundary measurements," *J. Acoust. Soc. Am.*, Vol. 88, No. 4, pp. 1884–1893, 1990.

[148] Photiadis, D. M., "The relationship of singular value decomposition to wave-vector filtering in sound radiation problems," *J. Acoust. Soc. Am.*, Vol. 88, No. 2, pp. 1152–1159, 1990.

[149] Sarkissian, A., "Acoustic radiation from finite structures," *J. Acoust. Soc. Am.*, Vol. 90, No. 1, pp. 574–578, 1991.

[150] Cunefare, K. A., "The minimum multimodal radiation efficiency of baffled finite beams," *J. Acoust. Soc. Am.*, Vol. 90, No. 5, pp. 2521–2529, 1991.

[151] Elliott, S. J. and Johnson, M. E., "Radiation modes and the active control of sound power," *J. Acoust. Soc. Am.*, Vol. 94, No. 4, pp. 2194–2204, 1993.

[152] Cunefare, K. A. and Currey, M. N., "On the exterior acoustic radiation modes of structures," *J. Acoust. Soc. Am.*, Vol. 96, No. 4, pp. 2302–2312, 1994.

[153] Chen, P.-T. and Ginsberg, J. H., "Complex power, reciprocity, and radiation modes for submerged bodies," *J. Acoust. Soc. Am.*, Vol. 98, No. 6, pp. 3343–3351, 1995.

[154] Peters, H., Kessissoglou, N., and Marburg, S., "Enforcing reciprocity in numerical analysis of acoustic radiation modes and sound power evaluation," *J. Comput. Acoust.*, Vol. 20, No. 03, 2012.

[155] Kuijpers, A., Rienstra, S., Verbeek, G., and Verheij, J., "The acoustic radiation of baffled finite ducts with vibrating walls," *J. Sound Vib.*, Vol. 216, No. 3, pp. 461–493, 1998.

[156] Kessels, P. H. L., *Engineering toolbox for structural-acoustic design: Applied to MRI-scanners*. Technische Universiteit Eindhoven, 2001.

[157] Naghshineh, K., Koopmann, G. H., and Belegundu, A. D., "Material tailoring of structures to achieve a minimum radiation condition," *J. Acoust. Soc. Am.*, Vol. 92, No. 2, pp. 841–855, 1992.

[158] Peters, H., Kessissoglou, N., and Marburg, S., "Modal decomposition of exterior acoustic-structure interaction," *J. Acoust. Soc. Am.*, Vol. 133, No. 5, pp. 2668–2677, 2013.

[159] Peters, H., Kessissoglou, N., and Marburg, S., "Modal decomposition of exterior acoustic-structure interaction problems with model order reduction," *J. Acoust. Soc. Am.*, Vol. 135, No. 5, pp. 2706–2717, 2014.

[160] Marburg, S., Lösche, E., Peters, H., and Kessissoglou, N., "Surface contributions to radiated sound power," *J. Acoust. Soc. Am.*, Vol. 133, No. 6, pp. 3700–3705, 2013.

[161] Wu, H., Jiang, W., and Liu, Y., "Analyzing acoustic radiation modes of baffled plates with a fast multipole boundary element method," *J. Vib. Acoust.*, Vol. 135, No. 1, p. 011007, 2013.

[162] Liu, Z.-B. and Maury, C., "An improved method for the calculation of near-field acoustic radiation modes," *J. Sound Vib.*, Vol. 363, pp. 316–328, 2016.

[163] Ji, L. and Bolton, J. S., "Sound power radiation from a vibrating structure in terms of structure-dependent radiation modes," *J. Sound Vib.*, Vol. 335, pp. 245–260, 2015.

[164] Liu, J., Liu, Y., and Bolton, J., "A study of the frequency and shape dependency of acoustic radiation modes," in *47th International Congress and Exposition on Noise Control Engineering, INTER-NOISE, 26-29 August 2018, Chicago, Illinois, USA*, 2018.

[165] Liu, J., Liu, Y., and Bolton, J. S., "Acoustic source reconstruction and visualization based on acoustic radiation modes," *J. Sound Vib.*, Vol. 437, pp. 358–372, 2018.

[166] Jones, C. B., Goates, C. B., Blotter, J. D., and Sommerfeldt, S. D., "Experimental validation of determining sound power using acoustic radiation modes and a laser vibrometer," *Applied Acoustics*, Vol. 164, p. 107254, 2020.

[167] Ruge, P., "Eigenvalues of damped structures: Vectoriteration in the original space of DOF," *Comput. Mech.*, Vol. 22, No. 2, pp. 167–173, 1998.

[168] Tisseur, F. and Meerbergen, K., "The quadratic eigenvalue problem," *SIAM Rev.*, Vol. 43, No. 2, pp. 235–286, 2001.

[169] Marburg, S., Dienerowitz, F., Fritze, D., and Hardtke, H.-J., "Case studies on structural-acoustic optimization of a finite beam," *Acta Acustica united with Acustica*, Vol. 92, No. 3, pp. 427–439, 2006.

[170] Wu, S. F., "On reconstruction of acoustic pressure fields using the Helmholtz equation least squares method," *J. Acoust. Soc. Am.*, Vol. 107, No. 5, pp. 2511–2522, 2000.

[171] Astley, R. and Hamilton, J., "The stability of infinite element schemes for transient wave problems," *Comput. Methods Appl. Mech. Eng.*, Vol. 195, No. 29-32, pp. 3553–3571, 2006.

[172] Goursaud, B., Hazard, C., and Prieto, A., "Pseudospectrum analysis of resonances in cavities with perfectly matched layers," in *3rd International Conference on Computational Methods in Structural Dynamics and Earthquake Engineering*, Papadrakakis, M., Fragiadakis, M., and Plevris, V., Eds., COMPDYN 2011, Corfu, Greece. National Technical University of Athens, 2011.

[173] Trefethen, L. N. and Embree, M., *Spectra and pseudospectra: The behavior of nonnormal matrices and operators*. Princeton University Press, 2005.

[174] Kaltenbacher, M., *Computational acoustics*. Springer, 2018.

[175] Kaltenbacher, M., "Fundamental equations of acoustics," in *Computational acoustics*, Kaltenbacher, M., Ed. Springer, 2018, Ch. 1, pp. 1–33.

[176] Bärwolff, G., *Höhere Mathematik für Naturwissenschaftler und Ingenieure (Advanced mathematics for scientists and engineers)*. Spektrum Akademischer Verlag, 2004, Vol. 2.

[177] Sommerfeld, A., "Die Greensche Funktion der Schwingungsgleichung," *Jahresbericht der Deutschen Mathematiker-Vereinigung*, Vol. 21, pp. 309–353, 1912.

[178] Atkinson, F., "On sommerfeld's "radiation condition."," *The London, Edinburgh, and Dublin Philosophical Magazine and Journal of Science*, Vol. 40, No. 305, pp. 645–651, 1949.

[179] Schot, S. H., "Eighty years of Sommerfeld's radiation condition," *Historia Mathematica*, Vol. 19, No. 4, pp. 385 – 401, 1992.

[180] De Bruijn, N. G., *Asymptotic methods in analysis*. Courier Corporation, 1981, Vol. 4.

[181] Rellich, F., "Über das asymptotische Verhalten der Lösungen von $\Delta u + \lambda u = 0$ in unendlichen Gebieten," *Jahresbericht der Deutschen Mathematiker-Vereinigung*, Vol. 53, pp. 57–65, 1943.

[182] Sommerfeld, A., "Partielle Differentialgleichungen der Physik, Vorlesungen über Theoretische Physik," *Verlag Harri Deutsch*, Vol. 6, 1947.

[183] Langer, P., Maeder, M., Guist, C., Krause, M., and Marburg, S., "More than six elements per wavelength: The practical use of structural finite element models and their accuracy in comparison with experimental results," *J. Comput. Acoust.*, p. 1750025, 2017.

[184] Arfken, G. B., *Mathematical Methods for Physicists*. Academic press, 1985, Vol. 3.

[185] Marburg, S. and Hardtke, H.-J., "A study on the acoustic boundary admittance. Determination, results and consequences," *Eng. Anal. Boundary Elem.*, Vol. 23, No. 9, pp. 737–744, 1999.

[186] Coyette, J.-P. and Van den Nieuwenhof, B., "A conjugated infinite element method for half-space acoustic problems," *J. Acoust. Soc. Am.*, Vol. 108, No. 4, pp. 1464–1473, 2000.

[187] Marques, J. M. M. C. and Owen, D. R. J., "Infinite elements in quasi-static materially nonlinear problems," *Computers & Structures*, Vol. 18, No. 4, pp. 739–751, 1984.

[188] Wilcox, C. H., "A generalization of theorems of Rellich and Atkinson," *Proc. Amer. Math. Soc.*, Vol. 7, No. 2, pp. 271–276, 1956.

[189] Cunefare, K. A. and Koopmann, G. H., "Global optimum active noise control: Surface and far-field effects," *J. Acoust. Soc. Am.*, Vol. 90, No. 1, pp. 365–373, 1991.

[190] Gerdes, K. and Demkowicz, L., "Solution of 3D-Laplace and Helmholtz equations in exterior domains using hp-infinite elements," *Comput. Methods Appl. Mech. Eng.*, Vol. 137, No. 3-4, pp. 239–273, 1996.

[191] Nobile, M. A. and Hayek, S. I., "Acoustic propagation over an impedance plane," *J. Acoust. Soc. Am.*, Vol. 78, No. 4, pp. 1325–1336, 1985.

[192] Ochmann, M. and Brick, H., "Acoustical radiation and scattering above an impedance plane," in *Computational Acoustics of Noise Propagation in Fluids - Finite and Boundary Element Methods*, Marburg, S. and Nolte, B., Eds. Berlin, Heidelberg: Springer Berlin Heidelberg, 2008, pp. 459–494.

[193] Melnikov, A., Chiang, Y. K., Quan, L., Oberst, S., Alù, A., Marburg, S., and Powell, D., "Acoustic meta-atom with experimentally verified maximum willis coupling," *Nat. Commun.*, Vol. 10, No. 1, pp. 1–7, 2019.

[194] Martínez-Sala, R., Sancho, J., Sánchez, J. V., Gómez, V., Llinares, J., and Meseguer, F., "Sound attenuation by sculpture," *Nature*, Vol. 378, No. 6554, p. 241, 1995.

[195] Montiel, F., Chung, H., Karimi, M., and Kessissoglou, N., "An analytical and numerical investigation of acoustic attenuation by a finite sonic crystal," *Wave Motion*, Vol. 70, pp. 135–151, 2017.

[196] Brillouin, L., *Wave propagation in periodic structures: Electric filters and crystal lattices*. Dover, 1953.

[197] Bloch, F., "Über die Quantenmechanik der Elektronen in Kristallgittern (On the quantum mechanics of electrons in crystal lattices)," *Zeitschrift für Physik*, Vol. 52, No. 7-8, pp. 555–600, 1929.

[198] Elford, D. P., Chalmers, L., Kusmartsev, F. V., and Swallowe, G. M., "Matryoshka locally resonant sonic crystal," *J. Acoust. Soc. Am.*, Vol. 130, No. 5, pp. 2746–2755, 2011.

[199] Claeys, C. C., Vergote, K., Sas, P., and Desmet, W., "On the potential of tuned resonators to obtain low-frequency vibrational stop bands in periodic panels," *J. Sound Vib.*, Vol. 332, No. 6, pp. 1418–1436, 2013.

[200] Sanchez-Perez, J. V., Rubio, C., Martinez-Sala, R., Sanchez-Grandia, R., and Gomez, V., "Acoustic barriers based on periodic arrays of scatterers," *Appl. Phys. Lett.*, Vol. 81, No. 27, pp. 5240–5242, 2002.

[201] Martins, M., Godinho, L., and Picado-Santos, L., "Numerical evaluation of sound attenuation provided by periodic structures," *Archives of Acoustics*, Vol. 38, No. 4, pp. 503–516, 2013.

[202] Koussa, F., Defrance, J., Jean, P., and Blanc-Benon, P., "Acoustical efficiency of a sonic crystal assisted noise barrier," *Acta Acustica united with Acustica*, Vol. 99, No. 3, pp. 399–409, 2013.

[203] Umnova, O., Attenborough, K., and Linton, C. M., "Effects of porous covering on sound attenuation by periodic arrays of cylinders," *J. Acoust. Soc. Am.*, Vol. 119, No. 1, pp. 278–284, 2006.

[204] Retka, S., "Numerische Umsetzung der Galbrun-Gleichung zur Modalanalyse strömender Medien in Außenraumproblemen unter Einsatz finiter und infiniter Elemente," Ph.D. dissertation, Institute of Mechanics, Universität der Bundeswehr München, Neubiberg, 2012.

[205] Chalmers, L., Elford, D. P., Kusmartsev, F. V., and Swallowe, G. M., "Acoustic band gap formation in two-dimensional locally resonant sonic crystals comprised of Helmholtz resonators," *Int. J. Modern Physics B*, Vol. 23, No. 20n21, pp. 4234–4243, 2009.

[206] Cheng, Y., Zhou, C., Yuan, B., Wu, D., Wei, Q., and Liu, X., "Ultra-sparse metasurface for high reflection of low-frequency sound based on artificial mie resonances," *Nat. Mater.*, Vol. 14, No. 10, p. 1013, 2015.

[207] Lu, G., Ding, E., Wang, Y., Peng, X., Cui, J., Liu, X., and Liu, X., "Realization of acoustic wave directivity at low frequencies with a subwavelength mie resonant structure," *Appl. Phys. Lett.*, Vol. 110, No. 12, p. 123507, 2017.

[208] Barbarosie, C., "Shape optimization of periodic structures," *Comput. Mech.*, Vol. 30, No. 3, pp. 235–246, 2003.

[209] Sigmund, O. and Søndergaard Jensen, J., "Systematic design of phononic band–gap materials and structures by topology optimization," *Philosophical Transactions of the Royal Society of London. Series A: Mathematical, Physical and Engineering Sciences*, Vol. 361, No. 1806, pp. 1001–1019, 2003.

[210] Ewins, D., "Vibration characteristics of bladed disc assemblies," *J. Mech. Eng. Sc.*, Vol. 15, No. 3, pp. 165–186, 1973.

[211] Irwanto, B., Hardtke, H.-J., and Pawandenat, D., "An efficient technique for the computation of eigenvalue and eigenvector derivatives of cyclic structures," *Computers & Structures*, Vol. 81, No. 24-25, pp. 2395–2400, 2003.

[212] Allemang, R. J., "The modal assurance criterion–twenty years of use and abuse," *J. Sound Vib.*, Vol. 37, No. 8, pp. 14–23, 2003.

[213] Mulder, W., "Spurious modes in finite-element discretizations of the wave equation may not be all that bad," *Appl. Numer. Math.*, Vol. 30, No. 4, pp. 425–445, 1999.

[214] Bermúdez, A., Durán, R. G., Rodríguez, R., and Solomin, J., "Finite element analysis of a quadratic eigenvalue problem arising in dissipative acoustics," *SIAM J. Numer. Anal.*, Vol. 38, No. 1, pp. 267–291, 2000.

[215] Balay, S., Abhyankar, S., Adams, M. F., Brown, J., Brune, P., Buschelman, K., Dalcin, L., Eijkhout, V., Gropp, W. D., Kaushik, D., Knepley, M. G., May, D. A., McInnes, L. C., Mills, R. T., Munson, T., Rupp, K., Sanan, P., Smith, B. F., Zampini, S., Zhang, H., and Zhang, H., "PETSc users manual," Argonne National Laboratory, Tech. Rep. ANL-95/11 - Revision 3.9, 2018. [Online]. Available: http://www.mcs.anl.gov/petsc

[216] Hernandez, V., Roman, J. E., and Vidal, V., "SLEPc: A scalable and flexible toolkit for the solution of eigenvalue problems," *ACM Trans. Math. Software*, Vol. 31, No. 3, pp. 351–362, 2005.

[217] Balay, S., Abhyankar, S., Adams, M. F., Brown, J., Brune, P., Buschelman, K., Dalcin, L., Eijkhout, V., Gropp, W. D., Kaushik, D., Knepley, M. G., May, D. A., McInnes, L. C., Mills, R. T., Munson, T., Rupp, K., Sanan, P., Smith, B. F., Zampini, S., Zhang, H., and Zhang, H., "PETSc Web page," 2018. [Online]. Available: http://www.mcs.anl.gov/petsc

[218] Marburg, S., "Boundary element method for time-harmonic acoustic problems," in *Computational acoustics*, Kaltenbacher, M., Ed. Springer, 2018, Ch. 3, pp. 69–158.

[219] Wylie, C. R., Barrett, L. C., and Wylie, C. R., *Advanced engineering mathematics*. McGraw-Hill New York, 1960.

[220] Fahy, F. and Walker, J., *Advanced applications in acoustics, noise and vibration*. CRC Press, 2018.

[221] Prieto, A., Personal communication, A Coruña, Spain, 2018.

Appendices

Publication A, pp. 62-83

Infinite elements and their influence on normal and radiation modes in exterior acoustics

Publication B, pp. 84-103

Normal modes and modal reduction in exterior acoustics

Publication C, pp. 104-129

Analysis of scattering by finite sonic crystals in free field with infinite elements and normal modes

Publication A

Journal of Computational Acoustics, Vol. 25, No. 4 (2017) 1650020 (20 pages)

DOI: 10.1142/S0218396X1650020X

INTERNATIONAL ASSOCIATION
FOR MATHEMATICS AND
COMPUTERS IN SIMULATION

Infinite Elements and Their Influence on Normal and Radiation Modes in Exterior Acoustics

Lennart Moheit* and Steffen Marburg
Chair of Vibroacoustics of Vehicles and Machines
Department of Mechanical Engineering
Technische Universität München
Boltzmannstraße 15, 85748 Garching, Germany
**Lennart.Moheit@tum.de*

Received 9 May 2016
Accepted 14 July 2016
Published 14 March 2017

Acoustic radiation modes (ARMs) and normal modes (NMs) are calculated at the surface of a fluid-filled domain around a solid structure and inside the domain, respectively. In order to compute the exterior acoustic problem and modes, both the finite element method (FEM) and the infinite element method (IFEM) are applied. More accurate results can be obtained by using finer meshes in the FEM or higher-order radial interpolation polynomials in the IFEM, which causes additional degrees of freedom (DOF). As such, more computational cost is required. For this reason, knowledge about convergence behavior of the modes for different mesh cases is desirable, and is the aim of this paper. It is shown that the acoustic impedance matrix for the calculation of the radiation modes can be also constructed from the system matrices of finite and infinite elements instead of boundary element matrices, as is usually done. Grouping behavior of the eigenvalues of the radiation modes can be observed. Finally, both kinds of modes in exterior acoustics are compared in the example of the cross-section of a recorder in air. When the number of DOF is increased by using higher-order radial interpolation polynomials, different eigenvalue convergences can be observed for interpolation polynomials of even and odd order.

Keywords: Infinite element method (IFEM); normal modes; acoustic radiation modes.

1. Introduction

The discretization and calculation of an acoustic exterior problem involves the problem of an infinite, unbounded domain with a nonreflecting boundary condition at the outside of the fluid-filled domain. Finite elements are only applicable for the discretization

of inner, circumscribed domains and imply reflecting outer borders. Two approaches have been established in order to calculate acoustic exterior problems numerically: Perfectly matched layers (PML)[1] and the infinite element method (IFEM).[2,3] The method of conjugated Astley–Leis infinite elements is applied by the authors, since these elements provide the frequency-independent system matrices of stiffness, damping and mass on the basis of the corresponding FE matrices. These system matrices are required for further investigations in modal decomposition. The IFEM implies the Sommerfeld radiation condition,[2,4] which provides a nonreflective boundary condition and decay to zero of the sound pressure at infinity. The sound pressure field in the radial direction in the domain with the infinite elements is interpolated by polynomials such as Lagrange polynomials, Legendre polynomials or Jacobi polynomials, which lead to differences in the matrix condition number of the discrete, global system matrices.[5,6]

The subject of this paper is the investigation of the influence of the choice of finite elements and the polynomial type for infinite element interpolation in the radial direction as well as the choice of the order of these polynomials on modes in exterior acoustics. The authors consider acoustic radiation modes (ARMs)[7–9] and normal modes (NMs),[10–12]which are based on eigenvalue problems of the acoustic impedance matrix $\mathbf{Z}_R$ and of a state-space formulation consisting of the discrete system matrices of stiffness, damping and mass, respectively.

The concept of radiation modes can be traced back to investigations of radiating velocity distributions carried out by Borgiotti[7] and Photiadis[8] and eigenvalue analysis of the real part of the impedance matrix performed by Sarkissian.[9] Cunefare and Currey[13–15] focus on the grouping behavior of the eigenvalues and radiation efficiencies. This line of research is further explored by Peters *et al.*[16] who investigate the symmetry characteristics of the real impedance matrix. Recent studies by Wu *et al.*[17] investigate fast multipole BEM and iterative methods for efficiently and accurately calculating the ARMs and the radiation efficiencies in the example of a baffled plate. Marburg *et al.*[18] apply ARMs in order to obtain surface contributions to the radiated sound power, which they compare to the acoustic intensity. Liu and Maury[19] focus on improvements to the ARMs in the near field of vibrating structures.

ARMs are regarded as frequency-dependent modes, because they have to be calculated separately for each frequency as opposed to NMs, which are obtained by solving of a single frequency-independent eigenvalue problem. The concept of NMs is extensively presented by Marburg *et al.*[10–12] Investigations of search algorithms for NM eigenvalues were carried out by Fuß *et al.*[20] with the example of a recorder as a long, slender and hollow object. By solving the Galbrun equation with an application of infinite elements, Retka and Marburg[21] solve the state-space eigenvalue problem for a duct with a thin wall and openings on both sides, while taking flow into consideration.

In the context of this paper, the authors will calculate the acoustic impedance matrix $\mathbf{Z}_R$ from FEM and IFEM system matrices rather than the boundary element method (BEM) as is suggested in the literature.[16,22] Recent studies on BEM in exterior acoustics were

published by Ramesh *et al.*[23] and Marburg.[24,25] The method is also applied for eigenvalue analysis in the exterior acoustic problem by Zheng *et al.*[26]

The convergence of the infinite elements was shown by Demkowicz and Gerdes[27,28] and proves the reliability of the approach, but there have been no studies yet on the influence of the infinite elements on modes in exterior acoustics. This paper will first give an overview of the formulation of the infinite elements and of the suitability of the considered polynomials as radial interpolation functions. Following this, both modes in exterior acoustics are summarized. In the simple example model of a circle in an unbounded domain, the reliability of the ARM approach is validated, using FEM and IFEM instead of BEM. Subsequently, the model of a cross-section of a recorder is considered.

Both ARMs and NMs are compared to each other and the influence of different radial interpolation polynomials and of different FE mesh sizes on the modes is discussed and interpreted. Afterwards, their convergence behavior is investigated as the degree of the radial interpolation polynomial is increased. Here, the convergence of the NM eigenvalues is obtained by application of the Modal Assurance Criterion (MAC).[29] Two different convergences are observed for even and odd orders of the interpolation polynomials for both ARM and NM eigenvalues.

2. Infinite Element Formulation

2.1. *Acoustics and discretization of the unbounded domain*

The spatial sound pressure field $p(\mathbf{x})$ in a fluid-filled domain can be described by the Helmholtz equation

$$\nabla^2 p(\mathbf{x}) + k^2 p(\mathbf{x}) = 0, \quad \mathbf{x} \in \Omega \subset \mathbb{R}^2, \tag{1}$$

where $k = \omega/c_f$ is the wave number with the angular frequency $\omega = 2\pi f$ and the speed of sound in the fluid c_f. At infinity the nonreflective Sommerfeld radiation condition causes the sound pressure to decay to zero.[2,4] On the surface of an obstacle, the normal fluid particle velocity $v_f(\mathbf{x})$ is assumed to be equal to the structural particle velocity $v_s(\mathbf{x})$. In other words, the coupling of the fluid and the structure is nondispersive.

Applying the finite element method (FEM) and IFEM leads to a discrete system of linear equations[30]

$$(\mathbf{K} - ik\mathbf{D} - k^2\mathbf{M})\mathbf{p} = i\omega\rho_f \mathbf{\Theta}\mathbf{v}_s = \mathbf{f}, \tag{2}$$

where ρ_f is the density of the fluid, $\mathbf{K}$, $\mathbf{D}$ and $\mathbf{M}$ are the system matrices for stiffness, damping and mass and $\mathbf{\Theta}$ is the boundary mass matrix, which was given by Marburg and Nolte[30] in discrete form

$$\mathbf{\Theta} = \int_\Gamma \Phi(\mathbf{x})\Phi^T(\mathbf{x}) \mathrm{d}\Gamma(\mathbf{x}). \tag{3}$$

The basis functions $\Phi(\mathbf{x})$ are required for the discretization of the sound pressure and the structural velocity at the surface of a solid structure in the fluid-filled domain

$$p(\mathbf{x}) = \sum_{l=1}^{N} \phi_l(\mathbf{x}) p_l = \Phi^T(\mathbf{x})\mathbf{p}, \tag{4}$$

$$v_s(\mathbf{x}) = \sum_{l=1}^{N} \phi_l(\mathbf{x}) v_{s,l} = \Phi^T(\mathbf{x})\mathbf{v}_s. \tag{5}$$

In the finite element domain, typical linear or quadratic Lagrangian basis functions as described by Ihlenburg[4] are applied.

The subsequent considerations use the concept of the so-called (mapped and conjugated) *Astley–Leis* infinite elements in reference to works by Astley *et al.*[2,3,31,32] as well as by Shirron and Babuška.[5] These elements are attached to the outer boundary of the finite elements to extend the fluid to infinity in the radial direction. The coordinate mapping is given in detail by Marques and Owen.[33] Here, it is sufficient to state that the global radial coordinate r is related to the local radial coordinate s by

$$\frac{a(t)}{r} = \frac{1-s}{2}, \tag{6}$$

where $a(t)$ is the radius of the circular boundary line between the FE and IFE domains as a function of the elementwise, local transverse coordinate t. Both s and t are defined in the range $[-1, 1]$. In the mapping in Eq. (6), the local radial distances $s = -1$, $s = 0$ and $s = 1$ correspond to $r = a(t)$, $r = 2a(t)$ and $r = \infty$ in the global space, respectively.

The frequency-dependent basis functions are constructed using an interpolation function $I_l(s,t)$ and a phase function $\mu(s,t)$, both of which are functions of the mapped coordinates s and t

$$\phi_l(s,t,\omega) = I_l(s,t) e^{-ik\mu(s,t)}, \tag{7}$$

where the phase function is given by

$$\mu(s,t) = a(t)\frac{1+s}{1-s}. \tag{8}$$

The interpolation function contains the product of the radial $P^s(s)$ and transverse $P^t(t)$ polynomial functions and a geometric factor to satisfy the Sommerfeld radiation condition. According to Shirron and Babuška,[5] the interpolation function in the two-dimensional case is defined as

$$I_l(s,t) = \sqrt{\frac{(1-s)}{2}} P^t_{l_t}(t) P^s_{l_s}(s), \tag{9}$$

such that $l = 1 \ldots n_{\mathrm{tr}} \cdot n_{\mathrm{rad}}$, where $l_t = 1 \ldots n_{\mathrm{tr}}$ is an index for the transverse interpolation polynomials and $l_s = 1 \ldots n_{\mathrm{rad}}$ is an index for the radial interpolation polynomials.

Investigations by von Estorff and Dreyer *et al.*[6,34] prove poor suitability of Lagrangian polynomials for higher orders and achieve better performance with Legendre and Jacobi polynomials. This was shown by calculating the condition number of the dynamic stiffness

matrix $\mathbf{A}$ in the system of linear equations in Eq. (2)

$$\mathbf{A}(\omega)\mathbf{p}(\omega) = (\mathbf{K} - ik\mathbf{D} - k^2\mathbf{M})\mathbf{p}(\omega) = \mathbf{f}(\omega). \tag{10}$$

Solving for the column vector $\mathbf{p}$ gives the unknown nodal pressure values p_k, which can be used to construct a continuous trial solution $\bar{p}(\mathbf{x}, \omega)$

$$\bar{p}(\mathbf{x}, \omega) \approx \sum_{k=1}^{N} p_k(\omega)\phi_k(s, t, \omega) = \mathbf{p}(\omega)\Phi(s, t, \omega) \tag{11}$$

with the infinite element basis functions $\phi_k(s, t, \omega)$ that are given in Eq. (7).

For conjugated Astley–Leis elements,[31] the test functions $\bar{q}(s, t, \omega)$ use the complex conjugates of the basis functions with an additional geometric weighting factor $(a/r)^2 = (1 - s)^2/4$ such that

$$\bar{q}(\mathbf{x}, \omega) \approx \left(\frac{1 - s}{2}\right)^2 \mathbf{p}(\omega)\Phi^*(s, t, \omega). \tag{12}$$

Taking the complex conjugates of the basis functions in the trial and test functions leads to the canceling of the frequency-dependent exponential term in Eq. (7) when the variational statement is formulated. The obtained stiffness, damping and mass matrices of the system are thus independent of frequency.

2.2. *Choice of radial polynomials*

Whereas in early infinite element concepts[35,36] solely Lagrangian polynomials were used for the radial interpolation functions, Legendre and Jacobi polynomials were found to be a good alternative in terms of improved matrix conditioning and performance.[3,5,6]

2.2.1. *Lagrange polynomials*

Lagrange polynomials are often applied as shape functions in FEM and were used in early concepts of Astley–Leis infinite elements, but led to ill-conditioned system matrices due to oscillatory behavior at high radial orders.[6] They are given by

$$P_j^s(s) = \prod_{\substack{k=1\ldots N \\ k \neq j}} \frac{s - s_k}{s_j - s_k} \tag{13}$$

and satisfy the condition that $P_j^s(s_i) = \delta_{ij}$, where δ_{ij} is the Kronecker delta. The transition at the boundary between FE and IFE domain is thus compatible.

2.2.2. *Legendre polynomials*

In order to improve the stability of the infinite element concept, Legendre polynomials $P_i^s(s)$ are applied such that they are orthogonal with respect to the product

$$\int_{-1}^{1} P_i^s(s)P_j^s(s)\mathrm{d}s = \mu_i\delta_{ij}, \tag{14}$$

where μ_i is a given constant. To ensure compatibility with the adjacent Lagrangian-discretized FE domain, the application of a shift pattern as described by Shirron and Babuška[5] is required.

2.2.3. *Jacobi polynomials*

As a generalization of the Legendre polynomials, Jacobi polynomials $P_i^s(s)$ were introduced by Dreyer and von Estorff[6] as radial interpolation functions for infinite elements. They are orthogonal with respect to the product

$$\int_{-1}^{1}(1-s)^{\alpha}(1+s)^{\beta}P_i^s(s)P_j^s(s)\mathrm{d}s = \mu_i\delta_{ij} \tag{15}$$

and depend on the choice of the parameters α and β. The product of trial and test functions in the variational statement in the two-dimensional case is of the same form as the orthogonality relationship of the Jacobi polynomials when $\alpha = 1$ and $\beta = 0$

$$\Phi_i(s,t)\Phi_j(s,t)^* = I_i(s,t)e^{-ik\mu(s,t)}I_j(s,t)e^{+ik\mu(s,t)} \sim \frac{(1-s)}{2}P_i^s(s)P_j^s(s), \tag{16}$$

which matches well with the orthogonality property.[34] The same shift pattern as for Legendre polynomials is applied.

2.2.4. *Shift pattern for polynomials*

The radial interpolation functions have to adapt to the Lagrangian finite-element interpolation. Therefore, the first radial polynomial is chosen to satisfy $P_1^s(-1) = 1$ on the boundary between the FE and IFE domains where $s = -1$. The remaining polynomials have to vanish at the infinite element base $P_i^s(-1) = 0$ with $1 < i \leq N$ by application of a constant shift as suggested by Shirron and Babuška[5]

$$P_i^s(s) = \begin{cases} 0, & i = 1, \\ \bar{P}_i^s(s) + 1, & i = 2n, \\ \bar{P}_i^s(s) - 1, & i = 2n+1, \end{cases} \qquad n \in \mathbb{N}, \tag{17}$$

where $\bar{P}_i^s(s)$ denotes the unshifted polynomial for radial interpolation. The constant shift is required if Legendre or Jacobi polynomials are chosen.

3. Normal and Acoustic Radiation Modes in Exterior Acoustics

3.1. *Normal modes*

Starting from the discrete, linear system of equations in Eq. (2), NMs can be found as the eigenvectors of the state-space formulation

$$(\mathbf{A} + ik\mathbf{B})\mathbf{z} = \mathbf{r} \tag{18}$$

with $\mathbf{r}^T = [\mathbf{0}, -\mathbf{f}] = [\mathbf{0}, -i\omega\rho_f \boldsymbol{\Theta}\mathbf{v}_s]$, where the hypermatrices $\mathbf{A}$ and $\mathbf{B}$ are constructed from the stiffness, damping and mass matrices

$$\mathbf{A} = \begin{bmatrix} \mathbf{M} & \mathbf{0} \\ \mathbf{0} & -\mathbf{K} \end{bmatrix}, \quad \mathbf{B} = \begin{bmatrix} \mathbf{0} & \mathbf{M} \\ \mathbf{M} & \mathbf{D} \end{bmatrix} \quad \text{and} \quad \mathbf{z} = \begin{bmatrix} -ik\mathbf{p} \\ \mathbf{p} \end{bmatrix}. \tag{19}$$

From the asymmetry of the stiffness and damping matrices, left and right eigenvectors are obtained[11]

$$(\mathbf{A} - \kappa\mathbf{B})\mathbf{x}_z = \mathbf{0} \quad \text{and} \quad \mathbf{y}_z^T(\mathbf{A} - \kappa\mathbf{B}) = \mathbf{0}, \tag{20}$$

which can be written in terms of the modal matrices $\mathbf{Y}$ and $\mathbf{X}$, which diagonalize $\mathbf{A}$ and $\mathbf{B}$

$$\mathbf{Y}_z^T\mathbf{A}\mathbf{X}_z = \text{diag}(\alpha_1, \ldots, \alpha_{2N-\delta}), \tag{21}$$

$$\mathbf{Y}_z^T\mathbf{B}\mathbf{X}_z = \text{diag}(\beta_1, \ldots, \beta_{2N-\delta}). \tag{22}$$

On the resulting diagonals, α_j and β_j can be found, the ratio of which is defined to be the jth NM eigenvalue $\kappa_j = \alpha_j/\beta_j$. Applying an additional scaling of $c_f/2\pi$ leads to a form in which the imaginary part of κ_j corresponds to the resonance frequency of the jth mode.[10] The real part of the NM eigenvalues represents a damping term.

3.2. *Acoustic radiation modes*

The eigenvalue problem of the real part of the frequency-dependent and symmetric impedance matrix $\mathbf{Z}$ leads to the eigenvalues λ_j and their corresponding right eigenvectors as mode shapes at the surface of solid structures, known as ARMs.[9] The acoustic impedance matrix can be derived from a quadratic form for the sound power in terms of the nodal velocity vector[22]

$$P = 0.5\mathbf{v}_\Gamma^T \Re\{\mathbf{Z}\}\mathbf{v}_\Gamma^*. \tag{23}$$

This is derived from the discrete formulation by means of the sound pressure and the structural velocity[11]

$$P = 0.5\Re\{\mathbf{p}_\Gamma^T \boldsymbol{\Theta}_{\Gamma\Gamma}\mathbf{v}_\Gamma^*\}, \tag{24}$$

where the subscript Γ ranges over the degrees of freedom (DOF) associated with the surface of the structure. The calculated sound power thus depends only on the choice of the impedance matrix $\mathbf{Z}$, which is often calculated from the boundary element method (BEM) matrices $\mathbf{G}$ and $\mathbf{H}$.[22] The relationship $\mathbf{H}\mathbf{p}_\Gamma = \mathbf{G}\mathbf{v}_\Gamma$ is rearranged for $\mathbf{p}_\Gamma^T$ and then substituted into the discrete expression for the sound power in Eq. (24), so that the real part of the acoustic impedance matrix can be found in the inner of the product of the nodal velocity vectors as given in Eq. (23). Peters *et al.*[16] show that $\mathbf{Z}_R = \Re\{\mathbf{Z}\}$ is required to be symmetric or — if not the case — can easily be symmetrized.

In this paper, the acoustic impedance matrix is obtained by fully inverting the system matrix $\mathbf{A}$ constructed by FEM and IFEM. The discrete system of linear equations (2) is subdivided into the DOF on the boundary of the solid structure (marked with the

subscript Γ) and those associated with the fluid (marked with the subscript $\circ$)

$$\begin{bmatrix} \mathbf{A}_{\Gamma\Gamma} & \mathbf{A}_{\Gamma\circ} \\ \mathbf{A}_{\circ\Gamma} & \mathbf{A}_{\circ\circ} \end{bmatrix} \begin{bmatrix} \mathbf{p}_\Gamma \\ \mathbf{p}_\circ \end{bmatrix} = -i\omega\rho_f \begin{bmatrix} \mathbf{\Theta}_{\Gamma\Gamma} & \mathbf{\Theta}_{\Gamma\circ} \\ \mathbf{\Theta}_{\circ\Gamma} & \mathbf{\Theta}_{\circ\circ} \end{bmatrix} \begin{bmatrix} \mathbf{v}_\Gamma \\ \mathbf{v}_\circ. \end{bmatrix} = \begin{bmatrix} \mathbf{f}_\Gamma \\ \mathbf{f}_\circ. \end{bmatrix}. \tag{25}$$

Written out in full and considering that there is no structural velocity in the fluid (i.e. $\mathbf{v}_\circ = 0$) gives

$$\mathbf{A}_{\Gamma\Gamma}\mathbf{p}_\Gamma + \mathbf{A}_{\Gamma\circ}\mathbf{p}_\circ = -i\omega\rho_f\mathbf{\Theta}_{\Gamma\Gamma}\mathbf{v}_\Gamma, \tag{26}$$

$$\mathbf{A}_{\circ\Gamma}\mathbf{p}_\Gamma + \mathbf{A}_{\circ\circ}\mathbf{p}_\circ = -i\omega\rho_f\mathbf{\Theta}_{\circ\Gamma}\mathbf{v}_\Gamma. \tag{27}$$

Solving the latter equation (27) for the sound pressure in the fluid $\mathbf{p}_\circ$ leads to

$$\mathbf{p}_\circ = \mathbf{A}_{\circ\circ}^{-1}[-i\omega\rho_f\mathbf{\Theta}_{\circ\Gamma}\mathbf{v}_\Gamma - \mathbf{A}_{\circ\Gamma}\mathbf{p}_\Gamma], \tag{28}$$

which is then substituted in Eq. (26) and rearranged, so that

$$[\mathbf{A}_{\Gamma\Gamma} - \mathbf{A}_{\Gamma\circ}\mathbf{A}_{\circ\circ}^{-1}\mathbf{A}_{\circ\Gamma}]\mathbf{p}_\Gamma = -i\omega\rho_f[\mathbf{\Theta}_{\Gamma\Gamma} - \mathbf{A}_{\Gamma\circ}\mathbf{A}_{\circ\circ}^{-1}\mathbf{\Theta}_{\circ\Gamma}]\mathbf{v}_\Gamma. \tag{29}$$

This expression has to be rearranged in order to substitute $\mathbf{p}_\Gamma^T$ in the equation for the discrete sound power in Eq. (24). It follows that the vector transpose of the nodal sound pressure values on the surface is given by

$$\mathbf{p}_\Gamma^T = -i\omega\rho_f\mathbf{v}_\Gamma^T[\mathbf{\Theta}_{\Gamma\Gamma} - \mathbf{A}_{\Gamma\circ}\mathbf{A}_{\circ\circ}^{-1}\mathbf{\Theta}_{\circ\Gamma}]^T[\mathbf{A}_{\Gamma\Gamma} - \mathbf{A}_{\Gamma\circ}\mathbf{A}_{\circ\circ}^{-1}\mathbf{A}_{\circ\Gamma}]^{-T}. \tag{30}$$

Chen and Ginsberg[37] have shown that the vectors of nodal velocities are extracted by the real part operator in the quadratic form of the sound power in Eq. (23), so that $\mathbf{Z}_R$ is given by

$$\mathbf{Z}_R = \Re\{\mathbf{Z}\} = \Re\{-i\omega\rho_f[\mathbf{\Theta}_{\Gamma\Gamma} - \mathbf{A}_{\Gamma\circ}\mathbf{A}_{\circ\circ}^{-1}\mathbf{\Theta}_{\circ\Gamma}]^T[\mathbf{A}_{\Gamma\Gamma} - \mathbf{A}_{\Gamma\circ}\mathbf{A}_{\circ\circ}^{-1}\mathbf{A}_{\circ\Gamma}]^{-T}\mathbf{\Theta}_{\Gamma\Gamma}\}. \tag{31}$$

As mentioned above, this impedance matrix is often calculated with the BEM with $\mathbf{Z}_R = \Re\{\mathbf{H}^{-1}\mathbf{G}\mathbf{\Theta}\}$, e.g. as done by Peters *et al.*[16]

4. Model and Numerical Implementation

4.1. *Circle*

The purpose of calculating this first model is to prove the reliability of the chosen approach using ARMs. The air surrounding a circle of diameter 0.2 m is built and meshed with COMSOL Multiphysics using triangular Langrangian finite elements of quadratic order. The air has a density of $\rho_f = 1.3\,\mathrm{kg\,m^{-1}}$ and a speed of sound of $c_f = 340\,\mathrm{ms^{-1}}$. After application of FEM and IFEM, the system matrix $\mathbf{A}$ is obtained, which is subdivided (Eq. (25)) and rearranged in order to calculate the acoustic impedance matrix from Eq. (31). The results of the eigenvalue problem of $\mathbf{Z}_R$ are presented in Sec. 5.1.

4.2. *Recorder*

In this paper, the authors adapt the model of a recorder by Retka *et al.*[20] to the two-dimensional case. Therefore, a circular fluid-filled domain ($\rho_f = 1.3\,\mathrm{kg\,m^{-1}}, c_f = 340\,\mathrm{ms^{-1}}$)

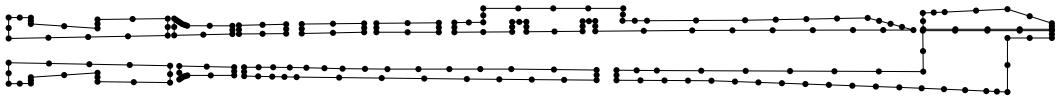

Fig. 1. Boundary mesh nodes at the recorder surface.

with a diameter of 0.67 m containing the cross-section of the recorder is meshed with COMSOL Multiphysics. Three different mesh sizes are investigated, such that 211 nodes on the recorder surface are shared by all three configurations. These mutual boundary nodes are depicted in Fig. 1. The meshes will be called coarse, normal and fine. The normal mesh consists of 1021 finite elements with a maximum element size of $h_{\max} = 3.78\,\text{cm}$ to ensure reliable results at about 3 kHz to 4 kHz.[38,39] The coarse and the fine mesh consist of 707 and 2102 elements, respectively, with maximum element sizes of $h_{\max} = 11.33\,\text{cm}$ and $h_{\max} = 2.27\,\text{cm}$. The total numbers of DOF for the sound pressure are 1569, 2197 and 4368 for the coarse, normal and fine meshes, respectively. The FE system matrices of stiffness, damping and mass are imported to Matlab, where the IFEM and subsequent studies are implemented. Mapped and conjugated Astley–Leis infinite elements are attached to the 56 (coarse), 56 (normal) and 60 (fine) elements of the outer boundaries of the three different FE meshes. The Lagrangian interpolation polynomials in the transverse direction inherit quadratic order from the finite elements along the circular FE–IFE-junction. In this paper, the influence of the IFEM on normal and ARMs is investigated. For this purpose, the IFEM system matrices are calculated for different radial interpolation polynomials of varying polynomial degree. Lagrange, Legendre and Jacobi$^{(1,0)}$ as well as Jacobi$^{(2,0)}$ polynomials with orders of 2 up to 20 are used with the normal FE mesh. In the case of the coarse and fine meshes, the subsequent investigations are confined to Jacobi$^{(1,0)}$ polynomials, since the same results are observed for all the radial interpolation polynomials as will be shown in the following results section. The radial interpolation points are positioned equidistantly between $[-1, 1)$ in the direction of the mapped radial coordinate s, such that the first interpolation point is located at $a = 0.33\,\text{m}$ on the circular junction of the FE and the IFE domain. According to the infinite element mapping approach in Eq. (6), the outer interpolation points in the global coordinate system can be found at the radii r_j in [m] for $j = 2 \ldots 20$: $[0.67, 1, 1.33, 1.67, 2, 2.33, 2.67, 3, 3.33, 3.67, 4, 4.33, 4.67, 5, 5.33, 5.67, 6, 6.33, 6.67]$.

The subsequent considerations are made in the frequency range 1 Hz–3000 Hz in frequency steps of 1 Hz.

5. Results

5.1. *Circle*

For the circle in air, the radiation modes of the acoustic impedance matrix are computed according to the derivation made in Sec. 3.2. In Fig. 2, the nine largest ARM eigenvalues λ_j are depicted as functions of the frequency. The largest eigenvalue (λ_1: ———) corresponds to a monopole mode and subsequent modes appear as pairs of eigenvalues of equal magnitude, corresponding to dipoles (λ_2 and λ_3: - - - -), quadrupoles (λ_4 and λ_5: – · – · –), hexapoles (λ_6

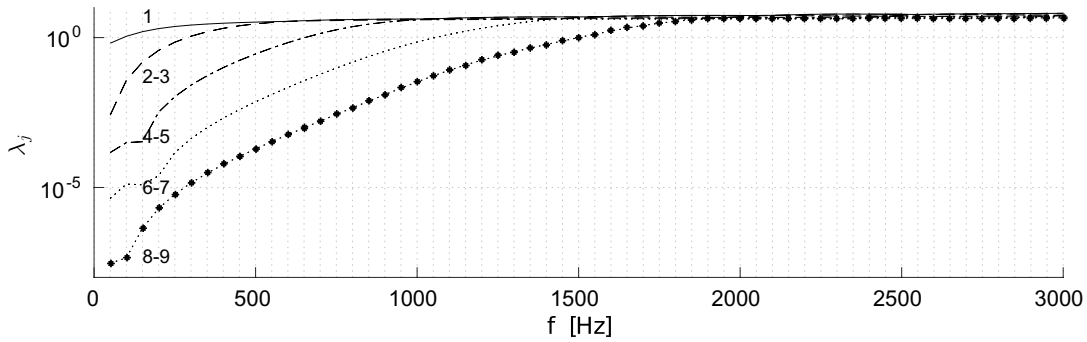

Fig. 2. The nine largest radiation mode eigenvalues λ_j as functions of the frequency, shown in groups of multipoles.

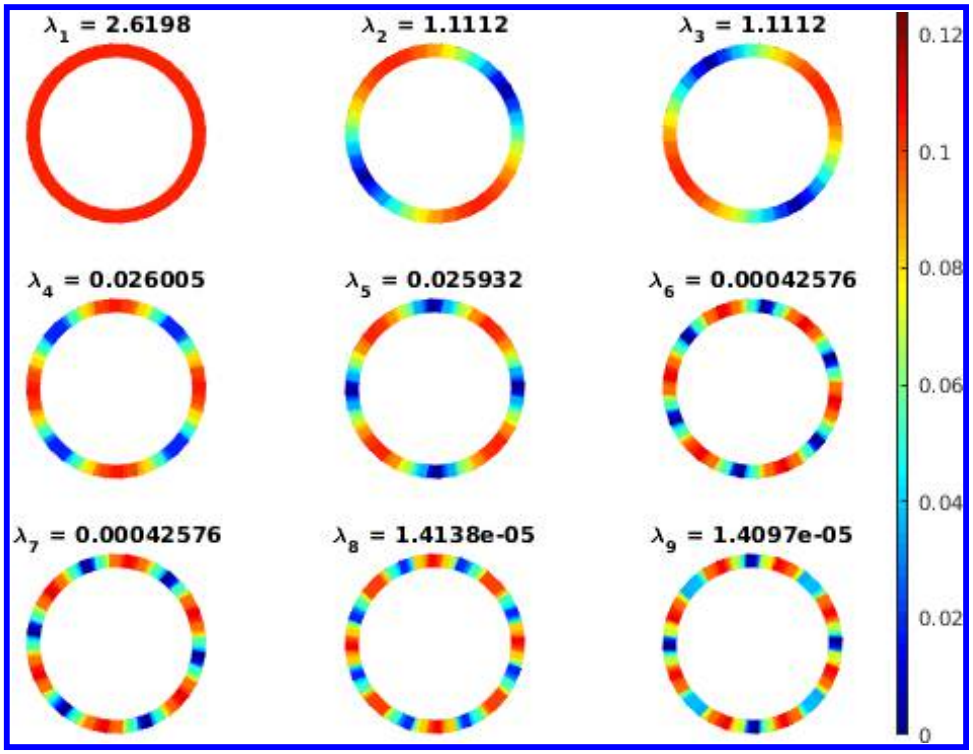

Fig. 3. ARM mode shapes corresponding to the nine largest eigenvalues λ_j at 300 Hz.

and λ_7: · · · · ·) as well as octupoles (λ_8 and λ_9: · ∗ · ∗ ·), depicted in Fig. 3. The grouping behavior of ARM eigenvalues or radiation efficiencies in terms of acoustical multipoles has already been presented by Cunefare *et al.*[15] for three-dimensional problems and by Wu *et al.*[40]

5.2. *Recorder*

5.2.1. *Matrix condition number*

As a first step, the condition number of the dynamic stiffness matrix $\mathbf{A}$ (cf. Eq. (10)) is calculated. The condition number $\kappa(\mathbf{A})$ is given by the ratio of the largest to the lowest

eigenvalue of the frequency-dependent matrix **A** and is calculated by power iteration and inverse iteration, respectively. As shown by Babuška *et al.*[41] Cremers *et al.*[42] and Dreyer *et al.*[6] the matrix condition increases with the polynomial order, which leads to ill-conditioned matrices for polynomials of degree > 8 in the case of Lagrange polynomials, whereas Legendre and Jacobi polynomials provide distinctly better-conditioned matrices. Tests performed by the authors of this paper have confirmed this observation, although the choice between the four polynomials had no considerable effect on the modes in exterior acoustics, as will be shown subsequently.

5.2.2. *Influence of infinite elements on radiation modes*

The eigenvalues λ_j and eigenvectors of the frequency-dependent, real acoustic impedance matrix $\mathbf{Z}_R$ from Eq. (31) were computed separately for each frequency step. The largest eigenvalues as a function of the frequency are shown in Fig. 4 for the four polynomials of degree 20 with the normal FE mesh. All polynomials exhibit virtually identical eigenvalue curves and do so for each degree of radial interpolation, not only for the 20th order. Despite the differences in matrix condition, the choice of polynomial for radial interpolation does not seem to matter for calculating the ARM.

In Fig. 4, the grouping behavior of the exterior radiation mode eigenvalues can be observed as described by Cunefare *et al.*[15] and by Wu *et al.*[40] and as obtained for the circle in Sec. 5.1, which is a pure exterior acoustic problem without holes or chambers with interior modes. These grouped curves are in superposition with interior resonances in the hollow recorder. This is indicated by single eigenvalues that show resonance peaks at certain frequencies above which they rapidly decrease, which leads to changes in the order of eigenvalue magnitudes. The distribution of eigenvalues at each frequency is related to the share of the corresponding mode shape in the total superimposed pressure field at the surface of the solid structure, since ARM eigenvalues are related to the radiation

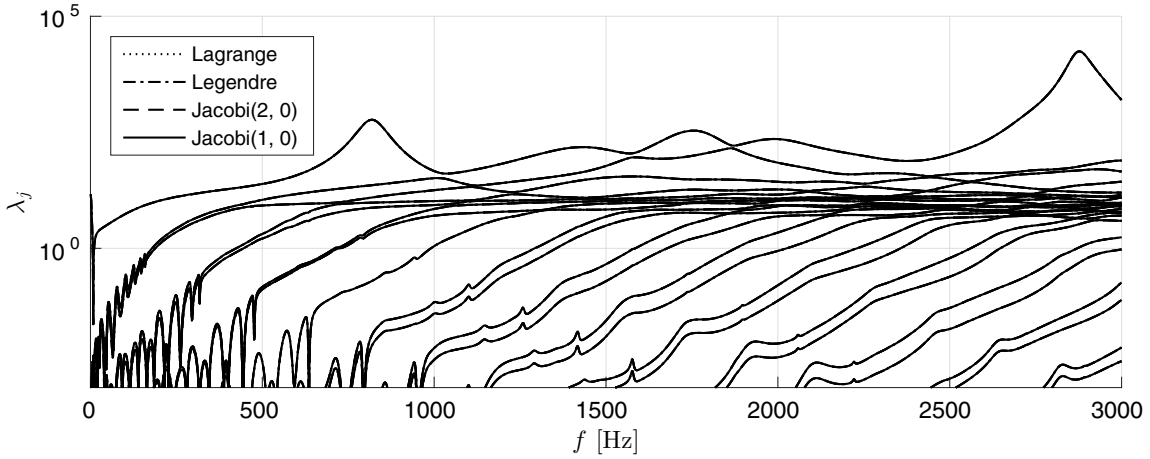

Fig. 4. Largest eigenvalues λ_j of the radiation modes as a function of the frequency for Lagrange, Legendre and two Jacobi polynomials of radial order 20 with the normal FE mesh. All polynomials lead to virtually identical eigenvalue curves.

(a) λ_1 at 840 Hz

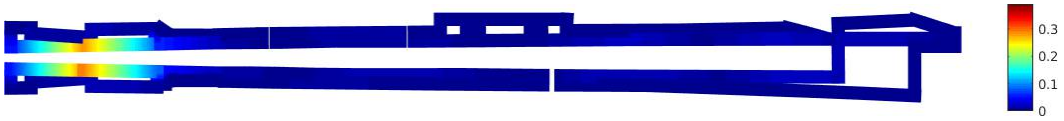

(b) λ_1 at 1760 Hz

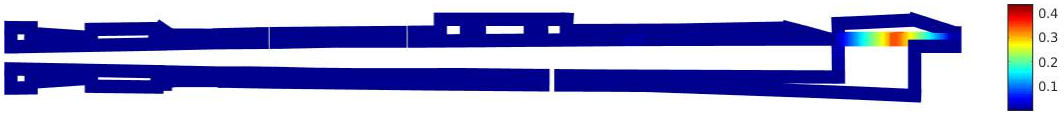

(c) λ_1 at 2880 Hz

Fig. 5. ARM shapes as eigenvectors of the acoustic impedance matrix corresponding to the largest eigenvalue at each of the given frequencies.

efficiency σ by $\lambda = \rho_f c_f \sigma$.[16] Three notable peaks can be found for the largest eigenvalue at approximately 840 Hz, 1760 Hz and 2880 Hz. The corresponding mode shapes — which can be found as eigenvectors of the acoustic impedance matrix $\mathbf{Z}_R$ — are depicted in Fig. 5 and show interior modes in the upper middle section (barrel), see Fig. 5(a), in the foot joint (Fig. 5(b)) and in the windway of the mouthpiece (Fig. 5(c)).

In the following, attention will be restricted to one single type of IFEM interpolation polynomial in the radial direction, the Jacobi(1, 0) polynomials. As shown before, the same results for the ARMs are obtained for all considered polynomials. Using the Jacobi(1, 0) polynomials leads to the best-conditioned problem due to the lowest matrix condition number $\kappa(\mathbf{A})$. Two further finite element meshes are taken into consideration and the infinite element system matrices are computed for Jacobi (1, 0) as radial interpolation polynomials of degree 2 up to 20. The ARM eigenvalues λ_j with $j = 1, \ldots, 8$ with coarse, normal and fine FE mesh are depicted in Fig. 6 for a degree of 20. The results show that the coarse and normal meshes lead to quite similar eigenvalue curves, whereas the fine FE mesh results in slightly smaller values of ARM eigenvalues.

Close to the eigenvalue resonance peaks it can be observed that each single eigenvalue converges as the degree of the radial interpolation polynomials increases, as can be seen in Fig. 7 in the example of the peak in λ_1 at about 2880 Hz. Polynomials of even and odd degrees respectively lead to curves that converge to two different eigenvalues. They do not necessarily approach from opposite sides, but sometimes both from below or from above. However, away from the resonance peaks, the difference between eigenvalue curves of low-order polynomials and the curves of the highest-order converged polynomials with degree 19 and 20 is negligible. This means that the loss of accuracy incurred by reducing the degree of radial interpolation polynomials only emerges at the modal resonances. In

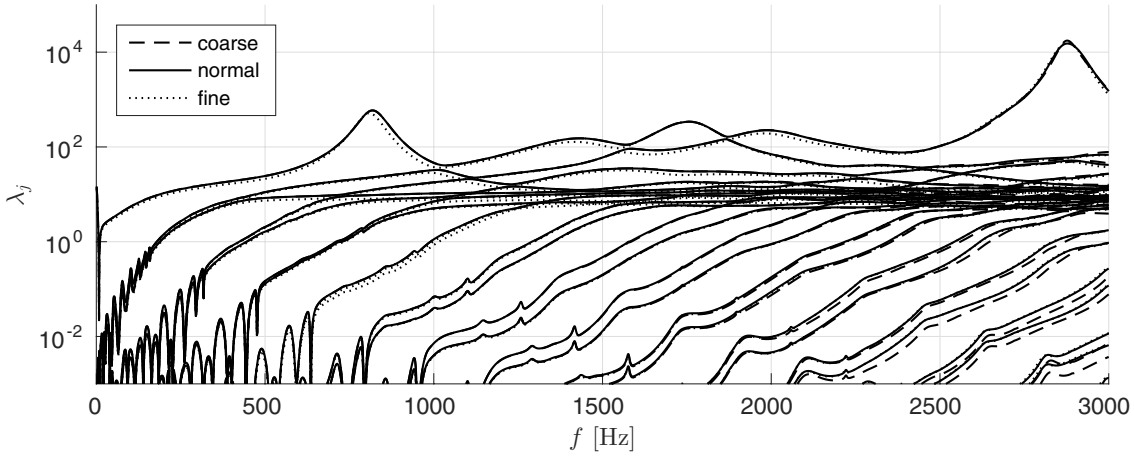

Fig. 6. Radiation mode eigenvalues λ_j for Jacobi(1, 0) interpolation polynomials of degree 20 for coarse, normal and fine FE mesh.

addition, convergence of the eigenvalues from both sides can be observed, depending on the FE mesh on which the computation is based. In the example of the peak considered earlier at about 2880 Hz, the eigenvalues obtained from IFEM radial interpolation polynomials with even degree converge from below for the coarse FE mesh (see Fig. 7(a)), whereas calculations based on the normal and the fine mesh lead to convergence from above, as can be seen in Figs. 7(b) and 7(c). The convergence of eigenvalues from odd-degree polynomials is observed to behave vice versa at this particular resonance. However, at least once, the curves cross and converge from opposite sides close to the resonance peaks.

5.2.3. *Influence of infinite elements on NMs*

Transforming the frequency-independent system matrices $\mathbf{K}$, $\mathbf{D}$ and $\mathbf{M}$ into the state-space form as given in Eq. (19) leads to the eigenvalue problem in Eq. (18) that yields the NMs as right eigenvectors. The corresponding eigenvalues κ_j are complex numbers with frequency information in the imaginary part and a damping term in the real part. Figure 8 shows the eigenvalues in the complex plane for all four polynomials at radial interpolation of degree $n_{\text{rad}} = 10$ and $n_{\text{rad}} = 20$ with the normal FE mesh. The focus is on eigenvalues with a positive frequency below 3 kHz (neglecting the complex conjugate eigenvalues) whose real part has comparatively small magnitude ($|\Re\{\kappa_j\}| < 100$), which means the considered modes are weakly damped and thus expected to have a major influence on the radiation of sound. Clearly, the eigenvalue solution does not depend on the choice of the radial interpolation polynomial for the infinite elements, since Lagrange, Legendre and both Jacobi polynomials lead to virtually the same eigenvalues in the complex plane as shown in Fig. 8. Since this parameter has no influence on the NM eigenvalues, only Jacobi(1, 0) polynomials are taken into consideration in the following.

Single eigenvalues or a certain number of eigenvalues on a curve can be observed, which can be recognized in all of the calculations, independent of the number of radial interpolation points n_{rad}. These eigenvalues are expected to converge as the order of the polynomials

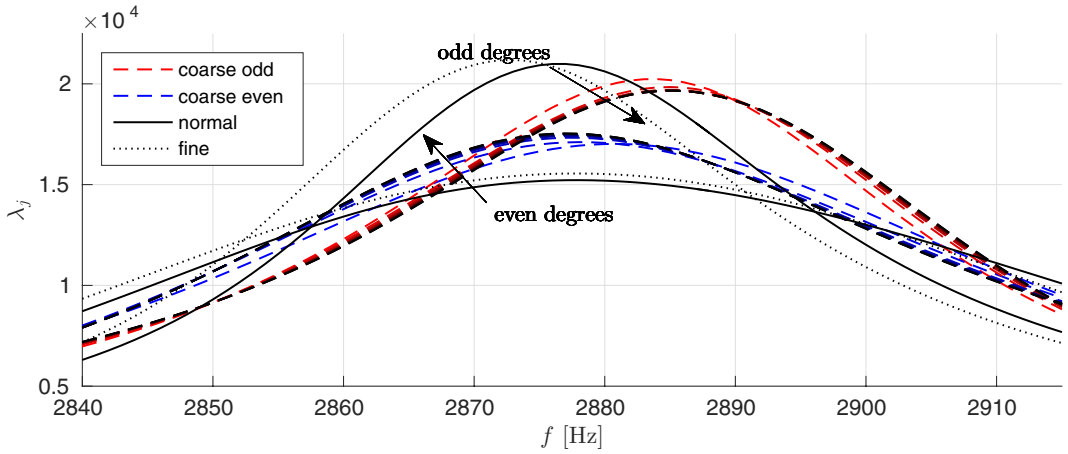

(a) ARM eigenvalues λ_j based on coarse FE mesh

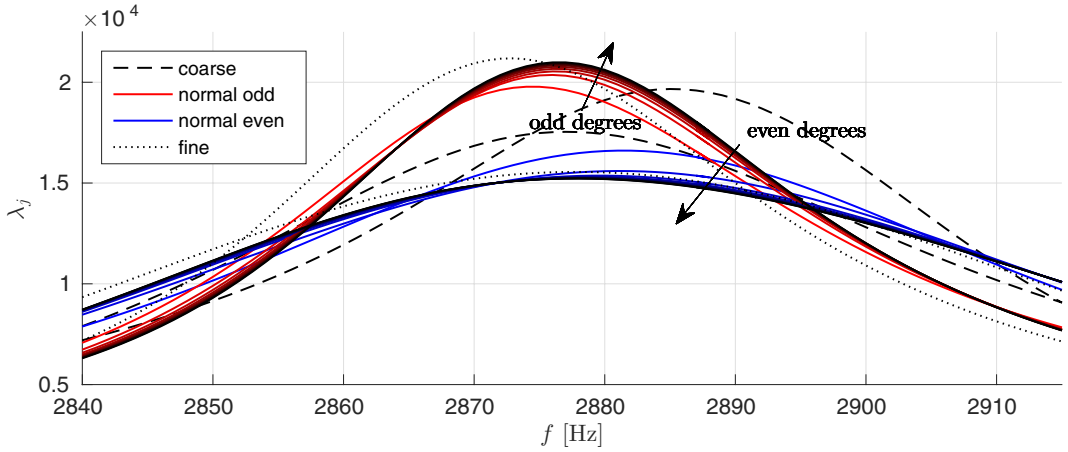

(b) ARM eigenvalues λ_j based on normal FE mesh

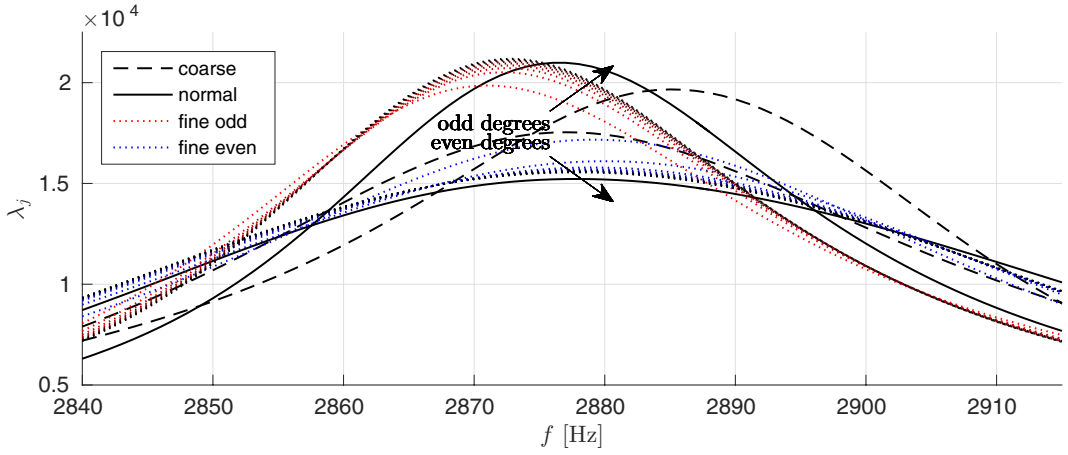

(c) ARM eigenvalues λ_j based on fine FE mesh

Fig. 7. (Color online) Convergence of ARM eigenvalues λ_j based on three different FE meshes (coarse – – – –, normal ——— and fine · · · · ·). Polynomials of even and odd degrees are denoted with blue and red lines, respectively. The black curves — in pairs, one for even and one odd order — denote the converged eigenvalues of degree 19 or 20 for all FE meshes.

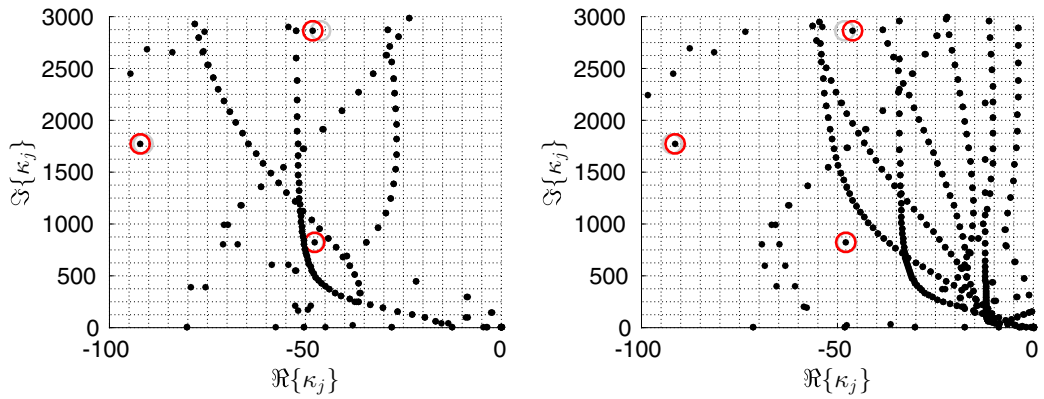

(a) κ_j at $n_{rad} = 10$ (b) κ_j at $n_{rad} = 20$

Fig. 8. (Color online) Complex plane with NM eigenvalues for Lagrange, Legendre, Jacobi(2, 0) and Jacobi(1, 0) polynomials, which all give virtually the same eigenvalues depicted as black dots. Radial interpolation polynomial of: (a) degree 10 and (b) degree 20. The red circles show the three related eigenvalues that were found for the ARMs in Figs. 4 and 5. The gray circles indicate the variation of the considered eigenvalues (red circles) between the polynomial degrees 10 and 20.

increases, whereas the additional eigenvalues that appear due to the growing number of DOF do not converge and are assumed to correspond to spurious modes. This was also observed by Marburg[11] when he investigated NMs in the fluids around an ellipse and an open box, respectively. The red circles indicate three eigenvalues κ_a, κ_b and κ_c which correspond to eigenvectors or mode shapes that were found in resonance at approximately 840 Hz (λ_1), 1760 Hz (λ_1) and 2880 Hz (λ_1) for the ARMs (cf. Fig. 4). Almost the same three frequencies can be found in the imaginary parts of the three red-marked NM eigenvalues $\kappa_{13} = -46.22+819.27i$ ($= \kappa_a$), $\kappa_{72} = -98.01+1743.25i$ ($= \kappa_b$) and $\kappa_{186} = -38.78+2880.84i$ ($= \kappa_c$) in the example of second-order Jacobi(1, 0) polynomials with the normal FE mesh. This single value in the imaginary part of the complex eigenvalues shows the frequency at which the respective NM is in resonance, whereas its damping ratio is given in the real part as described by Marburg.[10] The corresponding mode shapes in the fluid around the recorder — as right eigenvectors of the state space eigenvalue problem — are depicted in Fig. 9. As expected, the same mode shapes can be obtained in the barrel and in the mouthpiece of the recorder as for the ARMs in Fig. 5.

Similar to the eigenvalues of the ARMs, the NM eigenvalues differ for radial interpolation polynomials of even and odd degrees. This means that two different convergent complex conjugate pairs of eigenvalues are calculated, corresponding to the same mode shape. By application of the Modal Assurance Criterion (MAC),[29] the NM eigenvalues can be tracked throughout all the calculations. The MAC can be calculated by[29]

$$\mathrm{MAC}(\mathbf{a}, \mathbf{b}) = \frac{|\mathbf{a}^H \mathbf{b}|^2}{(\mathbf{a}^H \mathbf{a})(\mathbf{b}^H \mathbf{b})}, \tag{32}$$

where $\mathbf{a}$ and $\mathbf{b}$ are eigenvectors or columns of modal matrices and $(\cdot)^H = (\cdot)'^*$ is the Hermitian transpose (complex conjugate and transpose). The comparison of modal matrices

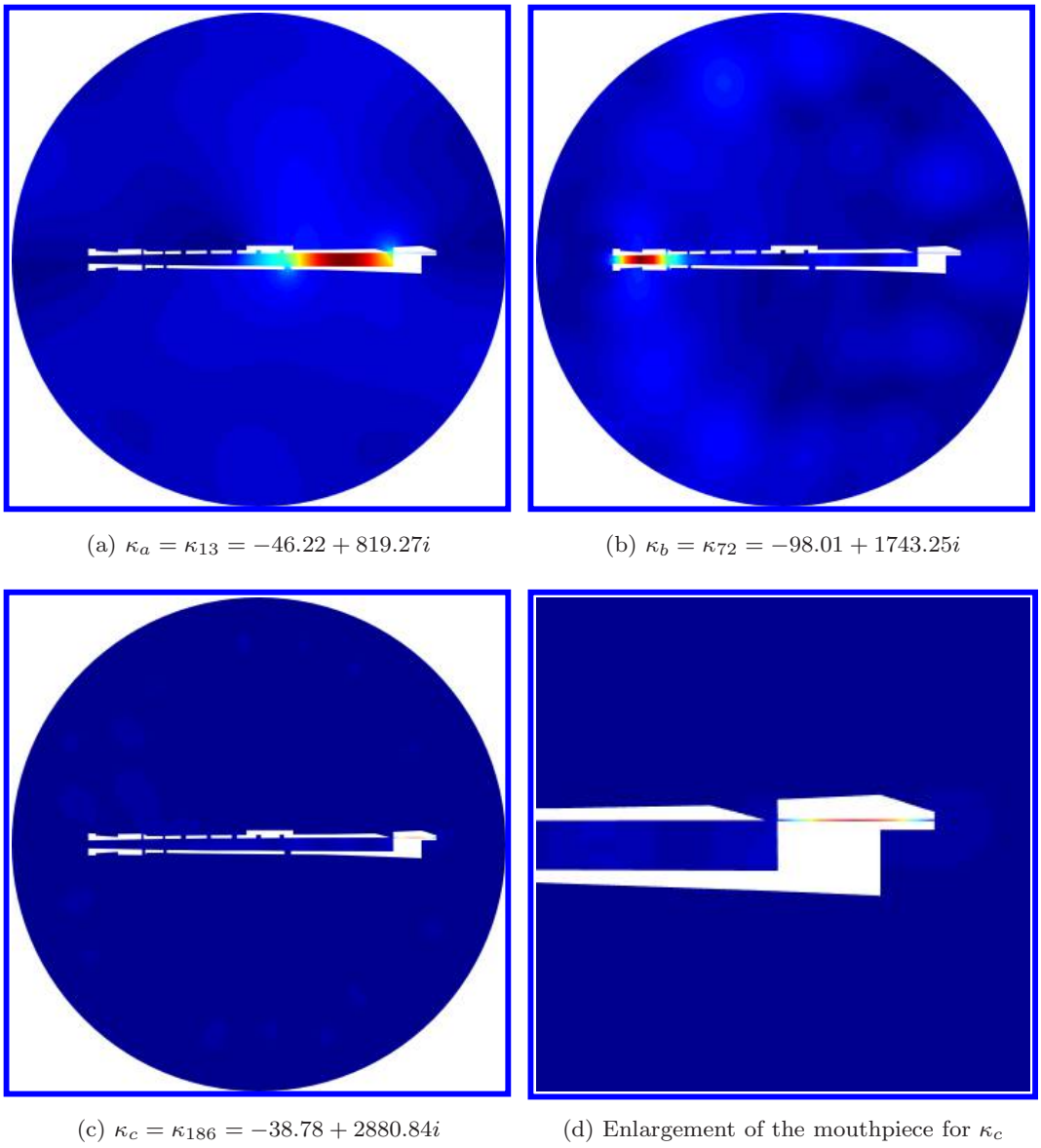

(a) $\kappa_a = \kappa_{13} = -46.22 + 819.27i$ (b) $\kappa_b = \kappa_{72} = -98.01 + 1743.25i$

(c) $\kappa_c = \kappa_{186} = -38.78 + 2880.84i$ (d) Enlargement of the mouthpiece for κ_c

Fig. 9. NM shapes as right eigenvectors corresponding to given complex eigenvalues ((a) κ_{13}, (b) κ_{72}, (c) and (d) κ_{186}) for Jacobi(1, 0) polynomials of second-order of radial interpolation, based on the normal FE mesh.

leads to a MAC matrix, whose maximum value(s) denote(s) the best accordance of two compared eigenvectors. The positions of the maxima indicate the corresponding eigenvalues of well-according mode shapes. The eigenvectors that are depicted in Fig. 9 (normal FE mesh and second-order interpolation polynomials) are compared to each of the remaining eigenvectors that were calculated with varying polynomial order based on three FE meshes. To ensure comparability between all modal matrices, eigenvectors are compared, which are narrowed to the mutual DOF on the recorder surface (211 DOF), cf. Sec. 4.2. Since the three tracked modes only have notable peaks in the interior and therefore directly at the surface of the recorder, this is a reasonable reduction.

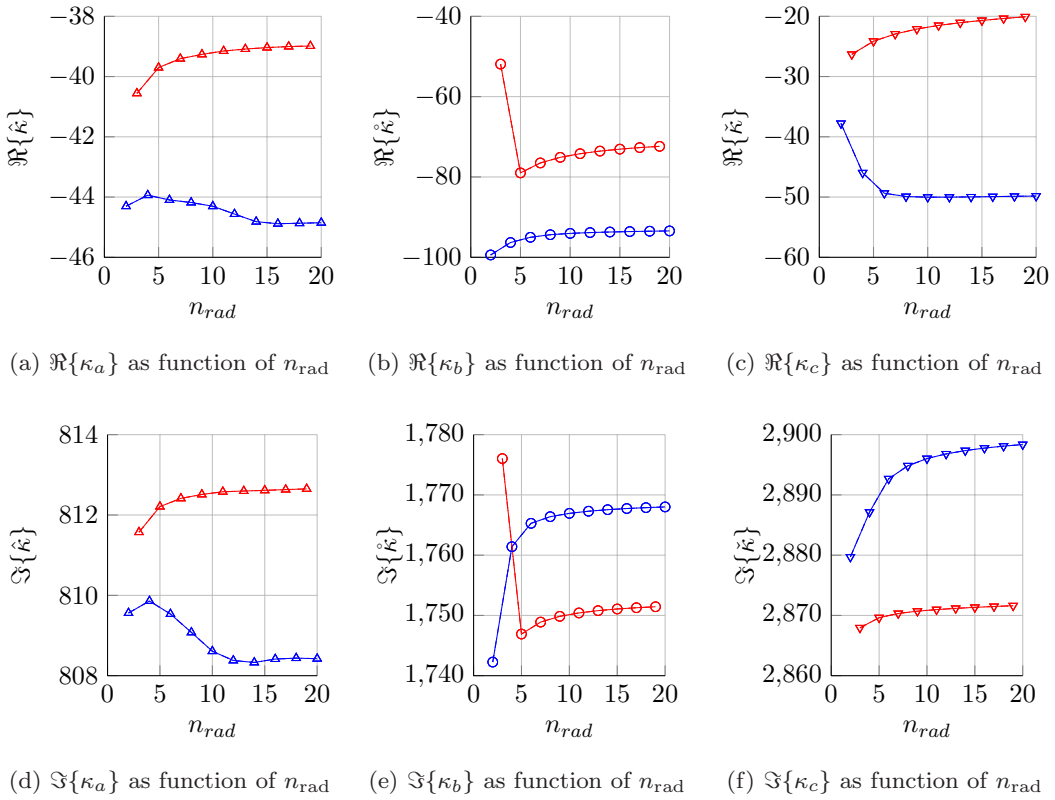

(a) $\Re\{\kappa_a\}$ as function of n_{rad} (b) $\Re\{\kappa_b\}$ as function of n_{rad} (c) $\Re\{\kappa_c\}$ as function of n_{rad}

(d) $\Im\{\kappa_a\}$ as function of n_{rad} (e) $\Im\{\kappa_b\}$ as function of n_{rad} (f) $\Im\{\kappa_c\}$ as function of n_{rad}

Fig. 10. (Color online) Convergence of the eigenvalues κ_a ($\triangle$), κ_b ($\bigcirc$) and κ_c ($\bigtriangledown$) as functions of even (blue) and odd (red) polynomial order for radial interpolation n_{rad} with three different FE meshes (coarse – – – –, normal ——— and fine · · · · ·), whose curves are virtually the same.

Figure 10 shows the convergence of the NM eigenvalues κ_a, κ_b and κ_c as the degree of the radial interpolation polynomials of the infinite elements is increased and considering the three different FE meshes. It can be seen that the choice of coarse, normal or fine FE mesh has hardly any effect, neither on the real part nor on the imaginary part of the converging eigenvalues. As already observed for the ARM eigenvalues, two different convergence curves of the NM eigenvalues for polynomials of even and odd orders are found.

6. Conclusion

In this work, the authors applied the FEM as well as the IFEM in order to discretize and calculate the spatial sound pressure field in fluid-filled unbounded domains around an inner solid structure. The obtained discrete system matrices were used for modal decomposition into ARMs and NMs. It was shown that the acoustic impedance matrix $\mathbf{Z}_R$ for the calculation of the radiation modes can also be determined from the matrices of the finite and the infinite elements, instead of the boundary element matrices that are usually used. Furthermore, the grouping behavior of exterior multipole eigenvalues was observed in the example of a circle and a recorder in a fluid-filled unbounded domain. In addition, resonances of interior radiation mode eigenvalues were found for the hollow model of the recorder. The

comparison between the ARMs and the NMs shows that both methods provide almost all the same eigenvectors (mode shapes) with an acceptable agreement for the corresponding frequencies. Radiation mode shapes only refer to the surface of the structure and NM eigenvectors can be visualized in the whole discretized fluid-filled domain.

The aim of this paper was to investigate the influence of FE mesh sizes as well as different IFE radial interpolation polynomials and polynomial degrees on the modes in exterior acoustics. The investigations show no differences, neither for ARM eigenvalues nor for NM eigenvalues, between the choice of Lagrange, Legendre or Jacobi polynomials. However, the matrix condition of the global system matrix $\mathbf{A}$ is the best with Jacobi(1, 0) polynomials, so that further investigations were limited to these polynomials. Variation of the finite element mesh size has no considerable effect on the NM eigenvalues and has a minor effect on some of the radiation mode eigenvalues in the whole frequency range. Increasing the degree of radial interpolation polynomials in the domain of the infinite elements reveals two convergence curves for the ARM eigenvalues for polynomials of even and odd degrees. Differences in the eigenvalue curves of lower- and higher-order interpolation polynomials mainly emerge close to the resonance peaks of the eigenvalues rather than over the whole frequency range. The investigations revealed no clear tendency for convergence of the eigenvalues from above or below. In order to track NM eigenvalues for different FE meshes and polynomial degrees, the corresponding eigenvectors were compared to each other by application of the MAC. In the example of three significant NM shapes, the NM eigenvalues were observed to converge as the order of the polynomials was increased. Similar to the convergence of the radiation modes, the authors found two convergences of the NM eigenvalues for polynomials of even and odd degree.

Future work is planned to further investigate the eigenvalue solver and alternative, iterative methods to reduce the calculation time. The role of the eigenvalue solver in the differences in polynomials of even and odd degree has to be clarified. Finally, a modal reduction is desirable in order to calculate the radiated sound power or sound pressure field with a reduced number of modal contributions.

Acknowledgments

We wish to gratefully acknowledge the support for this research provided by the Deutsche Forschungsgemeinschaft (DFG) under grant number MA 2395/11–1.

References

1. A. Bermúdez, L. Hervella-Nieto, A. Prieto and R. Rodríguez, Perfectly matched layers, in *Computational Acoustics of Noise Propagation in Fluids — Finite and Boundary Element Methods*, eds. S. Marburg and B. Nolte (Springer, Berlin, 2008), pp. 167–196.
2. R. J. Astley, G. J. Macaulay, J.-P. Coyette and L. Cremers, Three-dimensional wave-envelope elements of variable order for acoustic radiation and scattering. Part I. Formulation in the frequency domain, *J. Acoust. Soc. Am.* **103**(1) (1998) 49–63.
3. R. J. Astley, Infinite elements for wave problems: A review of current formulations and an assessment of accuracy, *Int. J. Numer. Methods Eng.* **49**(7) (2000) 951–976.

4. F. Ihlenburg, *Finite Element Analysis of Acoustic Scattering*, Vol. 132 (Springer Science & Business Media, 2006).
5. J. J. Shirron and I. Babuška, A comparison of approximate boundary conditions and infinite element methods for exterior Helmholtz problems, *Comput. Methods Appl. Mech. Eng.* **164**(1) (1998) 121–139.
6. D. Dreyer and O. von Estorff, Improved conditioning of infinite elements for exterior acoustics, *Int. J. Numer. Methods Eng.* **58**(6) (2003) 933–953.
7. G. V. Borgiotti, The power radiated by a vibrating body in an acoustic fluid and its determination from boundary measurements, *J. Acoust. Soc. Am.* **88**(4) (1990) 1884–1893.
8. D. M. Photiadis, The relationship of singular value decomposition to wave-vector filtering in sound radiation problems, *J. Acoust. Soc. Am.* **88**(2) (1990) 1152–1159.
9. A. Sarkissian, Acoustic radiation from finite structures, *J. Acoust. Soc. Am.* **90**(1) (1991) 574–578.
10. S. Marburg, Normal modes in external acoustics. Part I: Investigation of the one-dimensional duct problem, *Acta Acust. United with Acust.* **91**(6) (2005) 1063–1078.
11. S. Marburg, F. Dienerowitz, T. Horst and S. Schneider, Normal modes in external acoustics. Part II: Eigenvalues and eigenvectors in 2D, *Acta Acust. United with Acust.* **92**(1) (2006) 97–111.
12. S. Marburg, Normal modes in external acoustics. Part III: Sound power evaluation based on superposition of frequency-independent modes, *Acta Acust. United with Acust.* **92**(2) (2006) 296–311.
13. K. A. Cunefare, The minimum multimodal radiation efficiency of baffled finite beams, *J. Acoust. Soc. Am.* **90**(5) (1991) 2521–2529.
14. K. A. Cunefare and M. N. Currey, On the exterior acoustic radiation modes of structures, *J. Acoust. Soc. Am.* **96**(4) (1994) 2302–2312.
15. K. A. Cunefare, M. N. Currey, M. E. Johnson and S. J. Elliott, The radiation efficiency grouping of free-space acoustic radiation modes, *J. Acoust. Soc. Am.* **109**(1) (2001) 203–215.
16. H. Peters, N. Kessissoglou and S. Marburg, Enforcing reciprocity in numerical analysis of acoustic radiation modes and sound power evaluation, *J. Comput. Acoust.* **20**(3) (2012).
17. H. Wu, W. Jiang and Y. Liu, Analyzing acoustic radiation modes of baffled plates with a fast multipole boundary element method, *J. Vib. Acoust.* **135**(1) (2013) 011007.
18. S. Marburg, E. Lösche, H. Peters and N. Kessissoglou, Surface contributions to radiated sound power, *J. Acoust. Soc. Am.* **133**(6) (2013) 3700–3705.
19. Z.-B. Liu and C. Maury, An improved method for the calculation of near-field acoustic radiation modes, *J. Sound Vib.* **363** (2016) 316–328.
20. S. Fuß, S. C. Hawkins and S. Marburg, An eigenvalue search algorithm for the modal analysis of a resonator in free space, *J. Comput. Acoust.* **19**(1) (2011) 95–109.
21. S. Retka and S. Marburg, An infinite element for the solution of Galbrun equation, *ZAMM J. Appl. Math. Mech./Zeit. Angew. Math. Mech.* **93**(2–3) (2013) 154–162.
22. K. A. Cunefare and G. H. Koopmann, Global optimum active noise control: Surface and far-field effects, *J. Acoust. Soc. Am.* **90**(1) (1991) 365–373.
23. S. S. Ramesh, K.-M. Lim and B. C. Khoo, Comparison of constant and discontinuous quadratic boundary elements for exterior axisymmetric acoustic-wave propagation problems, *J. Comput. Acoust.* **23**(4) (2015) 1540003.
24. S. Marburg, The Burton and Miller method: Unlocking another mystery of its coupling parameter, *J. Comput. Acoust.* **24**(1) (2016) 1550016.
25. S. Marburg, Numerical damping in the acoustic boundary element method, *Acta Acust. United with Acust.* **102**(3) (2016) 415–418.
26. C.-J. Zheng, H.-B. Chen, H.-F. Gao and L. Du, Is the Burton–Miller formulation really free of fictitious eigenfrequencies?, *Eng. Anal. Bound. Elem.* **59** (2015) 43–51.

27. L. Demkowicz and K. Gerdes, Convergence of the infinite element methods for the Helmholtz equation in separable domains, *Numer. Math.* **79**(1) (1998) 11–42.
28. K. Gerdes, A summary of infinite element formulations for exterior Helmholtz problems, *Comput. Methods Appl. Mech. Eng.* **164**(1) (1998) 95–105.
29. R. J. Allemang, The modal assurance criterion–twenty years of use and abuse, *Sound Vib.* **37**(8) (2003) 14–23.
30. S. Marburg and B. Nolte, A unified approach to finite and boundary element discretization in linear timeharmonic acoustics, in *Computational Acoustics of Noise Propagation in Fluids — Finite and Boundary Element Methods*, eds. S. Marburg and B. Nolte (Springer, Berlin, 2008), pp. 1–34.
31. R. J. Astley, Infinite elements, in *Computational Acoustics of Noise Propagation in Fluids — Finite and Boundary Element Methods*, eds. S. Marburg and B. Nolte (Springer, Berlin, 2008), pp. 197–230.
32. R. J. Astley and J.-P. Coyette, Conditioning of infinite element schemes for wave problems, *Commun. Numer. Methods Eng.* **17**(1) (2001) 31–41.
33. J. M. M. C. Marques and D. R. J. Owen, Infinite elements in quasi-static materially nonlinear problems, *Comput. Struct.* **18**(4) (1984) 739–751.
34. O. von Estorff, S. Petersen and D. Dreyer, Efficient infinite elements based on Jacobi polynomials, in *Computational Acoustics of Noise Propagation in Fluids — Finite and Boundary Element Methods*, eds. S. Marburg and B. Nolte (Springer, Berlin, 2008), pp. 231–250.
35. R. J. Astley and W. Eversman, Finite element formulations for acoustical radiation, *J. Sound Vib.* **88**(1) (1983) 47–64.
36. O. C. Zienkiewicz, K. Bando, P. Bettess, C. Emson and T. C. Chiam, Mapped infinite elements for exterior wave problems, *Int. J. Numer. Methods Eng.* **21**(7) (1985) 1229–1251.
37. P.-T. Chen and J. H. Ginsberg, Complex power, reciprocity, and radiation modes for submerged bodies, *J. Acoust. Soc. Am.* **98**(6) (1995) 3343–3351.
38. S. Marburg and S. Schneider, Influence of element types on numeric error for acoustic boundary elements, *J. Comput. Acoust.* **11**(3) (2003) 363–386.
39. P. Langer, M. Güttler, C. Guist, M. Krause and S. Marburg, Six finite elements per wavelength reloaded: The practical use of finite element models and their accuracy in comparison with experimental results, *J. Comput. Acoust.* **25** (2017) 1750025.
40. H. Wu, W. Jiang, Y. Zhang and W. Lu, A method to compute the radiated sound power based on mapped acoustic radiation modes, *J. Acoust. Soc. Am.* **135**(2) (2014) 679–692.
41. I. Babuska, M. Griebel and J. Pitkaranta, The problem of selecting the shape functions for a p-type finite element, DTIC Document, Tech. Rep., (1988).
42. L. Cremers and K. R. Fyfe, On the use of variable order infinite wave envelope elements for acoustic radiation and scattering, *J. Acoust. Soc. Am.* **97**(4) (1995) 2028–2040.

Publication B

Journal of Computational Acoustics, Vol. 26, No. 0 (2018) 1850029 (18 pages)

DOI: 10.1142/S2591728518500299

INTERNATIONAL ASSOCIATION
FOR MATHEMATICS AND
COMPUTERS IN SIMULATION

Normal Modes and Modal Reduction in Exterior Acoustics

Lennart Moheit* and Steffen Marburg
Chair of Vibroacoustics of Vehicles and Machines
Department of Mechanical Engineering
Technical University of Munich, Garching 85748, Germany
**lennart.moheit@tum.de*

Received 31 December 2017
Accepted 29 March 2018
Published 14 June 2018

The Helmholtz equation for exterior acoustic problems can be solved by the finite element method in combination with conjugated infinite elements. Both provide frequency-independent system matrices, forming a discrete, linear system of equations. The homogenous system can be understood as a quadratic eigenvalue problem of normal modes (NMs). Knowledge about the only relevant NMs, which — when doing modal superposition — still provide a sufficiently accurate solution for the sound pressure and sound power in comparison to the full set of modes, leads to reduced computational effort. Properties of NMs and criteria of modal reduction are discussed in this work.

Keywords: Exterior acoustics; infinite element method; normal modes; modal reduction.

1. Introduction

Exterior acoustic problems comprehend the propagation and distribution of sound pressure in fluid-filled domains of infinite extent. This implies sound sources under free-field conditions in full- or half-space problems, with or without open cavities. For the description of sound sources, e.g. by means of their radiated sound power, free-field conditions are required in order to only determine the characteristics of the source and to exclude the influence of the measurement environment. This also applies for the numerical simulation of sound radiation, since in the context of virtual prototyping, it is desired for estimating acoustical properties in the development process. For this purpose, the Sommerfeld radiation condition[1] has to be satisfied, according to which the sound pressure decays with a defined rate and vanishes towards infinity.

The classical finite element method (FEM)[2] is restricted to interior acoustic problems in enclosed computational domains with reflecting or partially absorbing boundary conditions (ABCs). Givoli *et al.*[3,4] introduce and review the existing high-order local ABCs with the aim of applying the FEM to exterior acoustic problems. Rabinovich *et al.*[5] compare the high-order ABCs with perfectly matched layers (PMLs) that were introduced by Berenger[6] and optimized for frequency domain problems by Bermúdez *et al.*[7,8] PMLs ensure nonreflective

outer boundaries of the computational domain by attaching additional damped and finite computational domains to its outer boundary with perfect impedance matching at the junction. Similar to the PML approach, the infinite element method (IFEM) works with an outer layer around an inner spherical or ellipsoidal FE domain. Different formulations have been presented, e.g. by Bettess,[9] Burnett[10] and Astley.[11] The Astley–Leis IFEM formulation provides frequency-independent system matrices,[12,13] which is required for the subsequent investigations in this work. The radial interpolation of the sound pressure between the outer FE boundary and infinity can be realized by different polynomials. Using Legendre or Jacobi polynomials leads to improved matrix conditioning in comparison to conventional Lagrange polynomials, according to von Estorff and Dreyer *et al.*[14,15]

The Sommerfeld radiation condition is also implied in the boundary element method (BEM),[16,17] where an integral equation is found to solve the Helmholtz equation at the surface of the sound source for the given set of boundary conditions. This leads to discrete and frequency-dependent, single-layer and double-layer potential matrices that associate the sound pressure and fluid particle velocity at the boundary.

In order to determine the sound pressure or sound power using one of the above methods, linear systems of equations have to be solved and matrices have to be inverted for each frequency of interest separately. This leads to considerable computational effort for studies with a large number of degrees of freedom (DOFs) in a wide frequency range. A possible model reduction approach is modal analysis and superposition, in which the solution is decomposed into modes — or, in mathematical terms, eigenvalues and eigenvectors — which describe theoretically possible and orthogonal shapes of vibration that can be summed up or superimposed to the total solution.

The concept of normal mode (NM) was first adapted to exterior acoustic problems by Marburg *et al.*[18–20] and further investigated by Moheit and Marburg.[21,22] They apply the frequency-independent Astley–Leis IFEM in order to solve a single linearized eigenvalue problem referring to the works by Ruge[23] and Tisseur and Meerbergen.[24] The authors investigate the influence of the mesh and the radial interpolation of the IFEM on NMs and acoustic radiation modes (ARMs) and compare both kinds of modes in exterior acoustic problems. Fuß *et al.*[25] use an Arnoldi eigenvalue solver to calculate selected, weakly damped NMs in a proximity to the imaginary axis iteratively. The modal reduction of ARMs has been investigated by Kuijpers *et al.*,[26] Kessels[27] and Peters *et al.*[28–30] using BEM.

Model reduction is mainly associated with Krylov subspace-based methods such as Padé-via-Lanczos and Padé-via-Arnoldi. The latter approach has been applied to fluid-loaded structural modes by Peters *et al.* in Ref. 30 using a fully-coupled FEM/BEM model, whereas Baugart *et al.*[31] apply the Padé-via-Lanczos algorithm to FE- and IFE-discretized exterior problems in order to predict sound power efficiently. Wagner *et al.*[32] describe the concept of the Krylov subspace approach on the basis of Dirichlet-to-Neumann (DtN) boundary conditions and IFEs in exterior acoustics with the aim of solving the Helmholtz equation simultaneously at multiple frequencies.

In this phenomenological work, the authors recapitulate the NMs approach and the determination of the sound pressure and sound power and investigate the properties of

eigenvalues and eigenvectors for different geometries and load cases. In particular, the distinction between pure exterior problems and cavity problems is worked out. Finally, the errors of the radiated sound power are determined for reduced modal bases with certain criteria of modal reduction.

2. Method

According to the work by Marburg *et al.*,[18–20] NMs in numerical exterior acoustic problems can be determined as follows: For the description of the spatial sound pressure field $p(\mathbf{x})$ at a frequency f, the Helmholtz differential equation is used. It is discretized by the FEM and the IFEM according to Astley and Leis. The general setup is depicted in Fig. 1.

The resulting discrete system of N linear equations $-\omega^2\mathbf{M} - i\omega\mathbf{D} + \mathbf{K} = \mathbf{f}$ is solved as a linearized quadratic eigenvalue problem with $2N \times 2N$-sized hypermatrices $\mathbf{A}$ and $\mathbf{B}$:

$$\mathbf{A} = \begin{bmatrix} \mathbf{M} & \mathbf{0} \\ \mathbf{0} & -\mathbf{K} \end{bmatrix}, \quad \mathbf{B} = \begin{bmatrix} \mathbf{0} & \mathbf{M} \\ \mathbf{M} & \mathbf{D} \end{bmatrix}. \tag{1}$$

This leads to $2N$ eigenvalues κ_m corresponding to left and right eigenvectors $\mathbf{y}_{z,m}$ and $\mathbf{x}_{z,m}$ due to nonsymmetric system matrices for the IFEs

$$(\mathbf{A} - \kappa_m\mathbf{B})\mathbf{x}_{z,m} = \mathbf{0} \quad \text{and} \quad \mathbf{y}_{z,m}^T(\mathbf{A} - \kappa_m\mathbf{B}) = \mathbf{0}. \tag{2}$$

The subscript z indicates the twofold length of the eigenvectors as a consequence of the state-space linearization. The eigenvectors can be column-wisely comprised in modal matrices, which are indicated by the capital letters in what follows. The orthogonality of the modes is measured by the product of modal matrices and hypermatrices

$$\mathbf{Y}_z^T\mathbf{A}\mathbf{X}_z = \mathrm{diag}(\alpha_1, \ldots, \alpha_{2N-\delta}) \quad \text{and} \quad \mathbf{Y}_z^T\mathbf{B}\mathbf{X}_z = \mathrm{diag}(\beta_1, \ldots, \beta_{2N-\delta}), \tag{3}$$

where the ratio of the entries on the diagonals is found as the eigenvalues $\kappa_m = \alpha_m/\beta_m$. The eigenvalues are complex numbers and their real part contains information about the

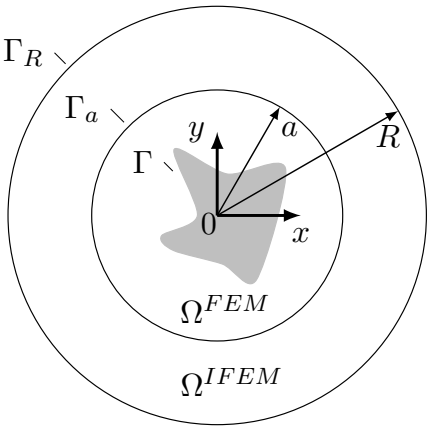

Fig. 1. General setup of the FEM/IFEM discretization: sound source as an obstacle (gray) in the fluid-filled computational domains Ω^{FEM} (radius a) and Ω^{IFEM} (outer radius R).

damping of the respective mode, whereas their imaginary part indicates its resonance frequency. δ is the rank deficiency of the mass matrix. A circular shape of the FE domain leads to an empty mass matrix for all DOFs of the IFEs.[12] Marburg[20] suggested canceling empty rows and columns, which leads to a system of equations of reduced size $2N - \delta$.

It is notable that only one single eigenvalue problem has to be solved, since the system matrices do not depend on the frequency and neither do the eigenvalues and eigenvectors.

2.1. *Modal sound pressure and sound power*

Up to this point, the eigensolution of the problem is frequency-independent and does not consider any right-hand-side excitation $\mathbf{f}$, e.g. caused by a structural particle velocity $v_s(\mathbf{x})$ at the boundary of inner obstacles. The discrete sound pressure field can be constructed by modal superposition of the truncated eigenvectors $\mathbf{y}_m$ and $\mathbf{x}_m$ of size $N \times 1$, considering only those N DOFs that are related to the pressure as shown by Marburg in Ref. 20:

$$\mathbf{p} = -\sum_{m=1}^{2N-\delta} \frac{\mathbf{y}_{\Gamma,m}^T \mathbf{f}_\Gamma}{\alpha_m + ik\beta_m} \mathbf{x}_m, \tag{4}$$

where the wave number $k = \omega/c_f$ is the ratio of the angular frequency $2\pi f$ and the speed of sound of the fluid. The index Γ indicates that only those DOFs in the right-hand-side vector and in the eigenvectors have to be taken into account that are related to the surface of the inner obstacles. The modal basis can be reduced if the sum is formed by the given eigenvectors and eigenvalues. In the same manner, the radiated sound power can be superimposed by a reduced number of modes. The discrete definition of the radiated sound power includes the discrete sound pressure and the particle velocities at the radiating boundaries[20,28]:

$$P = \Re\left\{\frac{1}{2}\mathbf{p}_\Gamma^T \Theta \mathbf{v}_\Gamma^*\right\}, \tag{5}$$

where Θ is the boundary mass matrix.[17] Hence, the sound power P_{NM} is found as the sum of modal sound power distributions P_m with

$$P_{\mathrm{NM}} = \Re\left\{-0.5\frac{1}{i\omega\rho_f}\sum_{m=1}^{2N-\delta} \frac{\mathbf{y}_{\Gamma,m}^T \mathbf{f}_\Gamma}{\alpha_m + ik\beta_m} \mathbf{x}_{\Gamma,m}^T \mathbf{f}_\Gamma^*\right\}. \tag{6}$$

The sound power P is called P_{Ainv} in what follows, as long as the included sound pressure vector in Eq. (5) is obtained by full inversion of the dynamic stiffness matrix $\mathbf{A}$ according to

$$\mathbf{p}_\Gamma = [\mathbf{A}^{-1}\mathbf{f}]_\Gamma = [(-\omega^2\mathbf{M} - i\omega\mathbf{D} + \mathbf{K})^{-1}(-i\omega\rho_f\Theta\mathbf{v}_s)]_\Gamma. \tag{7}$$

3. Models and Implementation

Three geometries are modeled and the respective FE matrices are computed by using the commercial software COMSOL Multiphysics®. The matrices as well as the mesh information are exported to MATLAB, where the subsequent processing is done. This includes the

implementation of the IFEM, the computation of the NMs and the radiated sound power as well as the visualization of the results. All models are two-dimensional problems that consider a solid structure as a sound-hard obstacle in a circular, fluid-filled FE domain, where the IFEs are attached to the outer boundary of the FE mesh according to the setup in Fig. 1.

The first model (a) is an ellipse-like structure with a rectangular insertion over the whole length of the ellipsoidal obstacle along the x-axis with a height of 0.1 m. The two semi-axes of the halfway stretched ellipses are $a = 0.9\,\mathrm{m}$ and $b = 17/30\,\mathrm{m} \approx 0.57\,\mathrm{m}$. The second geometry (b) is a slight modification of the first one. Here, a part of the inner rectangular insertion is cut out at the right side with a length of 1.7 m. The third obstacle (c) is the inversion of the second geometry, where the ellipse is removed and only the former cavity is an inner obstacle in the fluid domain. The geometries and meshes are depicted in Fig. 2.

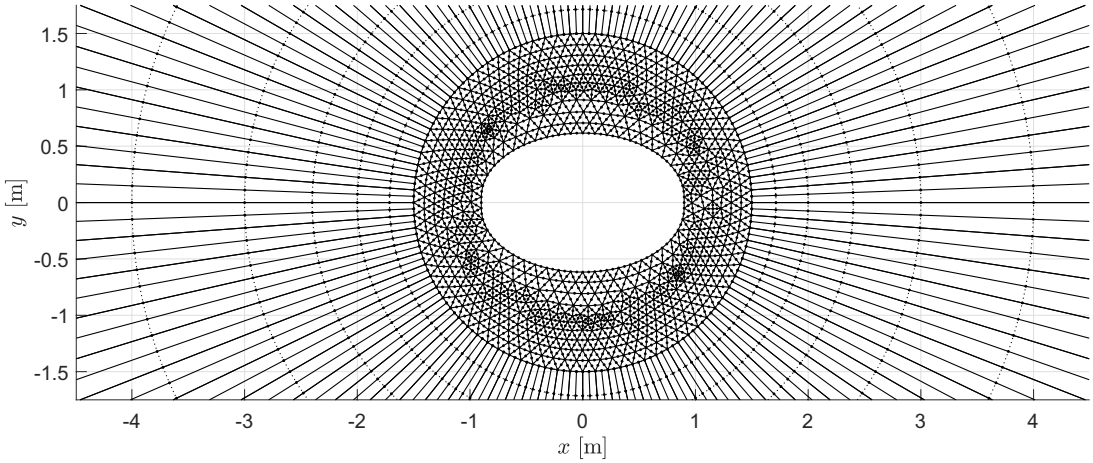

(a) Ellipsoidal obstacle

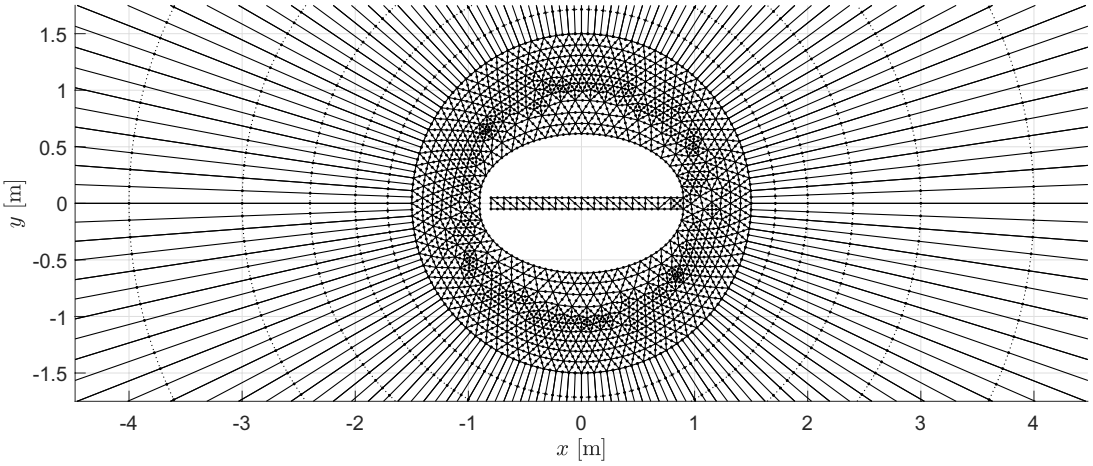

(b) Ellipsoidal obstacle with rectangular cavity

Fig. 2. Meshes in the fluid-filled domain around the three inner obstacles discretized by FE and IFEs.

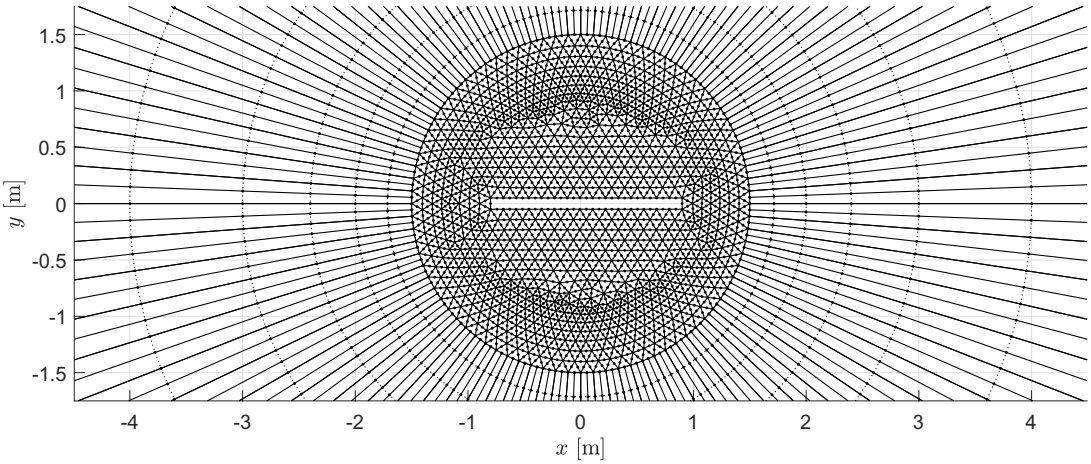

(c) Rectangular obstacle

Fig. 2. (*Continued*)

The three chosen geometries are motivated as follows: The fluid in the computational domain is air with a density of $\rho_f = 1.3\,\mathrm{kg\,m^{-3}}$ and a speed of sound of $c_f = 340\,\mathrm{ms^{-1}}$. In the case of a closed tube with a length of 1.7 m, the undamped eigenvalue problem leads to eigenfrequencies in 100 Hz-steps, starting from the first natural frequency at 0 Hz and corresponding to standing waves along the long side of the tube. In the case of the open cavity in the exterior acoustic domain, the eigenfrequencies are expected to appear damped at lower frequencies, but still can be found with roughly the same frequency step from one eigenfrequency to the next. This helps to better identify cavity-related resonance frequencies in the solution. In comparison to the ellipsoidal obstacle with the duct-like cut-out (b) and with these expected cavity modes inside, the ellipsoid (a) and the rectangle (c) are pure exterior problems. They all have the same IFE discretization and only differ in the inner area of the FE domain close to the surface of the obstacles, which might reveal similarities and differences in the spectral solution. In these examples, the role of pure real and complex eigenvalues and eigenvectors with respect to cavity-related resonances and outer multipole modes shall be investigated.

All surfaces of the obstacles behave reverberantly in such a way that the boundary admittance is zero $Y(\mathbf{x}) = 0$ and the particle velocities at the surfaces are the same in the fluid and in the structure $v_f = v_s$.[17] The FE mesh has a maximum element size of $h_{\max} = 11.33\,\mathrm{cm}$ in order to ensure at least six elements per wavelength at a frequency of 500 Hz for second-order Lagrangian FEs, which seems to be an appropriate sampling according to the literature Refs. 33 and 34.

At each of the 84 quadratic line elements at the outer circular FE boundary, an IFE is attached. Its polynomial order for the interpolation in the transversal direction is inherited from the corresponding boundary line. For the interpolation in the radial direction, the authors used 8-order Jacobi polynomials with the two corresponding exponents $\alpha = 1$ and $\beta = 0$. According to von Estorff *et al.*[14] and Dreyer *et al.*,[15] Jacobi polynomials provide a much better matrix condition number of the system matrices in comparison to Lagrange

Table 1. Number of DOFs of the three geometries.

Geometry	DOF FE	DOF IFE	DOF Total
Ellipsoid (a)	2746	1176	3922
Ellipsoid with cut-out (b)	2840	1176	4016
Rectangle (c)	3404	1176	4580

polynomials. This observation was confirmed by the authors in Ref. 21, however, the influence on NMs and ARMs was negligible. The number of DOFs in the used meshes is given in Table 1.

Two different load cases are investigated. In the first case, a structural particle velocity $v_{s,\mathrm{in}} = 1\,\mathrm{ms}^{-1}$ is applied to the inner left surface of the open duct. The other case is considered for two geometries, the ellipsoid and the ellipsoid with the cavity. A structural particle velocity $v_{s,\mathrm{out}} = 1\,\mathrm{ms}^{-1}$ is applied to all outer surfaces of the ellipsoid without the right surface of the rectangular insertion. Both excitations apply for all frequencies from 1 Hz to 500 Hz in 1 Hz-steps.

Reference solutions of the radiated sound power were computed by using COMSOL Multiphysics® and by applying a circular PML around the inner FE domain with a much finer mesh. The computation time of the presented method is not yet competitive to commercial codes, since it is not optimized for performance and only efficient if a reduced number of modes is considered during the modal superposition. Currently, the whole modal basis is computed in order to investigate the results regarding their characteristics and relevance and makes the approach hardly comparable to the PML approach, where the resulting radiated sound power is determined directly and efficiently.

4. Results

4.1. *Eigenvectors*

The NM eigenvectors are found in the whole computational fluid domain including FE and IFE DOFs. However, in general, the main focus is on the sound pressure distribution at the mesh nodes close to the inner obstacles, i.e. in the FE domain. Three typical mode shapes are column-wisely depicted in Fig. 3 in the example of the ellipsoidal with the open duct. The authors distinguish between modes with the sound pressure mainly concentrated at or close to the surface of the inner obstacles or inside a cavity, those with the sound pressure mainly concentrated at the junction between the FE and IFE domains and, finally, those modes with an even distribution.

In order to distinguish between these three kinds of mode shapes, the sum of certain eigenvector entries is set in relation to the sum of the remaining entries associated to the DOFs in the FE domain. In doing so, the concentration of the sound pressure — either at the surface of the inner obstacles or at the junction of the FE and the IFE domains — can be compared to the remaining share of the sound pressure distribution in the entire fluid, and the qualitative distinction can be done automatically to a certain extent. The eigenvectors

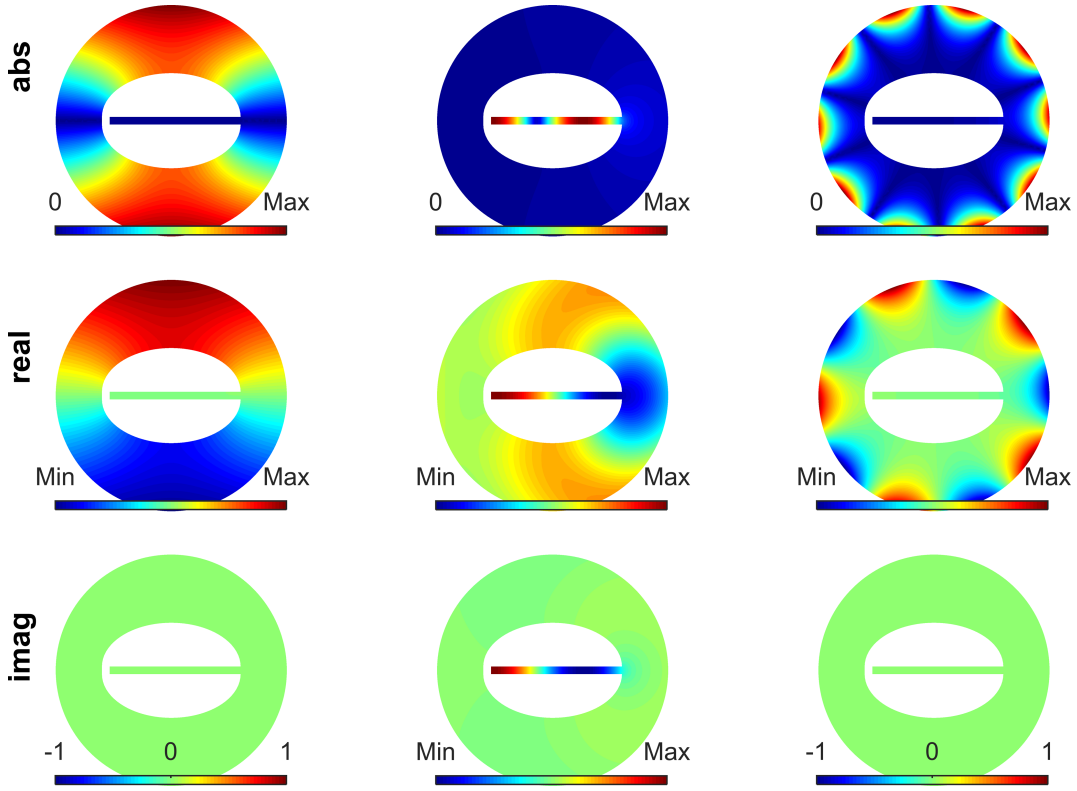

Fig. 3. Three exemplary kinds of NM shapes (one per column) as right eigenvectors $\mathbf{x}$ for the second geometry (b): even sound pressure distribution in the whole fluid domain (left); concentration of pressure peaks close to the surface of inner obstacles or cavity modes (middle); concentration of sound pressure peaks at the junction of the FE and IFE domains (right); Eigenvector magnitudes (first row), real parts (second row) and imaginary parts (bottom row).

were normalized to the length of one for this purpose and called $\hat{\mathbf{x}}$. In mathematical terms, the eigenvector distribution ratio χ_m for a certain mode m can be written as

$$\chi_m = \frac{\sum_i |\hat{\mathbf{x}}_{m,i}|}{\sum_j |\hat{\mathbf{x}}_{m,j}|} \quad \text{with } i \in \Gamma \text{ and } j \in \Omega \backslash \Gamma, \tag{8}$$

where $\Gamma = \Gamma_{\text{in}} \vee \Gamma_{\text{out}}$ includes either the DOFs at the inner boundaries of the obstacles Γ_{in} or at the outer FE boundary Γ_{out}.

As mentioned in Sec. 2, the asymmetry of the IFE matrices provides left and right eigenvectors that are both part of the orthogonal modal basis and are required for the computation of the modal sound pressure and sound power contributions, see Sec. 2.1. Examples of left and right eigenvectors are visualized in Fig. 4 for IFE DOFs only, since both mode shapes are almost the same in the FE domain. The similarity of left and right eigenvectors can be measured by the modal assurance criterion (MAC), which is presented in Sec. 4.3. The left eigenvectors show a much more extended radiation pattern in the radial direction in comparison to the right eigenvectors and are in antiphase to each other.

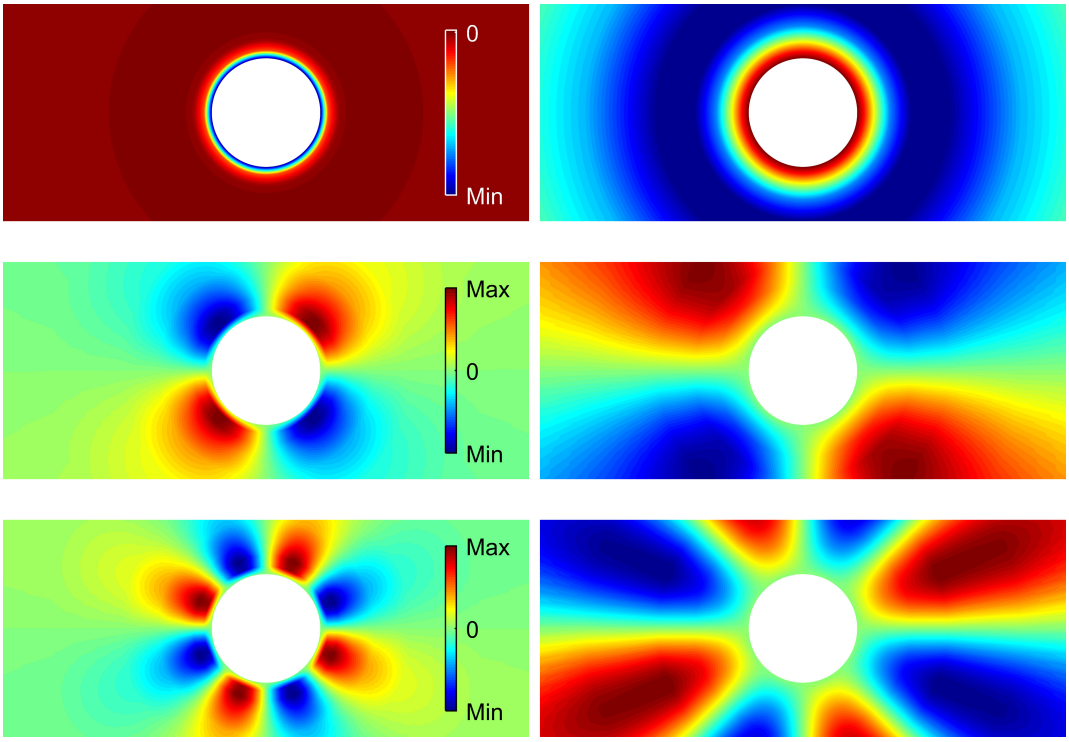

Fig. 4. Three examples of right eigenvectors $\mathbf{x}$ (left column) and the corresponding left eigenvectors $\mathbf{y}$ (right column) in the IFE domain, each both purely real and colored on the basis of the same color scale, respectively.

4.2. *Eigenvalues*

Initially, the NMs are sorted by increasing the magnitude of their eigenvalue κ_m. This order is not necessarily the best sequence of significance for the efficient superposition of NMs, even though weakly damped modes (small $\Re\{\kappa_m\}$) at low frequencies (small $\Im\{\kappa_m\}$) can be found in the very beginning in the list of ascending eigenvalue magnitudes. The subsequent modes might either have a weak damping or become in resonance at low frequencies in the audible frequency range, which is both an indicator of significance for the radiation of sound and therefore for the modal superposition of sound pressure or sound power. This leads to the research question of how a modified sorting algorithm could distinguish between relevant and nonrelevant modes.

The eigenvalues of the second problem (ellipse with the open duct inside) are depicted in the complex plane in Fig. 5. With each increment of the number of IFE radial interpolation points n_{rad}, a new straight line of highly damped eigenvalues comes up, where — at the same time — the other existing lines of eigenvalues move with a growing absolute angle in the polar form. As observed by the authors in Ref. 21, an even number for the polynomial order n_{rad} leads to a line of purely real eigenvalues (cf. Fig. 5 with $n_{\text{rad}} = 8$), whereas odd polynomial degrees do not induce these eigenvalues.

It can be observed that the eigenvalues are symmetric with respect to the real axis, which is due to the appearance of complex conjugated eigenvalues with a different sign of

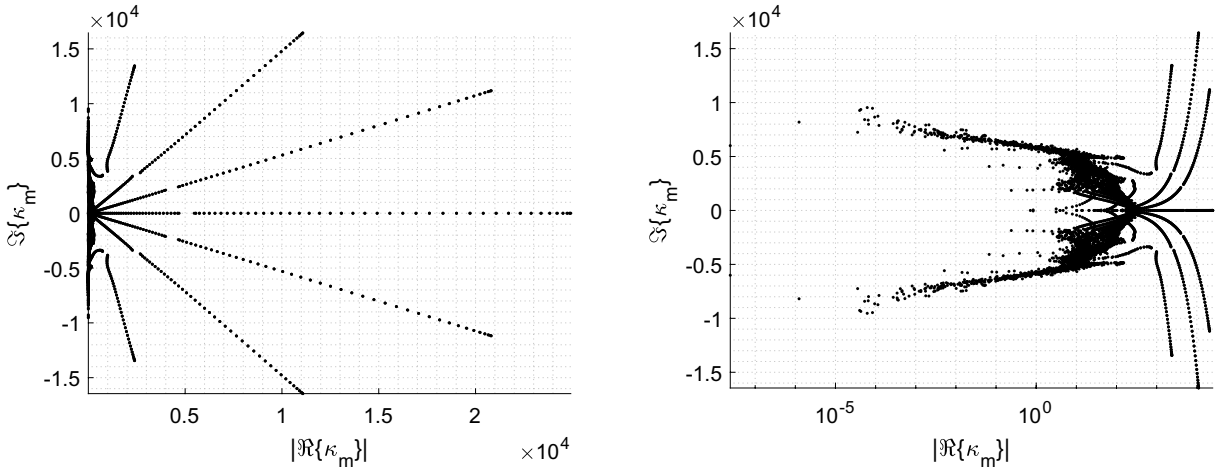

Fig. 5. NM eigenvalues of the cavity problem (second geometry) in the complex plane with linear (left) and logarithmic (right) scaling of the real axis.

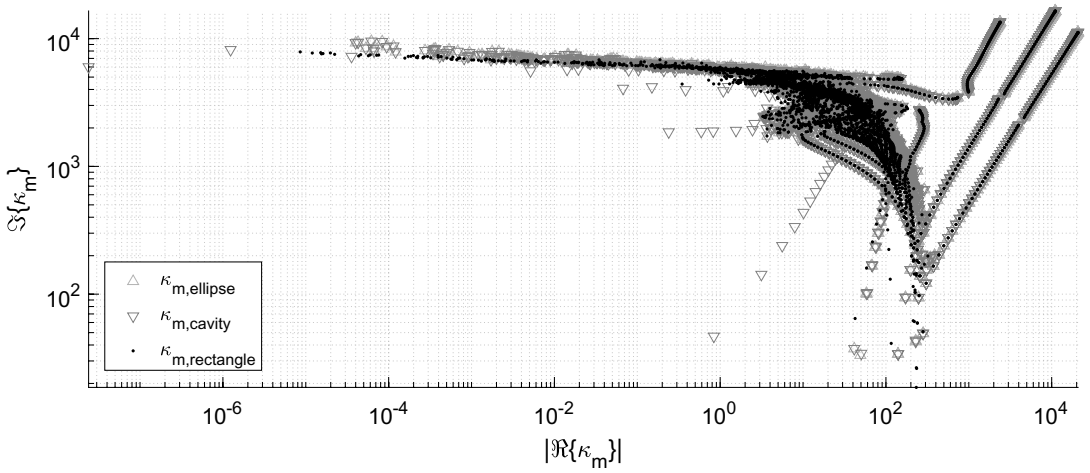

Fig. 6. Eigenvalues of the three models shown in one complex plane, considering only the positive part of the imaginary axis with double-logarithmic scaling, neglecting the purely real eigenvalues: ellipsoidal obstacle (gray deltas), ellipsoidal obstacle with the rectangular cavity (gray nablas) and rectangle (black dots).

their imaginary parts (resonance frequency), corresponding to — more or less — the same mode shape (cf. Secs. 4.1 and 4.3).

In Fig. 6, the eigenvalues of the three models are only shown in one complex plane for positive imaginary parts. In particular, most of the highly damped eigenvalues are very similar for all three problems and seem to be correlated with the properties of the IFEs. This is not the case for weakly damped eigenvalues whose positions in the complex plane seem to be more problem-dependent and therefore related to eigenvectors with a significant sound pressure distribution close to the inner obstacles. In the case of the cavity problem (b), additional lines of weakly damped eigenvalues at low frequencies can be observed. Some

of them appear roughly in 100 Hz-steps, which was expected by the choice of the 1.7 m-long, duct-like cavity in the ellipse. Another line of cavity-related eigenvalues at higher frequencies begins with a weaker damping once again. These eigenvalues correspond to eigenvectors with resonances in the lateral y-direction of the open duct. If no inner obstacle is placed inside the FE domain, the observations can be confirmed: the highly damped eigenvalues in lines and a few multipole modes in the FE domain with small real parts of their eigenvalues can be found in the complex plane, whereas there are no problem-specific mode shapes.

According to Sec. 4.1, the eigenvectors can be roughly classified by the concentration of their pressure distribution χ at inner Γ_{in} or outer boundaries Γ_{out} in relation to the remaining FE DOFs in the fluid domain, see Eq. (8) and the three examples in Fig. 3. The corresponding eigenvalues can thus be rated as inner, outer or mixed modes with respect to their eigenvector distribution ratio. This was done in Fig. 7 in the example of the second geometry with the eigenvalues in the complex plane and with χ in the third dimension and additionally colored from blue to red for small to high values of χ. It can be observed that the higher the real part of the eigenvalues, the higher the distribution ratio of the eigenvectors at the junction of the FE and the IFE domains (see Fig. 7(a)). The highest pressure concentration can be found for purely real eigenvalues with a real part in a range of about 10^3 to 10^4. On the other hand in Fig. 7(b), the highest pressure concentration at the inner obstacle is found for eigenvalues in the middle range of the real axis, where the cavity-related modes were expected in Fig. 6. The lowest concentration can be observed for highly damped modes, even though the ratios increase significantly at the very end of the real axis. In both cases, the behavior is the same for the complex conjugated partners in such a way that the lower pictures are virtually symmetric with respect to the real axis.

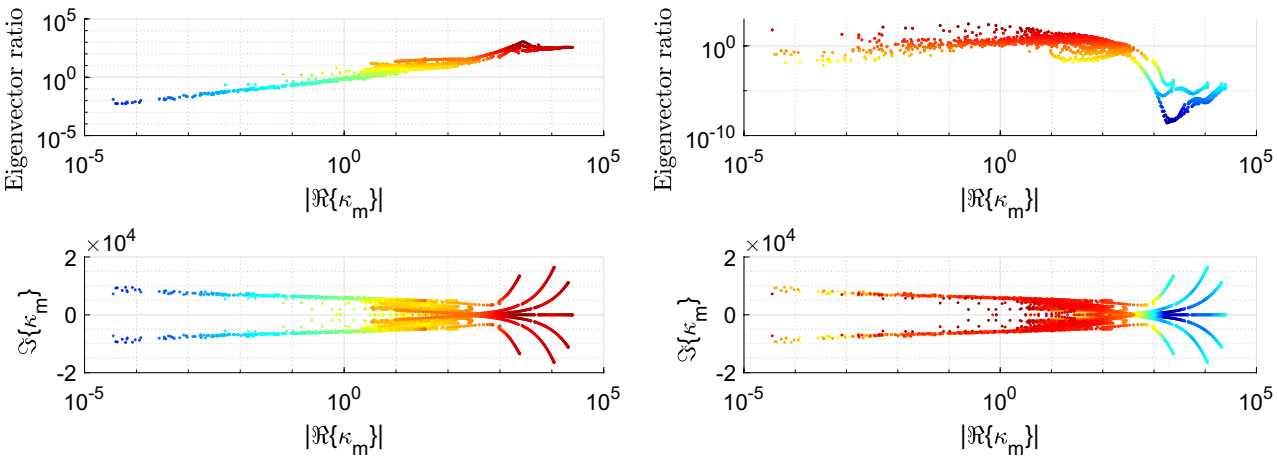

(a) Outer boundary modes

(b) Inner boundary modes

Fig. 7. (Color online) Eigenvalues in the complex plane with the ratios of the eigenvector distributions χ (see Eq. (8)) on the z-axis for the outer FE boundary Γ_{out} (left) and inner obstacle boundaries Γ_{in} (right) each with respect to the remaining DOFs; second geometry; each two views of a three-dimensional plot, where the color indicates the height on the z-axis (blue/small to red/high).

The authors observed that purely real eigenvalues are associated with purely real eigenvectors. This applies in the same manner for complex eigenpairs.

4.3. *Modal assurance criterion (MAC)*

By means of the MAC[35] the similarity of the eigenvectors to each other can be rated in an interval between zero and one. In previous work, the authors used the MAC in order to track the eigenvalues in convergence studies with different meshes and increasing orders of radial interpolation polynomials.[21]

The MAC values of the left and right eigenvectors of the second geometry are depicted in Fig. 8(a). Two cases are compared to each other: either only FE DOFs (gray) or all DOFs (including the FE and IFE domains; red) are considered. Left and right eigenvectors are almost the same (MAC ≈ 1) according to MAC in the first case. On the other hand, only a few pairs of left and right eigenvectors are virtually identical, when all DOFs are taken into account. Here, the MAC values are distributed in almost the whole range between zero and one. In Fig. 8(b), the MAC value is added in colors (blue/zero to red/one) and to the third dimension to the complex plane of NM eigenvalues. Obviously, the similarity of left and right eigenvectors is the best for weakly damped modes, which are primarily related to large eigenvector contributions at the inner boundary lines (cf. Fig. 7(b)). Accordingly, the single peaks (with small mode numbers m) of each two modes with a relatively high MAC value for FE and IFE DOFs (red) in Fig. 8(a) are the cavity modes. For eigenvalues with a real part larger than 1, the MAC values decrease virtually, logarithmically and with increasing damping until the values slightly grow for the very highly damped eigenvalues that do correspond to outer FE boundary modes (cf. Fig. 7(a)). The MAC values are virtually the same for both complex conjugated eigenvalue partners.

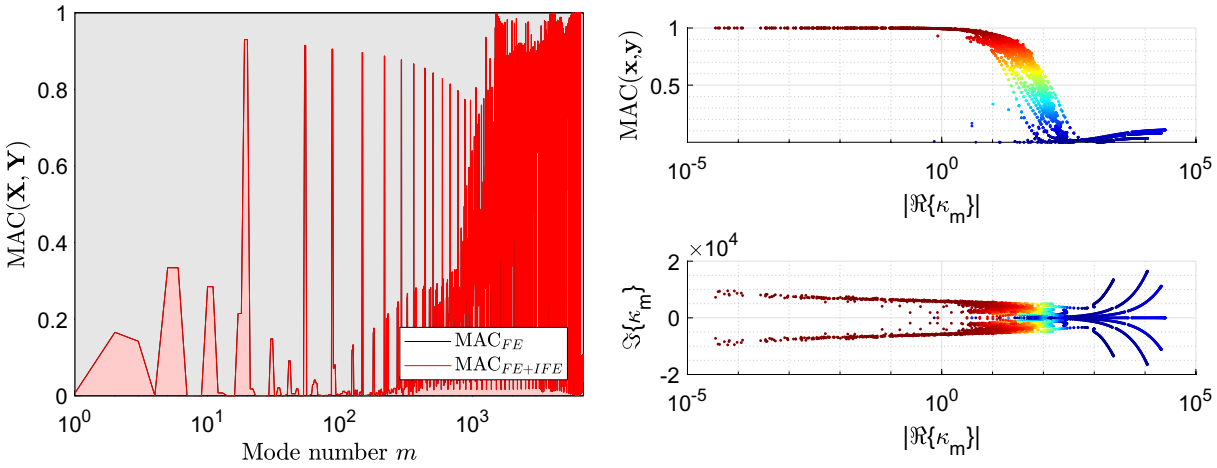

(a) (b)

Fig. 8. (Color online) MAC of left and right NM eigenvectors in the example of the ellipse with the rectangular cavity. (a) MAC for FE DOFs only (black; almost one for all modes) and for all DOFs in the FE and the IFE domains (red) and (b) Complex plane of NM eigenvalues κ_m with the MAC value in the third dimension and colored from blue/zero to red/one.

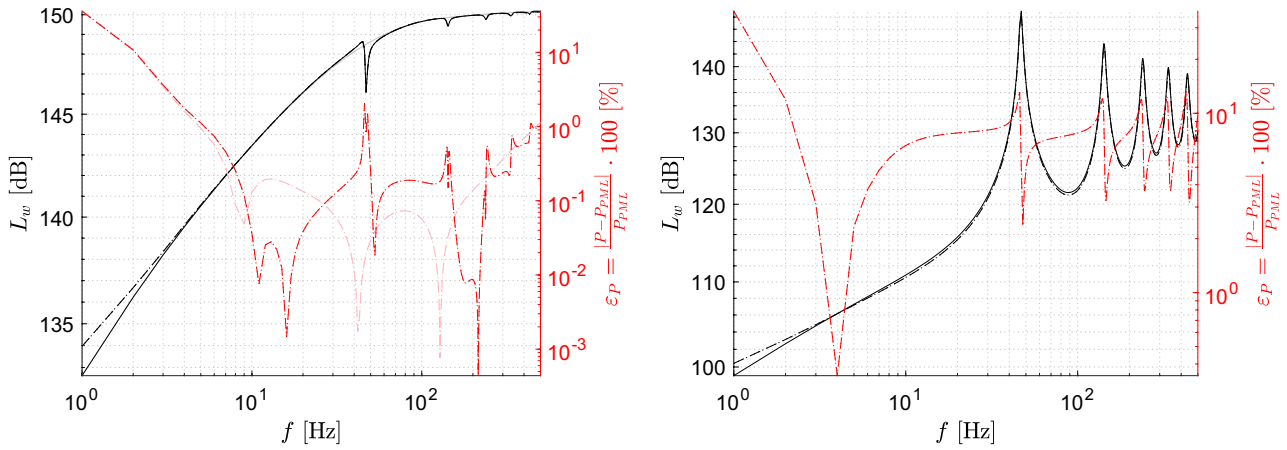

(a) $v_{s,\text{out}} = 1\,\text{ms}^{-1}$ geometries (a) and (b). (b) $v_{s,in} = 1\,\text{ms}^{-1}$; geometry (b).

Fig. 9. (Color online) Sound power level L_w and relative error ε_P with respect to the PML solution for two different load cases and geometries. Geometry (a): error curves (pink), sound power curves (gray); geometry (b): error curves (red), sound power curves (black); PML reference curves (————), full inversion P_{Ainv} in Eqs. (5) and (7) (– – – –), P_{NM} in Eq. (6) (· · · · ·).

4.4. *Modal sound power*

The two different load cases $v_{s,\text{out}}$ (for geometries (a) and (b)) and $v_{s,in}$ (for geometry (b)) lead to the radiation of sound power, which is depicted in Fig. 9 in terms of the sound power level L_w. The sound power is determined by three different approaches for each problem: $P_{A,\text{inv}}$ — full inversion of the dynamic stiffness matrix for the vector of nodal sound pressure values in Eq. (7) to be substituted into Eq. (5), P_{NM} — full summation of modal sound power contributions according to Eq. (6) and P_{PML} — a reference solution is computed by using the commercial FE software COMSOL Multiphysics® and by applying PMLs.

It can be observed in Fig. 9(a) that the radiated sound power is almost identical for both geometries and approaches if the structural velocity $v_{s,\text{out}}$ is applied to the outer ellipsoidal surfaces of the obstacles. At the resonance frequencies of the cavity modes, the sound power level collapses slightly for geometry (b) with the opening, while the relative errors, with respect to the PML reference solution, increase significantly. However, the relative errors are less than 1% above 10 Hz and differ for both geometries, but do not for the different approaches, respectively.

If the velocity excitation is applied to the left end of the duct-like cavity (b), the resonances in the tube can clearly be found in the curves of the sound power levels (see Fig. 9(b)). The relative errors of $P_{A,\text{inv}}$ and P_{NM} with respect to the PML solution are virtually the same and in the order of magnitude of $\approx 10\%$ even though the approximation of the sound power seems to be reasonable in the whole frequency range.

Each NM has its own contribution to the total radiated sound pressure $\mathbf{p}_m$ and sound power P_m (cf. Eqs. (4) and (6)). These two quantities are frequency-dependent and their modal contribution varies as the frequency changes. This is illustrated in Fig. 10(a) for 1 Hz and for multiple frequencies in Fig. 10(b) in the example of the second geometry and with

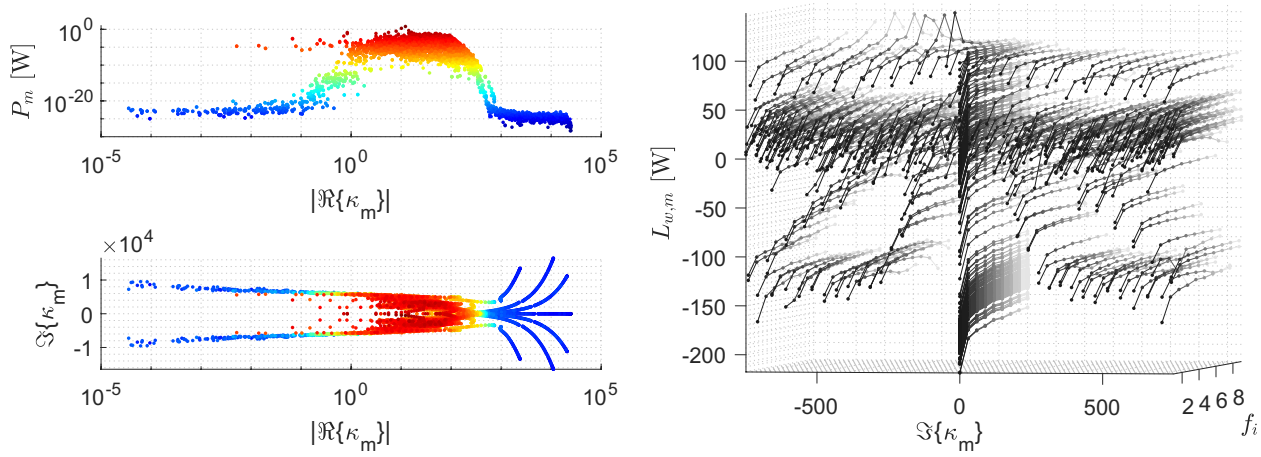

(a) (b)

Fig. 10. (Color online) Modal sound power and sound power level contributions P_m and $L_{w,m}$ of NM eigenvalues m for geometry (b) and $v_{s,in}$. (a) P_m at 1 Hz in the third dimension of the complex plane (blue/small to red/high) and (b) $L_{w,m}$ at frequency steps f_i (with increasing brightness) for $\Im\{\kappa\} \leq |\pm 750\,\text{Hz}|$.

the excitation inside the open duct $v_{s,\text{in}}$. The largest sound power is contributed by NMs with a real part in a range of about 0.01 o 1000, which are most likely related to inner boundary modes according to Fig. 7(b). At 1 Hz, the sound power share in the complex plane is virtually symmetric with respect to the real axis (see Fig. 10(a)), i.e. the sound power contribution of the eigenvalues is almost the same for both complex conjugated partners. In Fig. 10(b), the sound power levels for nine frequency steps f_i are only depicted for positive and negative imaginary parts of κ_m that are smaller than 750 Hz according to the amount, for the sake of clarity. Five of these frequency steps f_i are close to resonances of cavity modes. Most of the modal sound power contributions seem to increase as the frequency grows (which is emphasized by increasing the brightness of the lines), but only a few of them — primarily on the negative side of the imaginary axis — show clear peaks in particular at these resonance frequencies. This leads to an obviously asymmetric modal sound power level contribution for positive and negative imaginary parts of the complex eigenvalue partners. The differences of the modal sound power contributions of each of the two complex conjugated partners are depicted in Fig. 11, where the observations in Fig. 10(b) can be confirmed: The eigenvalue partners differ significantly at their corresponding cavity resonance frequencies only, where the radiation of sound is mainly due to the modes with the negative imaginary parts.

Different properties of the eigenvalues and eigenvectors have been discussed so far. With the aim of modal reduction during the summation process, a number of reduced modal bases is taken into account in Fig. 12, where the errors relative to P_{Ainv} (Eqs. (5) and (7)) are depicted for both $v_{s,\text{out}}$ (Fig. 12(a)) and $v_{s,\text{in}}$ (Fig. 12(b)) for the ellipsoidal geometry with the cavity (b). The relative error for the full modal basis is almost equal to zero over the whole frequency range for both velocity excitations and shown as a red, thick

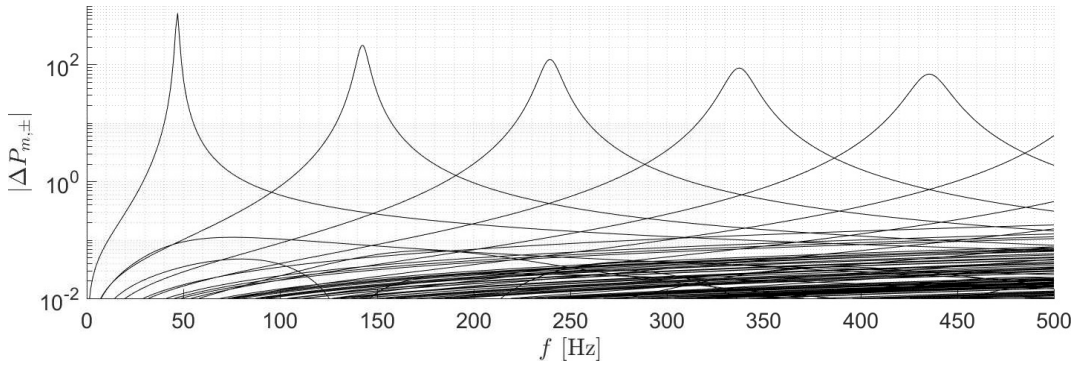

Fig. 11. Absolute sound power differences $|P_{m,\pm}|$ between 3316 complex conjugated eigenvalue partners m as functions of the frequency for geometry (b) and $v_{s,\text{in}}$.

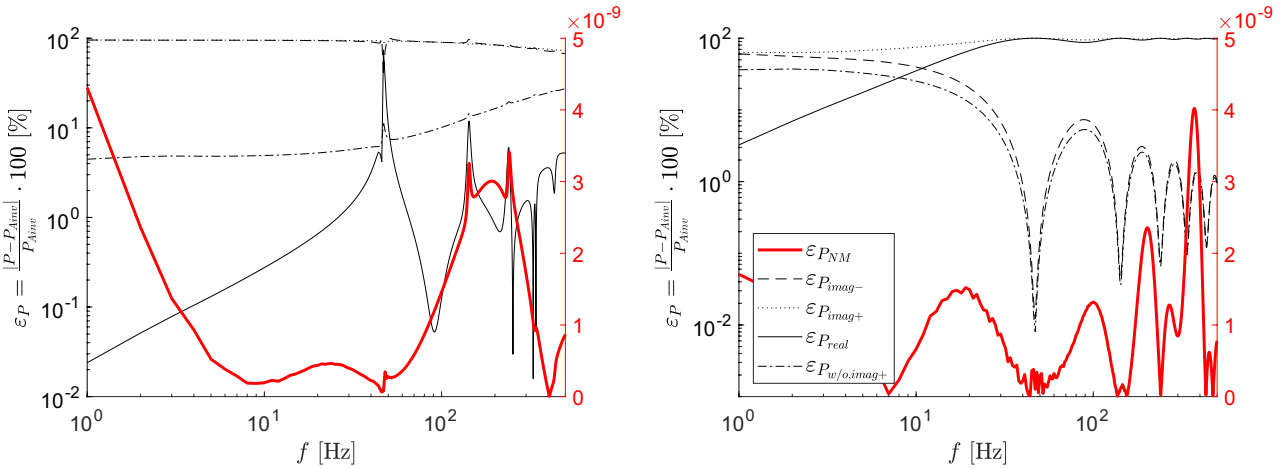

(a) (b)

Fig. 12. (Color online) Errors of the superimposed sound power curves (relative to P_{Ainv}) for geometry (b) and both load cases $v_{s,\text{out}}$ and $v_{s,\text{in}}$ considering the whole modal basis (red, thick line), only modes with negative imaginary parts (– – – –), only modes with positive imaginary parts (· · · · ·), only purely real modes (————) and neglecting only the modes with positive imaginary parts (– · – · –).

line, respectively. In the case of the outer excitation, the purely real eigenvalues lead to an acceptable relative error of less than 1%, except in the region of the cavity resonance frequencies. When considering only complex eigenvalues with only positive or only negative imaginary parts, respectively, the relative errors are not acceptable for the given geometry and excitation. In the last case, only the complex eigenvalues with a positive imaginary part are removed from the whole modal basis, which leads to a better result over the whole frequency range and less significant error peaks at the resonances in particular. However, the overall error is much worse in comparison to the purely real modal basis.

If the velocity excitation is applied inside the open duct, the purely real modal basis performs almost as poorly as the complex eigenvalues with a positive imaginary part, as can be seen in Fig. 12(b). The relative error is acceptable for frequencies higher than 10 Hz for

the two other methods: the eigenvalues with negative imaginary parts and — even better — the modal basis without the complex eigenvalues with a positive imaginary part.

Altogether, this leads to the assumption that pure exterior problems are mainly dominated by the purely real eigenvalues, and the cavity modes are due to the complex eigenvalues with a negative imaginary part. Neglecting the eigenvalues with a positive imaginary part only leads to acceptable results in the given example. However, better performance is desired and the criteria for reduced modal bases have to be further developed.

5. Conclusion

The sound pressure and sound power due to structural velocities in exterior problems could be determined by superposition of NMs. The major part of the eigenvalues is not problem-specific and due to the FE and IFE mesh. It was found that for weakly damped modes, the sound pressure is mainly concentrated at the surfaces of inner obstacles in the fluid, whereas highly damped modes have a large pressure distribution at the junction of the FE and the IFE domains. However, the largest share of radiated sound power is not due to the modes with the smallest damping coefficient, but it is mainly dominated by cavity resonances. The authors observed that the sound power peaks at these resonances are due to modes with a negative imaginary part, whereas the positive complex conjugated partners play a minor role in the radiation of sound. In order to further reduce the modal basis and — at the same time — minimize the errors during the modal superposition, additional criteria have to be developed in future work.

Acknowledgments

The support by the Deutsche Forschungsgemeinschaft (DFG project number 230029255) is gratefully acknowledged by the authors.

References

1. S. H. Schot, Eighty years of Sommerfeld's radiation condition, *Historia Math.* **19**(4) (1992) 385–401.
2. O. C. Zienkiewicz and R. L. Taylor, *The Finite Element Method for Solid and Structural Mechanics* (Butterworth-Heinemann, Oxford, 2005).
3. D. Givoli, T. Hagstrom and I. Patlashenko, Finite element formulation with high-order absorbing boundary conditions for time-dependent waves, *Comput. Methods Appl. Mech. Eng.* **195**(29) (2006) 3666–3690.
4. D. Givoli, Computational absorbing boundaries, in *Computational Acoustics of Noise Propagation in Fluids — Finite and Boundary Element Methods* (Springer, Berlin, 2008), pp. 145–166.
5. D. Rabinovich, D. Givoli and E. Bécache, Comparison of high-order absorbing boundary conditions and perfectly matched layers in the frequency domain, *Int. J. Numer. Methods Biomed. Eng.* **26**(10) (2010) 1351–1369.
6. J.-P. Berenger, A perfectly matched layer for the absorption of electromagnetic waves, *J. Comput. Phys.* **114**(2) (1994) 185–200.

7. A. Bermúdez, L. Hervella-Nieto, A. Prieto and R. Rodríguez, Perfectly matched layers, in *Computational Acoustics of Noise Propagation in Fluids — Finite and Boundary Element Methods*, eds. S. Marburg and B. Nolte (Springer, Berlin, Heidelberg, 2008), pp. 167–196.
8. A. Bermúdez, L. Hervella-Nieto, A. Prieto and R. Rodríguez, Perfectly matched layers for time-harmonic second order elliptic problems, *Arch. Comput. Methods Eng.* **17**(1) (2010) 77–107.
9. P. Bettess, Infinite elements, *Int. J. Numer. Methods Eng.* **11**(1) (1977) 53–64.
10. D. S. Burnett, A three-dimensional acoustic infinite element based on a prolate spheroidal multipole expansion, *J. Acoust. Soc. Am.* **96**(5) (1994) 2798–2816.
11. R. J. Astley, Infinite elements, in *Computational Acoustics of Noise Propagation in Fluids — Finite and Boundary Element Methods*, eds. S. Marburg and B. Nolte (Springer, Berlin, Heidelberg, 2008), pp. 197–230.
12. R. J. Astley, G. J. Macaulay, J.-P. Coyette and L. Cremers, Three-dimensional wave-envelope elements of variable order for acoustic radiation and scattering. Part i. Formulation in the frequency domain, *J. Acoust. Soc. Am.* **103**(1) (1998) 49–63.
13. R. J. Astley and J.-P. Coyette, Conditioning of infinite element schemes for wave problems, *Commun. Numer. Methods Eng.* **17**(1) (2001) 31–41.
14. O. von Estorff, S. Petersen and D. Dreyer, Efficient infinite elements based on Jacobi polynomials, in *Computational Acoustics of Noise Propagation in Fluids — Finite and Boundary Element Methods*, eds. S. Marburg and B. Nolte (Springer, Berlin, Heidelberg, 2008), pp. 231–250.
15. D. Dreyer and O. von Estorff, Improved conditioning of infinite elements for exterior acoustics, *Int. J. Numer. Methods Eng.* **58**(6) (2003) 933–953.
16. T. W. Wu, *Boundary Element Acoustics Fundamentals and Computer Codes* (WIT Press, Southampton, 2000).
17. S. Marburg and B. Nolte, A unified approach to finite and boundary element discretization in linear time-harmonic acoustics, in *Computational Acoustics of Noise Propagation in Fluids — Finite and Boundary Element Methods*, eds. S. Marburg and B. Nolte (Springer, Berlin Heidelberg, 2008), pp. 1–34.
18. S. Marburg, Normal modes in external acoustics. Part i: Investigation of the one-dimensional duct problem, *Acta Acust. United Ac.* **91**(6) (2005) 1063–1078.
19. S. Marburg, F. Dienerowitz, T. Horst and S. Schneider, Normal modes in external acoustics. part ii: Eigenvalues and eigenvectors in 2d, *Acta Acust. United Ac.* **92**(1) (2006) 97–111.
20. S. Marburg, Normal modes in external acoustics. Part iii: Sound power evaluation based on superposition of frequency-independent modes, *Acta Acust. United Ac.* **92**(2) (2006) 296–311.
21. L. Moheit and S. Marburg, Infinite elements and their influence on normal and radiation modes in exterior acoustics, *J. Comput. Acoust.* **25**(04) (2017) 1650020.
22. L. Moheit and S. Marburg, Acoustic radiation modes and normal modes in unbounded domains, in *Proc. Meetings on Acoustics 173EAA* (ASA Conference, Boston, MA USA, 2017), p. 022004.
23. P. Ruge, Eigenvalues of damped structures: Vectoriteration in the original space of dof, *Comput. Mech.* **22**(2) (1998) 167–173.
24. F. Tisseur and K. Meerbergen, The quadratic eigenvalue problem, *SIAM Rev.* **43**(2) (2001) 235–286.
25. S. Fuß, S. C. Hawkins and S. Marburg, An eigenvalue search algorithm for the modal analysis of a resonator in free space, *J. Comput. Acoust.* **19**(01) (2011) 95–109.
26. A. Kuijpers, G. Verbeek and J. Verheij, An improved acoustic fourier boundary element method formulation using fast fourier transform integration, *J. Acoust. Soc. Am.* **102**(3) (1997) 1394–1401.
27. P. H. L. Kessels, *Engineering Toolbox for Structural-acoustic Design*: *Applied to MRI-Scanners* (Technische Universiteit Eindhoven, Netherlands, 2001).

28. H. Peters, N. Kessissoglou and S. Marburg, Enforcing reciprocity in numerical analysis of acoustic radiation modes and sound power evaluation, *J. Comput. Acoust.* **20**(03) (2012) 1250005.
29. H. Peters, N. Kessissoglou and S. Marburg, Modal decomposition of exterior acoustic-structure interaction, *J. Acoust. Soc. Am.* **133**(5) (2013) 2668–2677.
30. H. Peters, N. Kessissoglou and S. Marburg, Modal decomposition of exterior acoustic-structure interaction problems with model order reduction, *J. Acoust. Soc. Am.* **135**(5) (2014) 2706–2717.
31. J. Baumgart, S. Marburg and S. Schneider, Efficient sound power computation of open structures with infinite/finite elements and by means of the Padé-via-Lanczos algorithm, *J. Comput. Acoust.* **15**(04) (2007) 557–577.
32. M. M. Wagner, P. M. Pinsky, A. A. Oberai and M. Malhotra, A Krylov subspace projection method for simultaneous solution of Helmholtz problems at multiple frequencies, *Comput. Methods Appl. Mech. Eng.* **192**(41) (2003) 4609–4640.
33. S. Marburg, Six boundary elements per wavelength: Is that enough? *J. Comput. Acoust.* **10**(01) (2002) 25–51.
34. P. Langer, M. Maeder, C. Guist, M. Krause and S. Marburg, More than six elements per wavelength: The practical use of structural finite element models and their accuracy in comparison with experimental results, *J. Comput. Acoust.* **25** (2017) 1750025.
35. R. J. Allemang, The modal assurance criterion–twenty years of use and abuse, *J. Sound Vib.* **37**(8) (2003) 14–23.

Publication C

Journal of Sound and Vibration 476 (2020) 115291

Contents lists available at ScienceDirect

Journal of Sound and Vibration

journal homepage: www.elsevier.com/locate/jsvi

Analysis of scattering by finite sonic crystals in free field with infinite elements and normal modes

Lennart Moheit *, Spyridon Anthis, Johannes Heinz, Felix Kronowetter, Steffen Marburg

Chair of Vibroacoustics of Vehicles and Machines, Technical University of Munich, 85748, Garching, Germany

ARTICLE INFO

Article history:
Received 1 May 2019
Revised 25 February 2020
Accepted 28 February 2020
Available online 6 March 2020
Handling Editor: I. Trendafilova

Keywords:
Exterior acoustics
Infinite element method
Normal modes
Sonic crystals
Meta-atoms
Noise barriers

ABSTRACT

Acoustic exterior problems are in this paper solved numerically using the Astley-Leis infinite element method (IFEM). Normal modes can be determined thanks to the frequency independence of the system matrices. Convergence properties of the harmonic sound pressure solution as well as of normal mode eigenvalues are investigated for two-dimensional elliptical computational domains to estimate the essential requirements of accuracy. A relationship between the half-axis ratio of the ellipses and the eigenvalues is identified. By solving half-space problems, symmetry of the computational domains is utilized, which is shown for the first time for frequency-independent normal modes in exterior acoustics. This paper discusses applicability of the modes in the example of sonic crystals—periodic arrays of scatterers, in this context denoted as acoustic meta-atoms—that have recently attracted attention for their possible use as noise barriers. It can be shown that the sound-insulating effect of finite sonic crystals and individual meta-atoms in the free field can be related to normal modes in exterior acoustics. With the help of this approach, the absorption by Helmholtz resonators and due to a boundary admittance inside are studied. This work provides a new point of view and physical insights into the effects and underlying physics of sound insulation by finite sonic crystals and acoustic meta-atoms in free field. Although it is not the intention of this article to optimize the arrays, the method of normal modes in exterior acoustics is presented as an appropriate and novel tool for their dimensioning and design.

1. Introduction

In recent years, sonic crystals have gathered much attention in the field of environmental acoustics, e.g. the design of noise barriers. Sonic crystals are periodic arrays of scatterers, most commonly designed as vertical cylinders. Their charm compared to standard noise barriers lies in that they are light, easily built and they can be extended or modified with little effort to be effective in a wide range of the frequency spectrum [1]. Another advantage is that they allow both light and air to pass through them freely, which ultimately leads to reduced wind loading on the noise barriers [2]. An interesting characteristic of sonic crystals are so-called *band gaps*, which are certain frequency ranges with ideally complete noise insulation in case of periodic, infinite arrangements of scatterers.

By altering their geometry or their arrangement, the effectiveness of sonic crystals can be controlled. Two of the most crucial factors are their diameter and the spacing between them, where mainly square and triangular lattices are discussed in the

* Corresponding author.
E-mail address: lennart.moheit@tum.de (L. Moheit).

https://doi.org/10.1016/j.jsv.2020.115291
0022-460X/

literature [1,3]. Gupta et al. [4] create a design of a radial sonic crystal with scatterers arranged periodically in the angular direction around a cylindrical sound source. Perforations or slits along their length can also adjust their range, if positioned suitably [2]. Krynkin et al. [5] found that increasing the number of slits also increases the frequency of the resonance. Van der Aa and Forssén [6] considered perforated scatterers filled with porous materials and found that they have both broader and lower resonance peaks. Chalmers et al. [7] showed that a sonic crystal consisting of c-shaped scatterers has two types of band gaps; one is attributed to the arrangement of the scatterers (Bragg band gap) and the other to the resonating fluid inside the scatterer (resonance band gap), which is referred to as meta-atom. Elford et al. [8] refer to the experimental results of their work and investigated concentric c-shaped ('Matryoshka') sonic crystals, whose resonance frequency is found to be independent of the periodic spacing within a sonic crystal. The resonance peak can be broadened by using multiple resonators with overlapping individual resonance peaks within a 'Matryoshka' scatterer. Montiel et al. [9] have analytically calculated the scattering sound pressure field and the transmission loss of finite sonic crystals for sound-hard cylindrical and c-shaped meta-atoms and compared them with numerical simulations. They relate the resonance frequencies of the Helmholtz resonators to sub-Bragg band gaps. 'Mie' type meta-atoms treated by Cheng et al. [10] and Lu et al. [11] indicate that sophisticated designs are conceivable and practicable and that numerous studies are still ongoing.

Romero-García et al. [12] present a genetic algorithm to create band gaps in predetermined frequency ranges. The optimization leads to quasiordered structures. Sigmund and Jensen [13] demonstrate the potential of topology optimization in order to maximize the relative size of acoustic band gaps of infinitely periodic *phononic band gap* materials and structures. In the frameworks of heat conduction and of linear elasticity in infinite, solid structures with periodic perforations, Barbarosie [14] applies numerical shape optimization techniques to obtain microstructures having extremal properties like good conductivity, high bulk modulus or high shear modulus. He describes the process of mesh deformation and mesh regeneration and gives several numerical examples, some of them having practical relevance. A practical example of a finite array and inspiration for sonic crystals noise barriers can be found in the work by Martínez-Sala et al. [15] on the sound attenuation of a sculpture. Experiments on sonic crystals are for example carried out with timber and bamboo rods with perforations [16,17]. References to review articles on sonic crystals include Gupta [18] and Miyashita [19].

For the investigation of the sound insulating *stop band* behavior of infinite periodic structures such as sonic crystals, the problem is usually reduced to a single meta-atom in a so-called unit cell with Floquet-Bloch boundary conditions [20,21]. The expression meta-atom is derived from the concept of acoustic metamaterials and describes subwavelength structures, which are arranged in periodic and infinite arrays [22–24]. Under the assumption of periodicity, the Floquet-Bloch theorem allows the description of the acoustic properties of the entire structure by analyzing a single unit cell. The considered acoustic Bloch wave function [25,26] ensures the amplitude and phase change of the acoustic wave when being scattered by the meta-atoms and traveling from one cell to the next. The resulting destructive interferences in distinct frequency bands are called stop bands. In the form of dispersion curves, both transmissive frequency bands and stop bands of the periodic sonic crystal can be read [21]. Bradley [26] applies the Floquet theorem to show theoretically and experimentally that acoustic Bloch wave functions exist as solutions in acoustic waveguides. Sugimoto and Horioka [27] investigate dispersion properties of sound waves propagating in an infinite waveguide with periodic Helmholtz resonators arranged laterally. They observe stop bands at frequencies where sound propagation is inhibited by the excitation of the lateral resonators and by Bragg reflections due to their periodic arrangement.

The above described approach using Floquet-Bloch boundary conditions is a very efficient technique for periodic, infinite structures. However, recent studies on acoustic metamaterials demonstrate that it is not suitable to fully reveal the acoustic properties, e.g. the transmission loss, of realistic arrays of finite length or with occasional defects that are not subject to periodicity [8,28,29]. This work suggests the method of frequency-independent normal modes (NM) based on the finite element method (FEM) and the Astley-Leis infinite element method (IFEM) as a novel approach for the investigation and design of more realistic finite sonic crystal arrays and arbitrarily shaped acoustic meta-atoms under free-field conditions.

There are numerous formulations to numerically approximate the boundary conditions posed by exterior acoustics, i.e. Sommerfeld's radiation condition [30,31], among them the boundary element method (BEM) [32,33] and FEM in combination with perfectly matched layers (PMLs) [34–36]. Quasi-periodic BEM is utilized in the example of Helmholtz-resonators and periodic noise barriers by Fard et al. [37,38] and by Ziegelwanger et al. [39] by application of the fast multipole method. Conjugated (Astley-Leis) infinite elements, however, used in this work have the great advantage that, in the same way as FEM, which is well established in interior acoustics, they provide frequency-independent system matrices and thus allow the solution of a single frequency-independent (normal modes) eigenvalue problem.

Various authors have published their own formulations of the IFEM, e.g. Burnett and Holford [40,41] and Astley et al. [31,42]. Burnett [43] found the method more efficient than the BEM, due to the local connectivity of degrees of freedom and sparsity. According to Prieto [44], a frequency-independent PML formulation is also conceivable, but the good absorbing properties get lost at low frequencies and the PML domain has to be much bigger. With the additionally required degrees of freedom, the advantage gained is at the same time canceled out again.

Since sonic crystals noise barriers are narrow, longitudinal arrays, this work discusses the potential of elliptical computational domains to minimize the performance required. The two-dimensional problem of elliptical domain shapes with infinite elements could yet not be found in the literature and therefore the coordinate transformation is elaborated according to Moon et al. [45] and Sun [46]. Burnett has introduced new elliptic coordinates to achieve the required convergence [40], which however were not considered in 2D.

The concept of normal modes is adapted to the application of sonic crystals and acoustic meta-atoms in two-dimensional exterior acoustics for the first time. The method is described in detail by Marburg et al.: In the first part of the series [47],

the continuous eigenspectrum of a one-dimensional, infinite waveguide is determined analytically and then, by means of a formulation provided by Ruge [48], the normal modes are determined as the quadratic eigensolution of the state space matrices, which are derived as a FE solution of the Helmholtz equation; in the second part [49] the authors describe the two-dimensional problem, which can be solved numerically with the Astley-Leis IFEM, they provide a solution for the calculation of the eigenvalue problem in case of circular FE domains that lead to singularities in the IFEM mass matrix, and they describe the presence of discrete eigenvalues in addition to the continuous spectrum in the exterior solution by means of two descriptive examples; the third part [50] proposes criteria for modal superposition and measures the sound power error for two different load cases.

Moheit and Marburg [51] further investigate the properties and dependencies of the normal modes on the discretization with infinite elements, in particular taking up research results on the choice of polynomials for radial interpolation [52]. They find out that NM eigenvalues converge towards two different values for IFE radial interpolation polynomials of even and odd degree, respectively. Furthermore, they show that acoustic radiation modes (ARM) can be calculated on the basis of FEM/IFEM and not as is usual on the basis of BEM (cf. e.g. Ref. [53]) and compare them with NM, which is also the subject of another work by the authors [54]. This shows that the real, symmetric and frequency-dependent impedance matrix, whose eigensolution represents ARM, can be constructed on the basis of NM and provides very good results. In Ref. [55] criteria for grouping the modes in multipole and cavity modes are developed and first promising results in modal superposition are obtained. In particular, it is found that the contribution of cavity modes to the radiated sound power is primarily due to the complex conjugated eigenpairs with a negative imaginary part.

Peters et al. [56,57] have illustrated the potential for modal reduction of ARM based on BEM taking into account fluid-structure interaction and Krylov subspace-based model order reduction (MOR) techniques for the coupled exterior problem, so that they could also be suitable for the analysis and design of sonic crystals. Compared to NM, however, ARM have the significant disadvantage that they are frequency-dependent and hence an eigenvalue problem has to be solved for each frequency of interest separately.

For the efficient investigation and design of finitely long sonic crystals noise barriers and arbitrarily shaped acoustic meta-atoms, the authors would like to present with this article the great potential of frequency-independent normal modes in exterior acoustics. The NM technique introduced here for the first time in this context is an enrichment for research in this field, as it provides new impressions and physical insights into their principle of operation, modal attenuation and sound insulation in view of the complex eigenvalues and eigenvectors. The advantage of the treatment of finite arrays over infinitely extended, periodic arrangements lies in the fact that diffraction effects occurring at the edge can be investigated, which have a considerable influence on the sound-reducing effect of the barriers. In addition, the investigation of single meta-atoms offers the advantage over those embedded in periodic arrays that a generalized statement on the efficacy and function of the meta-atoms can be made.

In the following Sec. 2, the authors briefly recapitulate the underlying theory for the harmonic analysis of incident and scattered sound pressure and present a well-known discrete system of linear equations as the numerical solution (FEM/IFEM) of the Helmholtz equation in exterior acoustics. Afterwards, the concept of normal modes is described in its essential aspects. The subsequent Sec. 3 is dedicated to the investigation of two-dimensional meta-atoms in free field and provides basic knowledge regarding the behavior and error of the numerical methods for varying meshes, elliptic and half-space computational domains, which are intended to pre-estimate the requirements for accuracy and computational effort. Basic studies on the relationship of sound insulation and normal modes are carried out in the example of a c-shaped meta-atom and the influence of an absorbing layer (boundary admittance) inside the cavity on the solution is investigated. In the next step in Sec. 4, the insertion loss of a selection of finite 2D sonic crystal noise barriers is simulated and frequency ranges with high sound attenuation are related to NM eigenvalues and eigenvectors, which can help to reveal and understand the underlying physical effects. Some of the geometries used are inspired by the work by Elford et al. [8] so that a certain reference can be made to the results already published.

2. Theoretical background

2.1. Acoustic pressure and velocity distribution of sources and plane waves in exterior acoustics

The homogeneous Helmholtz equation describes the spatial acoustic pressure field $p(\mathbf{x})$ with the harmonic time-dependency $\overline{p}(\mathbf{x}, t) = \mathrm{Re}\left\{p(\mathbf{x})e^{-\mathrm{i}\omega t}\right\}$. It is given by

$$\Delta p(\mathbf{x}) + k^2 p(\mathbf{x}) = 0, \qquad \mathbf{x} \in \Omega, \tag{1}$$

where Ω is the fluid-filled domain and k is the wave number, defined as $k = \omega/c_f$, ω being the angular frequency and c_f the speed of sound in the fluid. By splitting the computational domain Ω into a finite element (FE) and a conjugated infinite element (IFE) domain according to Astley and Leis [42,58], it can be assured that the system matrices are frequency-independent. This is ensured by the complex conjugation of the test and the basis functions leading to elimination of a frequency-dependent exponential term in the product of the two in the variational statement. Eq. (1) is then discretized by means of both methods and after implementation of appropriate boundary conditions [31,50,52,59] leading to the following discrete system of n equations, where n is the number of degrees of freedom (DOFs)

$$\left(\mathbf{K} - \mathrm{i}\omega\mathbf{D} - \omega^2\mathbf{M}\right)\mathbf{p} = \mathrm{i}\omega\rho_f\boldsymbol{\Theta}\mathbf{v_s} = \mathbf{f}, \tag{2}$$

where **K**, **D**, **M** are the frequency-independent matrices for stiffness, damping and mass, respectively, whereby for simplicity's sake it is assumed that the boundary admittance $Y(x) = (v_f(x) - v_s(x))/p(x)$ included in the FE damping matrix behaves constantly over frequency. $\boldsymbol{\Theta}$ is the boundary mass matrix [60], **p** is the acoustic pressure, **i** is the imaginary unit, ρ_f is the density of the medium and $\mathbf{v_s}$ is the structural particle velocity of any given obstacle. In the case of non-dispersive fluid-structure coupling (sound-hard walls), the structural particle velocity v_s is equal to the fluid particle velocity v_f at the obstacle surfaces with a zero boundary admittance $Y = 0$ [60–62].

If a source is present in the considered domain, the homogeneous Helmholtz equation must be expanded by a term denoting the source. It is then called the inhomogeneous Helmholtz equation and it is defined as

$$\Delta p(\mathbf{x}) + k^2 p(\mathbf{x}) = -q, \tag{3}$$

where q is the source, which is assumed to be a sphere of radius R. It is furthermore assumed, that the velocity and acoustic pressure fields of the domain consist of two components

$$p(\mathbf{x}) = p^i(\mathbf{x}) + p^s(\mathbf{x}) \tag{4}$$

$$v_f(\mathbf{x}) = v_f^i(\mathbf{x}) + v_f^s(\mathbf{x}), \tag{5}$$

where the superscripts s and i indicate the scattered and incident wave field components, respectively [60,63]. They are also known as complementary and particular solutions. For a monopole-like spherical scatterer, the incident acoustic pressure and velocity fields are given by

$$p^i(r) = p_0 \frac{R}{r} \mathrm{e}^{\mathrm{i}k(r-R)} \tag{6}$$

and

$$v_f^i(r) = \frac{\mathrm{i}p_0 R}{\rho_f \omega} \frac{1 - \mathrm{i}kr}{r^2} \mathrm{e}^{\mathrm{i}k(r-R)} \frac{\partial r}{\partial n}, \tag{7}$$

where p_0 is the constant surface pressure of the spherical source and r is the distance to the source [60].

The case of an incident plane wave field is handled in the same way, which means that equations (4) and (5) still hold. The incident acoustic pressure and velocity wave fields are now defined as

$$p^i(\mathbf{x}) = p_0 \mathrm{e}^{\mathrm{i}(\mathbf{k}\cdot\mathbf{n}+\phi_0)} \tag{8}$$

and

$$v_f^i(\mathbf{x}) = \frac{p_0}{\rho_f \omega} \mathbf{k}\cdot\mathbf{n} \, \mathrm{e}^{\mathrm{i}(\mathbf{k}\cdot\mathbf{n}+\phi_0)}, \tag{9}$$

where p_0 is the amplitude of the incident wave, ϕ_0 is the phase angle and $\mathbf{k}\cdot\mathbf{n}$ is the dot product of the normal vector **n** and the wave number vector **k**, which indicates the direction of the wave and whose magnitude is the wave number k [60].

The setup of an obstacle in the fluid-filled computational domains of finite and infinite elements as well as the concept of sources and incident and scattered pressure field is illustrated in Fig. 1.

2.2. Normal modes

The homogeneous system of linear equation (2) can also be interpreted as a quadratic eigenvalue problem. Since the conjugated IFEM formulation according to Astley and Leis ensures that the system matrices are independent of the frequency, it follows that neither the eigenvalues nor the eigenvectors depend on the frequency. Therefore, the eigenvalue problem must be solved only once. This assumes that the damping matrix for the degrees of freedom in the FE domain does not contain any frequency-dependent boundary absorption, e.g. in the form of a frequency-dependent boundary admittance. Section 3.4 deals with this in more detail.

The solutions of the two subsequent equations represent the left- and right-sided normal mode eigensolutions, for which the reader may refer to the literature for further details [47,49–51,55]

$$\left(\mathbf{A} - \overline{\kappa}_m \mathbf{B}\right) \mathbf{x_m} = \mathbf{0} \quad \text{and} \quad \mathbf{y_m^T} \left(\mathbf{A} - \overline{\kappa}_m \mathbf{B}\right) = \mathbf{0}, \tag{10}$$

where

$$\mathbf{A} = \begin{bmatrix} \mathbf{M} & \mathbf{0} \\ \mathbf{0} & -\mathbf{K} \end{bmatrix}, \quad \mathbf{B} = \begin{bmatrix} \mathbf{0} & \mathbf{M} \\ \mathbf{M} & \mathbf{D} \end{bmatrix}. \tag{11}$$

A and **B** are called hypermatrices and are of size $2N - \delta \times 2N - \delta$ with δ being the number of empty rows and columns in **M**, which according to Marburg [49,50] can be canceled to reduce the system of equations. This is applicable only in the case of a circular FE domain, because then the rows and columns of **M** corresponding to infinite elements are equal to zero [42]. The mth

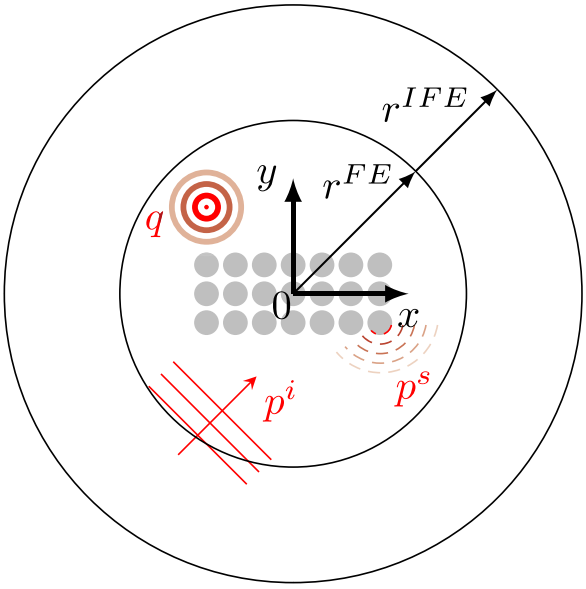

Fig. 1. Incident and scattered pressure field p^s due to a point source excitation q or an incoming plane wave field p^i around obstacles in exterior acoustics. The fluid is subdivided into an FE and an IFE domain.

eigenvalue is denoted by $\overline{\kappa}_m$, whereas $\mathbf{x}_m$ and $\mathbf{y}_m$ represent the corresponding right and left eigenvectors. Both exist due to the fact that the conjugated IFEM leads to asymmetric matrices **K** and **D**.

$$\mathbf{Y}^T\mathbf{A}\mathbf{X} = \mathrm{diag}(\alpha_1, \dots, \alpha_{2n-\delta}) \quad \text{and} \quad \mathbf{Y}_z^T\mathbf{B}\mathbf{X}_z = \mathrm{diag}(\beta, \dots, \beta_{2n-\delta}), \tag{12}$$

It is interesting to note that for distinct, complex eigenvalues $\overline{\kappa}_m = \alpha_m/\beta_m$. The diagonalization properties may not be valid for double-symmetric problems with duplicate eigenvalues that form blocks of ones around the diagonal of the matrix product. A scaled eigenvalue $\kappa = \frac{c}{2\pi f_0}\overline{\kappa}_m$ is introduced with $f_0 = 1$ Hz being a reference frequency so that the eigenvalues are unitless and their imaginary parts indicate the eigenfrequencies while their real parts describe the damping of the corresponding modes [49].

To classify normal mode shapes, Moheit and Marburg [55] develop criteria and roughly differentiate the eigenvectors into cavity modes and multipole modes. Marburg et al. [49] have previously observed the existence of a group of discrete eigenvalues in the continuous spectrum of NM in exterior acoustics and thus take up the discussion about so-called *trapped modes* [64–69], which Jones [70] has shown to exist as point eigenvalues in the spectrum of the Laplacian operator in unbounded domains using the theory of unbounded operators. The discretization of the free field by means of IFEM approximates the continuous spectrum of the exterior domain with discrete NM eigenvalues, which appear in lines in the complex plane [51]. While they move towards the imaginary axis with increasing mesh fineness, the trapped mode eigenvalues differ in that they converge.

Evans provides evidence for the existence of trapped modes in unlimited two-dimensional acoustic waveguides, once for a finite strip in the duct and in another work, together with Levitin and Vassiliev, for symmetrical obstacles and indentations in the waveguide [71,72]. They thus extend the spectrum of situations for which these modes have been proven to exist. Kaplunov and Sorokin [73] show the presence of a single trapped mode in a one-dimensional infinite waveguide in the form of an elastic string mounted on an elastic foundation with a concentrated mass rigidly attached to the string.

3. Results at meta-atom level

In the simple example of a two-dimensional, circular cross-section of a cylinder with diameter $d = 0.6$ m (see Fig. 2a), the authors' MATLAB IFEM code is verified and basic studies are evaluated by keeping some variables constant, while gradually altering others. The circular obstacle is treated as a multipole sound source with a structural normal surface velocity with the amplitude $v_s = 1\ \mathrm{ms}^{-1}$ for all frequencies. An analytical solution of the acoustic pressure solution is available [74]. The verification is required due to the lack of numerical experiences in two-dimensional elliptical infinite elements and their normal modes. The sensitivity of the solution in regard to certain parameters is tested: n_{el} the number of finite elements per wavelength (mesh size, Sec. 3.1.1), the size and aspect ratio of the FE domain and the number of IFE nodes in radial direction (Sec. 3.1.2) as well as the position of the circular obstacle along the x-axis (Sec. 3.1.3). The findings and minimum requirements from these fundamental studies are incorporated in the investigations on more complex geometries in what follows. This includes the utilization of the cylinder in a sonic crystals noise barrier in Sec. 4.

For simplicity, models that fall under this category are referred to as the letter C followed by the corresponding aspect ratio of the domain, e.g. C2.5 refers to a model of a circular obstacle, whose FE domain has an aspect ratio of 2.5 with the horizontal

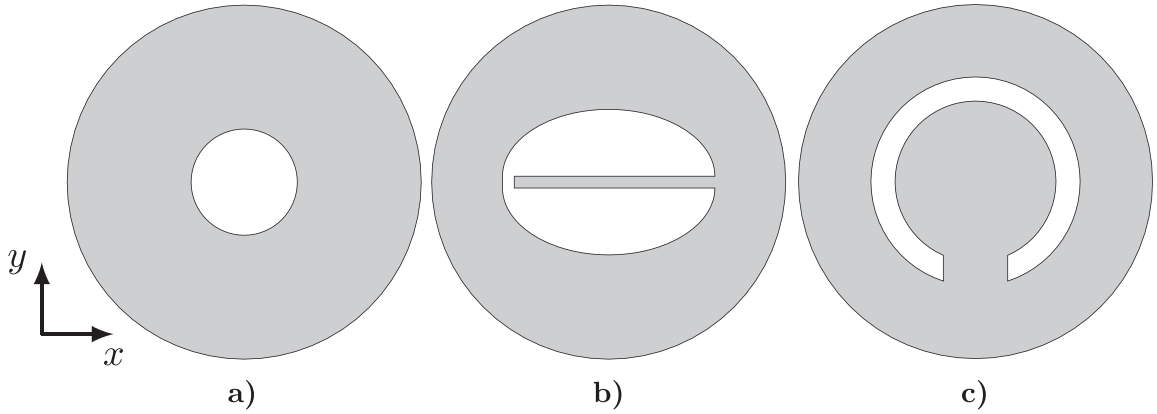

Fig. 2. Representation of the three considered meta-atoms: a) C (circle), b) E (ellipsoid with a 1.715 m long open cavity, cf. [55]) and c) M (c-shaped meta-atom, cf. [7]) in circular, fluid-filled computational domains (gray). Please note that the models shown are not scaled to the same size in relation to each other.

semi-axis $a = 2.5$ m, while the vertical semi-axis $b = 1$ m remains constant for all models of type C.

In the next step, the normal modes (see Sec. 2.2) are computed and evaluated using models that are inspired by previous work of the authors [55] in order to facilitate comparisons and build on preliminary findings and experiences—this model is virtually a prototype for the investigation of normal modes and trapped-mode frequencies in exterior acoustics with FEM/IFEM and NM. The obstacle is an ellipse-like structure with a rectangular cavity 1.715 m long, which is a convenient shape, since longitudinal cavity resonances are found in roughly 100 Hz-steps. The properties of this model are utilized to prove the existence of cavity modes (trapped modes) as well as multipole modes in exterior acoustics. It is shown in Fig. 2b and abbreviated with the letter E subsequently. The variables tested are: the aspect ratio of the FE domain, the IFE radial order and the position of the obstacle. Furthermore, the model E is investigated regarding the estimation and utilization of symmetry effects in half-space problems in Sec. 3.3 considering a cut-through variation and a mirrored problem.

The third model shown in Fig. 2c, a c-shaped meta-atom, is inspired by the work by Elford et al. [8]. The open ring has an outer diameter of 13 mm and a thickness of 1.5 mm. The opening on the side preferably facing the incident wave front has a width of 4 mm. The fluid domain shape remains circular for this model. In accordance with the abbreviations made for the previous models, the meta-atom will be referred to with the letter M in what follows. As the circle C, the c-shaped meta-atom M is examined in Sec. 4 in a sonic crystals array.

The idea of this model is the verification that the concept of normal modes is suitable for the investigation, understanding and design of sonic crystals with complex-shaped meta-atoms (e.g. c-shape, 'Matryoshka' meta-atoms [7,8] as well as 'Mie' type meta-atoms [10,11]). Furthermore, the influence of absorbing boundary conditions in terms of boundary admittances on the insertion loss is discussed in Sec. 3.4.

In contrast to the original work by Elford et al. [8], the modes of the meta-atom are not simulated with periodic boundary conditions (Floquet-Bloch), but are considered free in space, i.e. without consideration of the periodic effects in the unit cell. However, this makes the observation independent of the arrangement in the array and only the meta-atom is described individually. The resonator frequencies can therefore be determined with normal modes even for very complicated arrangements without the knowledge of analytical equations.

For all the subsequently used models, the FE domain is two-dimensional. This is equivalent to a sectional plane through three-dimensional cylinders of infinite height. The elliptical domain form varies in accordance with the chosen aspect ratio. The obstacle is considered as a hole in the computational domain with non-dispersive, sound-hard boundary conditions, but it is also imaginable to include solid structures and fluid-structure interaction even for modal analysis. Second-order Lagrangian finite elements are implemented and Jacobi (with exponents $\alpha = 1, \beta = 0$) polynomials are used for the radial interpolation of the infinite elements due to their improved matrix conditioning compared to classic Lagrange polynomials [52,75]. It could be confirmed that for radial interpolation Lagrange polynomials of order greater than eight lead to large errors. The fluid surrounding the models is air with density $\rho_f = 1.25\ \mathrm{kgm^{-3}}$ and speed of sound $c_f = 343\ \mathrm{ms^{-1}}$.

Geometry and mesh are created using COMSOL Multiphysics®. The system matrices are then passed to MATLAB, where the IFEM has been implemented. The solution of the normal mode eigenvalue problem from Eq. (10) is carried out using the LU algorithm with the software library SLEPc [76–78], which is based on PETSc [79–82].

3.1. Verification and evaluation of the acoustic pressure field

Within this section, an error measure is defined in order to describe the quality of the numerical solution with respect to an analytical solution for the circular obstacle C. The error is measured depending on the mesh size (Sec. 3.1.1), the aspect ratio of the finite element domain (Sec. 3.1.2) and on the position of the obstacle along the x-axis (Sec. 3.1.3). To the best of the authors' knowledge, there are no publications on the properties of ellipsoidal computational regions of infinite elements in two

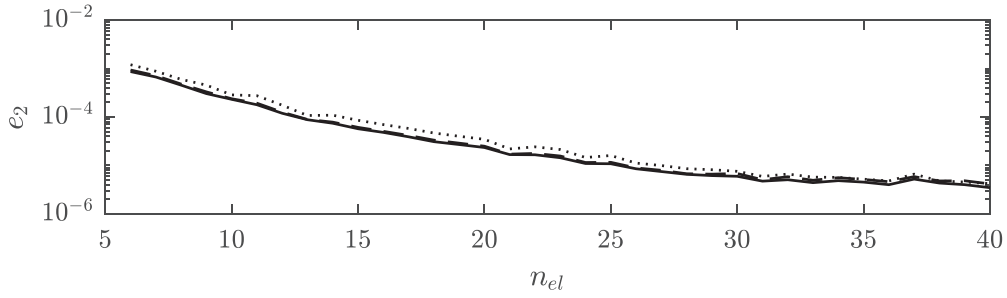

Fig. 3. e_2 in the FE domain in correlation with mesh size (number of finite elements per wavelength n_{el}) for a circular domain (C1) at 500 Hz for monopole $n = 0$ (——), dipole $n = 1$ (– – – –) and quadrupole $n = 2$ (· · · · ·) excitations.

dimensions; hence, they are investigated at the beginning for verification and error estimation of the results.

The simulations for the circular obstacle are verified by calculating the L^2-norm of the global relative error, which is considered as a sufficiently accurate error measure from an engineering point of view, although additional care is required for a mathematically substantiated consideration [83,84]. The error norm is defined as

$$e_2 = \sqrt{\frac{\sum_i |p_i^{num} - p^{an}(\mathbf{x}_i)|^2}{\sum_i |p^{an}(\mathbf{x}_i)|^2}}, \tag{13}$$

where p_i^{num} is the numerical solution using FEM and IFEM at node i and p_i^{an} is the analytical solution at position $\mathbf{x}_i$, given by [74]

$$p^{an}(r,\phi) = -\mathrm{i}\rho_f c_f v_s \frac{H_n^{(2)}(kr)}{H_n^{(2)\prime}(kb)} \cos(n\phi), \tag{14}$$

where $H_n^{(2)}(x)$ is the nth-order Hankel function of the second kind, $H_n^{(2)\prime}(x)$ is its derivative to x, b is the radius of the circular source, r is the radial distance of any given point to the surface of the circle, ϕ is the angle co-defining its position in polar coordinates and n is a constant that defines the nature of the multipole source. In the case of a monopole, n is equal to zero, for $n = 1$ the circle radiates as a dipole and for $n = 2$ as a quadrupole etc.

3.1.1. Dependence on mesh size

To quantify the FE mesh size, the number of quadratic elements per wavelength n_{el} is taken into consideration [84,85]. It is defined as

$$n_{el} = \frac{c_f}{f_{max} h_{max}} = \frac{\lambda_{min}}{h_{max}}, \tag{15}$$

where $f_{\max}$ is the maximum frequency of interest with the minimum wavelength $\lambda_{\min}$ and $h_{\max}$ is the corresponding maximum edge length of the finite elements during the meshing.

Fig. 3 shows a plot of e_2 over n_{el} in the case of C1 at 500 Hz.

For the model, eighth order Jacobian polynomials (with exponents $\alpha = 1, \beta = 0$) are used for the radial interpolation of the infinite elements and the source is located in the center of the domain.

The study is carried out for monopole, dipole and quadrupole excitations. It is evident that for higher-order multipole excitations, the deviations alter and the radial polynomial order of the infinite elements is required to be increased, where elements of order m are capable of representing the sound pressure field due to multipoles of order $m - 1$ [42]. With the choice of the polynomial order eight, the authors are on the safe side.

Using twelve finite elements per wavelength, the error is about 10^{-4} for all three excitations considered. However, this is true only for C1; models with higher aspect ratios produced results of lower quality, while keeping the other variables constant.

3.1.2. Elliptical computational domains

In many practical applications such as long slender obstacles or arrays, an elliptical domain shape can reduce the number of degrees of freedom in the FE mesh [40,41]. The authors could not find a discussion on sound pressure errors in two-dimensional elliptical IFE domains in the literature. The transformation between elliptical and cartesian coordinates is abstracted for 2D infinite elements based on the work of Burnett and Holford [40] in 3D, whose approach slightly differs from the usual transformation equations (cf. [45,46]) since it was derived specifically to satisfy Sommerfeld's radiation condition. As Astley and Coyette showed for three-dimensional problems [86], the error produced by high aspect ratios of elliptical domains can be counterbalanced by increasing the radial order n_{rad} of the IFE mesh. To investigate the effect the radial order can have on the error, models C1 to C5 are examined at three different radial orders (8, 16 and 24) and three different frequencies (100 Hz, 250 Hz and

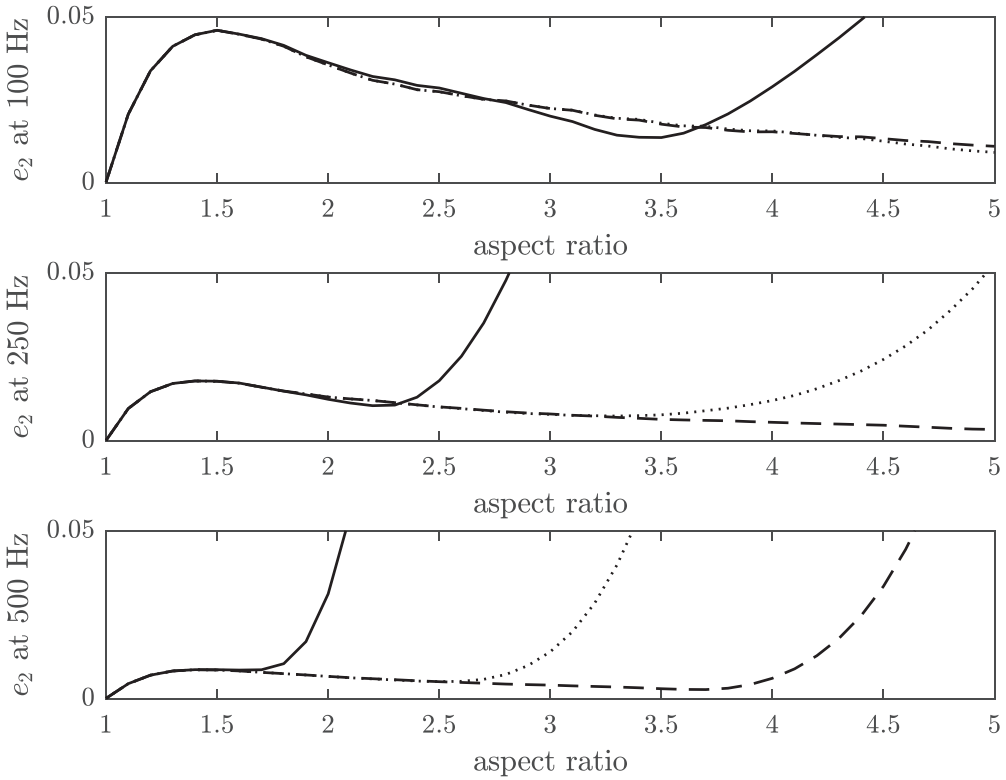

Fig. 4. e_2 for C1 to C5 in the FE domain of radial orders $n_{rad} = 8$ (——), $n_{rad} = 16$ (· · · · ·) and $n_{rad} = 24$ (– – – –) at (from top to bottom): 100 Hz, 250 Hz and 500 Hz.

500 Hz). The models apply twelve finite elements per wavelength in order to keep the mesh-related error low (cf. Sec. 3.1.1). The monopole-source ($n = 0$) is positioned at the center of the domain.

The resulting plots are shown in Fig. 4. Errors exceeding 5% are not plotted for brevity. These high errors occur with growing aspect ratios if the polynomial order of the infinite elements is too low for the radial interpolation. As the frequency increases, e_2 generally reduces, but obviously higher polynomial degrees are already required for lower aspect ratios, otherwise the error quickly becomes very large.

It is evident that the performance for models of large aspect-ratios is improved by implementing an IFE mesh of higher radial order. Furthermore, it is interesting to note that models with aspect ratios C1.4-C1.5 produce local error maxima at all frequencies and for all radial IFE orders. Neither the number of finite elements per wavelength n_{el}, nor the position of the obstacle along the x-axis (cf. Sec. 3.1.3) causes a noticeable shift of this error maximum towards other aspect ratios. Furthermore, not even a larger scaled FE domain leads to a shift of this peak. Instead, such scaling ensures that the error for elliptical half-axis ratios can be significantly reduced with increasing size of the FE domain. This may lead to the circumstance that the advantage of elliptical domains is eliminated by the higher number of degrees of freedom required.

Obviously, when introducing slightly elliptical computational domains, the error increases rapidly and momentarily in comparison to the circular shape and decreases afterwards for higher aspect ratios until the error grows rapidly as soon as the radial polynomial interpolation is no longer sufficient to describe the non-reflective decay of the sound pressure. For low frequencies, this effect is more pronounced: The error increases more strongly with slightly elliptical FE domains and decays linearly to higher aspect ratios. With an increasing frequency, the error grows to a lower extent at the beginning, but already at significantly smaller aspect ratios, higher polynomial orders are required for the infinite elements.

The authors did not find any evidence of the transformation in elliptical coordinates for two-dimensional problems with infinite elements in the literature. The chosen transformation is verified using analytical solutions, but still involves a few mathematical hitches to deal with, which might cause the observed numerical error at the transition from circular to elliptical domain shapes.

A possible explanation for the fact that the error is larger at low frequencies compared to higher frequencies might be that their respective wavelengths and—due to a constant number of finite elements per wavelength n_{el}—also the elements' edge length becomes large in relation to the obstacle and the computational domain, while large FE domains generally improve the quality of the solution. Furthermore, a coarse FE mesh is associated with less infinite elements in the circumferential direction, which might lead to discretization errors at the transition between FE and IFE domain.

Fig. 5 illustrates the extent to which the IFE radial order can influence the error of C2.The error virtually converged at different values for all three frequencies: for 100 Hz at about $n_{rad} = 8$, for 250 Hz at about $n_{rad} = 10$ and for 500 Hz at about $n_{rad} = 12$. The results confirm the observations in Fig. 4 for the half-axis ratio 2:1: With an increasing polynomial order n_{rad}, the error

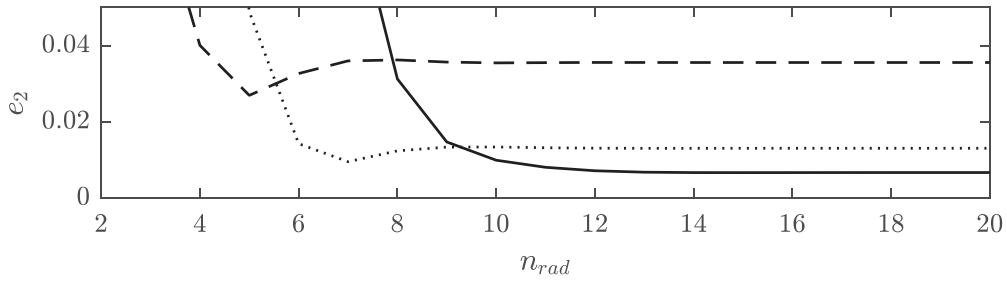

Fig. 5. e_2 of C2 correlated with the radial order at 100 Hz (– – – –), 250 Hz (· · · · ·) and 500 Hz (——).

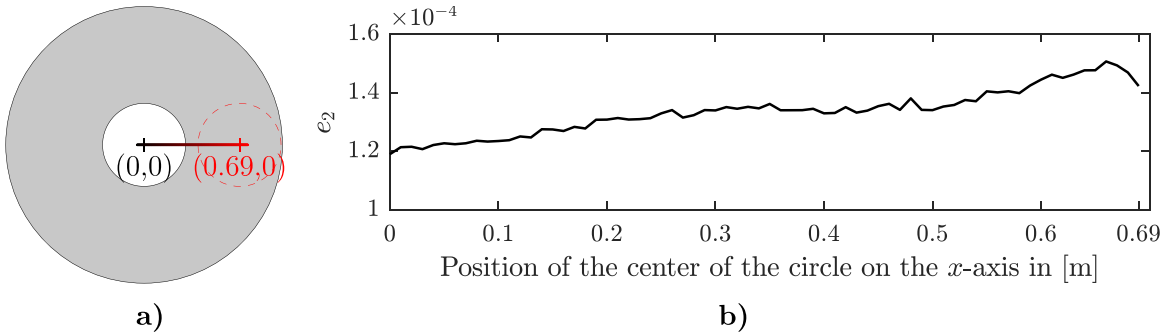

Fig. 6. Error of C1 depending on the position of the obstacle along the *x*-axis and thus the distance to the FE-IFE-interface at 500 Hz: a) geometric representation; b) the global relative error e_2 grows almost linearly with decreasing distances between the obstacle and the boundary of the FE domain, but at a very low level.

converges to a certain level. A further decrease can neither be achieved by an increase of n_{rad}, nor can it be achieved in a noticeable way by increasing n_{el}, but only by a larger FE domain.

It is noticeable that with an increasing frequency the error converges on a lower level (which obviously cannot be achieved for lower frequencies in the considered example), but a clearly higher polynomial order is necessary, from which the error is sufficiently low. This means that for elliptical computational domains the choice of the polynomial order of the infinite elements should depend on the considered frequency, although the practical application is likely to be very difficult. Generally speaking, the higher the frequency, the higher the polynomial order of the radial interpolation must be set.

3.1.3. Position of the obstacle

The correlation between the global relative error and the distance of the obstacle to the FE-IFE interface is examined with the aim of minimizing the size of the computational domain and investigating the stability of the numerical solution if the obstacle is very close to the outer boundary of the domain. This is intended to be exploited in widespread sonic crystals to require as few degrees of freedom as possible in the environment of the array. The model used is C1 with IFE of eighth radial polynomial order and with 20 elements per wavelength. The surface of the obstacle is vibrating with a monopole excitation at 500 Hz and the setup of the study is shown schematically in Fig. 6a.

In Fig. 6b, it can be observed that the error of C1 increases almost linearly, but at a very low level as the position of the obstacle moves from the central position to the outer FE boundary until the obstacle is 1 mm away from the interface.

3.2. Normal modes in elliptical computational domains

For harmonic analysis, the results of the subsequent studies are certainly known or easily accessible, but in this paper the authors want to further study the sensitivity of normal modes in exterior acoustics with respect to the underlying properties of finite and infinite element discretization.

This is done for the models E of an elliptical obstacle with a 1.715 m long cavity, see Fig. 2b. The geometry is chosen, since it is the subject of previous investigations on normal modes in exterior acoustics [55] and fundamental effects, e.g. cavity modes as trapped modes, can be clearly identified and discussed.

The normal mode eigenvectors can be roughly subdivided into two groups: cavity modes and exterior multipoles [55]. The cavity modes show sound pressure peaks inside the cavity, which can be considered as a Helmholtz resonator, whereas multipoles can be observed along the junction of FE and IFE domain.

In this section, the aspect ratio of the computational domain is varied while keeping the vertical semi-axis of the ellipse constant at $b = 1.5$ m. The behavior of the normal mode eigenvalues and eigenvectors is studied. Although the advantage of narrow, elliptic computational domains, given by their lower number of degrees of freedom, could possibly be eliminated by the higher demands for radial interpolation, it may nevertheless be useful for certain situations to use elliptical FE domains. In

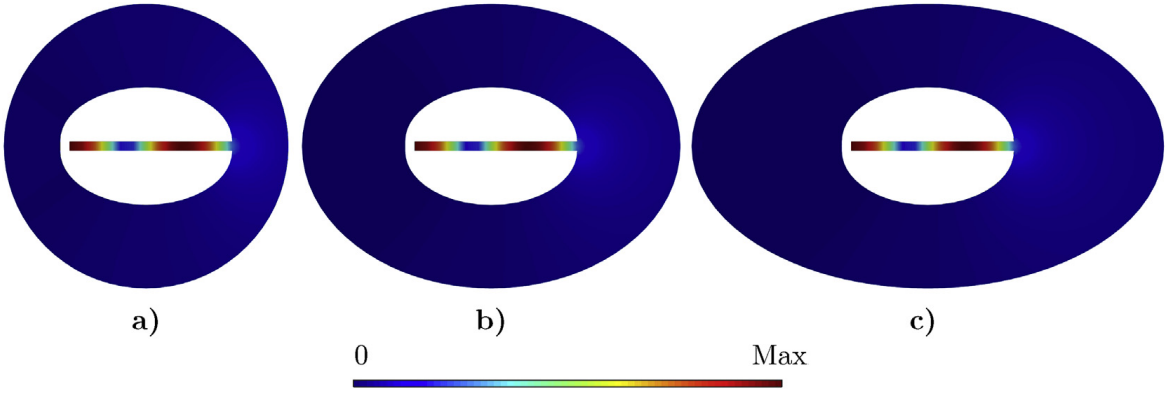

Fig. 7. Representation of a complex cavity mode as right eigenvector magnitude in the FE domain for the models: a) E1, b) E1.33 and c) E1.66, respectively. The corresponding eigenvalues are $\kappa_{E1} \approx -3.1 + 142.38\mathrm{i}$ ($|\kappa_{E1}| \approx 142.41$), $\kappa_{E1.33} \approx -3.13 + 142.36\mathrm{i}$ ($|\kappa_{E1.33}| \approx 142.39$), $\kappa_{E1.66} \approx -3.16 + 142.41\mathrm{i}$ ($|\kappa_{E1.66}| \approx 142.45$).

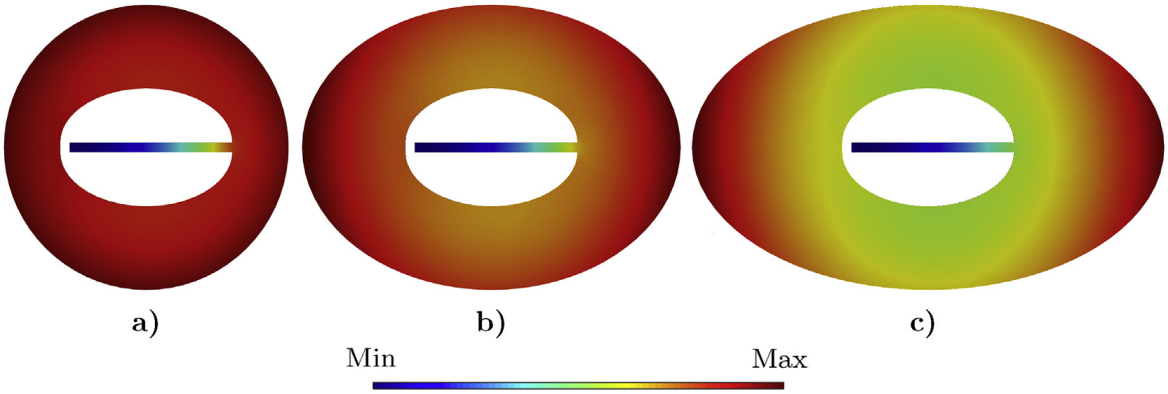

Fig. 8. Representation of a monopole mode as right eigenvector magnitude in the FE domain for the models: a) E1, b) E1.33 and c) E1.66, respectively. The corresponding eigenvalues are $\kappa_{E1} \approx -0.95$, $\kappa_{E1.33} \approx -0.71$, $\kappa_{E1.66} \approx -0.57$.

contrast to these, the mass matrix is singular for IFE degrees of freedom in circular problems [42]. This is of great importance for the choice of an appropriate eigenvalue solver for the normal modes. Three variations of the model E are considered: E1 with a circular FE domain shape and the two elliptical shapes E1.33 and E1.66.

The mesh has twelve quadratic finite elements per wavelength at 500 Hz. In regard to the proposed study of the general behavior of modes due to elliptic computational domains, the solution does not necessarily have to converge for a qualitative analysis and comparison. However, the radial polynomial order of the infinite elements has to be increased in the case of elliptical FE domains according to the observations made in Sec. 3.1.2. For this purpose, Jacobi (1,0) polynomials of 16th order are chosen for the subsequent studies.

Fig. 7 shows the mode shapes of a complex-valued cavity mode as right eigenvector magnitudes in differently shaped FE domains E1, E1.33 and E1.66. It can be observed that the modes mostly retain their form and the complex eigenvalues are comparable for all three aspect ratios, with their magnitude remaining virtually the same. This is true for all uniquely identifiable complex cavity modes (mixed forms and spurious modes are left out), since the domain shape should not have an influence on the cavity resonances.

Fig. 8 illustrates a purely real monopole mode for the circular and the two elliptical computational domains. The eigenvalue decreases and the sound pressure field of the mode appears to change as the aspect ratio increases. However, it is important to note that eigenvectors are freely scalable and therefore no absolute comparisons can be made. In addition, the greater distance to the obstacle leads to a higher difference between the minimum and maximum sound pressure, so that the color bar scale varies, respectively. It is known from earlier works [48,50,55] that a harmonic sound pressure solution in free field can be reconstructed by modal superposition of the normal mode eigenvalues and eigenvectors. This is independent of the shape of the FE domain.

The fluctuation in the eigenvalues can be predicted relatively accurately by the ratio of the respective aspect ratios:

$$\frac{\kappa_{Ea}}{\kappa_{Eb}} \approx \frac{b}{a}, \tag{16}$$

where a and b are two arbitrary aspect ratios, e.g. $0.953/0.714 \approx 1.33/1$ as for the shown example in Fig. 8. Eq. (16) is tested and confirmed on the first twenty modes—sorted by means of increasing magnitude—of the models C and E.

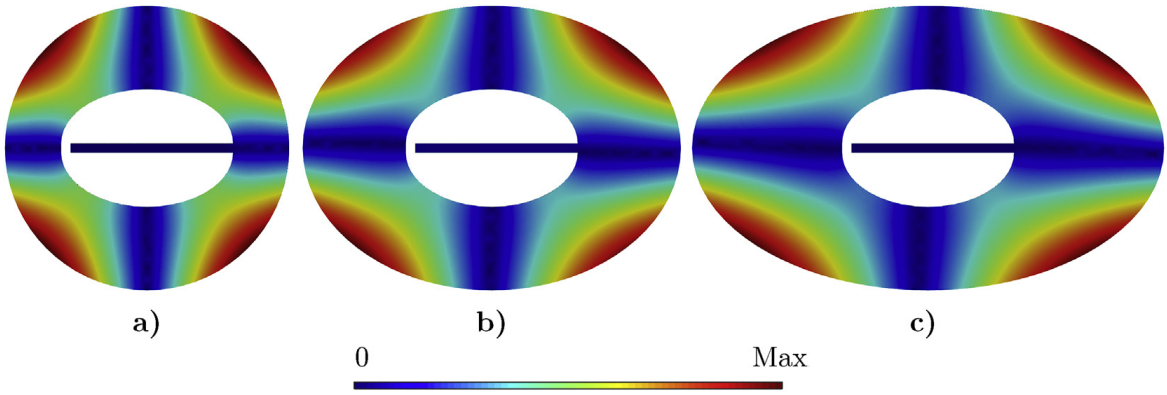

Fig. 9. Representation of a quadrupole mode as right eigenvector magnitude in the FE domain for the models: a) E1, b) E1.33 and c) E1.66, respectively. The corresponding eigenvalues are $\kappa_{E1} \approx -23.88$, $\kappa_{E1.33} \approx -17.81$, $\kappa_{E1.66} \approx -14.2$.

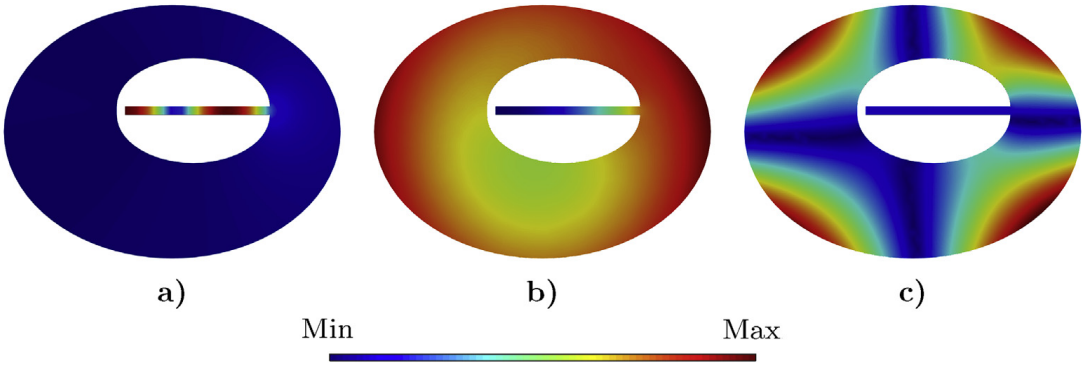

Fig. 10. The three chosen modes from Figs. 7–9 of the eccentric obstacle in E1.33 as right eigenvector magnitudes in the FE domain.

Fig. 9 shows a quadrupole mode for the three models. The symmetry of the mode in the circular domain is gradually but slightly lost in the elliptical domains and, once again, the aspect ratios indicate the decrease in the eigenvalues according to Eq. (16).

Each multipole group contains a number of modes, some of which differ greatly from each other. The more degrees of freedom a system has, the more multipoles per group can be expected. With increasingly elliptical shape of the FE domain, the assignment of some of the modes to a group becomes more difficult, since less clear multipoles occur compared to the circular FE domain. Instead, many of the modes in the elliptic domain are stretched and the sound pressure distribution along the outer FE boundary is irregular and asymmetrical. Consequently, it is not always possible to establish a direct relationship between the modes and those of modified domains. Modes that are highly variable and newly formed are likely to belong to the continuous spectrum of exterior problems. Marburg et al. [49] describe for a similar problem the occurrence of trapped modes, i.e. discrete eigenvalues in addition to the continuous spectrum, which converge with increasing IFE radial interpolation order, cf. Sec. 2.2. However, it is not within the scope of this paper to determine and investigate these trapped normal modes in more detail.

The associated modes are illustrated in Fig. 10 for the eccentric obstacle (shifted by 0.25 m in x- and y-direction, respectively) in E1.33. Since the eigenvalue magnitudes of the shown modes remain almost the same in comparison to those of the centered obstacle in E1.33 for multipole modes as well as for cavity modes (cf. Figs. 7–9), the assignment is straightforward. The three eigenvalues of E1.33 with the eccentric obstacle read as follows: $\kappa_{E1.33,a} \approx -3.1 + 142.35\mathrm{i}$ ($|\kappa_{E1.33,a}| \approx 142.38$), $\kappa_{E1.33,b} \approx -0.71$ and $\kappa_{E1.33,c} \approx -17.81$. As expected, the eigenvector of the cavity mode remains virtually unchanged from the position of the obstacle. The multipole modes in the exterior domain retain their essential character, but the sound pressure field is slightly influenced by the fact that the obstacle moves to a different position and partially affects the distribution of the acoustic waves. In modal superposition, this certainly leads to a change in the influence and contribution of individual modes to the total sound pressure field.

A precise comparison of the eigenvectors, for example by means of the modal assurance criterion (MAC), is not possible, since the position and number of mesh nodes varies with the modification of the computational domain. However, the eigenvalue ratio from Eq. (16) can be useful for assigning modes of different domain shapes.

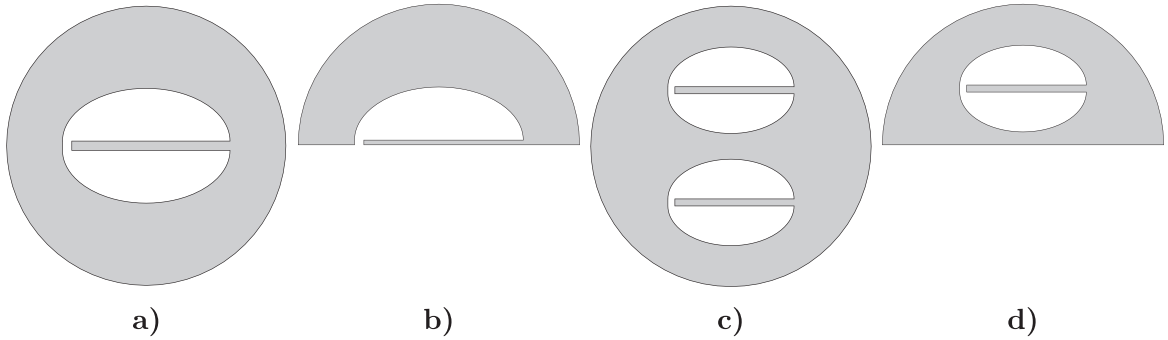

Fig. 11. Variations of model E for full-space and half-space problems.

3.3. Normal modes for symmetric half-space problems

Many applications in exterior acoustics are half-space problems such as vehicles on roads or railways and noise barriers as sonic crystals. On the other hand, half-space problems can be used for symmetric geometries in order to save computational costs. This approach is commonly used in structural dynamics, where the solution can be constructed as a superposition of symmetric and antisymmetric solutions analogous to the reconstruction of any function from the superposition of even and odd functions [87,88]. As long as the sound incidence in harmonic analysis has the same symmetry property as the sound pressure field, as assumed in the context of this work, it is in principle possible to consider only the half space.

In the example of variations of the elliptical structure E, it is investigated how the normal modes are influenced when working with half-space approximations for symmetric two-dimensional problems in order to estimate the differences in comparison to the whole computational domain. In all the subsequent examples, the mesh is symmetric, i.e. it remains the same for the compared full- and half-space problem using twelve elements per wavelength up to the maximum frequency of 500 Hz and 16 radial interpolation points. The four cases depicted in Fig. 11 are investigated.

For the first five cavity modes it could be ascertained that their eigenvalues remain almost the same for all four problems. The influence of the choice of the IFE radial polynomial order (either $n_{rad} = 8$, 16 or 24) has hardly any influence on the cavity mode frequencies. The respective difference between the full-space and the corresponding half-space problem is negligible for the centered obstacle in Fig. 11a and b as well as for the mirrored problem in Fig. 11c and d, respectively, where the deviation between the two is slightly higher for the mirrored problem and the fifth cavity mode frequency with a maximum error of about 1%. Due to the presence of a second obstacle and small reflections between the two, the results differ slightly for the centered and the mirrored obstacles, which amounts to a deviation between approx. 0.1%–0.9% compared to the reference solution E1 (Fig. 11a) with the finest IFE mesh. The error is generally growing as the frequency increases. The general nature and distribution of the multipole modes are very similar for all variations of E with the particularity that only symmetric modes occur for half-space problems. The effects of symmetry can be comprehended and exploited as long as the incident acoustic wave is subject to the same symmetry condition during harmonic analysis.

It is noticeable that, only for the third variation of E (Fig. 11c), each four cavity modes—two modes with each two complex conjugated partners with the eigenvalues very close to each other—can be found, whereas the other models provide only a single pair of complex conjugated eigenvalues per cavity mode.

The number of normal modes of the models 11a to 11d reads as follows: 32,553, 16,422, 48,400, 24,387, i.e. the number of degrees of freedom can be approximately halved by using half-spaces. Since asymmetric modes are insignificant in the case of symmetrical excitations and good agreement of the cavity modes is achieved across all models, the clear advantage of utilization of symmetry along the wave direction is taken into account for the investigations in the subsequent section on symmetric c-shaped meta-atoms and thereafter when considering the sonic crystals in Sec. 4.

3.4. C-shaped acoustic meta-atoms and damping by absorption

The insulating effect and the efficiency of sonic crystals noise barriers depends on their size and on the positioning and the shape of the meta-atoms in the array. It is known from the literature that the introduction of cavities in the meta-atoms causes additional effects. In this section, the unbounded sound pressure field around the c-shaped meta-atom M (shown in Fig. 2c) is decomposed by means of the normal modes and its insulating effect is investigated.

The chosen FE mesh with a maximum element size of approximately $h_{\max} = 1$ mm ensures twelve quadratic elements per wavelength at about 28 kHz—which still means more than 8.5 elements per wavelength at a frequency of 40 kHz—and the polynomial order of the infinite elements is three.

Initially, the surface of the obstacle is sound hard. In a next step, a boundary admittance $Y(x)$ is applied to the structural surface on the inside of the c-shaped meta-atom in order to investigate the influence of absorbing layers or imperfectly reflecting walls on damping and resonance frequencies of the normal modes. That could have been used specifically or might be due to contamination by dust or soil. Furthermore, in their studies on 3D-printed acoustic meta-atoms, Jordaan et al. [23] and Melnikov

et al. [24] observed that the assumption of non-dispersive, sound-hard boundary conditions does not apply for the material Polylactic Acid (PLA), from which the meta-atoms in their experimental works are fabricated. The viscoelastic material can be described well by an equivalent surface admittance. The boundary admittance relates the sound pressure to the difference of the fluid particle velocities v_f and the structural particle velocities v_s at the surfaces of the obstacle [60–62]

$$Y(x)p(x) = v_f(x) - v_s(x). \tag{17}$$

The relationship between the boundary admittance and the commonly used absorption coefficient α is as follows [89,90]

$$Y = \frac{\cos\vartheta}{\rho_f c_f} \frac{1-\sqrt{1-\alpha}}{1+\sqrt{1-\alpha}} \tag{18}$$

with $\rho_f = 1.25\ \mathrm{kgm}^3$ being the density of the fluid and $c_f = 343\ \mathrm{ms}^1$ being the speed of sound. As the Helmholtz equation does not take into account the angle of the incident acoustic waves ϑ, the boundary admittance is defined only for the normal component and ϑ is assumed to be zero. It follows that the admittance $Y_0 = 0$ is found for $\alpha_0 = 0$ in the case of sound-hard walls. In the absorbing case, $\alpha_1 = 0.017$ leads to a boundary admittance $Y_1 = 1 \times 10^{-5}\mathrm{m}^2\mathrm{skg}^1$. This value nearly equals the one found by Melnikov et al. [24] in experiments and thus seems to be a realistic assumption. The frequency-independent consideration of the boundary admittance serves a fundamental, simplified investigation of the resulting phenomena. A more realistic approach such as that of Marburg and Hardtke [89] is conceivable, in which the frequency is linearly proportional to the mass matrix and indirectly proportional to the stiffness matrix when considered individually.

A plane incident sound pressure field in positive y-direction with an amplitude of 2 Pa, which is equivalent to 100 dB, is implemented. A further consideration of asymmetric sound incidence other than along the x- or y-axis is left out in this paper, since then the utilization of symmetry properties is not possible and since this is also not the subject of the work of Elford et al. [8], on which the authors strongly rely when choosing their models and studies. The opening of the obstacle is aligned in the direction of the origin of the wave direction. In order to estimate and measure the sound insulation by a single meta-atom, the circular (full-space) finite element domain around the obstacle is chosen large (diameter $d = 80$ mm) in comparison to the size of the obstacle. A rectangular area (height $h = 25$ mm, width $w = 7.5$ mm) is positioned above the meta-atom in its sound-shadow (center point at $x = 0$ mm and $y = 20$ mm), and the sound pressure magnitude is measured and averaged in this area in order to quantify the efficiency of the obstacle by means of the sound pressure reduction due to the single meta-atom. The attenuation is termed insertion loss (IL) in what follows. It is the sound pressure level (SPL) difference of the incident wave i (which is constant in the entire domain if no obstacle is present) and the averaged SPL in the rectangular area behind the meta-atom

$$\mathrm{IL} = L_{p^i} - L_{\overline{p}} \tag{19}$$

with $L_{p^i} = 100$ dB for $p^i = 2$ Pa.

The IL of different meta-atoms is depicted as a function of the frequency in Fig. 12 for a circular obstacle (cf. model C with diameter $d = 13$ mm) and two variations of the c-shaped meta-atom M with the same outer diameter: one with sound-hard walls Y_0 and another one with the previously introduced boundary admittance Y_1 attached to the circular interior wall of the meta-atom.

It is noticeable that the upper frequency limit of the human hearing ability is exceeded, but since the specifications of the model are based on the example by Elford et al. [8], who presented their results up to 40 kHz, and interesting effects can be observed beyond the audible frequency range, a qualitative investigation will be carried out at this point. It can be assumed that the effects shown also occur for differently scaled models.

A single c-shaped meta-atom in the free field cannot be compared with that within the unit cell as given in Elfords work considering periodic Floquet-Bloch boundary conditions, because there it is assumed that, depending on the lattice constant, standing waves occur between the meta-atoms. This assumption is not valid for meta-atoms at the outer edges of the array. On the other hand, the consideration of a single meta-atom in the free field presented here is to be seen more universally. The consideration of the interaction of the meta-atoms with each other must then take place on the basis of the normal modes in the sonic crystals array, cf. Sec. 4.

The dashed curve in Fig. 12 stands for the insertion loss of the circular obstacle C. It shows a slight decrease between about 3 kHz and 5 kHz. Afterwards, the IL increases nearly proportional to the frequency. The meta-atom M shows a similar behavior, but three distinct insulating effects can be observed around 5 kHz, 21 kHz and 33 kHz. The effects can be assigned to the resonance frequencies of the cavity normal modes (Helmholtz resonator modes), which will be discussed below. The frequencies are given in the imaginary parts of the complex NM eigenvalues. Chalmers et al. [7] describe a single resonance band gap around the first Helmholtz resonator frequency. This work illustrates that in the regions of the higher-order resonator frequencies of a c-shaped meta-atom in free field or in a finite sonic crystal, a smaller but still considerable sound insulation can be observed on the basis of the same physical effects.

It is noticeable that the sound insulation is not the largest at the actual resonance frequency of a cavity mode. The eigenfrequency rather approximates the inflection point of the curve. It can be assumed that the IL curve of the c-shaped meta-atom M converges against the one of the cylinder C as the volume of the cavity is reduced towards zero.

Around the cavity resonance frequencies, the IL for the c-shaped meta-atom M shows a rapid increase and decrease (or vice versa), which can be utilized to insulate an incident sound pressure field if the effects are understood and advantageous in

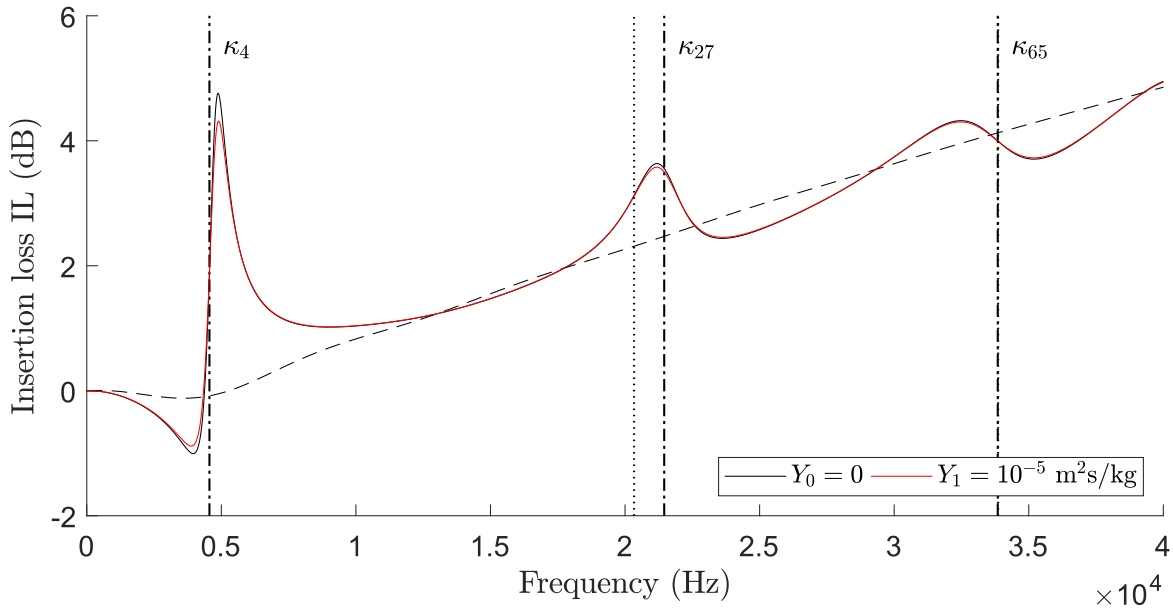

Fig. 12. Insertion loss (IL) according to Eq. (19) of the meta-atoms C (_ _ _ _) and M (_____) for two boundary admittances Y_0 and Y_1 as functions of the frequency. The modal resonance frequencies are indicated by vertical dash-dotted lines (_ . _ . _) for the eigenvalues $\kappa_4 \approx -447.85 + 4557.65\text{i}$, $\kappa_{27} \approx -1314.49 + 21455.45\text{i}$ and $\kappa_{65} \approx -2424.58 + 33848.26\text{i}$. The vertical dotted lines (. . . . .) at about 20,335 Hz and at about 33,863 Hz show the resonance frequencies of two eigenvectors, the imaginary parts of which are asymmetric with respect to the half-space axis, cf. Fig. 14.

Table 1
Alteration of eigenvalues of insulating modes according to Fig. 13 with two different boundary admittances Y_0 and Y_1.

Model	κ cavity mode 1	κ cavity mode 2	κ cavity mode 3
Y_0	$\approx -447.85 + 4557.65\text{i}$	$\approx -1314.49 + 21455.45\text{i}$	$\approx -2424.58 + 33848.26\text{i}$
Y_1	$\approx -413.45 + 4560.31\text{i}$	$\approx -1274.25 + 21461.39\text{i}$	$\approx -2374.55 + 33858.96\text{i}$

the specific application. The amplitude and the bandwidth of the insulation due to the c-shaped meta-atoms are larger at low frequencies, which might be indicated by the damping (real part of the eigenvalues) of the normal modes. The application of the boundary admittance Y_1 weakens the effects and both the rapid increase and decrease of the sound pressure are less distinct in comparison to the sound-hard problem. The effect is strongly frequency-dependent and diminishes with increasing frequency. It is already negligible around the third resonator frequency in the case of the small absorption coefficient $\alpha_1 = 0.017$. At least in this specific configuration with the c-shaped meta-atom M and the selected absorption α_1, no additional reduction effect by absorption can be read in the IL curve in the frequency range considered. However, it is conceivable that the reduction effect of absorber materials can be used specifically to reduce the incident sound pressure in certain frequency ranges, although at the same time there may be a reduction in insertion loss at other frequencies.

The normal mode eigenvalues of the undamped case Y_0 and the damped case Y_1 are given and compared in Table 1. Their real part decreases according to amount while the resonance frequency increases slightly.

The corresponding right eigenvectors or mode shapes illustrate the effect of the sound pressure within the air-column being in resonance. They can be referred to as the first and the two higher-order (second and third) Helmholtz resonator modes. Their magnitude, real part and imaginary part can be seen in Fig. 13 (consider the rotated view) in a half-space domain in order to utilize symmetry of the c-shaped meta-atom.

The sound pressure magnitudes (first row) give the impression that sound energy is trapped within the cavity, where for the second and even more so for the third resonator mode an interaction with the exterior can be observed. Like a Helmholtz resonator, the cavity acts like a tuned mass damper. Considering the additional, higher eigenfrequencies, one can speak of a tuned absorber. It is a well-known phenomenon that strongly attenuated tuned mass dampers do not work as effectively as weakly attenuated ones, which can be interpreted here from the proportions of the real parts of the eigenvalues.

In the second and third resonator modes, the sound pressure magnitude oscillates with one wavelength each in the y-direction and, for the third, additionally in the x-direction. Maximum sound pressure magnitudes can be found on the sound-hard boundary opposite the opening and directly in the opening itself so that it can be assumed that a sound pressure wave of the appropriate wavelength traveling through the opening excites this mode shape and thus gets caught inside the cavity.

The real and imaginary parts of the eigenvectors (second and third row) represent to some extent a radiative or reflective behavior.

Two more cavity normal modes are introduced in Fig. 14, which can only be found in full-space computational domains due to the asymmetric shape of the imaginary part of their right eigenvectors with respect to the y-axis as the mirror axis. These are

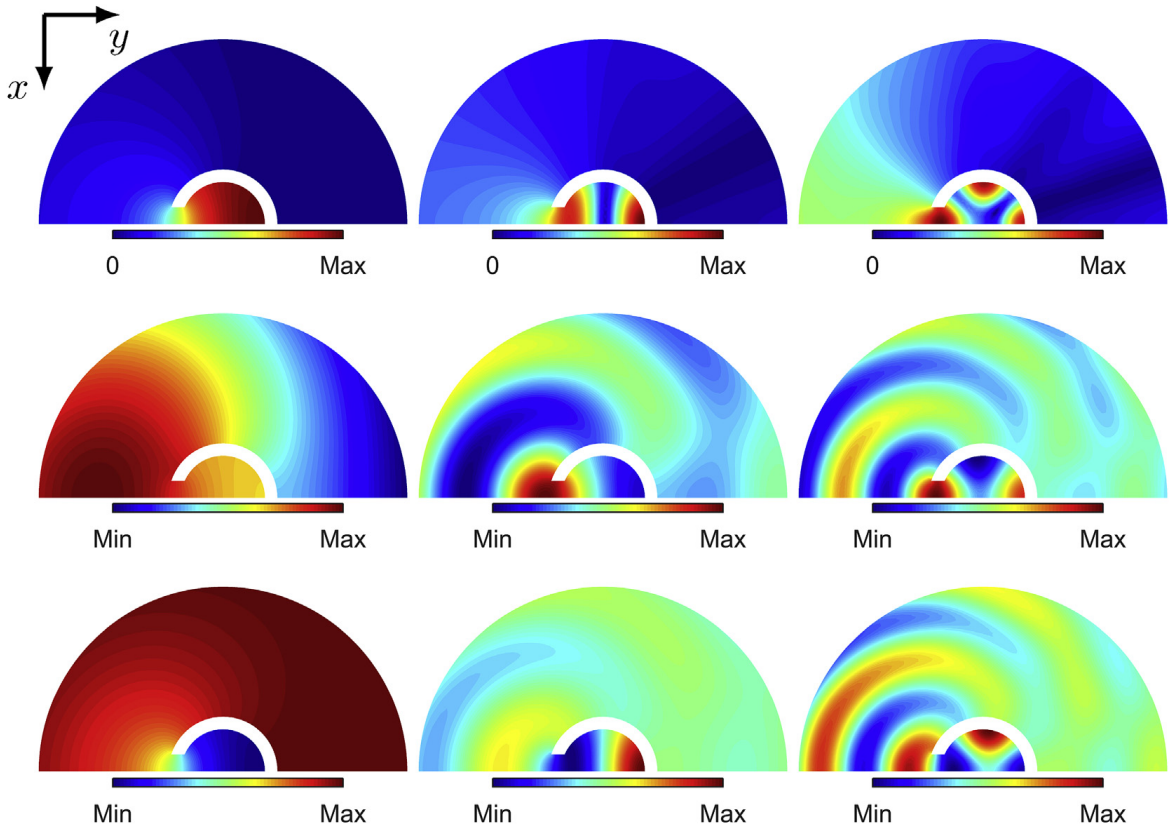

Fig. 13. Three considered insulating normal modes of $M1_{HS}$ (HS = half space, right eigenvectors in the FE domain) from left to right with the corresponding eigenvalues $\kappa_4 \approx -447.85 + 4557.65i$, $\kappa_{27} \approx -1314.49 + 21455.45i$ and $\kappa_{65} \approx -2424.58 + 33848.26i$. Eigenvector magnitude (first row), real part (second row) and imaginary part (third row). Note that the coordinate system is rotated for presentation reasons.

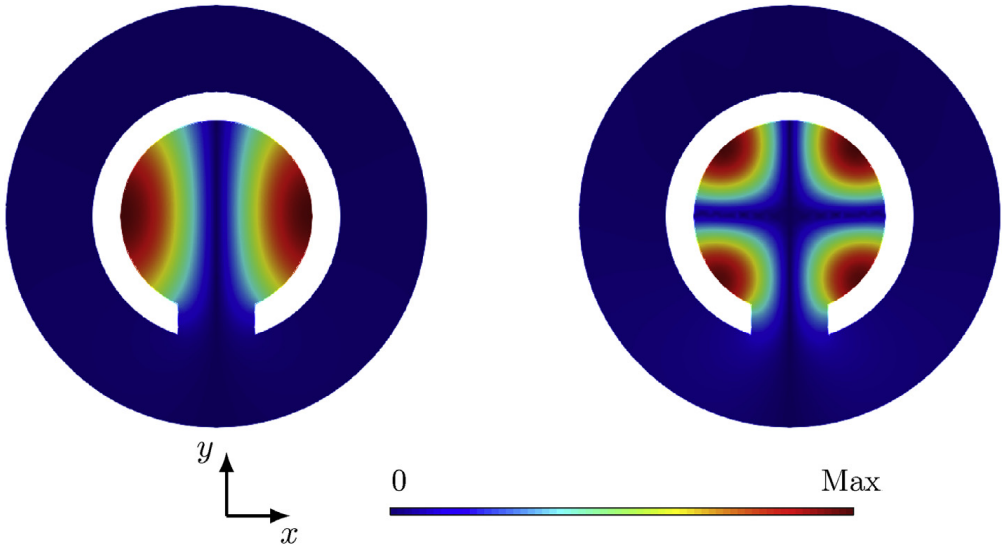

Fig. 14. Two cavity normal modes of M1 as right eigenvectors (magnitude) whose imaginary parts are asymmetrical with respect to the y-axis as the mirror axis. They cannot be determined in a half-space computation and are not substantially excited by a plane incident wave along the y-axis (symmetrical mirror axis). In this work they are called asymmetric modes. The corresponding eigenvalues are $\approx -3.36 + 20335.3i$ and $\approx -32.03 + 33862.7i$.

called asymmetric (cavity) modes in simplified terms in the following.

Even though the resonance frequencies of the two asymmetric modes in Fig. 14 are very close to those of the two symmetric Helmholtz resonator modes in the middle and on the right of Fig. 13—the similarity is related to the almost rotational symmetry of the meta-atom, which is only interrupted by the one-sided opening—the noise mitigation effect is mainly dominated by the symmetric modes in Fig. 13. This can be seen from the harmonic solution for the perpendicular and symmetrical incident sound pressure (in positive y-direction) in the fluid, in which only the symmetric mode shapes become clearly recognizable. The two

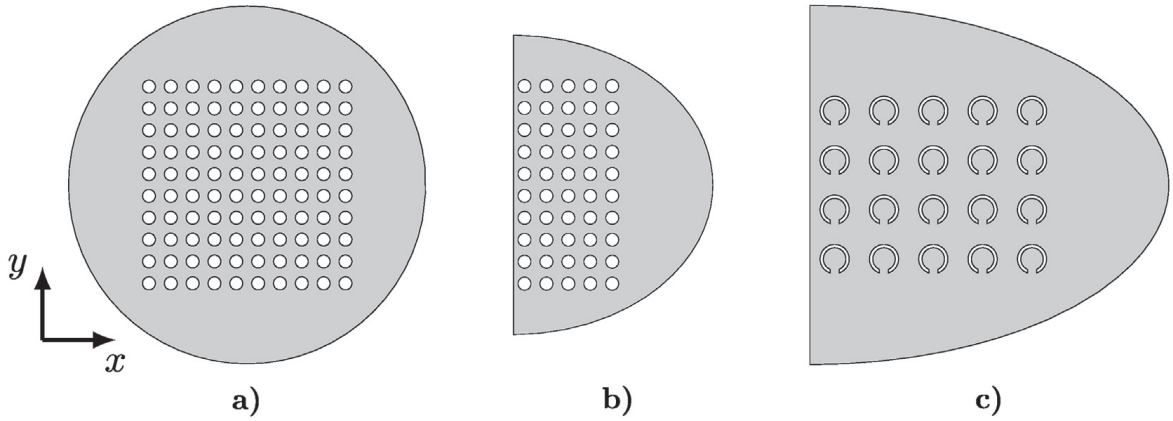

Fig. 15. Variations of the model S (sonic crystal) in a non-scaled representation: a) 10×10-array of meta-atoms C in a circular computational domain $\mathrm{S1}^{\mathrm{C}}10 \times 10$, b) 10×10-array of meta-atoms C in an elliptical, half-space computational domain $\mathrm{S1.33}^{\mathrm{C}}_{\mathrm{HS}}10 \times 10$ and c) 4×10-array of meta-atoms M in an elliptical, half-space computational domain $\mathrm{S2}^{\mathrm{M}}_{\mathrm{HS}}4 \times 10$. The fluid is illustrated gray.

asymmetrical modes do not interact with the exterior through the narrow opening, are therefore not significantly excited by the incident sound wave and are therefore not decisive for the noise-mitigating effect of the resonator.

It is obvious that the normal modes approach can determine and visualize the resonator frequencies and mode shapes very accurately, even for elaborated concepts such as the 'Matryoshka' design suggested by Chalmers et al. [7] and Elford et al. [8] as well as for the 'Mie' design presented by Cheng et al. [10] and Lu et al. [11]. The identification of the cavity modes can be carried out according to the criteria described by Moheit and Marburg [55].

The modal decomposition allows the clear distinction of the effects which lead to a high level of sound insulation. Here, no periodicity condition such as Floquet-Bloch in a unit cell is applied and the modal analysis is performed for a single meta-atom under free-field conditions. This has the advantage that one concentrates solely on the effect of the meta-atom itself. The interaction of the meta-atoms in finitely large arrays is discussed in the next section.

4. Results at sonic crystals level

Based on the findings from the results at meta-atom level in Sec. 3, the concept of normal modes is introduced in the context of finite sonic crystal noise barriers in order to provide a different point of view on the problem and form the basis for a thorough understanding of physical processes and effects.

Sonic crystals are periodic distributions of scatterers such as those of type C or M (cf. Fig. 2), which are embedded in an array allowing in specific conditions to produce acoustic band gaps (ABGs). These ABGs are frequency intervals where waves are forbidden to propagate. In this paper, the focus is on finitely long arrays for which the assumption of periodicity is limited and thus the effectiveness of the ABGs is influenced. The arrays are considered only in 2D in order to keep the computing requirements low. The view can therefore be understood as a sectional plane in 3D through an array of infinitely high cylinders. The surfaces of the scatterers are regarded as sound-hard walls.

For the investigations in this section, both the array and the shape of the computational domain are varied. An important feature of the sonic crystals is the arrangement of their elements, whereby in the scope of this work only square lattices are studied. The notation 4×10 indicates that the sonic crystal noise barrier is an array of four scatterers in the direction of the wave and ten in the direction perpendicular to it. Only incident plane waves along the x- or y-axis are considered in this work for the sake of simplicity and the possibility of exploiting symmetry properties. Symmetric problems are carried out using half-space domains due to the lower effort, cf. Sec. 3.3. The abbreviations for these models start with the letter S, half-space domains are indicated by the subscript HS.

Two arrays of scatterers (10×10 and 4×10) are investigated for both meta-atoms C and M. Variations of the models are depicted in Fig. 15.

Their specifications are inspired by the work of Elford et al. [8], for which experimental results are partly available in the earlier work of Chalmers et al. [7]. The lattice constant, which is the distance from the center of a scatterer to the center of the next one, is equal to 22 mm (the corresponding unit cell in Elford's work has a width of 11 mm), their diameter is 13 mm. The total depth of the considered barriers is thus 220 mm (ten times the lattice constant) and 88 mm (four times the lattice constant), respectively. The slender array 4×10 is calculated in an elliptical domain. The density of the fluid is $\rho_f = 1.25\,\mathrm{kgm}^3$ and the speed of sound is $c_f = 343\,\mathrm{ms}^1$.

According to the findings of the results at meta-atom level and weighing accuracy against computational effort for many degrees of freedom, infinite elements of radial polynomial order twelve with twelve second-order Lagrangian finite elements per wavelength at 20 kHz (i.e. $h_{\max} \approx 1.43$ mm and still six quadratic finite elements per wavelength at the maximum frequency 40 kHz) are used in the investigation of the sonic crystals. The coarser mesh resolution beyond the audible frequency range is acceptable in the present case, since on the one hand the results from preliminary investigations in Sec. 3.1 indicate a sufficient

Table 2
Mesh specifications of the sonic crystal models by means of degrees of freedom (DOF) and the number of finite elements.

Model	$S1^{C}10\times10$	$S1^{C}_{HS}10\times10$	$S2^{C}_{HS}4\times10$	$S1^{M}_{HS}10\times10$	$S2^{M}_{HS}4\times10$
DOF	289,429	145,075	57,789	156,931	62,553
N. of fin. elements	142,968	71,538	28,432	76,966	30,614

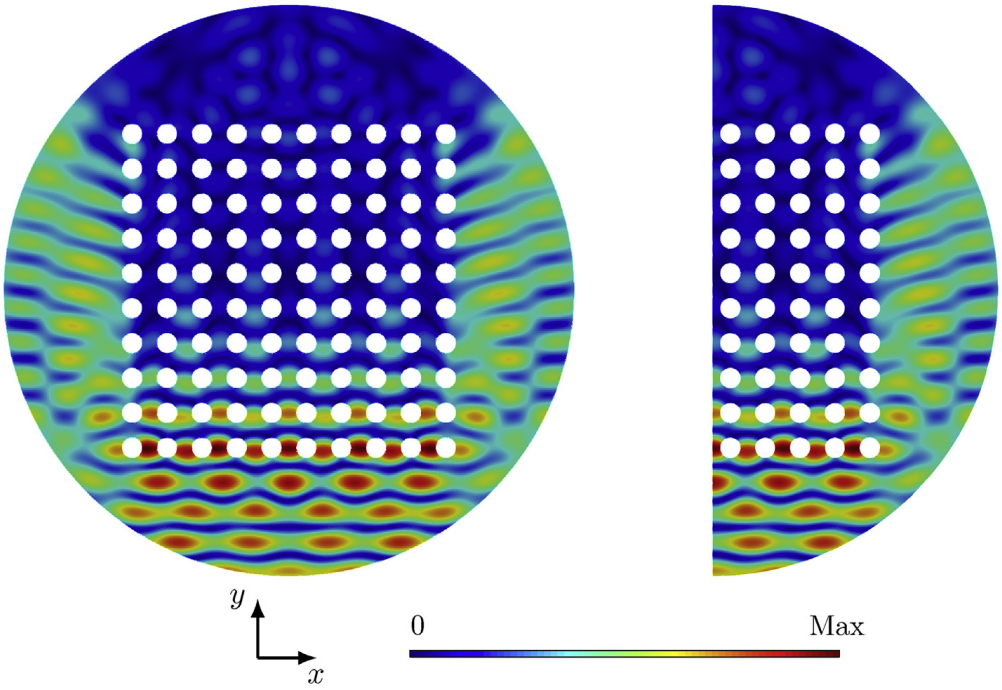

Fig. 16. Sound pressure magnitude distribution in the FE domain for an incident plane wave (traveling in positive y-direction) indicates a high sound pressure insulation at 9060 Hz for $S1^{C}10\times10$ (left) and $S1^{C}_{HS}10\times10$ (right) in the upper shadow of the 10×10 array.

accuracy and on the other hand no absolute results are of interest, but qualitative statements should be made. The number of degrees of freedom (DOF) and finite elements of the models are given in Table 2.

The procedure in this section is structured as follows: In the first step in Sec. 4.1, the noise barriers are subjected to incident sound pressure fields, resulting from plane waves, which lead to scattering fields as described in the theory Sec. 2.1. The insertion losses of the barriers are then calculated in a frequency spectrum ranging from 1 Hz to 40 Hz in 1 Hz-steps so that frequency bands with a low transmission of sound are identified and studied by means of normal mode eigenvalues and eigenvectors, which will be the subject of the second part Sec. 4.2. This procedure is intended to reveal relationships between the modes in exterior acoustics and the insulating effect of the noise barriers.

4.1. Harmonic scattering

An incident sound pressure field propagating in positive y-direction is implemented for each of the four models S with a variation of two different lattices and two different meta-atoms as described above. The amplitudes p_0 of the plane waves are 2 Pa ($L_p = 100$ dB) with the phase angle $\phi_0 = 0$. The problems are solved via harmonic analysis by inversion of the frequency-dependent system matrix according to Eq. (2).

Fig. 16 shows the distribution of the sound pressure magnitude at 9060 Hz in the circular and the half-space FE domain with cylindrical meta-atoms C in a 10×10 array.

The sound pressure distribution is virtually identical in full-space and in half-space and, due to the symmetry of the arrangement and of the incident sound pressure field, the results can be interpreted in the same way while saving computing power.

A significant sound insulation is yielded above the array, which seems to be controlled by the Bragg scattering effect of standing waves in the array of the scatterers [8]. In the sound pressure field, local maxima occur behind the array as a result of diffraction and interference, which do not occur with a periodically continued barrier, as there are no boundary effects (cf. [8]). The local effects are moreover heavily dependent on the frequency of the incident sound pressure field. For that reason, the noise mitigation by sonic crystals is measured by the insertion loss according to Eq. (19), wherein the difference of the averaged SPL is formed in a rectangular region behind the array between the case without mitigation measure and that with the barrier. The rectangular region has a thickness of 25 mm and it extends over the width of the barrier in a distance of 11 mm behind the last scatterers. The curves of the IL as functions of the frequency are depicted in Fig. 17 with a sampling in 1 Hz-steps.

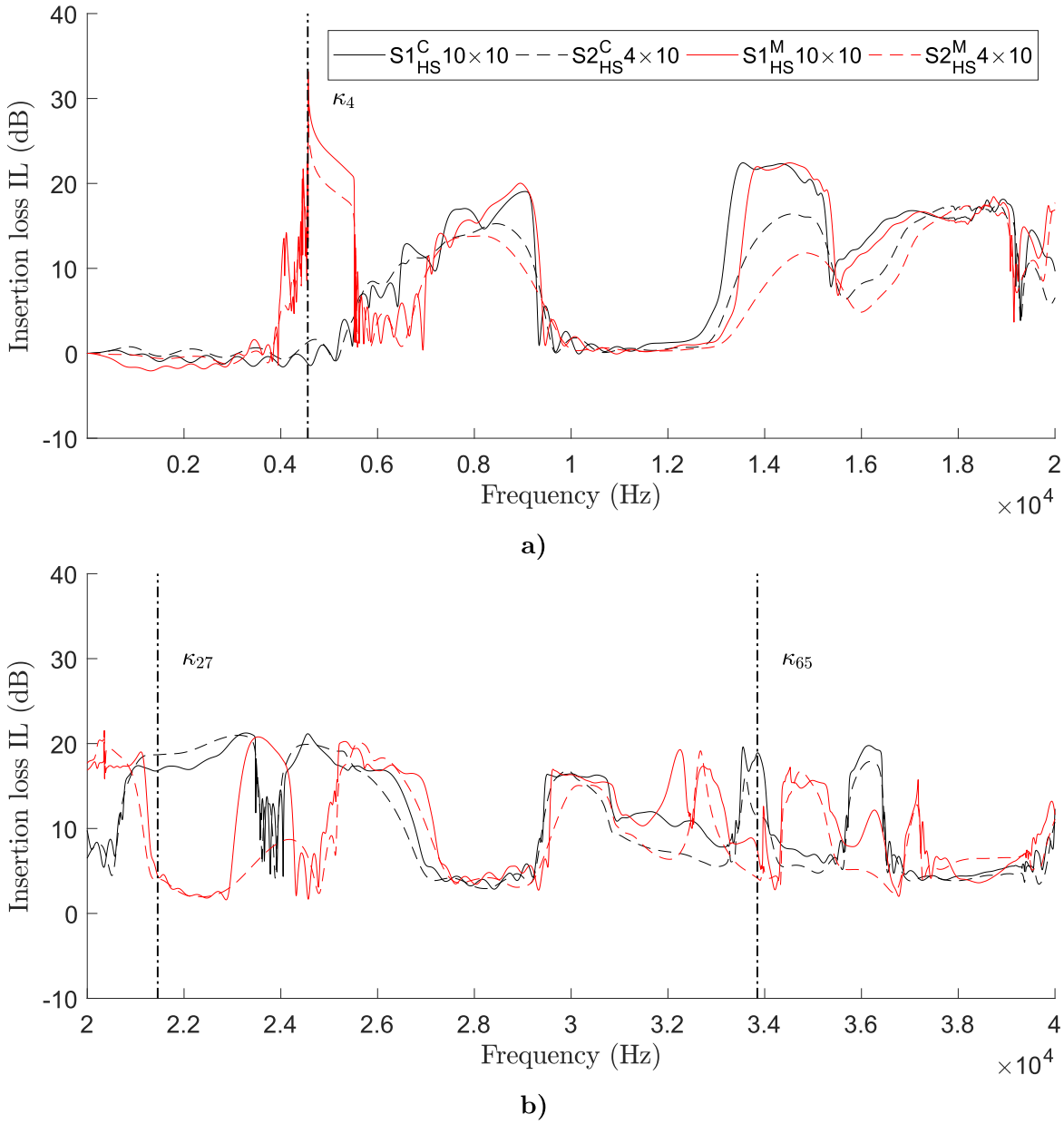

Fig. 17. Insertion loss IL for the two arrays 4 × 10 (_____) and 10 × 10 (_ _ _ _) and both meta-atoms C (black) and M (red): (a) frequency range from 1 Hz to 20,000 Hz and (b) from 20,000 Hz to 40,000 Hz. Vertical dash-dotted lines indicate the eigenfrequencies of the first and the two higher-order Helmholtz-resonator modes as described in Sec. 3.4. (For interpretation of the references to color in this figure legend, the reader is referred to the Web version of this article.)

It should be noted that the IL in the three-dimensional is of course considerably lower in the case of finitely high noise barriers due to the diffraction of the sound waves across the cylinders. For the basic description of the sound-insulating effect in the x-y-plane, however, the assumption of infinitely high cylinders in the two-dimensional is advantageous.

All four curves tend to show similarly high or low IL in certain frequency ranges, for example between 7 kHz to 9 kHz and 17 kHz–19 kHz. Virtually no sound-insulating effect is provided by all four considered configurations in the frequency range below approx. 3.5 kHz and in the range from 9.5 kHz to 13 kHz (IL $\approx$ 0.5 dB). A low mitigation is provided from 27 kHz to 29 kHz (IL $\approx$ 3 dB–4 dB). The similar behavior indicates that the effectiveness of the array in these frequency ranges does not primarily depend on the depth of the barrier and shape of the scatterers, but on the distance from each other in the lattice due to Bragg scattering. This will be referred to later in Sec. 4.2 by means of the modal analysis via normal modes.

The IL curves for the arrays of meta-atoms C and M show completely opposite effects between 3.7 kHz and 5.6 kHz, where the insertion loss of the array with c-shaped meta-atoms M is much greater than the one with the cylinders C and the other way round in the range from 21 kHz to 23 kHz. Both frequency ranges are close to the cavity mode resonance frequencies of the c-shaped meta-atom κ_4 at about 4558 Hz and κ_{27} at about 21,456 Hz, which are depicted and described in Sec. 3.4. The eigenfrequencies are drawn as vertical dash-dotted lines in Fig. 17. The peak value of the IL is reached for S1$^{M}_{HS}$10 × 10 at 4566 Hz with approximately 33 dB, which is to be justified with the Helmholtz resonator effect of the c-shaped meta-atom at this frequency.

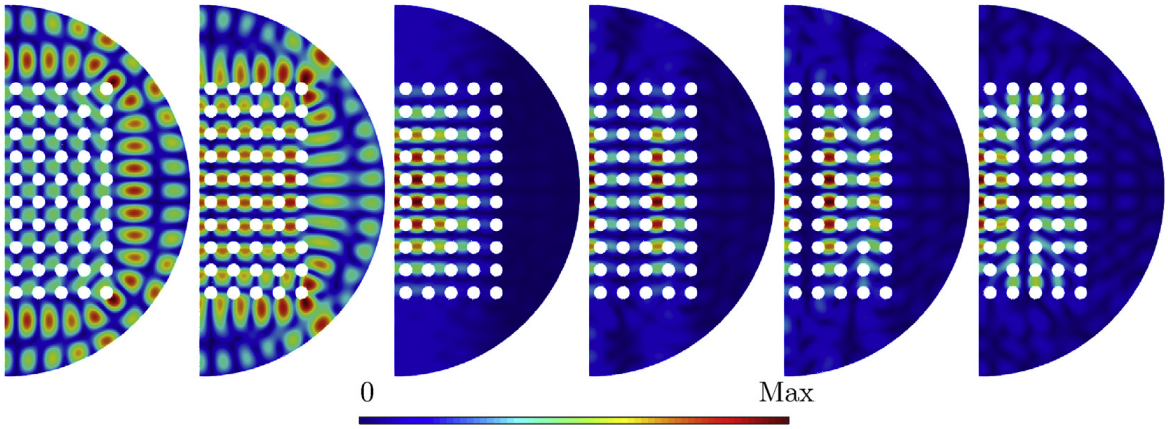

Fig. 18. Characteristic mode shapes as right eigenvectors in the FE domain with resonance frequencies in the range of the associated first Bragg-type band gap of the corresponding periodic array. Corresponding eigenvalues from left to right: $\kappa_{243} \approx 102.92 + 8844.85\mathrm{i}$, $\kappa_{245} \approx 95.18 + 8854.5\mathrm{i}$, $\kappa_{267} \approx 33.37 + 9252.59\mathrm{i}$, $\kappa_{269} \approx 40.98 + 9292.39\mathrm{i}$, $\kappa_{271} \approx 37.66 + 9344.87\mathrm{i}$ and $\kappa_{277} \approx 19.33 + 9409.02\mathrm{i}$.

Basically, the IL of the 4×10 arrays are only slightly lower than those of the 10×10 arrays with occasionally up to 5 dB, but in some cases even up to 15 dB less IL by 13.8 kHz and by 23.4 kHz. The effect is more pronounced with the c-shaped meta-atoms M.

The frequency ranges with a high sound-absorbing effect correspond qualitatively with those from the transmission analyses by Elford et al. [8] for both the circular and the c-shaped meta-atoms in the 10×10 array. Deviations can primarily be attributed to the varying determination of the IL as well as to the circumstance that the region lateral to the arrays is modeled differently and in this work, diffraction along the outer edge is considered, so that absolute comparability is not possible.

A noise reduction of 10 dB–20 dB can be achieved in wide frequency bands and it is conceivable that the effect can be greatly increased or the bandwidth can be broaden by the targeted introduction of Helmholtz resonators of different sizes and lattice widths as well as absorbers. It should be noted, of course, that the two-dimensional problem described is idealized and overestimates the results compared to reality.

4.2. Modal analysis

For a better understanding of the effects and as a tool for the efficient design and optimization of sonic crystal noise barriers, this paper proposes the normal modes in the acoustic exterior. Their requirements and specific properties have been considered in Sec. 3.

In the example of the array $\mathrm{S1}^{\mathrm{C}}_{\mathrm{HS}}10 \times 10$, some of the modes are depicted in Fig. 18, which are most likely responsible for the high sound insulation in the region of the associated Bragg-type band gap around 9060 Hz of a comparable, periodic array.

Its effect is shown in Fig. 16 for the harmonic sound pressure distribution as the sum of incident and scattered sound pressure field.

In Fig. 18, it can be observed how the sound energy is trapped inside the sonic crystals array at different positions. The first two shown modes are also in strong interaction with the surrounding fluid, but they are much more damped with respect to the larger real part of their eigenvalues and thus less excited than the others. With variable grid widths, it is conceivable that the sound insulating effect can be extended to a wider frequency range.

In what follows, the smaller array $\mathrm{S2}^{\mathrm{M}}_{\mathrm{HS}}4 \times 10$ (cf. Fig. 15c) shall be investigated exemplarily by NM to comprehend the underlying physics of both resonance and Bragg-type band gaps, which, in the case of the finitely extended array, result in finite sound insulation. The standing wave patterns are less pronounced in this example compared to the large 10×10-array due a stronger interaction with the exterior domain.

The distribution of the eigenvalues in the complex plane can be seen on the right-hand side in Fig. 19 in a cutout only for zero and positive imaginary parts. The imaginary axis of the complex plane represents the resonance frequencies of the modes, as discussed in Sec. 2.2. The general structure or distribution of the normal modes in the complex plane is similar to observations in previous studies by the authors [55], where a rough distinction is made between cavity modes, multipole modes and spurious modes. The frequency curves of the insertion loss due to the sonic crystal array $\mathrm{S2}^{\mathrm{M}}_{\mathrm{HS}}4 \times 10$ (black) and due to a single meta-atom M in free-field (gray) are depicted on the left-hand side in Fig. 19. Both images are shown side by side in order to compare the modes and the effect in the form of the IL directly with each other. Horizontal dash-dotted lines (- · - · -) indicate three cavity eigenfrequencies of the c-shaped meta-atom M under free-field conditions, cf. Fig. 13. Horizontal dashed lines (- - - -) connect two further distinctive peaks of the IL with eigenvalues in the complex plane. Selected eigenvalues κ_A to κ_L are tagged. Their corresponding mode shapes can be found in Fig. 20. Light gray areas indicate frequency regions with high insertion losses that can be attributed to associated Bragg band gaps (corresponding eigenvalues are indicated by ◇ markers). The corresponding eigenvalues of the Helmholtz resonator modes and asymmetric cavity modes are depicted as ○ and ☆, respectively.

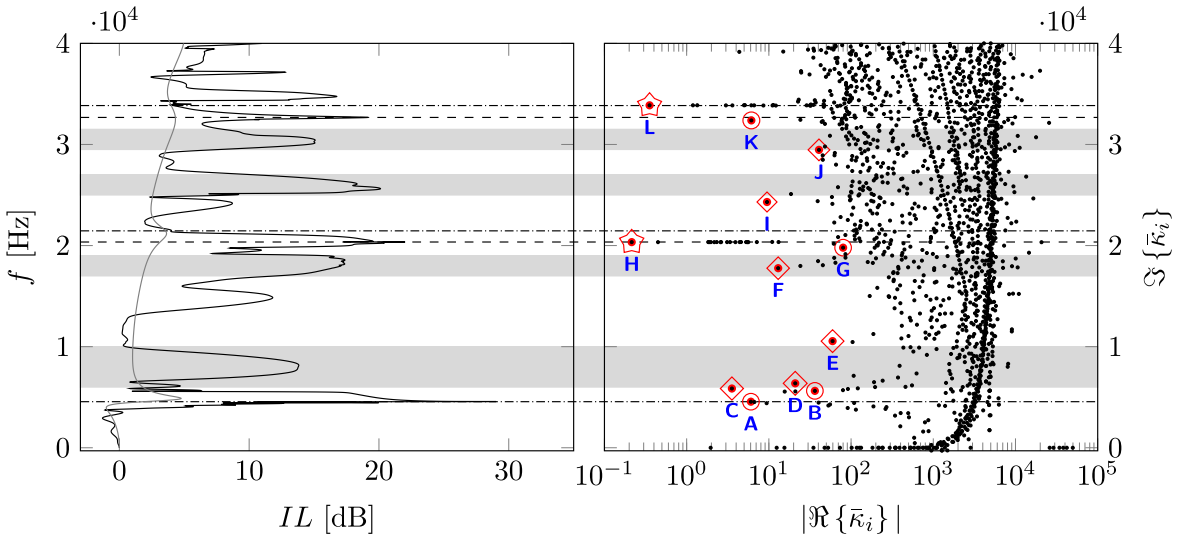

Fig. 19. Side-by-side of the insertion loss (IL) of $S2^{M}_{HS}4 \times 10$ (———) and a single meta-atom M in free-field (———) as functions of the frequency (left) and normal mode eigenvalues in the complex plane of eigenvalues κ_m (right, limited to $\mathrm{Im}\{\kappa_m\} \geq 0$).

The complex plane is symmetrical with respect to the real axis. All eigenvalues that appear on the positive side of the imaginary axis do also exist mirrored with a negative imaginary part. The corresponding complex-valued eigenvectors do therefore exist twice. The authors showed that the contribution of the two complex conjugated partners to a possible sound radiation by the scatterers is not identical [55]. The question to what extent the complex conjugated partners contribute to sound insulation to varying degrees is not to be investigated in the context of this work.

A large part of the determined normal modes are multipoles of different orders [55]. Due to the asymmetry of the arrangement by the one-sided opening of the meta-atoms and by the elliptical shape of the computational domain, some of the multipole-modes are slightly asymmetrical along the outer FE boundary line, similar to the representation in the preliminary studies at meta-atom level in Fig. 9.

The three dash-dotted lines in Fig. 19 indicate the eigenfrequencies of the three cavity modes of the single c-shaped meta-atom as described in Sec. 3.4 and shown in Figs. 12 and 13. The arrangement in the array shifts their natural frequencies and causes standing wave effects between the meta-atoms. As a consequence, the results of the free-standing meta-atoms are not directly comparable with those in the sonic crystal. Consequently, the peaks with very high IL do not necessarily occur at the same frequencies (dashed lines), except for the first Helmholtz resonator frequency, where the peak can still be assigned clearly; for the two higher ones, the deviation is already very significant.

The effects are described by the modes A, B, G and K (circular marker), which represents only a selection of the associated modes. In the surrounding frequency ranges, several modes of a similar kind scatter whereby only single, apparently randomly distributed cavities or small groups of meta-atoms vibrate per mode. Therefore, several modes are required for the entire effect of the arrangement. The interaction of individual, similar modes of the same group is reminiscent of studies on eigensolutions of mistuned rotor blades due to imperfect axial symmetry, for example by Ewins [91] and Irwanto et al. [92].

In the same way, multiple eigenvalues can be found for asymmetrical cavity modes as described in the previous section (cf. Fig. 14). Their eigenvectors are characterized by the fact that they are rotated by 45 and 90°, respectively, compared to the modes known as higher Helmholtz resonator eigenfrequencies in Fig. 13. Their corresponding eigenfrequencies lay quite exactly on only one frequency line at a time, which is virtually equivalent to the respective eigenfrequency of the single meta-atom as depicted in Fig. 12. This is due to the fact that the modes are weakly damped (small real part) and do hardly interact with the exterior domain. In one case, these eigenvalues are virtually in line with the frequency at which a particularly high IL is measured at about 20.35 kHz and once approximately at the level of the third Helmholtz resonator frequency at about 33.85 kHz. The asymmetric modes differ in frequency from the Helmholtz resonator modes solely due to the one-sided opening of the meta-atom but are otherwise almost rotationally symmetrical in shape and therefore have almost identical natural frequencies. In the complex plane in Fig. 19, two examples for asymmetrical cavity modes in the sonic crystals array are found as eigenvalues H and L (star-shaped marker).

The assignment of the peaks with high insertion loss due to the resonator effect (marked with dashed lines) can be done quite clearly. The modes of the first and the two higher Helmholtz resonator effects (circular markers) each scatter slightly around these dashed frequency lines and thus also influence the width of the peaks. Some of the resonator waveforms (especially the modes B and G) mix with the adjacent so-called Bragg-type effects, in which the sound energy remains trapped within the grid.

Bragg-type band gaps arise from the periodic nature of the crystal [7]. In the case of local periodicity as given here, a high level of sound insulation in the associated frequency regions can still be attributed to the underlying physical effect of Bragg band gaps. In order to approach their phenomenon, first, four exemplary frequency bands are selected in which a high IL occurs (light gray background marking). Using the imaginary parts of their eigenvalues, meaningful eigenvectors are identified, which

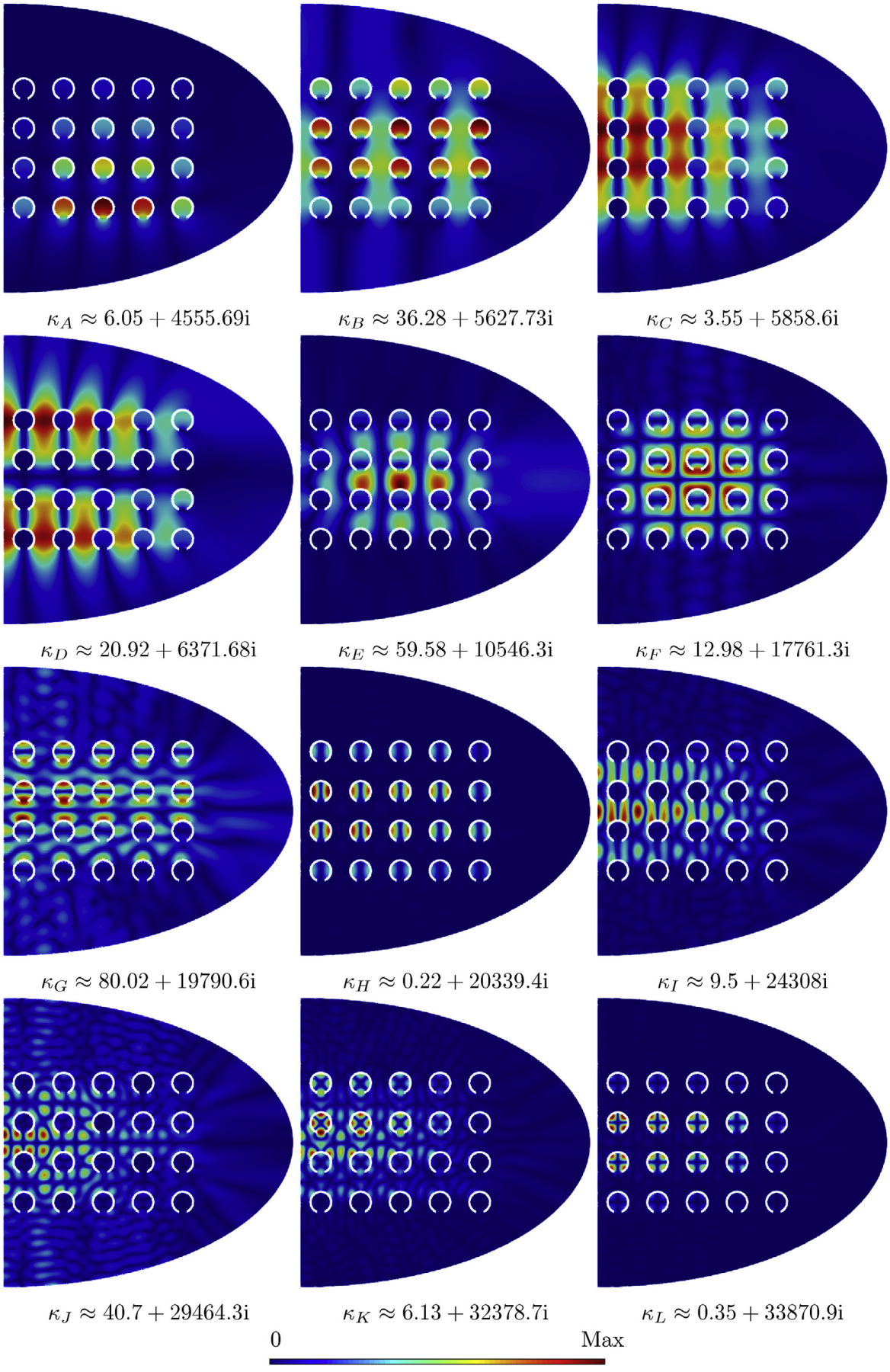

Fig. 20. Normal mode shapes as right eigenvectors in the FE domain (magnitude) corresponding to the eigenvalues κ_A to κ_L as depicted in Fig. 19.

contribute to the description of the insulating Bragg effect within the array. The eigenvalues C, D, E, F, I and J are indicated by diamonds in the complex plane in Fig. 19. The most different patterns and forms can be observed for the eigenvector magnitudes and it becomes obvious that on the one hand the Bragg-type modes often interact with the resonator modes and on the other hand their eigenfrequencies depend strongly on the lattice width and the number of zero crossings of the standing waves in the array. With the introduction of different lattice widths within the array, the frequency ranges with high IL could be specifically influenced. The knowledge about the normal modes of the single meta-atoms and the whole arrangement can contribute to a targeted design and optimization of sonic crystals.

5. Conclusions

In this work, it could be confirmed that the IFEM is applicable at circular and elliptical FE domains of various aspect ratios for the computation of incident and scattered sound pressure fields and for the frequency-independent normal modes. The focus of this work is on two-dimensional models of sonic crystal noise barriers and their components, which can be referred to as meta-atoms. The requirements for the FE mesh size and for the IFE radial order, however, are initially examined for simple, known models and they serve as the basis for the error estimation of the subsequent investigations.

The concept of normal modes is introduced in this field, since the complex eigenvalues and eigenvectors provide information on damping and resonance frequencies of modes in exterior domains and offer a new point of view on standing waves, diffraction and interference effects in the unbounded fluid around and in between the array of scatterers. The modal decomposition of the exterior sound pressure field around arbitrarily-shaped meta-atoms can be utilized in the process of design and dimensioning of noise barriers or acoustic metamaterials in general. It could be suggested that the sound insulation is due to the superposition of a few normal modes in and around the frequency ranges of the associated band gaps of the related periodic array. Their eigenvectors show standing wave patterns between the acoustic meta-atoms in the array. Obviously, these mode shapes are responsible for the reflection or withdrawal of sound energy.

The investigations at sonic crystals always focus on the attempt to broaden the bandwidth of sound insulation, for example by introducing differently scaled and shaped meta-atoms and varying lattice widths in order to overlap the individual effects. The method of normal modes is presented in this work as a suitable tool for the conception of complex arrays and for a better understanding of their mode of action.

With regard to the insulating effect of individual c-shaped meta-atoms, it can be concluded that—in contrast to the filled obstacle—their efficiency is dominated by the first and higher-order Helmholtz resonator modes or cavity modes around their respective resonance frequencies while the insulation of sound pressure also involves an amplification with the result that both effects have to be weighted. The effects are softened if a boundary admittance is attached to the interior walls of the c-shaped meta-atom as could be the case for slightly soiled or elastic materials.

The effects of elliptical domain shapes and half-space problems on the normal modes is estimated, since finite sonic crystals can be considered as long, slender and symmetric arrays and the number of degrees of freedom can be reduced significantly, if the domain shape is adapted to the shape of the obstacle(s). It is found that, while the eigenvalues of the complex Helmholtz resonator or trapped modes remain virtually the same for both circular and elliptical domains, the eigenvalues of exterior multipole modes change according to the aspect ratios of the compared domains. The number of degrees of freedom can be reduced significantly by utilization of symmetry in half-space domains, which is shown to have a negligible influence on the cavity modes.

Summarizing it can be said that elliptic computational domains in 2D should be used with care, since the global relative error grows considerably compared to circular computational domains and unpredictable effects might occur. Furthermore, the polynomial order for the radial interpolation of the IFEM has to be strongly increased, so that the advantage of narrow computational domains may be lost.

Future work should include a further investigation of the physical effects inside the arrays in order to improve and adapt the design and configuration in regard to unique applications. The computational costs of the method can be reduced by the utilization of model order reduction (MOR) techniques, such as modal reduction. The authors suggested criteria for the distinction between relevant and non-relevant normal modes in previous work [55], which can be adapted and enhanced in the present example. It is also interesting to study the collaboration of differently shaped and aligned meta-atoms in sonic crystals and further develop understanding for the insulating processes of meta-atoms with absorbing or porous layers or integrated mass damper structures subject to fluid-structure interaction by means of the normal modes approach. More realistic simulations can be conducted for three-dimensional sonic crystals with cylinders of finite height on an absorbing ground (ellipsoidal half-space FE domain).

Acknowledgements

The authors kindly acknowledge the anonymous reviewers for their constructive advises during the peer review process. This research was thankfully supported by the Deutsche Forschungsgemeinschaft (DFG), grant number 230029255.

References

[1] J.V. Sanchez-Perez, C. Rubio, R. Martinez-Sala, R. Sanchez-Grandia, V. Gomez, Acoustic barriers based on periodic arrays of scatterers, Appl. Phys. Lett. 81 (27) (2002) 5240–5242.
[2] S.M.B. Fard, N. Kessissoglou, H. Peters, Locally resonant sonic crystal barrier for low frequency noise control, in: J. Parnell (Ed.), Proceedings on Acoustics 2015 Hunter Valley, Australian Acoustical Society, Australian Acoustical Society, 2015.
[3] M. Martins, L. Godinho, L. Picado-Santos, Numerical evaluation of sound attenuation provided by periodic structures, Arch. Acoust. Q. 38 (4) (2013) 503–516.
[4] A. Gupta, K.-M. Lim, C.H. Chew, Design of radial sonic crystal for sound attenuation from divergent sound source, Wave Motion 55 (2015) 1–9.
[5] A. Krynkin, O. Umnova, A.Y.B. Chong, S. Taherzadeh, K. Attenborough, Scattering by coupled resonating elements in air, J. Phys. D Appl. Phys. 44 (12) (2011) 125501.
[6] B. Van der Aa, J. Forssn, Scattering by an array of perforated cylinders with a porous core, J. Acoust. Soc. Am. 136 (5) (2014) 2370–2380.
[7] L. Chalmers, D.P. Elford, F.V. Kusmartsev, G.M. Swallowe, Acoustic band gap formation in two-dimensional locally resonant sonic crystals comprised of Helmholtz resonators, Int. J. Mod. Phys. B 23 (20n21) (2009) 4234–4243.
[8] D.P. Elford, L. Chalmers, F.V. Kusmartsev, G.M. Swallowe, Matryoshka locally resonant sonic crystal, J. Acoust. Soc. Am. 130 (5) (2011) 2746–2755.
[9] F. Montiel, H. Chung, M. Karimi, N. Kessissoglou, An analytical and numerical investigation of acoustic attenuation by a finite sonic crystal, Wave Motion 70 (2017) 135–151.
[10] Y. Cheng, C. Zhou, B. Yuan, D. Wu, Q. Wei, X. Liu, Ultra-sparse metasurface for high reflection of low-frequency sound based on artificial mie resonances, Nat. Mater. 14 (10) (2015) 1013.
[11] G. Lu, E. Ding, Y. Wang, X. Peng, J. Cui, X. Liu, X. Liu, Realization of acoustic wave directivity at low frequencies with a subwavelength mie resonant structure, Appl. Phys. Lett. 110 (12) (2017) 123507.
[12] V. Romero-Garca, E. Fuster, L. Garca-Raffi, E.A. Snchez-Prez, M. Sopena, J. Llinares, J.V. Snchez-Prez, Band gap creation using quasiordered structures based on sonic crystals, Appl. Phys. Lett. 88 (17) (2006) 174104.
[13] O. Sigmund, J. Sndergaard Jensen, Systematic design of phononic bandgap materials and structures by topology optimization, Philos. Trans. R. Soc. London, Ser. A: Math., Phys. Eng. Sci. 361 (1806) (2003) 1001–1019.
[14] C. Barbarosie, Shape optimization of periodic structures, Comput. Mech. 30 (3) (2003) 235–246.
[15] R. Martnez-Sala, J. Sancho, J.V. Snchez, V. Gmez, J. Llinares, F. Meseguer, Sound attenuation by sculpture, Nature 378 (6554) (1995) 241.
[16] C. Lagarrigue, J. Groby, V. Tournat, Sustainable sonic crystal made of resonating bamboo rods, J. Acoust. Soc. Am. 133 (1) (2013) 247–254.
[17] L. Godinho, P.G. Santos, P. Amado-Mendes, A. Pereira, M. Martins, Experimental and numerical analysis of sustainable sonic crystal barriers based on timber logs, in: Proceedings of the EuroRegio2016, Portugal, Porto, 2016, pp. 13–15.
[18] A. Gupta, A review on sonic crystal, its applications and numerical analysis techniques, Acoust Phys. 60 (2) (2014) 223–234.
[19] T. Miyashita, Sonic crystals and sonic wave-guides, Meas. Sci. Technol. 16 (5) (2005) R47.
[20] L. Brillouin, Wave Propagation in Periodic Structures: Electric Filters and Crystal Lattices, 1953.
[21] C.C. Claeys, K. Vergote, P. Sas, W. Desmet, On the potential of tuned resonators to obtain low-frequency vibrational stop bands in periodic panels, J. Sound Vib. 332 (6) (2013) 1418–1436.
[22] S.A. Cummer, J. Christensen, A. Al, Controlling sound with acoustic metamaterials, Nat. Rev. Mater. 1 (3) (2016) 16001.
[23] J. Jordaan, S. Punzet, A. Melnikov, A. Sanches, S. Oberst, S. Marburg, D.A. Powell, Measuring monopole and dipole polarizability of acoustic meta-atoms, Appl. Phys. Lett. 113 (22) (2018) 224102.
[24] A. Melnikov, Y.K. Chiang, L. Quan, S. Oberst, A. Al, S. Marburg, D. Powell, Acoustic meta-atom with experimentally verified maximum willis coupling, Nat. Commun. 10 (1) (2019) 1–7.
[25] F. Bloch, ber die Quantenmechanik der Elektronen in Kristallgittern (On the quantum mechanics of electrons in crystal lattices), Z. Phys. 52 (78) (1929) 555–600.
[26] C.E. Bradley, Acoustic Bloch Wave Propagation in a Periodic Waveguide, Tech. rep., 1991.
[27] N. Sugimoto, T. Horioka, Dispersion characteristics of sound waves in a tunnel with an array of Helmholtz resonators, J. Acoust. Soc. Am. 97 (3) (1995) 1446–1459.
[28] Z. Liu, X. Zhang, Y. Mao, Y. Zhu, Z. Yang, C.T. Chan, P. Sheng, Locally resonant sonic materials, Science 289 (5485) (2000) 1734–1736.
[29] C. Claeys, E. Deckers, B. Pluymers, W. Desmet, A lightweight vibro-acoustic metamaterial demonstrator: numerical and experimental investigation, Mech. Syst. Signal Process. 70 (2016) 853–880.
[30] S.H. Schot, Eighty years of Sommerfeld's radiation condition, Hist. Math. 19 (4) (1992) 385–401.
[31] R.J. Astley, Infinite elements, in: S. Marburg, B. Nolte (Eds.), Computational Acoustics of Noise Propagation in Fluids - Finite and Boundary Element Methods, Springer Berlin Heidelberg, Berlin, Heidelberg, 2008, pp. 197–230.
[32] T.W. Wu, Boundary Element Acoustics Fundamentals and Computer Codes, WIT Press, Southampton, 2000.
[33] S. Marburg, Boundary element method for time-harmonic acoustic problems, in: M. Kaltenbacher (Ed.), Computational Acoustics, Springer, 2018, pp. 69–158. Ch. 3.
[34] J.-P. Berenger, A perfectly matched layer for the absorption of electromagnetic waves, J. Comput. Phys. 114 (2) (1994) 185–200.
[35] A. Bermdez, L. Hervella-Nieto, A. Prieto, R. Rodrguez, Perfectly matched layers, in: S. Marburg, B. Nolte (Eds.), Computational Acoustics of Noise Propagation in Fluids - Finite and Boundary Element Methods, Springer Berlin Heidelberg, 2008, pp. 167–196.
[36] A. Bermdez, L. Hervella-Nieto, A. Prieto, R. Rodrguez, Perfectly matched layers for time-harmonic second order elliptic problems, Arch. Comput. Methods Eng. 17 (1) (2010) 77–107.
[37] S.M. Fard, H. Peters, N. Kessissoglou, S. Marburg, Three-dimensional analysis of a noise barrier using a quasi-periodic boundary element method, J. Acoust. Soc. Am. 137 (6) (2015) 3107–3114.
[38] S. Fard, H. Peters, S. Marburg, N. Kessissoglou, Acoustic performance of a barrier embedded with Helmholtz resonators using a quasi-periodic boundary element technique, Acta Acustica united Acustica 103 (3) (2017) 444–450.
[39] H. Ziegelwanger, P. Reiter, M. Conter, The three-dimensional quasi-periodic boundary element method: implementation, evaluation, and use cases, Int. J. Comput. Methods Exp. Meas. 5 (3) (2017) 404–414.
[40] D.S. Burnett, R.L. Holford, An ellipsoidal acoustic infinite element, Comput. Methods Appl. Mech. Eng. 164 (12) (1998) 49–76.
[41] D.S. Burnett, R.L. Holford, Prolate and oblate spheroidal acoustic infinite elements, Comput. Methods Appl. Mech. Eng. 158 (12) (1998) 117–141.
[42] R.J. Astley, G.J. Macaulay, J.-P. Coyette, L. Cremers, Three-dimensional wave-envelope elements of variable order for acoustic radiation and scattering. Part I. Formulation in the frequency domain, J. Acoust. Soc. Am. 103 (1) (1998) 49–63.
[43] D.S. Burnett, A three-dimensional acoustic infinite element based on a prolate spheroidal multipole expansion, J. Acoust. Soc. Am. 96 (5) (1994) 2798–2816.
[44] A. Prieto, Personal Communication, 2018.
[45] P. Moon, D.E. Spencer, Field Theory Handbook: Including Coordinate Systems, Differential Equations and Their Solutions, Springer, 2012.

[46] C. Sun, Explicit equations to transform from cartesian to elliptic coordinates, Math. Modell. Appl. 2 (4) (2017) 43–46.
[47] S. Marburg, Normal modes in external acoustics. Part I: investigation of the one-dimensional duct problem, Acta Acustica united Acustica 91 (6) (2005) 1063–1078.
[48] P. Ruge, Eigenvalues of damped structures: vectoriteration in the original space of dof, Comput. Mech. 22 (2) (1998) 167–173.
[49] S. Marburg, F. Dienerowitz, T. Horst, S. Schneider, Normal modes in external acoustics. Part II: eigenvalues and eigenvectors in 2D, Acta Acustica united Acustica 92 (1) (2006) 97–111.
[50] S. Marburg, Normal modes in external acoustics. Part III: sound power evaluation based on superposition of frequency-independent modes, Acta Acustica united Acustica 92 (2) (2006) 296–311.
[51] L. Moheit, S. Marburg, Infinite elements and their influence on normal and radiation modes in exterior acoustics, J. Comput. Acoust. 25 (4) (2017) 1650020.
[52] D. Dreyer, S. Petersen, O. von Estorff, Effectiveness and robustness of improved infinite elements for exterior acoustics, Comput. Methods Appl. Mech. Eng. 195 (29-32) (2006) 3591–3607.
[53] H. Peters, N. Kessissoglou, S. Marburg, Enforcing reciprocity in numerical analysis of acoustic radiation modes and sound power evaluation, J. Comput. Acoust. 20 (3) (2012).
[54] L. Moheit, S. Marburg, Acoustic radiation modes and normal modes in unbounded domains, Proc. Meet. Acoust. 30 (1) (2017) 022004.
[55] L. Moheit, S. Marburg, Normal modes and modal reduction in exterior acoustics, J. Theor. Comput. Acoust. 26 (3) (2018) 1850029.
[56] H. Peters, N. Kessissoglou, S. Marburg, Modal decomposition of exterior acoustic-structure interaction, J. Acoust. Soc. Am. 133 (5) (2013) 2668–2677.
[57] H. Peters, N. Kessissoglou, S. Marburg, Modal decomposition of exterior acoustic-structure interaction problems with model order reduction, J. Acoust. Soc. Am. 135 (5) (2014) 2706–2717.
[58] R. Astley, Mapped spheroidal wave-envelope elements for unbounded wave problems, Int. J. Numer. Methods Eng. 41 (7) (1998) 1235–1254.
[59] D. Dreyer, O. von Estorff, Improved conditioning of infinite elements for exterior acoustics, Int. J. Numer. Methods Eng. 58 (6) (2003) 933–953.
[60] S. Marburg, B. Nolte, A unified approach to finite and boundary element discretization in linear timeharmonic acoustics, in: S. Marburg, B. Nolte (Eds.), Computational Acoustics of Noise Propagation in Fluids - Finite and Boundary Element Methods, Springer Berlin Heidelberg, Berlin, Heidelberg, 2008, pp. 1–34.
[61] S. Suzuki, S. Maruyama, H. Ido, Boundary element analysis of cavity noise problems with complicated boundary conditions, J. Sound Vib. 130 (1) (1989) 79–96.
[62] S. Marburg, R. Anderssohn, Fluid structure interaction and admittance boundary conditions: setup of an analytical example, J. Comput. Acoust. 19 (1) (2011) 63–74.
[63] J.-P. Coyette, B. Van den Nieuwenhof, A conjugated infinite element method for half-space acoustic problems, J. Acoust. Soc. Am. 108 (4) (2000) 1464–1473.
[64] F. Rellich, Das Eigenwert problem von *uu*0 in Halbrhren (The eigenvalue problem of *uu*0 in half ducts), in: Studies and Essays Presented to R. Courant on his 60th Birthday, 1948, pp. 329–344.
[65] P. Werner, Ein Resonanzphnomen in der Theorie akustischer und elektromagnetischer Wellen (A resonance phenomenon in the theory of acoustic and electro-magnetic waves), Math. Methods Appl. Sci. 6 (1) (1984) 104–128.
[66] P. Werner, Zur Asymptotik der Wellengleichung und der Wrmeleitungsgleichung in zweidimensionalen Auenrumen (On the asymptotics of the wave equation and the heat conduction equation in two-dimensional exterior spaces), Math. Methods Appl. Sci. 7 (1) (1985) 170–201.
[67] S. Hein, T. Hohage, W. Koch, On resonances in open systems, J. Fluid Mech. 506 (2004) 255–284.
[68] S. Hein, T. Hohage, W. Koch, J. Schberl, Acoustic resonances in a high-lift configuration, J. Fluid Mech. 582 (2007) 179–202.
[69] W. Koch, Acoustic resonances and trapped modes in annular plate cascades, J. Fluid Mech. 628 (2009) 155–180.
[70] D. Jones, The eigenvalues of $^2uu0$ when the boundary conditions are given on semi-infinite domains, in: Mathematical Proceedings of the Cambridge Philosophical Society, vol. 49, Cambridge University Press, 1953, pp. 668–684.
[71] D. Evans, Trapped acoustic modes, IMA J. Appl. Math. 49 (1) (1992) 45–60.
[72] D. Evans, M. Levitin, D. Vassiliev, Existence theorems for trapped modes, J. Fluid Mech. 261 (1994) 21–31.
[73] J.D. Kaplunov, S.V. Sorokin, A simple example of a trapped mode in an unbounded waveguide, J. Acoust. Soc. Am. 97 (6) (1995) 3898–3899.
[74] G. Mller, M. Mser, Handbook of Engineering Acoustics, Springer Science & Business Media, 2012.
[75] O. von Estorff, S. Petersen, D. Dreyer, Efficient infinite elements based on Jacobi polynomials, in: S. Marburg, B. Nolte (Eds.), Computational Acoustics of Noise Propagation in Fluids - Finite and Boundary Element Methods, Springer Berlin Heidelberg, 2008, pp. 231–250.
[76] V. Hernandez, J.E. Roman, V. Vidal, SLEPc: a scalable and flexible toolkit for the solution of eigenvalue problems, ACM Trans. Math Software 31 (3) (2005) 351–362.
[77] V. Hernandez, J.E. Roman, V. Vidal, SLEPc: scalable library for eigenvalue problem computations, Lect. Notes Comput. Sci. 2565 (2003) 377–391.
[78] J.E. Roman, C. Campos, E. Romero, A. Tomas, SLEPc Users Manual, Tech. Rep. DSIC-II/24/02 - Revision 3.9, D. Sistemes Informtics I Computaci, Universitat Politcnica de Valncia, 2018.
[79] S. Abhyankar, J. Brown, E.M. Constantinescu, D. Ghosh, B.F. Smith, H. Zhang, Petsc/ts: A Modern Scalable Ode/dae Solver Library. arXiv:1806.01437, 2018.
[80] S. Balay, S. Abhyankar, M.F. Adams, J. Brown, P. Brune, K. Buschelman, L. Dalcin, V. Eijkhout, W.D. Gropp, D. Kaushik, M.G. Knepley, D.A. May, L.C. McInnes, R.T. Mills, T. Munson, K. Rupp, P. Sanan, B.F. Smith, S. Zampini, H. Zhang, H. Zhang, PETSc Web Page, 2018, http://www.mcs.anl.gov/petsc, http://www.mcs.anl.gov/petsc.
[81] S. Balay, S. Abhyankar, M.F. Adams, J. Brown, P. Brune, K. Buschelman, L. Dalcin, V. Eijkhout, W.D. Gropp, D. Kaushik, M.G. Knepley, D.A. May, L.C. McInnes, R.T. Mills, T. Munson, K. Rupp, P. Sanan, B.F. Smith, S. Zampini, H. Zhang, H. Zhang, PETSc Users Manual, Tech. Rep. ANL-95/11 - Revision 3.9. Argonne National Laboratory, 2018http://www.mcs.anl.gov/petsc.
[82] S. Balay, W.D. Gropp, L.C. McInnes, B.F. Smith, Efficient management of parallelism in object oriented numerical software libraries, in: E. Arge, A.M. Bruaset, H.P. Langtangen (Eds.), Modern Software Tools in Scientific Computing, Birkhuser Press, 1997, pp. 163–202.
[83] I. Babuka, F. Ihlenburg, T. Strouboulis, S. Gangaraj, A posteriori error estimation for finite element solutions of Helmholtz equationpart II: estimation of the pollution error, Int. J. Numer. Methods Eng. 40 (21) (1997) 3883–3900.
[84] F. Ihlenburg, Finite Element Analysis of Acoustic Scattering, vol. 132, Springer Science & Business Media, 2006.
[85] P. Langer, M. Maeder, C. Guist, M. Krause, S. Marburg, More than six elements per wavelength: the practical use of structural finite element models and their accuracy in comparison with experimental results, J. Comput. Acoust. (2017) 1750025.
[86] R. Astley, J.-P. Coyette, The performance of spheroidal infinite elements, Int. J. Numer. Methods Eng. 52 (12) (2001) 1379–1396.
[87] K.H. Huebner, D.L. Dewhirst, D.E. Smith, T.G. Byrom, The Finite Element Method for Engineers, John Wiley & Sons, 2001.
[88] W. Wunderlich, W.D. Pilkey, Mechanics of Structures: Variational and Computational Methods, CRC press, 2002.
[89] S. Marburg, H.-J. Hardtke, A study on the acoustic boundary admittance. determination, results and consequences, Eng. Anal. Bound. Elem. 23 (9) (1999) 737–744.
[90] M. Mser, Engineering Acoustics, Springer, 2014.
[91] D. Ewins, Vibration characteristics of bladed disc assemblies, J. Mech. Eng. Sci. 15 (3) (1973) 165–186.
[92] B. Irwanto, H.-J. Hardtke, D. Pawandenat, An efficient technique for the computation of eigenvalue and eigenvector derivatives of cyclic structures, Comput. Struct. 81 (2425) (2003) 2395–2400.